



2015

# Design, Synthesis, and Biological Evaluation of Folate Targeted Photosensitizers for Photodynamic Therapy

Laura Jean Donahue  
*Loyola University Chicago*

---

## Recommended Citation

Donahue, Laura Jean, "Design, Synthesis, and Biological Evaluation of Folate Targeted Photosensitizers for Photodynamic Therapy" (2015). *Dissertations*. Paper 1940.  
[http://ecommons.luc.edu/luc\\_diss/1940](http://ecommons.luc.edu/luc_diss/1940)

This Dissertation is brought to you for free and open access by the Theses and Dissertations at Loyola eCommons. It has been accepted for inclusion in Dissertations by an authorized administrator of Loyola eCommons. For more information, please contact [ecommons@luc.edu](mailto:ecommons@luc.edu).



This work is licensed under a [Creative Commons Attribution-Noncommercial-No Derivative Works 3.0 License](https://creativecommons.org/licenses/by-nc-nd/3.0/).  
Copyright © 2015 Laura Jean Donahue

LOYOLA UNIVERSITY CHICAGO

DESIGN, SYNTHESIS, AND BIOLOGICAL EVALUATION OF  
FOLATE TARGETED PHOTSENSITIZERS  
FOR PHOTODYNAMIC THERAPY

A DISSERTATION SUBMITTED TO  
THE FACULTY OF THE GRADUATE SCHOOL  
IN CANDIDACY FOR THE DEGREE OF  
DOCTOR OF PHILOSOPHY

PROGRAM IN CHEMISTRY

BY

LAURA J. DONAHUE

CHICAGO, IL

AUGUST 2015

Copyright by Laura J. Donahue, 2015  
All rights reserved.

## **ACKNOWLEDGMENTS**

I would like to acknowledge my research advisor, Dr. David Crumrine, for all of his guidance, patience, and support throughout my years of graduate work. I would also like to thank the members of my dissertation committee, Dr. James Babler, Dr. Ken Olsen, Dr. Martina Schmeling, and Dr. Stefan Kanzok for their continued guidance, support, and participation as members of my committee. I would like to thank other graduate students at Loyola who have been of assistance to me, in particular, Jeff Trautmann, Matthew Reichert, Brian Levenson, Cory Reidl, and RoJenia Jones. In addition, I would like to thank other faculty and staff at Loyola who have been very helpful, including Dr. Robert Polak, Dr. Rodney Dale, Dr. Matthew Bartucci, Dr. David French (dec.), Dr. Jessica Eisenberg, Dr. Paul Chiarelli, Doug Steinman, Peidong Zhao, Denise Hall, Carol Grimm, and Stacey Lind. I would like to thank the many undergraduate students, especially Sana Hira, who worked with cell cultures and cell killing studies, Munira Munshi, who worked on the oxidation studies of the phenothiazine trimer, and all of the others who worked with me in the research group, as their assistance was invaluable. I am also grateful for the financial assistance from Loyola University in the form of teaching assistantships and a 3<sup>rd</sup> year teaching fellowship, without which this research would not have been possible.

Finally, I would like to thank my family and my most beloved friend, John Sahagian, for their support of me throughout this entire endeavor.

## TABLE OF CONTENTS

ACKNOWLEDGMENTS	iii
LIST OF SCHEMES	vii
LIST OF FIGURES	viii
LIST OF TABLES	xiii
LIST OF ABBREVIATIONS	xv
ABSTRACT	xxii
CHAPTER ONE: CANCER AND PHOTODYNAMIC THERAPY	1
Introduction	1
Photodynamic Therapy	2
Mechanisms of Photodynamic Therapy	3
Role of Oxygen in Photodynamic Therapy	9
Importance of Light Dosimetry and Types of Light Sources for PDT	12
Characteristics of a Good Photosensitizer	14
Historical Uses of Phototherapy	15
First Generation Photosensitizers	18
Second Generation Photosensitizers	20
Third Generation Photosensitizers	25
Folate Targeted Cancer Therapy	32
Folate Receptor Expression Patterns	33
Current Uses of PDT for Non-cancerous Conditions	34
Vascular Targeting in Photodynamic Therapy	46
Inflammation and Immune Responses to PDT	51
Photobleaching and Quenching of Singlet Oxygen in PDT	57
Buchwald-Hartwig Chemistry for Pd-Catalyzed Cross Coupling	
Reactions Forming C-N Bonds	59
Pd-Catalyzed Cross Coupling Reactions Forming C-C Bonds	64
Ullmann Conditions for Catalysis of Cross Coupling Reactions	
Forming C-N Bonds	66
HeLa Cells to Test Cancer Cell Killing Potential	68
CHAPTER TWO: PURPOSE OF THE RESEARCH	70

CHAPTER THREE: EXPERIMENTAL RESEARCH & DEVELOPMENT	74
Experimental Description of Research	74
Experimental Materials	96
Chemical Materials	96
Biological Materials	97
Experimental Procedures	97
Synthesis of N-benzylphenothiazine	97
Synthesis of N-benzyl-3,7-dibromophenothiazine	98
Attempted Ullmann Synthesis of N-benzyl-3,7-diphenothiazinylphenothiazine	99
Buchwald-Hartwig Synthesis of N-benzyl-3,7-diphenothiazinylphenothiazine	100
Procedure for Deprotection of N-benzylphenothiazine	101
Synthesis of Acetyl Phenothiazine Using Acetyl Chloride	102
Synthesis of Acetyl Phenothiazine Using Acetic Acid NHS Ester	103
Synthesis of Methyl 4-N-methylenephenothiazinylbenzoate	103
Synthesis of Methyl (3,7-dibromo)-4-N-methylenephenothiazinylbenzoate	104
Synthesis of Methyl (3,7-diphenothiazinyl)-4-N-methylenephenothiazinylbenzoate	105
Synthesis of N-Octadecylbenzamide	106
Ullmann Synthesis of Methyl 4-phenothiazinylbenzoate	107
Synthesis of Chlorin e6-PEG-Folate Conjugate	108
CHAPTER FOUR: EVALUATION OF A CHLORIN e6-PEG-FOLATE CONJUGATE AS A PHOTODYNAMIC THERAPY AGENT	110
Determination of the Phototoxicity of the Chlorin e6-PEG-FA Conjugate	110
Results and Discussion	113
Cytotoxicity / Phototoxicity Assays	116
Conclusions	125
CHAPTER FIVE: CONCLUSION	129
APPENDIX A: LIST OF FIGURES	133
APPENDIX B: LIST OF TABLES	211
REFERENCE LIST	241
VITA	284

## LIST OF SCHEMES

Scheme 1. Synthesis of N-benzylphenothiazine	74
Scheme 2. Synthesis of N-benzyl-3,7-dibromophenothiazine	75
Scheme 3. Ullmann Reaction Attempt to Produce Phenothiazine Trimer	76
Scheme 4. Buchwald-Hartwig Reaction to Produce Phenothiazine Trimer	76
Scheme 5. Synthetic Approach to N-benzyl-3,7-diiodophenothiazine	77
Scheme 6. Buchwald-Hartwig Synthesis of Phenothiazine Trimer	79
Scheme 7. Model Deprotection of N-benzylphenothiazine	81
Scheme 8. Model Acetylation of Phenothiazine using Acetyl Chloride	82
Scheme 9. Model Acetylation of Phenothiazine using Acetic Acid NHS Ester	84
Scheme 10. Phenothiazine Protection using methyl 4- (bromomethyl)benzoate	85
Scheme 11. Bromination of methyl 4-N- methylenephenothiazinylbenzoate	85
Scheme 12. Synthesis of methyl (3,7-diphenothiazinyl)-4-N- methylenephenothiazinylbenzoate	86
Scheme 13. Model Reaction Synthesis of N-octadecylbenzamide	86
Scheme 14. Ullmann Synthesis of methyl 4-N-phenothiazinylbenzoate	88
Scheme 15. Synthesis of Chlorin e6-PEG-Folate	89



## LIST OF FIGURES

Figure 1. Type 1 and 2 Mechanisms of Forming ROS	4
Figure 2. Structure of 8-oxo-7,8-dihydroguanosine	6
Figure 3. Buchwald-Hartwig Cross Coupling Reaction	63
Figure 4. Structure of Losartan	66
Figure 5. Endocytosis	71
Figure 6. Cross-linked Hemoglobin	72
Figure 7. Other Heterocyclic Compounds to Replace Bromine	75
Figure 8. Structures of XPhos Ligand and Pd Catalyst	79
Figure 9. Structure of PEG linker with COOH group	83
Figure 10. Structure of PEG linker with NHS ester group	83
Figure 11. Mechanism of Aminolysis Using TBD Catalyst	87
Figure 12. Structure of NH <sub>2</sub> -PEG-FA	88
Figure 13. Mechanism of Amide Coupling of Chlorin e6 to NH <sub>2</sub> -PEG-FA (Note – RCOOH indicates the carboxylic acid group at C-17 of Chlorin e6)	90
Figure 14. UV-VIS Spectrum of Ce6-PEG-FA in PBS	91
Figure 15. Reduction of Resazurin to Resorufin	111
Figure 16. Cytotoxicity / Phototoxicity of Ce6-PEG-FA	112
Figure 17. Chlorin e6-PEG-Folate Structure and FR Interactions	114
Figure 18. Structural Interactions of Folate with the Folate Receptor	115

Figure 19. Average Fluorescence Counts for Cells Only Control: 4 Expts.	116
Figure 20. Cytotoxicity Average % Viability for Cells Control, Ce6 Controls, and CPF: 4 Expts.	117
Figure 21. Average % Viability for Ce6 Control: 4 Expts.	118
Figure 22. Average % Viability for Ce6–PEG–FA: 4 Expts.	120
Figure 23. Average % Viability for Ce6 / CPF 10 $\mu$ M: 4 Expts.	121
Figure 24. Average % Viability for All Compounds: 4 Expts.	123
Figure 25. Average % Viability for Ce6 / CPF 5 $\mu$ M: 4 Expts.	124
Figure 26. Diagram of N-benzyl-3,7-diphenothiazinylphenothiazine Showing Delocalization of a Lone Electron	131
Figure 27. UV-VIS Spectrum of N-benzyl-3,7-diphenothiazinylphenothiazine	134
Figure 28. UV-VIS Spectrum of methyl (3,7-diphenothiazinyl)-4-N-methylenephenothiazinylbenzoate	135
Figure 29. UV-VIS Spectrum of Ullmann methyl 4-N-phenothiazinylbenzoate	136
Figure 30. UV-VIS Spectrum of Folic Acid Dihydrate Standard	137
Figure 31. UV-VIS Spectrum of Folic Acid Dihydrate Standard	138
Figure 32. UV-VIS Spectrum of Folic Acid Dihydrate Standard	139
Figure 33. UV-VIS Spectrum of Folic Acid Dihydrate Standard	140
Figure 34. UV-VIS Spectrum of Ce6 Standard	141
Figure 35. UV-VIS Spectrum of Ce6 Standard	142
Figure 36. UV-VIS Spectrum of Ce6 Standard	143
Figure 37. UV-VIS Spectrum of Ce6 Standard	144

Figure 38. IR Spectrum of N-benzyl-3,7-diphenothiazinylphenothiazine	145
Figure 39. IR Spectrum of methyl (3,7-diphenothiazinyl)-4-N-methylenephenothiazinylbenzoate	146
Figure 40. Mass Spectrum of N-benzyl-3,7-diphenothiazinylphenothiazine	147
Figure 41. Mass Spectrum of methyl 4-N-methylenephenothiazinylbenzoate	148
Figure 42. Mass Spectrum of methyl (3,7-diphenothiazinyl)-4-N-methylenephenothiazinylbenzoate	149
Figure 43. Mass Spectrum of Chlorin e6	150
Figure 44. Mass Spectrum of Ce6-PEG-FA	151
Figure 45. Mass Spectrum of Ce6-PEG-FA	152
Figure 46. <sup>1</sup> H NMR of N-benzylphenothiazine	153
Figure 47. <sup>1</sup> H NMR Expansion of N-benzylphenothiazine	154
Figure 48. <sup>13</sup> C NMR Expansion of N-benzylphenothiazine	156
Figure 49. <sup>1</sup> H NMR of N-benzyl-3,7-dibromophenothiazine	157
Figure 50. <sup>1</sup> H NMR Expansion of N-benzyl-3,7-dibromophenothiazine	158
Figure 51. <sup>13</sup> C NMR of N-benzyl-3,7-dibromophenothiazine	160
Figure 52. <sup>13</sup> C NMR Expansion of N-benzyl-3,7-dibromophenothiazine	161
Figure 53. <sup>1</sup> H NMR Expansion of N-benzyl-3,7-diphenothiazinylphenothiazine	162
Figure 54. <sup>1</sup> H NMR Expansion of N-benzyl-3,7-diphenothiazinylphenothiazine	163
Figure 55. <sup>13</sup> C NMR of N-benzyl-3,7-diphenothiazinylphenothiazine	166
Figure 56. <sup>13</sup> C NMR Expansion of N-benzyl-3,7-diphenothiazinylphenothiazine	167

Figure 57.	<sup>13</sup> C NMR Expansion of N-benzyl-3,7-diphenothiazinylphenothiazine	168
Figure 58.	<sup>13</sup> C NMR Expansion of N-benzyl-3,7-diphenothiazinylphenothiazine	169
Figure 59.	2D COSY Spectrum of N-benzyl-3,7-diphenothiazinylphenothiazine	173
Figure 60.	2D COSY Spectrum Expansion of N-benzyl-3,7-diphenothiazinylphenothiazine	175
Figure 61.	2D COSY Spectrum Expansion of N-benzyl-3,7-diphenothiazinylphenothiazine	176
Figure 62.	2D COSY Spectrum Expansion of N-benzyl-3,7-diphenothiazinylphenothiazine	178
Figure 63.	2D HSQC Spectrum of N-benzyl-3,7-diphenothiazinylphenothiazine	180
Figure 64.	2D HSQC Spectrum Expansion of N-benzyl-3,7-diphenothiazinylphenothiazine	182
Figure 65.	<sup>1</sup> H NMR of methyl 4-N-methylenephenothiazinylbenzoate	184
Figure 66.	<sup>1</sup> H NMR Expansion of methyl 4-N-methylenephenothiazinylbenzoate	185
Figure 67.	<sup>13</sup> C NMR of methyl 4-N-methylenephenothiazinylbenzoate	187
Figure 68.	<sup>13</sup> C NMR Expansion of methyl 4-N-methylenephenothiazinylbenzoate	188
Figure 69.	<sup>13</sup> C NMR Expansion of methyl 4-N-methylenephenothiazinylbenzoate	190
Figure 70.	<sup>1</sup> H NMR of methyl (3,7-dibromo)-4-N-methylenephenothiazinylbenzoate	192
Figure 71.	<sup>1</sup> H NMR Expansion of methyl (3,7-dibromo)-4-N-methylenephenothiazinylbenzoate	193

Figure 72.	<sup>13</sup> C NMR Expansion of methyl (3,7-dibromo)-4-N-methylenephenothiazinylbenzoate	195
Figure 73.	<sup>13</sup> C NMR Expansion of methyl (3,7-dibromo)-4-N-methylenephenothiazinylbenzoate	196
Figure 74.	<sup>1</sup> H NMR Expansion of methyl (3,7-diphenothiazinyl)-4-N-methylenephenothiazinylbenzoate	197
Figure 75.	<sup>1</sup> H NMR Expansion of methyl (3,7-diphenothiazinyl)-4-N-methylenephenothiazinylbenzoate	198
Figure 76.	<sup>13</sup> C NMR Expansion of methyl (3,7-diphenothiazinyl)-4-N-methylenephenothiazinylbenzoate	199
Figure 77.	<sup>13</sup> C NMR Expansion of methyl (3,7-diphenothiazinyl)-4-N-methylenephenothiazinylbenzoate	200
Figure 78.	<sup>13</sup> C NMR Expansion of methyl (3,7-diphenothiazinyl)-4-N-methylenephenothiazinylbenzoate	201
Figure 79.	<sup>13</sup> C NMR Expansion of methyl (3,7-diphenothiazinyl)-4-N-methylenephenothiazinylbenzoate	202
Figure 80.	<sup>1</sup> H NMR Expansion of methyl 4-N-phenothiazinylbenzoate	203
Figure 81.	<sup>1</sup> H NMR of Ce6-PEG-FA	204
Figure 82.	<sup>1</sup> H NMR Expansion of Ce6-PEG-FA	205
Figure 83.	<sup>1</sup> H NMR Expansion of Ce6-PEG-FA	206
Figure 84.	<sup>1</sup> H NMR Expansion of Ce6-PEG-FA	207
Figure 85.	<sup>13</sup> C NMR of Ce6-PEG-FA	208
Figure 86.	<sup>13</sup> C NMR Expansion of Ce6-PEG-FA	209
Figure 87.	<sup>13</sup> C NMR Expansion of Ce6-PEG-FA	210

## LIST OF TABLES

Table 1. UV-VIS Data of Known Concentrations of Ce6 and Folate	93
Table 2. Calculations of Concentration of Folate and Chlorin from UV-VIS Data and Epsilons of Known Concentrations (1:40 Dilution in PBS)	94
Table 3. Calculations of Concentration of Folate and Chlorin from UV-VIS Data and Epsilons of Known Concentrations (1:20 Dilution in PBS)	95
Table 4. Fluences of Irradiated Light Delivered to Various Cell Culture Plate Rows	113
Table 5. Cytotoxicity Data: August 1, 2014	212
Table 6. Phototoxicity Data: August 1, 2014	213
Table 7. Cytotoxicity Data: November 21, 2014	214
Table 8. Cytotoxicity Data (cont.): November 21, 2014	215
Table 9. Phototoxicity Data: November 21, 2014	216
Table 10. Phototoxicity Data (cont.): November 21, 2014	217
Table 11. Cytotoxicity Data: December 5, 2014	218
Table 12. Cytotoxicity Data (cont.): December 5, 2014	219
Table 13. Phototoxicity Data: December 5, 2014	220
Table 14. Phototoxicity Data (cont.): December 5, 2014	221
Table 15. Cytotoxicity Data: February 6, 2015	222
Table 16. Cytotoxicity Data (cont.): February 6, 2015	223

Table 17. Cytotoxicity Data (cont.): February 6, 2015	224
Table 18. Phototoxicity Data: February 6, 2015	225
Table 19. Phototoxicity Data (cont.): February 6, 2015	226
Table 20. Phototoxicity Data (cont.): February 6, 2015	227
Table 21. Cytotoxicity Data: April 3, 2015	228
Table 22. Cytotoxicity Data (cont.): April 3, 2015	229
Table 23. Cytotoxicity Data (cont.): April 3, 2015	230
Table 24. Cytotoxicity Data (cont.): April 3, 2015	231
Table 25. Cytotoxicity Data (cont.): April 3, 2015	232
Table 26. Phototoxicity Data: April 3, 2015	233
Table 27. Phototoxicity Data (cont.): April 3, 2015	234
Table 28. Phototoxicity Data (cont.): April 3, 2015	235
Table 29. Phototoxicity Data (cont.): April 3, 2015	236
Table 30. Phototoxicity Data (cont.): April 3, 2015	237
Table 31. Phototoxicity Data (cont.): April 3, 2015	238
Table 32. Compiled Cytotoxicity Data: 4 Experiments	239
Table 33. Compiled Phototoxicity Data: 4 Experiments	240

## LIST OF ABBREVIATIONS

AIDS	Autoimmune Deficiency Syndrome
AK	Actinic Keratosis
ALA	Aminolevulinic acid
AMD	Age-related Macular Degeneration
Anh	Anhydrous
APCs	Antigen-presenting cells
BH	Buchwald-Hartwig
BINAP	2,2'-Bis(di-p-tolylphosphino)-1,1'-binaphthyl
BPD-MA	Benzoporphyrin Derivative-Monoacid Ring A
BSA	Bovine Serum Albumin
BSA-Ce6-Mal	Bovine Serum Albumin-Chlorin e6-Maleimide
BSA-Pc	Bovine Serum Albumin Phthalocyanine
CDCl <sub>3</sub>	Deuterated Chloroform
Ce6	Chlorin e 6
CH <sub>2</sub> Cl <sub>2</sub>	Methylene Chloride
CH <sub>3</sub> CN	Acetonitrile
CNV	Choroidal Neovessels
COSY	CH Correlation Spectroscopy
COX	Cyclooxygenase



CsCO <sub>3</sub>	Cesium Carbonate
CuI	Copper (I) Iodide
DAMPs	Damage-associated Molecular Patterns
DBSF	Bis(3,5-dibromosalicyl)fumarate
DC	Dendritic Cells
DCC	Dicyclohexylcarbodiimide
DCM	Dichloromethane
DMF	Dimethylformamide
DMSO	Dimethylsulfoxide
DNA	Deoxyribonucleic Acid
dppf	diphenylphosphinoferrocene
DSAP	Disseminated Actinic Purokeratosis
EPR	Electron Paramagnetic Resonance
FR	Folate Receptor
GePc	Germanium Phthalocyanine
Hb	Hemoglobin
HBr	Hydrogen Bromide
HCOOH	Formic Acid
HDLs	High Density Lipoproteins
HeLa	cells from Henrietta Lacks
HIO <sub>3</sub>	Iodic Acid
HIV	Human Immunodeficiency Virus

HOBt	1-hydroxybenzotriazole
HP	Hematoporphyrin
HP-BSA	Hematoporphyrin-Bovine Serum Albumin
HpD	Hematoporphyrin Derivative
HP-LDL	Hematoporphyrin-Low Density Lipoprotein
HPPH	2-(1-hexyloxyethyl)-2-devinylpyropheophorbide-a
HPV	Human Papilloma Virus
HS	Hidradenitis Suppurativa
HSP70	Heat Shock Protein 70
HSQC	Heteronuclear Single Quantum Correlation
IH	Intimal Hyperplasia
IPL	Intense Pulsed Light
IR	Infrared
IV	Intravenous
JosiPhos	(S)-1-((RP)-2-[Bis[3,5-bis(trifluoromethyl)phenyl]phosphino]-ferrocenyl)ethyl-dicyclohexylphosphine (one of many types of these ligands)
K <sub>2</sub> CO <sub>3</sub>	Potassium Carbonate
KH	Potassium Hydride
KI	Potassium Iodide
K <sub>3</sub> PO <sub>4</sub>	Potassium Phosphate
LASER	Light Amplification by Stimulated Emission of Radiation
LDA	Lithium Diisopropyl Amide

LDL-Ce6	Low Density Lipoprotein-Chlorin e6
LDLs	Low Density Lipoproteins
LED	Light Emitting Diode
LOOH	Lipid hydroperoxides
LOX	Lipoxygenase
Lutex	Lutetium Texaphyrin
Mal-BSA-Ce6	Maleimide-Bovine Serum Albumin-Chlorin e6
MgSO <sub>4</sub>	Magnesium Sulfate
MHC	Major Histocompatibility Complex
MRI	Magnetic Resonance Imaging
MRSA	Methicillin-Resistant Staphylococcus Aureus
m-THPC	meta-tetrahydroxyphenylchlorin
MTT	3-(4,5-dimethylthiazol-2-yl)-2,5-diphenyltetrazolium bromide
Na <sub>2</sub> CO <sub>3</sub>	Sodium Carbonate
NADH	Nicotinamide Adenine Dinucleotide (reduced form)
NADPH	Nicotinamide Adenine Dinucleotide Phosphate (reduced form)
NaHCO <sub>3</sub>	Sodium Bicarbonate
NaOC(CH <sub>3</sub> ) <sub>3</sub>	Sodium <i>tert</i> -butoxide
NHS	N-hydroxysuccinamide
NK	Natural Killer
NMR	Nuclear Magnetic Resonance

NOE	Nuclear Overhauser Effect
NOX	NADPH oxidase
NPe6	mono-L-aspartyl chlorin e6
8-oxo-dG	8-oxo-7,8 dihydro-guanosine
$^1\text{O}_2$	excited singlet state oxygen
$^1\Delta_g$	first excited singlet state oxygen
$^1\Sigma_g^+$	second excited singlet state oxygen
$^3\text{O}_2$	ground state oxygen
PBS	Phosphate Buffered Saline
$\text{Pd}(\text{dba})_2$	Bis(dibenzylideneacetone)palladium(0)
$\text{PdCl}_2(\text{PPh}_3)_2$	Bis(triphenylphosphine)palladium(II) dichloride
$\text{Pd}_2(\text{dba})_3$	Tris(dibenzylideneacetone)dipalladium(0)
PDT	Photodynamic Therapy
PEG	Polyethylene Glycol
PpIX	Protoporphyrin IX
PRRs	Pattern Recognition Receptors
PS / PSs	Photosensitizer / Photosensitizers
PT	Pressure Tube
PTA	Percutaneous Transluminal Angioplasty
PUVA	Psoralen + Ultraviolet A
RB	Round Bottom
RNA	Ribonucleic Acid

ROS	Reactive Oxygen Species
RuPhos	2-Dicyclohexylphosphino-2',6'-diisopropoxybiphenyl
S <sub>0</sub>	Ground state
S <sub>1</sub>	Excited singlet state
SDS	Sodium Dodecyl Sulfate
SnET2	Tin ethyl etiopurpurin
SOCl <sub>2</sub>	Thionyl Chloride
SOD	Superoxide Dismutase
SRA	Scavenger Receptor Class A
T <sub>1</sub>	Excited triplet state
TBD	1,5,7-Triazabicyclo[4.4.0]dec-5-ene
TCFA	Thin-cap Fibroatheroma
THF	Tetrahydrofuran
TLC	Thin Layer Chromatography
TLRs	Toll-like Receptors
TNF $\alpha$	Tumor Necrosis Factor Alpha
UV-A	Ultraviolet A
UV-B	Ultraviolet B
UV-C	Ultraviolet C
VEGF	Vascular Endothelial Growth Factor
vWF	vonWillebrand Factor
XantPhos	4,5-Bis(diphenylphosphino)-9,9-dimethylxanthene

XPhos	2-Dicyclohexylphosphino-2',4',6'-triisopropylbiphenyl
ZnPc	Zinc Phthalocyanine
ZnPc-LDL	Zinc Phthalocyanine-Low Density Lipoprotein

## ABSTRACT

Photodynamic therapy (PDT) is used to treat cancer, and involves a highly conjugated molecule, called a photosensitizer (PS), which is excited by wavelengths of light from visible to infrared. Photosensitizers that are highly conjugated will absorb longer wavelengths (600 – 900 nm), and have the potential to destroy cells of deeper tissue cancers. In PDT, a PS is administered to the patient, and after an appropriate time delay, the tissue is then exposed to light of a specific wavelength necessary for excitation of the PS. A transfer of energy can take place between the excited PS and oxygen that is nearby. This process allows the PS to relax back to the ground state, while creating an excited singlet state oxygen molecule ( $^1\text{O}_2$ ).

Buchwald-Hartwig conditions using Pd catalysts and phosphorus containing ligands can be utilized to synthesize the photosensitizer. The reaction involves a Pd-catalyzed cross coupling of an aryl halide with a nitrogen nucleophile to form a new carbon-nitrogen bond. The PS will be PEGylated with an amine-PEG-Folate complex. Since many tumors over-express folate receptors, the PS-PEG-FA complex will be transported to cancer cells via receptor mediated endocytosis, providing greater selectivity.

The killing efficiency of the PS will be tested using HeLa cells. Solutions containing PS only, PS-PEG-FA, and media only will be added to cancer

with folate restricted media. After exposure to light, the cells will be counted to determine the percentage of cells killed by the singlet oxygen and other radical species. Variables that must be controlled in this study are the following: length of time cells have been growing; specific concentration of PS-PEG-folate complex; length of time for PS-PEG-folate complex uptake into the cell; length of time of exposure to light; length of time from light exposure to cell counting to determine necrosis. The goal of the research is to determine the concentration of PS and length of time of light exposure that is maximally effective for killing tumor cells.



# **CHAPTER ONE**

## **CANCER AND PHOTODYNAMIC THERAPY**

### **Introduction**

A normal cell has a specific lifespan of growth, division, and death that occurs in an orderly fashion. A critical balance is maintained between cell growth, proliferation, differentiation, and death; and, in the presence of factors that promote tumor formation, such as an inherited genetic defect, a chemical carcinogen, a viral infection, or irradiation, this balance is disrupted. Cancer develops when cellular growth in a part of the body becomes out of control. Three major changes must occur in order for a cell to become cancerous, which are:

1. **Immortalization** – the cancer cell acquires the ability to grow and divide indefinitely.
2. **Transformation** – the normal growth constraints are not observed, that is, growth occurs independently of cell growth factors. The transformed cells can form a solid tumor; however, in order for the tumor to grow, a blood supply is needed, and angiogenesis (growth of new blood vessels) must occur.
3. **Metastasis** – cancer cells often migrate from the tissue of origin to other areas of the body where they begin to grow and replace normal tissue. This process, known as metastasis, occurs as cancer cells invade the bloodstream or lymph vessels and other tissues.

Cancer is not only one disease, but a group of genetically diverse disorders, with each unique tumor that has its own “genetic signature.” Gene

mutations acquired by a tumor can subsequently become a heritable trait of all cells of future generations. Cancer is a disease of many steps. A tumor cell emerges after the cell accumulates many (estimates are between four to eight) genetic alterations over the course of years.

Gene mutations which increase a person's risk for cancer can be inherited or acquired. Genetic changes that are acquired result from spontaneous or environmentally inflicted errors during deoxyribonucleic acid (DNA) replication. Genetic changes associated with tumor growth are divided into two major categories: those that result from a gain of function, which involves inappropriate activation of oncogenes; and those that result from a loss of function, which involves inactivation of tumor suppressor genes. Oncogenes stimulate growth, and can cause cancer when hyperactive; whereas, tumor suppressor genes inhibit cell growth, and these genes can cause cancer when not expressed (1).

### **Photodynamic Therapy**

Photodynamic therapy (PDT) is a treatment that destroys cells in the presence of oxygen and upon exposure to light which is absorbed by a photosensitizer (PS) (2). The PS becomes excited, and a transfer of energy converts triplet oxygen to the highly reactive singlet oxygen (3). Singlet oxygen causes destruction of vital cellular organelles, resulting in cell death, as well as vascular shutdown, and activation of an immune response against cellular targets. Some of the advantages of PDT as opposed to conventional therapies include the following: noninvasiveness, selectivity to target tissue, the ability for

repeated dosing to patients without initiating resistance or exceeding total dose limitations (as is associated with radiation therapy), rapid healing with little or no scarring, ability to treat patients in an outpatient setting, and lack of deleterious side effects (4).

Current clinical applications of PDT include: treatment of solid tumors of the skin (basal cell carcinomas), lung, esophagus, bladder, head and neck, brain, ocular melanoma, ovarian, prostate, renal cell, cervix, pancreas, and bone carcinomas (5, 6). Other non-cancerous conditions have also been treated with PDT, which include: dysplasias, papillomas, rheumatoid arthritis, actinic keratosis, cosmetic procedures, psoriasis, neovascularization in age associated macular degeneration, endometrial ablation, port wine stains, and atherosclerotic plaques (6, 7). PDT has also been used to treat bacterial and fungal infections for over 30 years (8).

### **Mechanisms of Photodynamic Therapy**

Three elements are required for successful PDT, which involves the generation of singlet oxygen. These elements include a PS, light of the appropriate wavelength, and oxygen. When a PS in the ground state is exposed to light of a specific wavelength, the PS absorbs a photon and is promoted from its ground state ( $S_0$ ) to the excited singlet state ( $S_1$ ), which has a lifetime of approximately 1  $\mu$ s (2, 9). The energy of the excited singlet state can be dissipated by thermal decay or the emission of fluorescence (2). Alternatively, by intersystem crossing, the excited singlet state can be converted to a lower

energy excited triplet state ( $T_1$ ), which has a lifetime of approximately 0.01 s (2, 9). In the excited singlet state, the PS can produce reactive species via two mechanisms, Type I and Type II processes (3). In the Type I process, an electron can be transferred from the excited singlet state PS to receptor molecules, giving rise to free radicals, including the superoxide anion ( $O_2^-$ ), hydroxyl radical ( $OH^\cdot$ ), or hydrogen peroxide (10). In addition to electron transfer, Type I processes can involve hydrogen abstraction, photoadditions, and various other bimolecular photochemical reactions (11). In the Type II process, the PS in the excited singlet state intersystem crosses to the excited triplet state, and interacts directly with molecular oxygen to produce singlet oxygen ( $^1O_2$ ), which is very reactive (12).

Figure 1., diagramming Type 1 and 2 mechanisms, is shown below.

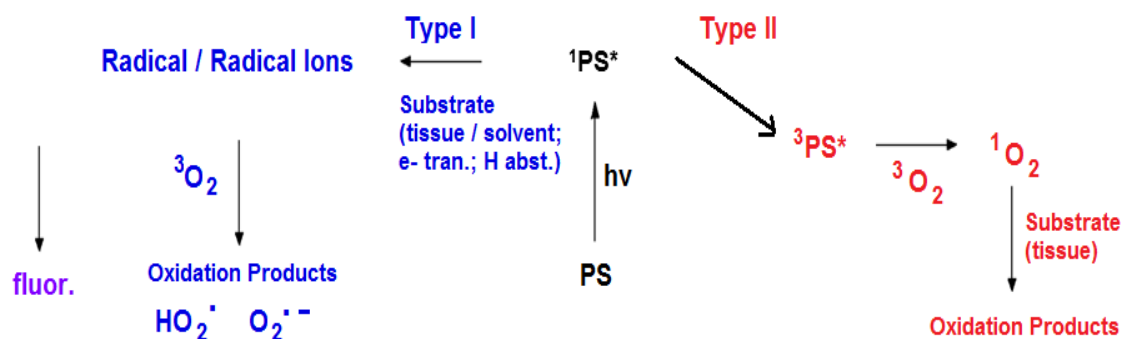


Figure 1. Type 1 and 2 Mechanisms of Forming ROS

The production of  $^1O_2$  occurs by inversion of the spin of one of the outermost electrons in an antibonding orbital. For ground state oxygen ( $^3O_2$ ) the two outermost electrons occupy separate antibonding orbitals and have identical

spins  $\{(\sigma_{2p})^2(\pi_{2py})^2(\pi_{2pz})^2(\pi_{2py}^*)^1(\pi_{2pz}^*)^1\}$ . In the lower energy form of  $^1\text{O}_2$ , the two highest energy electrons are found in the same antibonding orbital with opposing spins  $\{(\sigma_{2p})^2(\pi_{2py})^2(\pi_{2pz})^2(\pi_{2py}^*)^2\}$ , and in the higher energy form of  $^1\text{O}_2$ , the two highest energy electrons are found in two antibonding orbitals with opposing spins  $\{(\sigma_{2p})^2(\pi_{2py})^2(\pi_{2pz})^2(\pi_{2py}^*)^1(\pi_{2pz}^*)^1\}$ . The position of these highest energy electrons in  $^1\text{O}_2$  accounts for its high reactivity (9). Singlet oxygen in the first excited state ( $^1\Delta_g$ ) has an energy that is 22 kcal/mol (92 kJ/mol) higher than ground state triplet oxygen, whereas  $^1\text{O}_2$  in the second excited state ( $^1\Sigma_g^+$ ) has an energy that is 37 kcal/mol (155 kJ/mol) higher than ground state triplet oxygen. Type II processes are most relevant, and  $^1\text{O}_2$  that is generated is responsible for the destruction of the targeted tissues (12). The lifetime of  $^1\text{O}_2$  ( $^1\Delta_g$ ) is approximately 10-100  $\mu\text{s}$  (13) in most organic solvents, which restricts its activity to a spherical volume 10 nm in diameter centered at the actual point of production. The lifetime of  $^1\text{O}_2$  in water is approximately 1-3  $\mu\text{s}$  because the excited state energy of  $^1\text{O}_2$  is nearly equal to the energy of the O-H stretching in the water molecule; therefore, it is easy to dissipate the energy of  $^1\text{O}_2$  as heat due to the stretching and vibrational motions of water molecules (14). Of even greater importance is the lifetime of  $^1\text{O}_2$  ( $^1\Delta_g$ ) in cellular systems, which ranges from 100 ns in the lipid regions of membranes to 250 ns in the cytoplasm. Due to these short lifetimes, the diffusion range of  $^1\text{O}_2$  is predicted to be approximately 45 nm in cellular media. The diameter of human cells ranges from approximately 10 to 100  $\mu\text{m}$ ; therefore,  $^1\text{O}_2$  cannot diffuse more than a single cell length. The

site in the cell where the primary generation of  $^1\text{O}_2$  occurs determines which subcellular structures will be attacked, and  $^1\text{O}_2$  is an indiscriminate oxidant which can react with a variety of biological molecules (15).

Oxidative stress due to  $^1\text{O}_2$  interaction with cellular components such as lipids, amino acid residues, and nucleic acids leads to cell death (11). Singlet oxygen is an electrophile and it can undergo the “ene” reaction, adding to double bond systems and also form endoperoxides upon insertion into ring systems via a 4 + 2 Diels Alder cycloaddition reaction. Addition of  $^1\text{O}_2$  to unsaturated lipids forms hydroperoxides (16) which can lead to further chain lipid peroxidation reactions. Also, the formation of protein peroxides (17) disrupts the protein structure and function. Nucleic acid base oxidation favors the purines, especially guanine, and eventually forms the mutagenic product, 8-oxo-7,8-dihydroguanosine (8-oxo-dG) (see structure shown below) (18).

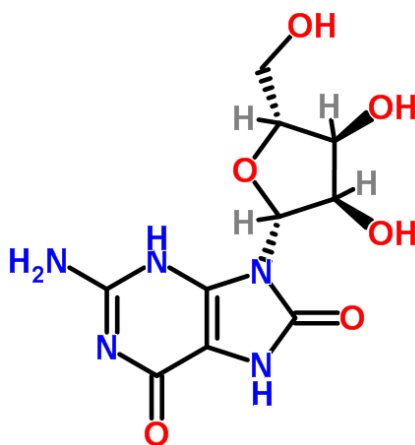


Figure 2. Structure of 8-oxo-7,8-dihydroguanosine

There are three unique mechanisms of cell death, which are apoptosis, necrosis, and autophagy. The process of apoptosis is characterized by cellular shrinkage,

condensation of chromatin, and fragmentation of the cell into membrane-bound bodies that can be eliminated by phagocytosis. Apoptosis is also termed programmed cell death. Necrosis refers to the morphological changes which indicate cell death that are caused by progressive enzymatic degradation. Autophagy refers to the process of digestion of the cytoplasmic material of the cell by lysosomes (19). Whether cell death occurs by apoptosis or necrosis depends upon two factors, which are: localization of the PS within the cell; and amount of  $^1\text{O}_2$  produced (12). Some evidence suggests that a PS localized in the mitochondria or endoplasmic reticulum is better at inducing apoptosis, whereas a PS localized in the plasma membrane or lysosomes is more conducive to necrosis (4). Photodynamic therapy can also cause local inflammation, which produces an immune response against cancer cells (20).

In addition to the overall mechanism of cellular oxidation that results from PDT, there are secondary processes that occur after the light illumination ceases which must be considered. Singlet oxygen also produces secondary reactive oxygen species (ROS) and these species play a role in the whole photodynamic effect. The various pathways to generating secondary ROS can have postillumination effects in PDT. Products of the initial generation of  $^1\text{O}_2$  can initiate further oxidation reactions. For example, membrane lipid hydroperoxides, which are relatively unstable, can be broken down to form free radicals that cause further chain peroxidation. These reactions can seriously impact the cell. Damage to mitochondria can lead to a loss of function and an uncoupling of

electron transport in oxidative phosphorylation. The subsequent leakage of electrons can generate  $O_2^-$ , and then hydrogen peroxide ( $H_2O_2$ ) in the presence of the antioxidant enzyme superoxide dismutase (SOD). The primary photodynamic reactions often lead to increases in intracellular calcium ( $Ca^{2+}$ ), which acts as a signaling event. Other oxidative pathways which can be initiated include activation of phospholipase A2, lipoxygenase (LOX), and cyclooxygenase (COX) enzymes in response to oxidation of membranes and  $Ca^{2+}$  increases. These pathways can increase the level of peroxide in the cell and the overall oxidative stress (21). Activation of NADPH oxidase (NOX) is another enzymatic process that can contribute to delayed oxidative damage. The NOX enzyme accepts an electron from an intracellular flavin donor and transfers the electron to molecular oxygen to form  $O_2^-$ , which can then be converted to  $H_2O_2$  by SOD catalysis and reaction with protons (22). These secondary processes can extend the spatial range of photodynamic action in cells (23). The diffusion distance of an ROS is inversely proportional to its lifetime in a given environment, with the lifetime dependent on its reactivity. The highly reactive hydroxyl radical ( $HO^\cdot$ ) and other  $\alpha$ -oxyl radicals ( $RO^\cdot$ ) will not travel far from the site where they were generated. However, less reactive species like lipid hydroperoxides (LOOH),  $H_2O_2$ , peroxy radicals ( $ROO^\cdot$ ) and carbon radicals ( $C^\cdot$ ) can have effects at more distant sites and be delayed in time with respect to their shorter-lived relatives (21). Oxidative stress caused by secondary ROS can also lead to effects at the extracellular level. There is a bystander effect, which describes the generation of



effects in cells that were not exposed to a primary insult, but are in close proximity to cells that were (24). Less reactive secondary ROS such as  $\text{H}_2\text{O}_2$  and LOOH may be candidates for mediating bystander responses in cells and tissues exposed to photodynamic treatment (11).

For Type II photochemical reactions, ground state molecular oxygen ( $^3\text{O}_2$ ) is necessary. Conditions such as anoxia or hypoxia have potential to arise if tumors are not well oxygenated, and in these cases Type I mechanisms can predominate. In an anoxic situation, the excited PS singlet state transfers its energy to substrates by oxidation of the substrate, thereby transferring the PS to the triplet state. During a hypoxic condition, the triplet state PS interacts with  $^3\text{O}_2$  to produce superoxide anions and highly reactive  $\text{HO}^\cdot$  (25, 26).

### **Role of Oxygen in Photodynamic Therapy**

The generation of  $^1\text{O}_2$  (Type II reaction) is the primary mechanism activated in PDT (25), and PDT has been found to be inefficient in cases of anoxia (27-29). There are several other routes that oxygen has to influence the outcome of PDT. The formation of  $^1\text{O}_2$  depends on the collision of an excited photosensitizer (usually in the triplet state) and an oxygen molecule in the ground state. The quantum yield of  $^1\text{O}_2$  is dependent upon three factors: 1) quantum yield of triplet state PS (usually 0.2 – 0.9) (30), 2) influence of quenchers which can react with the PS before they collide with molecular oxygen, 3) yield of  $^1\text{O}_2$  per collision. Factors 2 and 3 do not play a significant role, since the yield of  $^1\text{O}_2$  is not much smaller than the yield of triplet state PS and is about 0.2 to 0.7 (31-

35). Once  $^1\text{O}_2$  is formed in cells or extracellular fluid, it can react with quenchers before it reaches the biological target. The lifetime of  $^1\text{O}_2$  in cells and the diffusion length are critical (36). Fluorescence quenching experiments have determined the lifetime of  $^1\text{O}_2$  ( $^1\Delta_g$ ) in tissues to be 10 to 40 ns and the diffusion length to be 10 – 20 nm (37). Because the singlet oxygen diffusion length and the triplet PS diffusion length are both so short, the PDT induced cell and tissue damage occurs in the place where the PS concentration is the highest (23, 38, 39). The following cellular targets of PDT have been identified, and include: all membranes, mitochondria, lysosomes (38, 40), endoplasmic reticulum (38), and Golgi complex (41). Experimentation has proven that almost no photosensitizers localize in the nucleus; therefore, PDT causes little damage to DNA and few chromosomal changes, which indicates a low carcinogenic potential (41-52). Since the lifetime of the PS in the triplet state is longer than 10  $\mu\text{s}$  (53, 54), it is long enough for the triplet excited state to react with oxygen to form  $^1\text{O}_2$ . The action of the PS is very dependent on the oxygen concentration for PDT to be effective. Experiments were done to measure the importance of oxygen concentration on the formation of  $^1\text{O}_2$ ; and production of  $^1\text{O}_2$  was found to be effective at oxygen levels of 100 % to 5 %, but was halved at oxygen levels of 1 % (25). PDT is unable to kill cells in hypoxic tumor regions. Also, pressure against a superficial tumor can diminish blood perfusion and oxygen concentration to render PDT ineffective (55, 56).

Most normal tissues contain approximately 5 % oxygen, which is supplied by the blood circulation, and since tumor areas are often poorly vascularized, the oxygen concentration can be much lower (57, 58). Hypoxic tumors can be made more vulnerable to PDT by increasing the oxygen tension, and several methods have been proposed: 1) breathing hyperbaric oxygen, 2) breathing using oxygen-carrying fluorocarbons combined with carbogen made of 95 % O<sub>2</sub> (carbogen is a mixture of CO<sub>2</sub> and O<sub>2</sub> gases ranging from 1.5 – 50 % CO<sub>2</sub>), 3) using nicotinamide injection and carbogen breathing, 4) using oxygen releasing substances, 5) modulating the oxygen binding capacity of hemoglobin (Hb), 6) decreasing the respiration rate, 7) increasing the oxygen solubility, 8) using blood flow modifiers, and 9) destroying hypoxic cells with bioreductive drugs or hypothermia (59). Tumor hypothermia can be advantageous because the oxygen binding by Hb will increase (the Bohr effect), and the metabolic activity will decrease (60-63). The Bohr effect refers to the dissociation of a proton when Hb binds to O<sub>2</sub>. When Hb is in the conformation known as the R state (relaxed), the Hb has a greater affinity for O<sub>2</sub>. In a hypothermic state, O<sub>2</sub> does not need to be given off to the tissues since metabolism will be slowed; therefore, the O<sub>2</sub> can stay bound to the Hb molecule (64). Since the result of PDT is photooxidation, one oxygen molecule is consumed for every <sup>1</sup>O<sub>2</sub> molecule that reacts with and oxidizes another molecule (65). Experiments in the clinical setting have shown that PDT with Photofrin at fluence rates larger than 100 mW / cm<sup>2</sup> leads to oxygen depletion (66-68). Secondary reactions of PDT are due to vascular

damage (69-77). The time for vessel damage is dependent on tissue type (80, 81), PS hydrophilicity (hydrophilic photosensitizers give more vascular damage than lipophilic ones) (79), and on the time between PS application and light exposure (80) (short time leads to more vascular damage because of larger PS concentrations in blood) (78, 81). A mild erythema, an indicator of invasion of inflammatory cells or release of vasoactive substances, can occur after PDT (69, 71, 82-85). This process leads to an increase in blood flow and temperature (86-89), which leads to higher oxygen concentrations in the treated tissue (67, 87). Fluence rates of light delivery will effect oxygen depletion. At high fluence rates, primary oxygen depletion will occur quickly and lead to a low PDT efficiency (66-68, 90). At low fluence rates, long exposure times are required, and vessel damage (vasoconstriction and thrombosis) can occur which will reduce the effectiveness of PDT (67, 90, 91). Intermediate fluence rates ( $\sim 30 \text{ mW} / \text{cm}^2$ ) may give better results since they avoid primary oxygen depletion while still giving complete tumor destruction before the introduction of vascular effects (67, 92-94). Following light exposure, however, vascular effects have been shown to contribute greatly to tumor destruction (74).

### **Importance of Light Dosimetry and Types of Light Sources for PDT**

Light dosimetry is also a critical factor to consider to determine the efficiency of PDT treatment. Light dosimetry involves two parameters, which are fluence and fluence rate. Fluence refers to the total energy of exposed light across a sectional area which has been irradiated (the energy per unit area of

exposed light,  $\text{J} / \text{m}^2$ ). Fluence rate refers to the radiant energy incident per second across a sectional area which has been irradiated (power per unit area of light,  $\text{J} / \text{s} / \text{m}^2$  or  $\text{W} / \text{m}^2$ ;  $1 \text{ W} = 1 \text{ J} / \text{s}$ ). As the fluence rate lowers, the time of exposure gets longer so that the same fluence (dose) of light is provided. High fluence rates are typically used to reduce treatment time. However, reports have demonstrated that high fluence rate may not elicit an optimal effect on the patient (9). It has been reported by Wilson *et al.* that in conditions of high fluence rates, oxygen depletion can occur, which results in a reduced photodynamic effect, since there is not an effective production of cytotoxic species. Studies are ongoing in several laboratories to develop oxygen diffusion models in which lower fluence rates generate  $^1\text{O}_2$  more efficiently so that more  $^1\text{O}_2$  is exposed to the tumor for longer time periods (95).

Lasers are most frequently used for PDT. Lasers produce coherent monochromatic light which can be focused and passed down through an optical fiber and delivered directly to the target tissue. Earlier laser systems were bulky, expensive, and fit only for laboratory research purposes; but modern diode lasers are portable, lightweight, and much less expensive (9). Light emitting diodes (LEDs) can also be used for PDT, and they have narrow spectral bandwidths and high fluence rates (96, 97). Inflatable balloons which are covered on the interior with a strongly scattering material and formed to fit an organ are also available for treatment using PDT (98). Light sources may also be implanted in solid organs deep in the body under image guidance (19). The efficacy of PDT

depends upon the depth of light penetration through tissue. The light penetration is also dependent upon the optical properties of the tissue and depending on the tissue type, light may be reflected, scattered, absorbed, or transmitted. Tissues rich in pigment, such as melanoma, are resistant to PDT. The depth of tissue penetration is also affected by the wavelength of light, as both absorption and scattering of light by tissue increases as the wavelength decreases. For example, light with wavelengths shorter than 580 nm is unsuitable due to a strong absorption by hemoglobin. The depth of light penetration is approximately 3 – 8 mm for light in the wavelength range from 630 – 800 nm (99).

### **Characteristics of a Good Photosensitizer**

The ideal photosensitizer should fulfill the following requirements: 1) Singlet oxygen is the key cytotoxic agent in tumor destruction; therefore, the PS must produce  $^1\text{O}_2$  efficiently. 2) The PS should have no dark toxicity and selectively accumulate in tumor tissue to minimize skin photosensitivity (9). 3) It should be amphiphilic, water soluble with a hydrophobic matrix to facilitate the crossing of cell membranes. 4) A limited *in vivo* stability is preferred so that rapid removal from tissues is possible. 5) The PS should absorb in the red to near IR region of the electromagnetic spectrum in order to increase the depth of penetration into tissues. 6) It should have a high extinction coefficient to increase the number of photons of light absorbed. 7) The absorption of the PS should not overlap absorption bands of other chromophores present in tissue such as Hb, melanin, DNA, RNA, *etc* (33). 8) The PS should be stable and easy to dissolve in

injectable solvents. 9) It should be pure and prepared by a relatively straightforward synthetic technique to give high yield in order to minimize the cost of production as well as cost to the patient (9).

### **Historical Uses of Phototherapy**

Phototherapy involves the use of visible light or light of wavelengths near the visible region to treat disease. The process involves electronic transitions which lead to photochemical reactions, which subsequently may be followed by dark reactions of the initial products. There are two broad categories of phototherapy: direct and indirect. In direct phototherapy, no drug is administered. An effect will be observed if light is absorbed by molecules already present in the organism. In indirect phototherapy, a light sensitive chemical (a PS) is administered prior to irradiation. Another term to describe this reaction is photochemotherapy. Light is absorbed by the PS, which initiates the therapeutic process. The benefits of sunlight on bone growth and for treatment of other various human maladies was known as far back as 460 BC (*100, p. 3*). However, the introduction of phototherapy which utilized scientific methods is credited to Niels Rydberg Finsen, who is generally regarded as the father of the subject. Finsen carried out experiments on the effects of different colored light on animals. He advocated the use of red light for the amelioration of scarring in cases of smallpox. He found that sunlight, or, even better, light generated from a carbon arc that was filtered to eliminate infrared light, could be used to treat and cure *lupus vulgaris*, a tubercular condition of the skin. A symptom of this

condition was the development of reddish brown plaques, especially on the face. Finsen received a Nobel Prize in Physiology-Medicine in 1903 for his work in phototherapy (101). Interest in phototherapy became stagnant between the two World Wars, however, the process has seen a revival over more recent decades. Four main areas of treatment are the following: Vitamin D and rickets, psoriasis, newborn jaundice, and tumors (100, p. 4).

Vitamin D is responsible for calcium and phosphate absorption and metabolism in the deposition of bone and in bone maintenance. A Vitamin D deficiency is known as rickets when used to describe the condition during childhood, and osteomalacia when used to describe the condition during adulthood (most often elderly persons) (100, p. 4). This disease could be prevented by incorporating fish oil into the diet or by exposing the skin to sunlight. Experiments with animals fed a diet deficient in calcium and phosphate showed that irradiation of the food supply followed by direct irradiation with ultraviolet light had a curative effect. In 1978, Jung and colleagues treated adults with osteomalacia, who had poor absorption of Vitamin D, with short exposures of ultraviolet light. Whole body treatment had a marked beneficial effect, which led to a rapid rise in the concentration of 25-hydroxyvitamin D<sub>3</sub> in the plasma. A negative effect of this treatment is that the substrates for this photochemical process have absorption maxima (ca. 280 – 300 nm) with wavelengths close to where the purine and pyrimidine bases of DNA absorb. This creates the potential for a carcinogenic effect of radiation in this region (UV-B and UV-C) (100, p. 6).



Various skin diseases have been treated with plant extracts known to contain furocoumarins (psoralens). In India, for example, extracts of *Psoralea corylifolia* were given orally, followed by sunlight exposure, to treat *vitiligo*, a disorder of the skin which is associated with the loss of pigmentation (100, p. 6). In 1974, Parrish and colleagues found that oral administration of 8-methoxypsoralen, followed by exposure to ultraviolet light in the 320 – 400 nm range could be used as a treatment modality for psoriasis. Since a PS was required, this treatment is known as indirect sensitized phototherapy, or photochemotherapy. The 320 – 400 nm region is known as the UV-A region; therefore, this treatment is called PUVA (psoralen + UVA) (102).

Bilirubin is a linear tetrapyrrole, which is formed as a product of the breakdown of the heme from hemoglobin. After about 3 months, the red blood cells are worn out and begin to leak, and are subsequently destroyed and replaced. The heme in the red blood cells is oxidatively opened to yield carbon monoxide and biliverdin (a blue green substance). The biliverdin is reduced to bilirubin (an orange yellow compound which is the chromophore of jaundice). Bilirubin is insoluble in water and must be enzymatically converted to bilirubin D-glucuronide so that it can be solubilized in water, secreted in the bile, and passed out of the body (100, p. 7). An enzyme known as uridine diphosphoglucuronyl transferase allows the bilirubin to be conjugated to D-glucuronic acid to yield the product bilirubin D-glucuronide. In newborns, this conjugation is sometimes impaired, resulting in bilirubin remaining in circulation.

The skin of the infant becomes yellow (jaundiced) due to bilirubin (*100, p. 8*).

Phototherapy of jaundiced infants came about rather serendipitously. In 1956, a charge nurse in England noticed that when the skin of a newborn was exposed to sunlight, it became less yellow as compared to the skin that was covered. It was discovered that bilirubin levels were reduced after exposure of the jaundiced skin to sunlight. Since sunlight was sporadic in England, a controlled source was used to irradiate the skin of the newborns. Again, it was found that bilirubin levels dropped following exposure to irradiation. These findings represented the first scientific demonstration of the phototherapy of neonatal hyperbilirubinemia. Today, the phototherapy of neonatal hyperbilirubinemia using white light or blue-enriched white light emitted by fluorescent lamps is a standard procedure in pediatric units worldwide (*103*).

### **First Generation Photosensitizers**

The phototherapy of cancer is termed PDT, because the three requirements of light, a PS, and oxygen must be met. In 1903, Jesionek and von Tappeiner from Munich reported results from experiments in which tumors had been treated topically with eosin, and then exposed to visible light. Two years later, these scientists reported an extension of their work in which various sensitizers and sunlight and an arc lamp were utilized. The sensitizer was applied at or near the surface in patients with basal cell carcinoma, and the results were promising. In 1924, Policard and Lyons observed a natural porphyrin fluorescence in experimental tumors, which is indicative of an association

between porphyrins and cancer tissue (100, p. 9). In 1942, Auler and Banzer injected tumor bearing animals with Photodyn (a hematoporphyrin), followed by irradiation with a powerful quartz lamp. These animals showed necrosis, fluorescence, and cellular softening of the tumors (104). In 1961, Lipson and colleagues introduced a preparation called "Haematoporphyrin Derivative" (HpD), which was shown to be somewhat selectively localized in tumor tissue. When irradiated with 366 nm light, the tumor was able to be visualized by its red fluorescence emission. HpD was investigated for 10 years as a diagnostic agent for cancer. Eventually, it was realized that by changing the irradiation conditions, the tumor could be identified by its red fluorescence, and then subsequently undergo photodegradation. In 1972, Diamond and his colleagues reported the photodegradation of glioma implants in the rat after administration of HpD. In 1974, Dougherty discovered that intraperitoneal administration of fluorescein reduced the growth rate of mammary tumor implants in irradiated animals (100, p. 10). The first photodynamic experiment in humans was published by Kelly and Snell in London in 1976. These scientists found that HpD could be used to aid the diagnosis and treatment of bladder cancer (105). In 1993, Photofrin was the first PDT drug to be approved by Canadian authorities to treat human superficial papillary bladder cancer. Photofrin was originally derived from HpD. Additional approvals of Photofrin for limited applications have been made in other countries (100, p. 11). HpD and Photofrin, which was derived from HpD, are known as first generation photosensitizers. The advantages of first generation photosensitizers

include: 1) Material is synthesized from readily available starting materials by a simple procedure. 2) Extensive clinical activity has been demonstrated repeatedly. 3) This material was the first preparation known to show effectiveness in PDT. 4) It was the first substance to receive regulatory approval (initially in Canada in 1993, and subsequently in several other countries). The disadvantages of these photosensitizers include: 1) The compound is a very complex mixture, with positional and stereoisomerism, and also contains inter-porphyrin linkages. As a result, the composition of this mixture is difficult to reproduce; the relationship of the clinical response to the molecular structure is almost impossible to predict. 2) HpD is active in PDT for treating cancer, but its activity is very modest. 3) Selectivity is poor, since sensitivity to light of normal tissue (skin, in particular) remains for weeks following treatment. 4) HpD has a spectrum at which the absorption band at lowest energy ( $\lambda_{\max} = 630 \text{ nm}$ ) has the weakest absorption (*100, p. 129*). Irradiation is done at this wavelength since transmittance through tissue is highest in the red region of the spectrum. Substances with low molar absorptivity in this region will require higher PS doses or higher doses of light (or both) in order to generate an adequate level of excited PS with subsequent production of  $^1\text{O}_2$  (*100, p. 130*).

### **Second Generation Photosensitizers**

More recently, there has been development of more powerful and specific tumor photosensitizers known as second generation sensitizers (*100, p. 129*). Verteporfin is a PS that is a benzoporphyrin derivative (*106*). This PS is activated

at 690 nm, which allows for deeper tissue penetration. This drug is cleared rapidly from the body so that skin photosensitivity is minimized (107). Treatment occurs within 15 – 30 minutes after injection, and clinical response is based on vascular disruption and shutdown (108, 109). Verteporfin has been used to treat age related macular degeneration (AMD), which is the leading cause of blindness. The pathophysiology of this disease is based on the hemorrhaging of neovascular vessels which destroys the choroids of the eye. The drug is administered at doses of 6 mg / kg via I.V. injection, and light of 100 J / cm<sup>2</sup> illumination is applied to the leaky eye vessels within 30 minutes of infusion. In most cases, neovascular occlusion occurs and visual loss is curtailed in 80 % of patients (110). Verteporfin has also been used to treat choroidal melanoma with the same dosage and amount of light used for macular degeneration (111, 112).

Texaphyrins are synthetic expanded porphyrins, and they have been used for many years to enhance imaging for magnetic resonance imaging (MRI) (113-115). The PS Lutetium texaphyrin is sold under the trade names of Lu-tex or Optrin for cutaneous formulations, and Antrin for vascular formulations (cardiac, peripheral, and ophthalmic). This PS is water soluble, and is activated at 730 nm, which allows for deeper light penetration. Lutetium binds well to low density lipoproteins, which means that it may be useful against arteriosclerotic plaque (116). The texaphyrin photosensitizers fluoresce at 750 nm which could allow their use to improve localization and dosimetry of PDT (117).

Foscan, a member of the chlorin family of photosensitizers, has been used

for a variety of cutaneous lesions (118-120), as well as pulmonary (121, 122-126), esophageal (127, 128), and head and neck tumors (129-135). The drug dosage is 0.15 mg / kg, which is lower than with Photofrin (one of the first generation photosensitizers). The patient is irradiated 4 days following injection, and the drug activates at 660 nm, which gives it a greater depth of penetration (136).

m-Tetrahydroxyphenylchlorin (m-THPC), which is used for head and neck tumors, is highly efficient in converting light so that only 20 J / cm<sup>2</sup> is needed. This allows for rapid treatment, lasting for a few minutes; however, the drawback is that significant pain can be experienced during the procedure. Also, this PS is so efficient, and time of treatment is so short, that patient movement (from breathing, for example) can move the treatment field, which can result in under dosage to the tumor tissue, and over dosage to normal tissue. Since significant reflection can occur in mucosal regions, scattering of the light can be a problem. Care must also be taken to cover all regions that are not intended to be illuminated. The potential for improper illumination as well as light scattering is always present, and it is easy to make a treatment mistake given the efficient nature of this PS and the short time needed to create a PDT reaction. Excellent outcomes have been achieved for cutaneous squamous cell and basal cell lesions, head and neck lesions, and lung and esophageal lesions, provided that the appropriate blocking of light to normal tissues is achieved (136).

Purlytin, chemically known as tin-ethyl-etiopurpurin (SnET2), is a product

of the degradation of chlorophyll (137). This drug is also categorized as a chlorin. Although the drug is synthetic and pure, it has poor stability in water, so it must be carefully formulated. This drug is activated at 660 nm, which will allow for good depth of penetration. A drawback is that the agent used as a carrier creates an egg based allergic reaction. Therefore, patients with egg allergies cannot be infused with this drug. This drug has been shown to be effective in the treatment of basal cell, squamous cell, chest wall metastasis, and Kaposi sarcoma (138-141).

Another product of the chlorin family is NPe6, which is mono-L-aspartyl chlorin e6. This chlorin has been involved in Phase 1 clinical trials on cutaneous lesions (142-144). Tumor control was not achieved with drug doses below 1.6 mg / kg; however, at doses between 2.5 and 3.5 mg / kg, the majority of tumorous lesions were resolved. Studies of this drug revealed that light doses of  $100 \text{ J / cm}^2$  at 664 nm given 4 h after drug infusion were favorable. There was no tissue selectivity achieved at drug doses of 1.6 mg / kg or greater, which limits the use of this drug in clinical situations. A potential use for NPe6, however, could exist for ophthalmic lesions (145).

HPPH [chemically known as 2-(1-hexyloxyethyl)-2-devinyl pyropheophorbide-a], also known as Photochlor, is a chlorin based photosensitizer (146). This PS is active at 665 nm and has been used successfully to treat naturally occurring tumors in dogs and cats (147, 148). The drug is introduced intravenously and is effective at a concentration of 0.15 mg /

kg (6 mg / m<sup>2</sup>) and a light dose of 150 J / cm<sup>2</sup> at 665 nm administered after 48 h post drug exposure. Eight of eight patients with esophageal cancer achieved an excellent response. Other types of cancers that were treated successfully with Photochlor are basal cell, Barrett's esophageal, and endobronchial recurrence from lung cancer. Photosensitivity of patients to sunlight for several days after injection appears to be dose dependent (149).

Most of the activity of photosensitizers in the dye family come from phthalocyanines and related compounds such as naphthocyanines (150). These structures require activation at 100 J / cm<sup>2</sup> at wavelengths in the 650 – 850 nm range. Most of the dyes are hydrophobic and require delivery agents for clinical use. Dyes have been linked to a variety of metals, which has increased their efficacy. The best PDT activity appears to be with the use of aluminum, zinc, and silicon (151). Although dyes are of interest in PDT, there has been limited published clinical literature in existence. Aluminum phthalocyanine tetrasulfate has had an excellent response in the treatment of naturally occurring tumors in cats (152). This dye and others allowed for fluorescence that could enhance treatment by imaging cancerous tissues (153). Photosens, which is a sulfonated aluminum phthalocyanine has been used for cutaneous and endobronchial lesions to treat malignancy and infection. This photosensitizer has been formulated to allow for delivery via aerosol, direct injection into lesions, and intravenous delivery (154). Photosens has successfully treated head and neck tumors, including lip, pharynx, larynx, and tongue (155, 156). Tumors that failed



with initial therapy often were successfully treated after two PDT sessions. Complete response was reported about 60 % of the time (157).

### **Third Generation Photosensitizers**

Third generation photosensitizers not only have improved activity and selectivity, but also contain a system which allows the targeting of the PS to a receptor on the cancer cell (100, p. 129). When administered into the bloodstream, most drugs will associate with serum proteins, including high and low density lipoproteins (HDLs; LDLs) and albumin. The exact type of interaction depends upon the characteristics of the drug and the serum protein involved. Various methods of interaction include hydrogen bonding, van der Waals forces,  $\pi$  bond stacking, hydrophobic interactions, and ion pairing. Serum proteins are mainly responsible for the transport of photosensitizers throughout the body. Improved photodynamic action can be accomplished with the *in situ* generation of these carrier systems, as they may lead to enhanced intracellular dye accumulation via receptor-mediated endocytosis with improved targeting (158).

Albumin is the most abundant human serum protein, and is approximately 10 times more concentrated than the total concentration of all lipoproteins (159). Serum albumin has a unique capability to bind a large number of endogenous and exogenous compounds, either covalently or reversibly, and with high affinity (160). Initial studies utilizing serum albumin as a targeting substance involved non-covalent binding of Zinc phthalocyanine (ZnPc) into bovine serum albumin (BSA) prior to intravenous administration (161). EMT-6 mouse mammary tumors

on Balb/c mice and T380 human colon carcinomas on nude mice showed tumor regression with no liver toxicity using the ZnPc – BSA conjugate (162). Studies have been undertaken to covalently bond several different photosensitizers to BSA. Physically altered albumin is targeted by scavenger receptors which are over-expressed on macrophages. The scavenger receptors are able to bind many different ligands and transport them to endosomal and lysosomal cellular compartments (163). Since over 50 % of tumor mass is of macrophage lineage in several cancers, photosensitizers can be targeted to tumor volume (164). It has been observed that higher levels of PS accumulate in tumor-associated macrophages as compared to neighboring tumor cells, with a 9 fold increase observed with porphyrin photosensitizers (165).

Hamblin and Newman covalently coupled hematoporphyrin (HP) to BSA to yield monomeric and cross-linked conjugates. Singlet oxygen quantum yields were comparable to those of free porphyrins. In NIH 3T3 fibroblast cells and HT29 tumor cells, native albumin did not compete with the uptake of HP-BSA conjugate. Most likely, the HP-BSA was associated with the plasma membrane of these cells (165). Maleylated BSA (synthesized by reaction with maleic anhydride) has also been investigated as a possible PS target agent (166). The maleylated BSA-phthalocyanine complex conjugate showed a greater affinity for the scavenger receptor compared to BSA-Pc. This complex exhibited increased uptake and higher photodynamic efficiency in the macrophage-like J774 cells (158). Chlorin e6 (Ce6) was also studied by covalently attaching it to BSA and

further modifying the BSA by maleylation (167, 168). These photosensitizers displayed increased uptake and higher photodynamic activity in J774 cells. *In vivo* studies showed that the mal-BSA-Ce6 had a significant effect on tumor growth delay and reduction of tumor growth in scavenger receptor negative EMT-6 tumors (158).

Lipoproteins have also been used as targets for photosensitizers. A lipoprotein is a particle with a central core of hydrophobic lipids surrounded by hydrophilic polar lipids and apoproteins. These particles have two functions: solubilization of highly hydrophobic lipids which allows transport throughout the body, and signaling to regulate the movement of the particular lipid into and out of specific tissues (158). The most important lipoprotein in terms of drug delivery is LDL. LDLs are the major carriers of cholesterol in the blood (169). The outer shell of LDLs contains a single copy of the large B-100 apolipoprotein which is responsible for recognition and binding by the LDL receptor and leads to receptor-mediated endocytosis of the LDL particle. Cholesterol is a key component of all eukaryotic cell membranes and is necessary for growth of cells; therefore, tumor cells and tumor vascular endothelial cells overexpress the LDL receptor due to either increased proliferation or increased membrane turnover (170). LDL can then become a good target for drug delivery. Another advantage of using LDL during PDT, is that following irradiation, the LDLs will become highly oxidized. These oxidized products are cytotoxic towards endothelial cells, which further extends the effect of photodynamic action (171). To investigate the role of

the LDL receptor, the amphiphilic HP and hydrophobic ZnPc were bound to human LDL (172). Using human HT1080 fibroblasts, HP-LDL complex accumulated on the LDL receptors, but the ZnPc-LDL complex was internalized through non-specific endocytosis. The complexation of the LDL with the phthalocyanine resulted in changes in the apolipoprotein B structure on the LDL, which accounts for the lack of LDL receptor affinity with the ZnPc-LDL complex (173). Incorporation into LDLs enhances the PDT efficiency of most photosensitizers (174). Conjugates of HP and LDL exhibited increased uptake in NIH 3T3 cells (175) and the HP-LDL complex was also taken up by J774.2 macrophages (158). Ce6 has also been covalently bound to LDL via a carbodiimide and the LDL-Ce6 complexes were compared to free Ce6 and Ce6 complexed non-covalently to LDL with a fibroblast and retinoblastoma cell line (176). The covalent bonding of Ce6 to LDL increased uptake significantly in both cell lines (158).

All rapidly dividing cells require a continuous influx of iron for cell division, and transferrin is the major circulating iron transport protein (177). Cells express transferrin receptors, which allows for binding and internalization of the iron saturated transferrin, with subsequent delivery of iron to the necessary sites in the cell (178, 179). Many types of cancers exhibit over-expression of transferrin receptors. Also, the expression of the transferrin receptor is correlated with tumor grade, stage, progression, and metastasis (178). Transferrin has potential for transporting photosensitizers to cancer cells (180). In one study, transferrin was

covalently coupled to HP using the N-hydroxysuccinimide (NHS) ester of HP (165), and the conjugate was found to have similar  $^1\text{O}_2$  quantum yields. The uptake of HP-transferrin in NIH 3T3 and HT29 cells was shown to be receptor-mediated (158). Transferrin was also covalently bonded to Ce6 (181, 182), and the resulting complex had a  $^1\text{O}_2$  quantum yield of approximately 70 % of that of the free Ce6. During *in vitro* studies with MTLn3 rat mammary adenocarcinoma cells, the transferrin-Ce6 conjugate was 10 – 40 times more photocytotoxic than the free Ce6 (158).

The human skeleton is continually being built and destroyed (183), and the physiological balance is maintained by osteoclasts (mediate bone resorption) and osteoblasts (mediate new bone formation)(184, 185). Enhanced bone resorption is typical of many metabolic bone disorders, including malignant hypercalcemia and bone metastases (186). It has been proposed that PDT may be useful for treatment of these conditions by selectively destroying osteoclasts. Bisphosphonates have been proposed as the PDT targeting agents (187). Bisphosphonates bind to hydroxyapatite crystals in bone matrix and inhibit osteoclast recruitment and function (186, 188). In addition, bisphosphonates stimulate osteoblasts to produce inhibitors of osteoclast function, while avoiding degradation by cellular enzymes. The following photosensitizers have been proposed as potential for targeting to bisphosphonate in PDT: indocyanine green, methylene blue, chlorins, phthalocyanines, porphyrins, purpurins, and texaphyrins (187).

Germanium phthalocyanine (GePc) with two cholesterol moieties bound to the germanium central metal atom has been synthesized. The cholesterol molecules are bound via a diphenylsilanediol (189). The overall amphiphilicity of the molecule is altered by the length of the spacer chain between the cholesterol and the silane. The quantum yield of  $^1\text{O}_2$  for these conjugates was quite good in organic solvents (190).

Steroids are also useful as an ancillary therapy to PDT. For example, 2-methoxyestradiol potentiates the anti-tumor effects of PDT (191). When 2-methoxyestradiol was incubated with five human tumor cell lines prior to PDT, a synergistic anti-tumor effect was seen. When this combination therapy was used *in vivo*, retardation of tumor growth and prolonged survival of tumor-bearing mice was observed. In another study, the photodynamic efficiency of HP derivatives was potentiated when glucocorticoids were administered following irradiation (192). Steroids and other hormones can deliver the photosensitizer to the nucleus, which is one of the most photosensitive sites in the cell. Estrogens, androgens, progesterone, mineralocorticosteroids, glucocorticosteroids, thyroid hormones, retinoic acid, vitamin D and ecdysone bind with high affinity to specific members of the nuclear hormone receptor superfamily (193). The members of this family of receptors have both a ligand binding domain and a DNA binding domain (194). Since the DNA binding domain varies for the various members of this family of receptors, the family is divided into two subgroups (195). The steroid receptor family (except the estrogen receptor) are distributed in the

cytoplasm in the absence of ligand (196). When the ligand diffuses through the plasma membrane and binds to the ligand binding site, the receptors undergo a conformational change and are trafficked to the nucleus where they target sequences of DNA. The estrogen receptor, however, is found exclusively in the nucleus. Nuclear receptors will attract and selectively localize their ligands into cells where these receptors are expressed. These ligands are important for targeting these cells with photosensitizers and other drugs (158). The estrogen receptor binds estradiol, estriol, estrone, and synthetic estrogen agonists / antagonists. Breast tumors are known to over-express estrogen receptors in high levels (197-199), which makes these receptors excellent sites for directing photosensitizers to both increase cellular uptake and to deliver the dye to the nucleus of the cell. Several attempts have been made to covalently attach estrogen and other hormone receptor ligands to photosensitizers (200, 201). The major problem, however, with the PS-steroid conjugate is the decrease or loss of receptor recognition, which is why it is essential to identify positions on the parent steroid where a PS can be attached without compromising receptor binding (202-205). Experiments with Ce6 to improve photocytotoxicity of hormone PS conjugates were completed with Ce6 attached to estradiol (206). Binding to the receptor was poorer than with estradiol alone; however, these conjugates were photoactive against estrogen receptor-positive MCF-7 breast cancer cells. Additional conjugates were prepared using 4-hydroxytamoxifen, an anti-estrogen that binds to the estrogen receptor. When the conjugate was

covalently bound to Ce6, estrogen receptor binding was still observed, but only in a small amount. The MCF-7 breast cancer cells were killed upon light irradiation, which demonstrates that the tamoxifen conjugates were photoactive (207).

### **Folate Targeted Cancer Therapy**

The strategy behind targeting therapy involves using a ligand that binds specifically to a receptor that is expressed to a greater degree on tumor cells relative to normal cells. When the ligand (folate) is linked to a therapeutic drug, the drug can be carried specifically into the cancer cell (208). Some of the advantages and disadvantages of ligand targeted therapies will now be discussed. Ligand targeted therapies are remarkably flexible and adaptable. Most potent drugs can be targeted to tumor tissue if the drug can be linked reversibly to a targeting ligand that is specific for a pathologic cell type. Also, an imaging agent can almost always be synthesized using the identical targeting ligand. This imaging agent can then be used to select for patients with tumors that overexpress the ligand's receptor (209, 210). Ligand targeted therapies are preferred for delivery of drugs which are membrane impermeable because the targeting ligand can deliver the drug via receptor mediated endocytosis, which increases the efficacy of the drug (211, 212). There are also some disadvantages to ligand targeted therapies, which will now be discussed. Most endocytic pathways transport few molecules into a cell, which requires the ligand targeted drugs to be effective at low concentrations. Delivery to the cancer site does not guarantee efficacy, since the drug must be released within the cell as well as



being internalized within the cell. Drugs must contain a limited number of chemical moieties ( $-\text{SH}$ ,  $-\text{COOH}$ ,  $-\text{OH}$ , or  $-\text{NH}_2$ ), because only a few functional groups allow for facile release of a covalently attached drug after targeted cell uptake (213, 214). Also, an efficient drug release mechanism must be part of the drug conjugate – one that is inert during transport to the cancer cell, but is activated after target cell binding and internalization to insure drug release only at the disease site. Finally, for some membrane impermeable drugs, following receptor mediated endocytosis, the drug will still need to pass through the endosomal membrane to reach its target within the cancer cell (211).

### **Folate Receptor Expression Patterns**

Folic acid is a vitamin needed for the proliferation and maintenance of all cells. Folate is needed for the synthesis, repair, and functioning of DNA. Deficiencies of folate may result in DNA damage which can lead to cancer. Folate is especially important for cells and tissues undergoing rapid division; therefore, cancer cells overexpress folate receptors (FRs) to ensure that they obtain an adequate supply. This FR overexpression, as well as the high affinity recognition by the receptor ligand binding, has meant that FRs have become popular tumor targets by conjugating folic acid to anticancer molecules (11). Most mammalian cells obtain their normal folate requirement via a low affinity reduced folate carrier or proton-coupled folate transporter (215, 216). Accessible folate receptors are normally overexpressed on cancer cells (217-219), activated macrophages (220-223), and the proximal tubules of the kidneys (224). Folate

conjugates have no affinity for the reduced folate carrier or proton-coupled folate transporter; they bind to FRs with high affinity and enter FR-expressing cells by receptor mediated endocytosis (225, 226).

Cancer cells have an increased requirement for folic acid, which is essential for synthesis of nucleotide base pairs in cell proliferation. Overexpression of FRs on cancer cells may have evolved because folate is often a limiting nutrient in human serum, and up-regulation of a high affinity FR may enable malignant cells to compete more aggressively for the vitamin. Many, but not all, cancer cells express either the  $\alpha$  or  $\beta$  FR isoform (217, 218). Cancers that most aggressively up-regulate the FR include ovarian, lung, kidney, endometrial, breast, brain, colon, and myeloid cells of hematopoietic lineage. Other tumors may up-regulate the reduced folate carrier or proton-coupled folate transporter to satisfy increased folate needs (215, 217).

### **Current Uses of PDT for Non-cancerous Conditions**

Use of PDT to treat microbial infections is becoming more popular due to the emergence of antibiotic resistance, the rise of human immunodeficiency virus (HIV), cancer patients with intractable infections, and the greater likelihood of spread of infection among global travel between developed and developing countries (11). Treatment with conventional antibiotics is facing serious limitations due to the following: the development of resistance to many classes of antibiotics leading to lethal effects (an example is the methicillin-resistant *Staphylococcus aureus* – MRSA) (227); excessive or inappropriate prescription

of antibiotics coupled with failure of patients to complete the treatment regimen (11); the large variety of strategies adopted by microorganisms to potentiate a degree of resistance to antibiotics (228); the broad differences in structure and organization by microbial cells (examples are the formation of protective biofilms, and lifecycles which include a resistant cystic stage)(11). Research has suggested that a suitable choice of PS dose and irradiation conditions for treating infectious diseases allows one to overcome the limitations of antibiotic therapies (8). Approaches under consideration involve the administration of the PS in the infected areas through topical application, spray formulations, or instillation, followed by irradiation of the photosensitized area with full spectrum visible light or selected intervals of visible wavelengths (229). The application of PDT for treatment of infectious diseases is still at the experimental stages. This therapy has several potentially favorable properties, since it is characterized by a high level of safety, is efficient against a large variety of pathogens (conventional antibiotics show activity to one or two pathogenic varieties), and has a possibility for repeating treatment due to insufficient response or recurrences. Clinical applications of antimicrobial PDT are reinforced by promising results that have been obtained in studies involving animal models as well as the encouraging reports of initial clinical trials (230, 231).

Cardiovascular disease is the leading cause of death across the globe. One of the main manifestations of the disease is atherosclerosis, which can occur in coronary or peripheral arteries. The understanding of what

atherosclerosis is has changed, and it is no longer considered a build up of fat leading to progressive narrowing of the arterial wall. Instead, plaque is a collection of cells (mostly macrophages and smooth muscle cells) which arise where the endothelial layer is injured or as a response to chronic infection. The underlying mechanism for the majority of sudden cardiac deaths has been suggested to be plaque rupture followed by occlusive thrombosis. It has been observed that photosensitizers commonly used for PDT specifically accumulate in the plaques in the arterial wall that are the hallmark of atherosclerosis. This accumulation has lead to suggestions that PDT could be used as therapy for atherosclerosis. If a PS could be delivered systemically or locally to the affected artery, along with an intravascular catheter fitted with a diffusing tipped fiber and placed at the affected lesion, illumination of an appropriate wavelength may kill pathogenic cells within the plaque. Cells involved in cardiovascular disease are the following: endothelial cells that line the inside of the blood vessels (these cells can regrow after injury to recoat the blood vessel wall and allow smooth blood flow); smooth muscle cells which provide contractility in the arteries (these cells can grow after injury and may lead to recurrent blockages in the artery known as intimal hyperplasia); fibroblasts which produce collagen and are components of fibrous plaques; macrophages that are thought to be a major cell type in atherogenesis and in the inflamed plaque; lymphocytes and other inflammatory cell types. There have been studies *in vitro* on how these cell types behave after incubation with various photosensitizers followed by illumination

(11). A technology was developed to target photosensitizers to macrophages. The approach involves covalently attaching a PS to a macromolecule that is recognized by the cell surface receptors that are expressed on macrophages. The diseased arterial wall was the only part that was illuminated, which resulted in localized and specific destruction of macrophages (232). Specific ligands of scavenger receptors, such as maleylated albumin, were utilized. Scavenger receptors are expressed mainly on mature macrophages, and Class A scavenger receptor (SRA) is a good target for macrophage specific PDT (233). The SRA is a multidomain trimeric transmembrane protein and has a high capacity to internalize ligands. One of the molecular designs to target SRAs is BSA. Three molecules of the Ce6 PS were covalently attached to the BSA via amide bonds between the carboxyl groups of chlorin and the epsilon amino groups of lysine in the BSA. Further modifications included the maleylation to give BSA – Ce6 – mal. There was a high degree of selectivity of this SRA-targeted PS conjugate for macrophages. Several experiments have used various photosensitizers such as photofrin, Hp, Ce6, and lutetium texaphyrin to study atherosclerosis *in vivo* in animal models. Some experiments have focused on fluorescence to detect atherosclerosis, while others have focused on potential therapeutic effects of PDT. In many cases, dramatic reductions in plaque were seen as a result of PDT treatments. Fluorescence was also seen in areas containing plaque, which shows that the PS accumulates in the atherosclerotic tissue (11). PDT has also been used for prevention and treatment of intimal hyperplasia (IH). Intimal

hyperplasia is a thickening of the *tunica intima* of a blood vessel which occurs as a complication of a reconstruction procedure or angioplasty. The arterial wall thickens and the lumen narrows due to accumulation of vascular smooth muscle cells in the *intima*, which secrete matrix proteins. Various animal studies have used PDT to prevent IH from occurring (a few days after injury) or to treat established IH several weeks after arterial injury. There have been few cardiovascular studies involving human subjects (three clinical studies known up to 2008). The first study in 1999 by Jenkins *et al.* investigated aminolevulinic acid (ALA) PDT following femoral percutaneous transluminal angioplasty (PTA). The study involved eight PTAs in seven patients (median age of 70) who had previously undergone conventional angioplasty at the same site which resulted in restenosis or occlusion between 2 and 6 months. The patients were dosed with oral ALA (60 mg / kg) 5 to 7 hours before the procedure. After having a second femoral angioplasty, up to 50 J / cm<sup>2</sup> of 635 nm light was delivered to the angioplasty site via a laser fiber within the angioplasty balloon. All of the patient's vessels remained open and no lesion became restenosed. The second study used the texaphyrin PS Antrin, or motexafin lutetium (234). The patients had claudication (pain and cramping in the legs due to poor blood circulation) and peripheral arterial insufficiency. A photoangioplasty of a single atherosclerotic lesion was performed in the external iliac, common femoral, or superficial femoral artery. In the first phase, the drug doses were escalated from 1 to 5 mg / kg at a constant 732 nm wavelength with light fluence of 400 J / cm<sup>2</sup>. In the second

phase, escalating drug doses from 2 to 4 mg / kg and light fluences of 500, 625, and 781 J / cm<sup>2</sup> were used. The median change in arterial stenosis was 24 % less and 62 % of patients showed improvement, while 36 % showed no change, and 2 % showed moderate worsening (235). The third study was a phase I trial which studied drug and light dose-escalation of motexafin lutetium and intravascular illumination in patients with coronary artery disease undergoing percutaneous coronary intervention and stent deployment. Therapeutic changes were achieved without adverse vascular responses or any treatment limiting phototoxicity (236).

Treatment of cardiovascular disease in the past consisted of balloon angioplasty followed by application of bare-metal stents, and subsequently drug-eluting stents (237). However, problems still remain with each of these treatments. Stenosis (arterial blockage or narrowing of the vessel) can be a problem with the bare-metal stents, and late thrombosis events are problematic with drug-eluting stents (238, 239).

PDT can play a role in the treatment of heart disease. PDT can also play a role in the problem of vulnerable plaque. Vulnerable plaque includes various types of high-risk plaques which predispose patients to developing acute thrombotic coronary syndrome / death. The aim with vulnerable plaque is not to remove or ablate the plaque to allow reestablishment of blood flow, but rather to reduce the inflammatory elements in the plaque that allow rupture and thrombosis to occur. The stabilization of these thin-cap fibroatheroma (TCFA)

lesions may be well suited to PDT, since photosensitizers can selectively target inflammatory cells such as macrophages (11).

Age-related macular degeneration is the main cause of a significant loss of vision among people who are over age 50 (240-242). AMD is most prevalent in the elderly population (238, 240). Blood vessels of the choroid (choroidal neovessels or CNV), which are poorly regulated and leaking, represent only about 15 % of the AMD cases (240, 244), but neovascular AMD causes nearly all the rapid and extensive vision loss (240, 245). Nonvascular AMD is characterized by lipid deposits which contain lipofuscin in and under the retinal pigment epithelium. These deposits are called drusen and show up as yellowish spots upon visual inspection of the retina (246, 247). Verteporfin (Visudyne) was the first approved PS for PDT treatment of AMD. PDT changed everything for both patients and eye care professionals, as legal blindness was no longer the main outcome of this disease. Since the year 2000, several hundreds of thousands of eyes have been treated and saved from blindness by PDT (11). SnET2 and Lutetium texaphyrin were tested in phase I and II clinical trials; however, these drugs failed to reach the market. Other compounds are being developed in order to achieve even higher treatment selectivity. Higher selectivity implies less damage induced by PDT to the surroundings of the CNV, and also less closure of the normal choriocapillaries. An example of this is the creation of a conjugate between benzoporphyrin derivative monoacid ring A (BPD-MA) and a peptide that selectively binds to endothelial cell receptors that are up-regulated in CNV,



such as the vascular endothelial growth factor (VEGF) receptor 2 (248). PDT of subfoveal CNV uses freshly made verteporfin solution that is injected via IV over a 10 minute interval. Fifteen minutes after starting perfusion of the drug, light is applied to the retina from a diode laser at a wavelength of 689 nm. This beam targets the retina so that the diseased area is able to be visualized. The treatment beam is coaxial and operates at a 630 nm wavelength. The target area, which includes the leaky CNV, is visualized by fluorescein angiography. The eye is irradiated via a planar-concave contact lens that is placed on the eye. The fluence rate at the retina is  $600 \text{ mW} / \text{cm}^2$ , which is delivered over a time period of 83 seconds, giving a fluence rate of  $50 \text{ J} / \text{cm}^2$  (11). There are many aspects of selectivity in the PDT treatment of the angioocclusion of CNV in AMD. First of all, there is selectivity of vascular damage and the subsequent stasis of blood flow. This selectivity is seen in the short time interval between the drug injection and application of light. The 83 second irradiation takes place 15 minutes after the start of the IV injection of Visudyne, and at that point, most of the drug that is in the retina is still within the blood vessels, and more specifically, on or in the endothelial cells lining the CNV, which will undergo the angioocclusion. This represents the main photodynamic effect which takes place in the endothelium being irradiated. During the phase I and II trials that took place during the development of Visudyne, the second reason for the selective angioocclusion of the targeted CNV became evident. Visudyne angiography was done in the early clinical tests. What was observed in these experiments was that

the retinal vessels emptied of Visudyne fluoresced significantly faster than the choroidal vessels. At the time of irradiation, the retinal capillaries appeared to have much less drug in them compared to the CNV and choroidal vessels. This may have implied a significant level of protection of the retinal capillaries. Occlusion of retinal capillaries must be avoided due to immediate and heavy loss of visual acuity. A third reason for selectivity in the closure of CNV is that retinal capillaries are protected by the blood retinal barrier, which signifies tighter junctions between endothelial cells, and probably more resistance to PDT. The CNV are new leaky vessels with somewhat weak junctions between the endothelial cells, without significant reinforcement of the capillary walls by pericytes and connective tissue, which means that the CNV should be more prone to angioocclusion induced by PDT. A fourth reason for the selective angioocclusion of the CNV is that these rapidly growing neovessels tend to have a relatively high activity of LDL receptors on their endothelium. Verteporfin, a fairly lipophilic drug, is transferred to a significant extent to LDL. The rapidly proliferating CNV endothelium may be selectively loaded with verteporfin (this was effectively shown in rabbit eye neovessels) (249). Finally, another reason for selectivity in CNV angioocclusion by PDT may be a lower level of tissue molecular oxygen in the region of the retinal vessels as compared to the choroid (250). Angioocclusion induced by PDT begins with the light-drug interaction that generates reactive intermediates that damage different sites in and on the endothelium. It has been shown (251-253) that the cytoskeleton of the

endothelial cells can be damaged, leading to shrinkage and rounding of these cells. This can then cause rupture of the tight junctions between the CNV's endothelial cells. This break up of the tight endothelial junctions is followed by release of von Willebrand factor (vWF). vWF is a glycoprotein that is present in the endothelial cells and the subendothelium. One of its functions is related to adhesion and aggregation of platelets. Together with fibrinogen it helps to develop a thrombus (that is, the release of vWF causes platelets to stick to the capillary wall). More platelets continue to stick to the immobilized platelets, forming a plug. This thrombus is then stabilized by the activation of fibrinogen to fibrin. PDT of subfoveal CNV does not damage photoreceptors or other neighboring parts of the retina so that retinal function is maintained (11).

The uses of PDT in dermatology include the following: nonmelanoma skin cancer, acne, photorejuvenation, hidradenitis suppurativa (a chronic skin inflammation with presence of blackheads and one or more red, tender lesions – a severe form of acne), psoriasis, cutaneous T-cell lymphoma, disseminated actinic porokeratosis (DSAP; a rare inherited skin condition that causes dry, itchy lesions on the arms and legs), localized scleroderma, vulval lichen sclerosis, bacterial infections, and verruca vulgaris. The skin has easy access to light-based therapy, and this has lead dermatologists to apply PDT to cutaneous disorders (254). Photofrin, which is a purified HpD, was used in conjunction with UV light to locate tumors, and then in combination with visible light to treat tumors (255). The drawbacks of using HpD as a PS is that this drug accumulates

in skin and clears out slowly. The result is that the patient experiences cutaneous photosensitivity that may last several months, and during this time, the patient is at risk of phototoxic reactions (256). Actinic keratosis (AK) is caused by long term exposure to the sun, and this condition is often the beginning stage of invasive squamous cell carcinoma (SCC) (257, 258). PDT has been reviewed among the conventional treatments of cryotherapy, curettage, and 5-fluorouracil (259-262). ALA has been applied to diffuse areas and is selectively uptaken by abnormally keratinized cells. This cellular uptake paves the way for PDT to be used for prevention of AK by eradicating populations of abnormal cells before they become confluent and manifest as visible actinic keratoses. In a clinical study, Szeimies *et al.* used 10 % ALA, and applied ALA-PDT once to 36 AK lesions on the hands, arms, and heads of 10 patients. They irradiated the lesions with red and infrared light (580 – 740 nm, 150 J / cm<sup>2</sup>), and monitored the patients for 3 months. After twenty-eight days, complete remission had occurred in 71% of the head lesions. No lesions on the hands and arms showed complete remission (263). More recently, a phase IV trial of 110 patients were treated with 20 % Levulan Kerastick, and the results of the study were a clearance of 76 %, with an increase of 86 % with two treatments, and an overall recurrence rate of 24 % over a 1 year follow-up (264). In a study in 2000, Hongcharu *et al.* (265) applied ALA-PDT with filtered red light (550 – 700 nm) for the treatment of mild to moderate acne. This study demonstrated that Protoporphyrin IX (PpIX) accumulates in pilosebaceous glands. The authors reported statistically

significant clearance for 10 weeks after one treatment, and for 20 weeks after four weekly treatments. The authors also showed that after ALA-PDT, sebum excretion was decreased, bacterial fluorescence was decreased, and sebaceous glands were damaged (266, 267). In another study, Goldman and Boyce (268) showed that with ALA-PDT using blue light, the effectiveness against acne was better than with blue light alone, and also that short-contact ALA (< 1 hour) provided efficacy and minimal side effects. Hidradenitis suppurativa (HS) is a chronic, inflammatory disease of the apocrine glands in the skin, particularly in the axilla, anogenital region, and breasts. The condition results in painful abscesses and sinus tract formation. HS can be progressive with marked morbidity related to chronic pain, draining sinuses, and scarring with restricted mobility. Complications of this condition can lead to fistulas of the urethra, bladder, and rectum if the anogenital region is affected, and limited mobility and lymph edema if the axilla are affected. Previous treatments included oral and topical antibiotics, antiandrogens, oral retinoids, immunosuppressive therapy, biologics, and surgery. PDT has been studied due to limitations of the aforementioned therapies (11). Gold *et al.* studied four patients with chronic HS that were unresponsive to previous therapies. The patients received three to four treatments at 1 to 2 week intervals which consisted of 15 to 30 minutes of incubation of Levulan followed by exposure to blue light. All subjects showed 75 % - 100 % clearance of HS three months after the final treatment. The treatments were painless and patients reported no adverse events (269). DeVita

and Taub also supported this finding in case studies of four persons with moderate to severe HS who were unresponsive to previous therapies. Patients were treated with either blue light or intense pulsed light (IPL) after 30 to 60 minutes incubation with Levulan. The treatments were given at 2 to 4 week intervals, followed by maintenance treatments every 1 to 2 months. The patients achieved 50 % – 75 % clearance with the initial treatment series and were either maintained or improved with further treatments during the maintenance phase (270).

### **Vascular Targeting in Photodynamic Therapy**

After studying the process of PDT, it is now known that PDT can kill cancer cells directly or can indirectly induce tumor cell death as a result of damage to tumor stroma (73). Direct toxicity to tumor cells is often limited due to inadequate supplies of PS, light, and / or oxygen in tumor tissues (252). Tumor vasculature is an important part of PDT and is often responsible for the decrease in tumor burden following PDT. Vascular damage is the main PDT effect and is primarily responsible for the final outcome following PDT treatment (73).

Vascular targeting has been developed to further potentiate vascular damage. Solid tumors are unable to grow larger than 1 mm<sup>3</sup> without a vascular network (271). Like normal tissues, tumor tissues require a functioning vascular system to supply the tumor with nutrients and to remove metabolic wastes. In order to sustain growth, tumor tissues depend upon existing vessels and also develop new blood vessels for blood supply. Tumor blood vessels exhibit abnormalities in

vessel architecture (tortuosity, dilatation, irregular branching, and lack of pericyte and basement membrane coverage) and function (stagnant blood flow, increased vascular permeability), as compared to normal blood vessels (272).

There are two categories of vascular targeting therapy, which are:

antiangiogenic therapy that inhibits the formation of new vessels, and vascular disrupting therapy that targets existing blood vessels (273). The overall goal of vascular therapy is to disrupt tumor vascular function without affecting the function of normal tissues. This therapy can be used alone or in conjunction with traditional cellular PDT or other cancer treatments. There are several advantages to tumor vascular therapy as compared to the tumor cellular targeting approach (271, 274). First, vascular targets are readily accessible to the intravenous delivery of therapeutic agents, whereas the various physiological barriers make cellular targets difficult to reach. Second, vascular targeting is highly efficient and potent in killing tumor cells, because not all of the endothelial cells need to be targeted to disrupt tumor vascular function. Damage to a single endothelial cell or a portion of a blood vessel can have a catastrophic effect on the perfusion of the tumor. This, in turn, results in killing thousands of tumor cells dependent upon that vessel for blood supply. Third, since endothelial cells are considered to be more stable genetically than tumor cells, the risk of acquiring drug resistance is low (11). Photodynamic vascular targeting uses site-directed delivery of photosensitizing agents to the blood vessel system followed by light irradiation to induce photosensitizing effects in the vasculature. There are two approaches,

passive and active. The passive approach is based on the fact that the concentration of the PS is often high shortly after intravenous administration of a PS. The goal with active vascular targeting PDT is to direct the drugs to the vasculature and to alter the pharmacokinetic properties of the PS via drug structure modification or drug formulation into a targeted delivery system (73). A target that has a high affinity to endothelial cell markers (for example, integrins, VEGF receptors, tumor endothelial markers) or vessel supporting structures (for example, the extra domain B of fibronectin which is a marker of tissue angiogenesis expressed in solid human tumors) is often used to modify the PS. The PS conjugates are expected to selectively accumulate in the targeted blood vessels, and become activated upon irradiation by light. The mechanism of vascular targeted PDT is the same as cellular PDT in that  $^1\text{O}_2$  is produced and is responsible for the subsequent vessel structural and functional alterations (275). The ultimate goal is to obtain maximal tumor cell killing by inducing tumor vascular shutdown. Fluorescence studies have shown that microcirculation dysfunction is induced by vessel occlusion due to thrombus formation and vessel constriction / collapse caused by mechanical compression and vasoactive substances. Photosensitizing damage to either blood cells or endothelial cells can induce thrombus formation. It has been demonstrated that PDT can damage platelets and red blood cell membranes, thereby causing platelet aggregation and thrombus formation (276, 277). Thromboxane, a vasoactive substance, is stimulated by damage to the platelets. Thromboxane has potent vessel



constriction and thrombus formation effects. Damage to the endothelial cells occurs in addition to damage to blood cells. The endothelium serves as an interface between blood and tissue underneath. If the endothelial barrier is lost due to vascular photosensitization, this exposes the extracellular tissue matrix to the circulation, which activates platelets and leukocytes. This will subsequently induce blood cell adherence to the damaged endothelial cells (278). Endothelial cells also influence the balance of blood clotting by release of vWF that facilitates thrombus formation (279) and prostacyclin which inhibits thrombus formation and dilates blood vessels (280). Blood clot formation is the net effect that is most likely favored in the early stages of photosensitization. Blood clots will cause obstruction to blood flow; however, some of these clots are unstable and will be dissolved and dislodged by anticoagulants within the body. Only stable clots will occlude blood vessels and shut down vascular function (281). Thrombus formation is only partially responsible for PDT induced vascular damage. Vessel constriction is often observed after vascular photosensitization, and this also contributes to blood flow stasis. The release of vasoactive substances, such as thromboxane and leukotrienes, can cause vessel constriction (69). However, an increase of interstitial fluid pressure is also a strong inducer of vasoconstriction and collapse in tumor tissues (272). Tumor tissues have higher interstitial pressure than normal tissues due to leaky tumor blood vessels. Mechanical compression due to high tumor interstitial pressure can cause collapse of tumor blood vessels even without treatment. This is one of the mechanisms involved in

acute hypoxia development in tumor tissues (282). Since PDT is able to cause vascular barrier disruption and further increase tumor interstitial pressure, vessel compression and collapse effects are aggravated by PDT (283, 284). One of the challenges of PDT vascular targeting, is that in spite of extensive tumor vascular shutdown leading to tumor cell death, functional blood vessels are typically detected at tumor peripheral areas. Existence of these functional vessels can lead to tumor recurrence, which is often observed at the peripheral tumor area (285, 286). It is unclear why tumor peripheral and central blood vessels react differently to photosensitization. The hypothesis is that the variation in response is due to differences in tumor interstitial pressure and the structure of blood vessels in the tumor central versus peripheral areas. The central tumor vessels have a higher interstitial pressure than the peripheral vessels, and are therefore more likely to collapse because of higher mechanical compression (287, 288). Also, peripheral tumor vessels are usually larger and have more vessel support structures as compared to central tumor vessels. The current status of PDT vascular targeting involves the use of verteporfin for treating AMD, and other photosensitizers such as SnET2 (Purlytin), and lutetium texaphyrin (Lu-Tex, Optrin), which are under clinical trials for AMD (73). The PS Tookad is in a phase I / II clinical trial for locally recurrent prostate cancer after radiation therapy (289). These photosensitizers are being studied for the passive form of vascular targeted PDT. Less studies have been undertaken for the active form of vascular targeted PDT, but this avenue is being pursued for cancerous and noncancerous

diseases. Some promising results have been achieved from several studies using conjugated photosensitizers with blood vessel homing peptides (290-294).

### **Inflammation and Immune Responses to PDT**

The therapeutic outcome after cancer treatment by PDT is the result of the photooxidative damage, effects on tumor vasculature and other tumor stromal elements, and the elicited host response (252, 295). The host response includes two major processes, inflammation and the acute phase response, and the two main parts of immunity, the innate and adaptive immune reactions. These host responses have a pronounced systemic impact. The inflammatory response occurs because of localized oxidative stress which is associated with a wide range of photooxidative lesions produced in the membranes and cytoplasm of tumor cells, stroma, and vasculature (296). The PDT-induced insult is experienced by the host (patient) as a local trauma. The inflammatory response is initiated as this is the body's way for dealing with localized injury. The acute inflammation first prevents the spread of tissue damage and contains the disrupted homeostasis. Next, the damaged and dead tissue is removed, and then local healing is promoted to restore tissue function at the affected site (297). The inflammation resulting from PDT-treated tumor tissue is a tumor antigen nonspecific process orchestrated by the innate immune system which detects the inflicted tumor-localized insult (296, 298). The sensors of the innate immune system recognize the insult as a state of "altered self" (299). This alert system is called into action upon detection of alarm / danger signals from the injured /

distressed tumor tissue (300, 301). The sensors of the innate immune system recognize damage-associated molecular patterns (DAMPs). Basically, DAMP can be any molecule that is abnormally exposed, misfolded, or residing at a wrong location, as well as breakdown products of damaged biomolecules. There are three major types of DAMPs generated by tumor PDT: cell-derived molecules, extracellular matrix degradation products, and extravasated plasma proteins (299, 302). Degradation products of cellular membranes (lysophospholipids and arachidonic acid metabolites) are PDT-induced DAMPs that are massively released from PDT-treated areas (303, 304). Intracellular molecules originating from necrotic cells are also DAMPs. PDT can induce damage to extracellular matrix (305), and the degradation of this tissue-supporting scaffold will liberate fragments of fibronectin, hyaluronan, collagen, and laminin that are also danger signals (301, 306-308). Tissue injury induced by PDT includes breakdown of blood vessels, which leads to the escape of plasma proteins, which leads to increased accumulation of protein such as fibrinogen (302). Extravascularly localized fibrinogen is also recognized as a danger signal and promotes the development of a host response against PDT-treated tumor tissue (309). DAMPs of proinflammatory danger signals following tumor PDT treatment are detected by specialized pattern recognition receptors (PRRs) (310). These PRRs can be soluble, membrane-anchored, or cytoplasmic (the latter two are found on macrophages, mast cells, dendritic cells, and endothelial cells) (311). The engagement of PRRs by tumor PDT-induced injury associated

DAMPs is what triggers the inflammatory process. The inductive phase of inflammation (including inflammation induced by PDT) involves the vascular component of the affected tissue. When using photosensitizers that do not target the vasculature, such as Photofrin, m-THPC, and PpIX induced by 5-ALA, the process of inflammation is initiated by signals originating from photooxidative damage. This photooxidative damage is produced in perivascular regions with chemotactic gradients that reach the vascular endothelium. The conversion of vascular endothelium from a nonthrombotic nonadhesive barrier to a proadhesive surface for inflammatory cells that becomes leaky to blood components represents the onset of inflammation (312, 313). There are several underlying changes that occur during the process of inflammation, which include vasodilatation (due to the action of arachidonic acid metabolites (314) and elevated production of nitric oxide from activated nitric oxide synthase) that increases blood flow and leukocyte delivery, appearance of leukocyte adhesion molecules on the endothelium, opening of junctions between endothelial cells, and activation of platelets (triggered by activating factor induced in endothelial cells by lysophosphatidylcholine) (313). Next, there is rapid and massive invasion by neutrophils into PDT-treated tumors, followed by mast cells and monocytes (315-317). These inflammatory effector cells neutralize the source of danger signals by destroying compromised tissue elements and eliminating dead and injured cells. Studies into the signaling pathways initiated by inflammation following PDT will lead to insights into tumor cell death by the three mechanisms

of apoptosis, necrosis, and autophagy. The immune response that occurs after successful PDT is also thought to play a critical role in the long-term outcome of tumor treatment. Factors that determine the strength of the immune response will likely be further studied (11).

PDT has a significant effect on the immune system (318-320), which can either stimulate the immune system or suppress the immune system in some circumstances. Administration of photosensitizers along with the appropriate light activation causes an unusual mixture of both apoptotic and necrotic cell death (14). Some reports show that apoptotic tumor cells are more effective in the induction of the immune response than necrotic tumor cells (321, 322), however, there are other reports showing the opposite findings (323, 324). The acute inflammation caused by PDT-induced necrosis may stimulate immunity by attracting host leukocytes into the tumor, and enhancing antigen presentation. Antigen-presenting cells (APC) have the unique ability to induce a primary immune response. One of the most characteristic features of the APCs is the expression of the major histocompatibility complex (MHC) class II molecules and the ability to present exogenous antigens to T helper lymphocytes. The types of APCs include dendritic cells (DC), macrophages, and B lymphocytes. Dendritic cells can acquire the antigens, process them, and present them in the context of MHC class II molecules. The DCs express Toll-like receptors [TLRs; TLRs are a class of protein receptors on macrophages or dendritic cells that recognize structurally conserved molecules derived from microbes; an immune response is

activated after microbes have penetrated the skin or intestinal mucosa and are recognized by TLRs (302)] as well as costimulatory molecules needed for successful DC-T cell interactions. They can travel to the lymph nodes and interact with T cells to start the primary immune response. One of the most important factors induced by PDT is the release of extracellular heat shock protein 70 (HSP70) from necrotic tumor cells. When HSP70 remains intracellular, it chaperones unfolded proteins and prevents cell death by inhibiting aggregation of cellular proteins (325). Intracellular HSP70 can inhibit tumor cell death by apoptosis and also promote formation of stable complexes with cytoplasmic tumor antigens that can be either expressed at the cell surface or escape intact from dying necrotic cells to interact with antigen presenting cells to stimulate an antitumor immune response (326). Extracellular HSP70 binds to high affinity receptors on the surface of the APCs, which leads to activation of DCs. This process subsequently enables the cross-presentation of the antigen cargo of HSP70 by the APC to cytotoxic T-cells (327). PDT mediated by NPe6 and SnET2 increased HSP70 protein levels in mouse tumor cells *in vitro* and in tumor cells *in vivo* (328). Agents derived from microbial stimulators of innate immunity can be injected into the tumor or surrounding area before, during, or after PDT in order to activate TLRs or similar pattern recognition molecules on macrophages and dendritic cells (329). Combination therapy that involves administering immunoadjuvants (often potential TLR ligands) and different PDT regimens has proven to be effective. There have been reports that macrophages can be

activated by low, sublethal doses of PDT (330). It has been shown that PDT-treated macrophages secrete tumor necrosis factor alpha (TNF $\alpha$ ) (331). Evidence indicates that macrophages can show preferential cytotoxicity towards tumor cells that have been treated with a sublethal dose of PDT (332). Another report showed that the tumoricidal effect of peritoneal macrophages removed from mice after PDT was unaltered; however, there was a reduction in natural killer (NK) cell function. Studies have demonstrated that the acute inflammation produced by PDT and a systemic and tumor-localized increase in neutrophils are very important in obtaining tumor cures. It is likely that these phenomena will also be important in developing a memory T-cell antitumor immune response following PDT. Studies with NK cells suggest that these cells may play a significant role in post-PDT activity of CD8+ T cells and control of distant metastases. In the absence of NK cells, SCID mice exhibited a significant increase in lung tumor number (11). Canti and colleagues examined the effects of PDT with the PS aluminum disulfonated phthalocyanine on the antitumor immune response in immunosuppressed and normal mice with MS-2 fibrosarcomas. All of the mice were cured, but resistance to a new challenge with MS-2 tumors was evident in animals cured by PDT. Immunosuppressed animals and animals cured by surgery died after tumor rechallenge. These results suggest that PDT may induce the activation of the tumor-specific cytotoxic T lymphocytes (333).



### **Photobleaching and Quenching of Singlet Oxygen in PDT**

Photobleaching refers to the loss of absorbance and / or fluorescence of the PS upon exposure to light. Photobleaching can lead to chemical change, including the total destruction of the PS. Two types of photobleaching are possible, which are: 1) photomodification – refers to the loss of absorbance or fluorescence at some wavelengths with the PS retained in a modified form. 2) true photobleaching, in which the chemical change results in small fragments which no longer have significant absorption in the visible region. Ideally the PS should be completely selective for tumor tissue; however, some will be found in normal tissues, where it may cause undesirable photosensitization. If the PS exhibits moderate sensitivity to photobleaching, after the tumor tissue is destroyed, the residual PS located in normal tissue would be susceptible to photobleaching under ambient light conditions. This situation is a potential value of photobleaching, as the period of post-treatment sensitivity of the patient to sunlight would be reduced and the clearance of the residual PS from the body is hastened. Photobleaching will affect dosimetry, both of the PS and of the light. If the PS exhibits some photobleaching, a stronger light dose may be needed to compensate. Allowances may also need to be made for photobleaching in determining drug dosages (*100, pp. 237-238*).

Other considerations that may affect the efficacy of treatment with PDT involve the quenching of  $^1\text{O}_2$  before it has the opportunity to react with cellular organelles leading to destruction of tissues. There are two mechanisms of

quenching of singlet oxygen: 1) Physical quenching –  $^1\text{O}_2 + \text{A} \rightarrow ^3\text{O}_2 + \text{A}$  In this situation, interaction leads to deactivation of  $^1\text{O}_2$  with no consumption of  $\text{O}_2$  or product formation. 2) Chemical quenching –  $^1\text{O}_2 + \text{A} \rightarrow \text{P}$  In this situation, the quencher reacts with  $^1\text{O}_2$  to give a new product. Early research with  $^1\text{O}_2$  showed that  $^1\text{O}_2$  could oxidize substrates that were not affected by oxygen in its normal triplet energy state. Oxygen is more oxidizing in its singlet state, and is therefore more electrophilic, making it very reactive with unsaturated carbon-carbon bonds, neutral nucleophiles such as sulfides and amines, as well as with anions (33). Singlet oxygen can also react with double bonded compounds containing two or more allylic substituents, causing a shift in the double bond, and formation of an allylic hydroperoxide. This reaction is relevant to biological systems in the reaction of  $^1\text{O}_2$  with the amino acids tryptophan and histidine, as well as unsaturated fatty acids which are part of cellular membranes (334, 335). Singlet oxygen may also form dioxetanes by reacting via cycloaddition with the pi electrons of olefins (336, 337). Excited triplet state photosensitizers can produce  $^1\text{O}_2$ ; however, in many cases, these same photosensitizers can also quench  $^1\text{O}_2$  once formed. This situation can lead to photobleaching and photodegradation. Photodegradation refers to the process in which  $^1\text{O}_2$  reacts with a material and results in its degeneration, and photobleaching refers specifically to the degradation of dyes by  $^1\text{O}_2$ . This process is undesirable, since it is the generation of  $^1\text{O}_2$  which allows PDT to be successful (33).

## **Buchwald-Hartwig Chemistry for Pd-Catalyzed Cross Coupling Reactions**

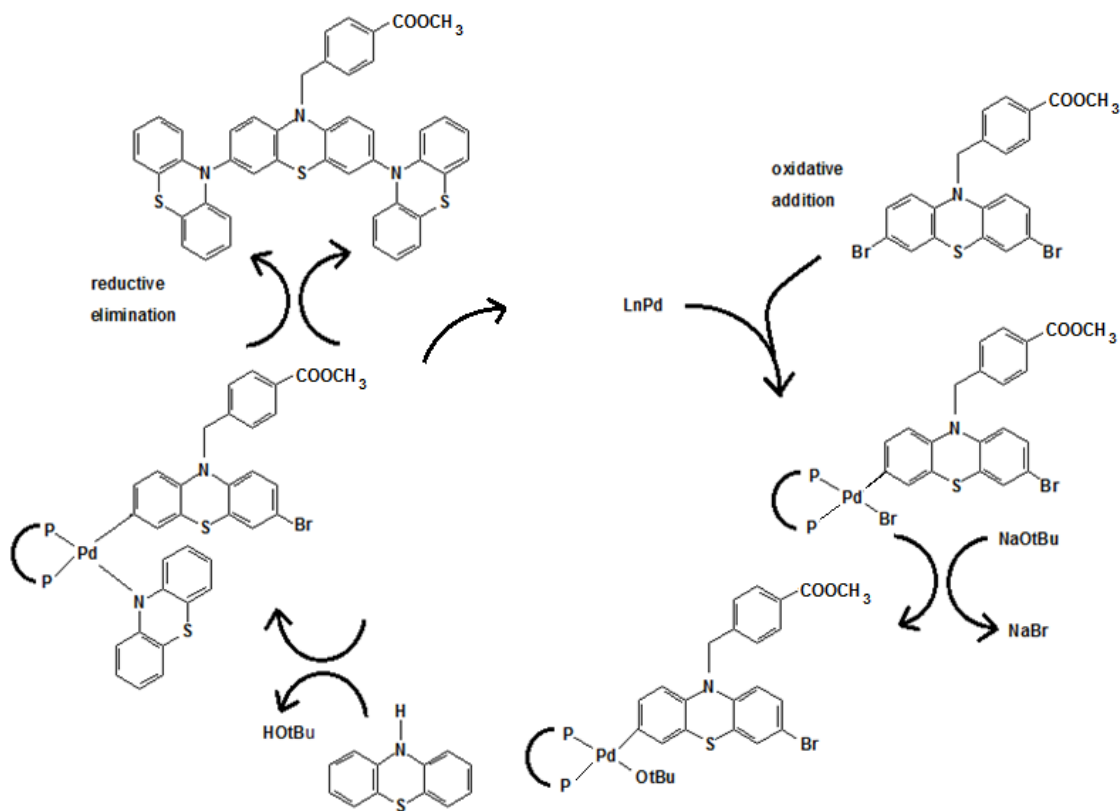
### **Forming C-N Bonds**

Palladium catalyzed amination using aryl, vinyl, and heteroaryl halides has rapidly emerged as a tool for the synthesis of many pharmaceuticals and natural products (338-341). This method of synthesis stems from the prevalence of aromatic amines in molecules that are biologically active (342). Important classes of these molecules include kinase inhibitors (343, 344), antibiotics (345, 346), and central nervous system agents (347). Major breakthroughs in this area of synthesis have been in the implementation of new types of ligands. Some specific examples include chelating diphenylphosphino ligands such as BINAP (348, 349), dppe (350), and Xantphos (351). In addition, more electron-rich chelating phosphines such as Josiphos (352), N-heterocyclic carbenes (353), and trialkylphosphines (354, 355) have allowed an increase in types of substrates utilized and have rendered the reactions more efficient (356, 357). In spite of the fact that a number of systems are available for Pd-catalyzed C-N coupling, only a limited group of types have been applied in practice. Catalysts based on dialkylbiaryl phosphines compare favorably with other systems, and have been used extensively in the synthesis of biologically active molecules (341). Professor Stephen Buchwald first described the use of these systems for Pd-catalyzed cross-coupling in 1998 (358). Since then, further work (359-371) has led to the development of many structurally related ligands that can generate highly active catalysts for a number of reactions, such as Pd-catalyzed amination

(341) and etherification of aryl halides (372, 373), arylation of enolates (374), and Suzuki-Miyaura cross-coupling (375, 376). These ligands have an advantage over others in that they are able to be utilized without the need for a dry-box and can be used with standard laboratory glassware (377). The choice of ligand as well as other parameters (Pd catalyst, base, solvent, temperature) needed to optimize the reaction will vary for different substrate combinations. This is due in part to the wide variation in electronic and steric properties of the nitrogen nucleophiles when compared to other cross-coupling processes such as the Suzuki-Miyaura reaction (see next section). Due to differences in nucleophilicity and  $pK_a$  of the amine and amide substrates, the rate determining step of the catalytic cycle can vary, which contributes to the difficulty in selecting the best reaction conditions (378). The structure of the ligand is critical to the success of a given amination reaction when using a dialkylbiaryl phosphine compound. Many ligands have been developed which are air stable, easily handled crystalline solids, and are commercially available (379). Improved reactivity in a variety of amination reactions became possible with the discovery of XPhos and RuPhos (380, 381). The use of an extra equivalent of ligand relative to the Pd catalyst is often needed to stabilize the catalyst for difficult reactions which require long reaction times (382, 383). This tactic is effective for dialkylbiaryl phosphine ligands because when an extra equivalent of ligand is used, the  $L_1Pd$  complex can still be the main species in solution (384). An extra quantity of ligand may also be necessary for activation of the Pd catalyst. The efficiency of formation of

the catalytically active  $L_1Pd(0)$  complex before entry into the catalytic cycle is a key factor in the selection of the reaction conditions for Pd-catalyzed amination. If a Pd salt is used as the catalyst, the Pd must be reduced from the +2 oxidation state to a 0 oxidation state before the cross coupling reaction can take place. The need for a reduction step from Pd(2) to Pd(0) can be avoided by using a stable Pd(0) complex such as  $Pd_2(dba)_3$  or  $Pd(dba)_2$ , which are suitable for a variety of conditions (380, 381, 385-391). The coordination of dba to the metal, however, can attenuate the activity of the Pd catalyst (392, 393). A wide variety of solvents can be used for Pd-catalyzed amination reactions using dialkylbiaryl phosphine ligands, although toluene and 1,4-dioxane are the most commonly used solvents. The choice of base for amination depends on the functional groups present in the substrate (394). Selection of the base by noting the  $pK_a$  of the free N nucleophile is not possible since the  $pK_a$  is altered significantly by binding to the Pd, which occurs before deprotonation. Sodium t-butoxide is the most versatile base for Pd-catalyzed amination reactions with dialkylbiaryl phosphine ligands since it often gives the highest reaction rates with the lowest catalyst loadings. However, because sodium t-butoxide is a fairly strong base ( $pK_a = 17.0$ ) it can participate in undesirable side reactions with electrophilic functional groups and some aromatic heterocycles and cause epimerization at acidic centers (395). Reaction conditions will depend on the structures of both the electrophile (aryl bromide in this research) and the nucleophile (phenothiazine in this research). The various aryl halides (chlorides, bromides,

and iodides) and aryl sulfonates have distinct properties with respect to how easily they undergo oxidative addition (396-398). The presence of electron donating or withdrawing groups on the aromatic ring or of heteroatoms within the ring affects the rate of all steps of the catalytic cycle. Substituents that are ortho to the aryl halide can facilitate some steps of the catalytic cycle (reductive elimination), while retarding others (oxidative addition). The N nucleophile can also possess differences in nucleophilicity and  $pK_a$  in addition to steric properties. These properties can also affect the rates of various steps in the catalytic cycle such as amine binding (378), deprotonation, and reductive elimination (377). Initial studies on Pd-catalyzed aminations were carried out predominantly with aryl bromides as electrophiles; however, aryl chlorides are now typically more attractive substrates since they are more cost effective and more widely available (399, 400). A diagram of the Buchwald-Hartwig oxidative addition, reductive elimination cross coupling reaction to form C-N bonds for the protected phenothiazine trimer, as well as a description of the steps is shown in Figure 3.



### Description of Buchwald-Hartwig Mechanism

- **Br and methyl bromo-4-N-methylenephenthiazinylbenzoate add to Pd (0) ligand and Pd  $\rightarrow$  +2 oxidation state (oxidative addition)**
- **Na t-butoxide displaces Br atom from ligand (NaBr byproduct)**
- **t-butoxide anion deprotonates phenothiazine N atom (t-butyl alcohol byproduct)**
- **Deprotonated phenothiazine adds to Pd ligand**
- **Methyl bromo-4-N-methylenephenthiazinylbenzoate and phenothiazine released from catalyst (phenothiazine dimer formed); new C-N bond formed**
- **Final product of methyl (3,7-diphenothiazinyl)-4-N-methylenephenthiazinylbenzoate (benzoate protected phenothiazine trimer) formed after reaction cycles through mechanism twice**
- **Pd catalyst reduced back to 0 oxidation state (reductive elimination)**

Figure 3. Buchwald-Hartwig Cross Coupling Reaction

Ref: <http://www.organic-chemistry.org/namedreactions/buchwald-hartwig-reaction.shtm>

## **Pd-Catalyzed Cross Coupling Reactions Forming C-C Bonds**

The 2010 Nobel Prize in Chemistry was awarded to three scientists who were all working on Pd-catalyzed cross coupling reactions involving the formation of new C-C bonds. The three Nobel laureates were Professor Richard Heck, Professor Ei-ichi Negishi, and Professor Akira Suzuki. In order for a specific area of research to be recognized for a Nobel Prize, its real world application must be demonstrated within 20 to 30 years of its discovery (401). The area of metal-catalyzed cross coupling was initiated in the early 1970s; however, there were a limited number of publications and patents in this area prior to the 1990s. This area of research has grown rapidly, especially since the year 2000. In terms of scientific publication, patents, and industrial applications, Suzuki coupling is the largest area, followed by Heck coupling, and then Negishi coupling. The popularity of Negishi's work is growing due to the functional group tolerance of the zinc reagent compared to magnesium, its potential in  $sp^3$ - $sp^2$  coupling, natural product synthesis, and asymmetric carbon-carbon bond forming reactions (402). Between 1968 and 1972, Heck and coworkers as well as Mizoroki and coworkers independently discovered the use of Pd(0) catalysts for coupling aryl, benzyl, and styryl halides with olefinic compounds. This reaction is now known as the Heck coupling reaction, since Heck was the first to elucidate the mechanism of the reaction. This reaction combines an aryl, vinyl, or alkyl halide with an alkene to create a new R-R' bond, using a Pd catalyst and base. This chemistry can be applied to the synthesis of hydrocarbons, conducting polymers, light-



emitting electrodes, pharmaceuticals, and dyes. Heck reactions have a broader range of uses than other coupling reactions because they can make products of different regio (linear and branched) and stereo (cis and trans) isomers. Alkenes with electron-withdrawing groups favor linear products, while electron-donating groups give a mixture of branched and linear products. Selectivity is also influenced by other factors such as the nature of the ligand, halide, additives, solvents, and the palladium source. Chiral C-C bonds can also be made by the Heck coupling reaction (403-407). During the period from 1976 – 1977, Negishi and coworkers as well as other groups of researchers reported the use of zinc reagents in cross-coupling reactions (408-410). The Negishi coupling reaction uses organozinc reagents containing halide (organic portion can be aryl, vinyl, or alkyl) which react with an alkyl, vinyl, or aryl halide to create a new R-R' bond in a cross-coupling reaction utilizing a Pd catalyst. This reaction has been used in the synthesis of natural products and fine chemicals (411-413). Suzuki recognized that boron was the last element of the three (Zn, Sn, B) that were identified by Negishi as suitable counterions for cross-coupling reactions. The Suzuki reaction involves Pd catalysis to cross-couple aryl or vinyl boronic acids or boronic esters with aryl or vinyl halides to create new R-R' bonds (414). Heck, however, had already demonstrated the transmetalation of a vinyl boronic acid in 1975 (415). Suzuki identified  $\text{PdCl}_2(\text{PPh}_3)_2$  as an efficient cross-coupling catalyst, and demonstrated the easy reduction of Pd(II) to Pd(0) during catalysis. The

Suzuki reaction is used in the synthesis of pharmaceutical ingredients such as losartan (see structure below) (402).

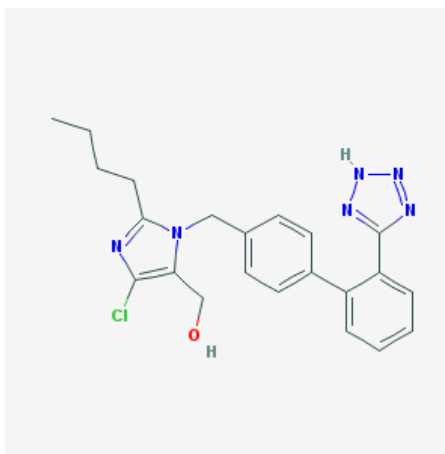


Figure 4. Structure of Losartan

## Ullmann Conditions for Catalysis of Cross Coupling Reactions

### Forming C-N Bonds

Copper mediated C-N, C-O, and C-C bond formation reactions were first reported a hundred years ago in the pioneering work of Ullmann and Goldberg. Harsh reaction conditions and low substrate scope hampered these reactions in the synthesis of natural products. In the past 10 years or so, the development of highly efficient catalytic systems has allowed reactions to be conducted under milder conditions and with dramatically enhanced yields compared to the classical methods. Copper mediated catalysis now has applications in natural product synthesis. An array of copper mediated procedures have been successfully employed to make many complex targets with new and efficient

bond disconnections. Copper-catalyzed cross-coupling reactions are often not too sensitive to the choice of the copper source [copper (I) in most cases]; however, the choice of ligand, base, and solvent are often critical to the success of the reaction. The quality and particle size of inorganic bases can have a dramatic impact on the yields and kinetics of the reaction (416). In 1998, Chan (417) and Lam (418) independently published reports of copper-mediated arylation of N-nucleophiles using stoichiometric copper (II) acetate and boronic acids at room temperature with a wide range of nucleophiles. Over the last 10 years this arylation of N-nucleophiles with arylboronic acid has become a standard (419). More recently, the introduction of chelating ligands has led to dramatic improvements, and many milder Ullmann-type procedures have been reported, which have allowed for the use of simpler arylating agents such as aryl halides. The basis for the Ullmann reaction is the use of a copper catalyst, which includes Cu, CuI, CuBr, CuCl, CuCN, Cu<sub>2</sub>O, as well as copper compounds in the +2 oxidation state. An organic ligand is also often used. Substrates can be aryl or alkyl halides with the halide portion being Cl, Br, or I, as well as boronic acid, which reacts with a primary amine, secondary amine, amino alcohol, or N-heterocyclic amine. The final product consists of a new C-N bond between the RX and the N-nucleophile amine compound, where the N of the amine is attached to the carbon originally bearing the halide. Various bases used for the reaction include potassium or sodium t-butoxide, potassium carbonate, cesium carbonate, potassium phosphate, and sodium hydroxide. Solvents used include

dioxane, toluene, DMF, acetonitrile, DMSO, methylene chloride, isopropyl alcohol, and methanol. In some cases, the solvent plays a dual role as ligand and solvent (416).

### **HeLa Cells to Test Cancer Cell Killing Potential**

The term HeLa refers to the first two letters of the first and last name of Henrietta Lacks, from whom the original cells were cultured. Ms. Lacks was 30 years old when she was diagnosed with an aggressive form of a glandular adenocarcinoma of the cervix in 1951. Cervical cancer is typically slow growing, and the survival period for most patients is five years from the time of diagnosis. Henrietta Lacks did not have an ordinary cancer, and according to Dr. Howard Jones, her gynecologist, her cancer was purple and soft, unlike any cancer he had ever seen before. This cancer did not respond to radiotherapy. It was a rare adenocarcinoma (420) and not of epidermal origin as is usually the case with cervical cancers. Henrietta Lacks died only eight months after her initial diagnosis with cervical cancer (421).

In February of 1951, Dr. George Gey, a respected researcher at Johns Hopkins hospital in Baltimore, Maryland, was given a small sample of cells from Henrietta Lacks. He established a tissue culture using these cells by using plasma obtained from a chicken heart, extract from calf embryos, and human placental blood from umbilical cords. These cells became an immortal line of cancer cells that have been used to gain knowledge of every fundamental process that occurs in human cells (421). Research on the Human Papilloma

Virus (HPV) uncovered how Henrietta's cancer began. HPV inserted its DNA into her eleventh chromosome and turned off her p53 tumor suppressor gene. Scientists learned from studying HeLa that cancer cells could divide indefinitely. They also knew that there was a portion of DNA at the end of each chromosome called a telomere. These telomeres shortened a little bit each time a cell divided. When the telomeres are almost gone, the cells stop dividing and begin to die. In the early nineties, a scientist at Yale used HeLa cells to discover that human cancer cells contain an enzyme called telomerase. The purpose of this enzyme is to rebuild telomeres. Telomerase allows cells to regenerate their telomeres indefinitely. This explained the immortality of the HeLa cells – telomerase continued to rebuild Henrietta's telomeres so that the cells never grew old and never died (422).

## CHAPTER TWO

### PURPOSE OF THE RESEARCH

The goal of the research is to synthesize a conjugated photosensitizer that will absorb light in the wavelength range of 600 – 900 nm, and produce significant amounts of singlet oxygen so that tumor cells are killed. Absorption of light in the long wavelength visible region to the near IR region will allow deeper tissue tumors to be treated with PDT.

If the PS is attached to cross-linked hemoglobin, upon the absorption of the light, O<sub>2</sub>, which is present in the heme pocket, could become converted to singlet oxygen. The PS does not have to be attached to hemoglobin to be effective; however, if tumor tissue is hypoxic, an available supply of oxygen is present in the heme. If the photosensitizer is linked to folic acid, the molecule can be taken in more readily by tumor cells. The reason for this is that folate receptors are over-expressed in cancerous tissue. This allows photodynamic therapy to have greater specificity for tumor cells, leaving normal cells less damaged. Because traditional chemotherapy targets not only the tumor, but also healthy cells, especially fast growing cells, such as hair follicles and the lining of the colon, side effects such as hair loss and diarrhea result. This weakens the patient (423); therefore, targeting tumor cells is less toxic to the patient. The photosensitizer complex, which will consist of the PS with a polyethylene

glycol linker, folate, and Hb, will enter the cell by a process known as endocytosis. During the process of endocytosis, the substance enters the cell without directly passing through the cell membrane. In the specific type of endocytosis known as receptor-mediated endocytosis, the specific molecules are ingested into the cell due to a receptor ligand interaction. Receptors on the plasma membrane of the target tissue will specifically bind to ligands on the outside of the cell. This process results in the formation of an intracellular vesicle by invagination of the plasma membrane and membrane fusion (424). See Figure 5. below.

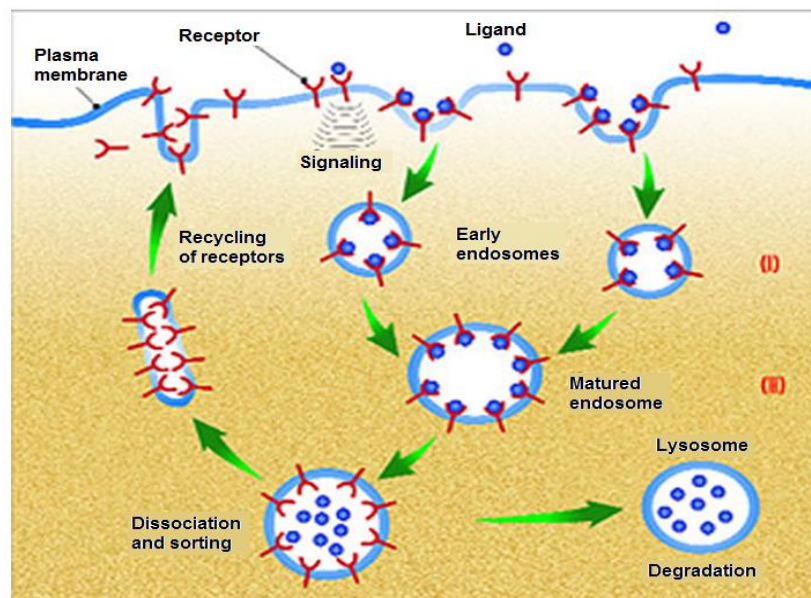


Figure 5. Endocytosis

Ref: <http://www.expresspharmaonline.com/20060815/research03.shtml>

Since Hb will be traveling in the body outside of the red blood cell, this molecule must be stabilized by reacting the beta<sub>1</sub>-82 and beta<sub>2</sub>-82 lysines with

DBSF [Bis(3,5-dibromosalicyl)fumarate] (425). See Figure 6. Once the PS complex is in the cell, when light in the IR region is directed to the patient, reactive singlet oxygen is generated, resulting in cell destruction.

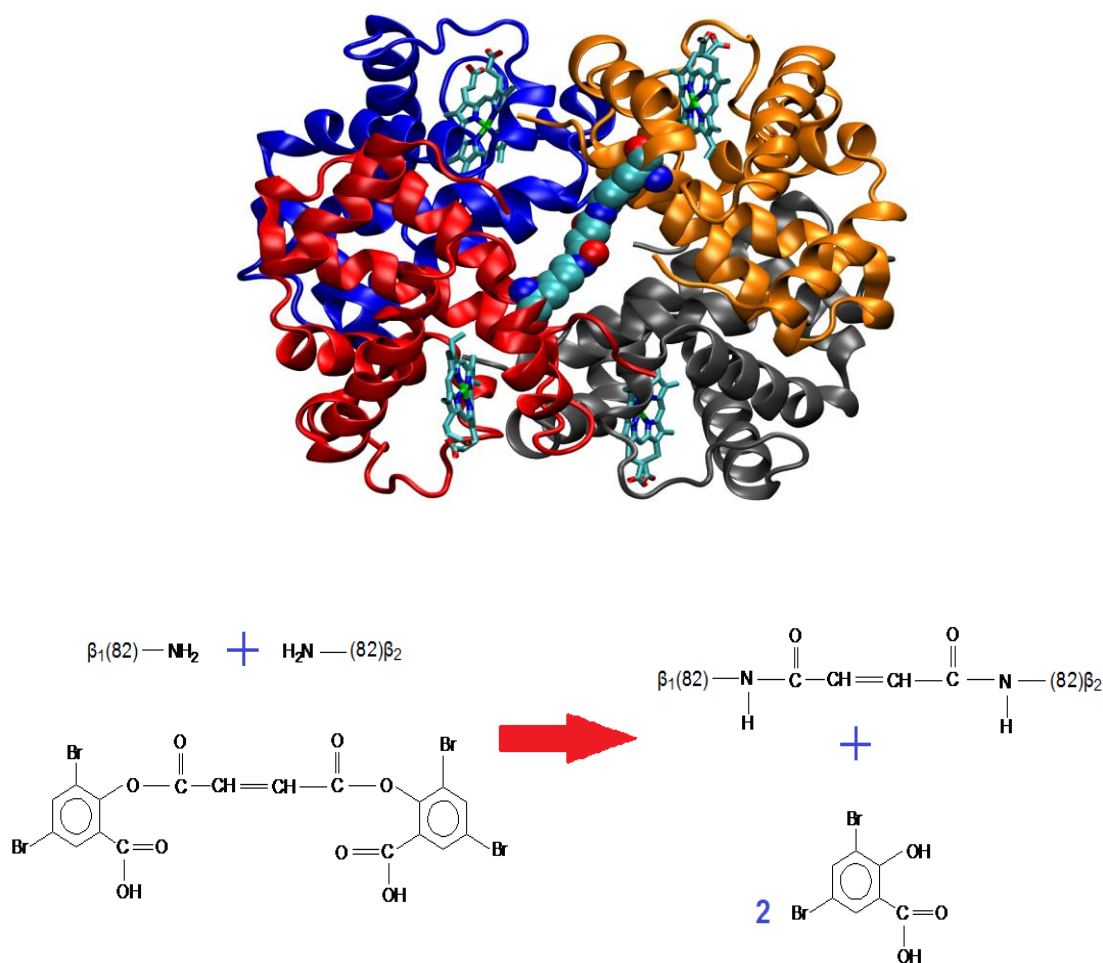


Figure 6. Cross-linked Hemoglobin

Due to the large molecular weight of the PS complex, oral administration is not possible according to Lipinski's rules, which state that a molecular weight greater than 500 will not be orally bioavailable (426). Therefore, administration



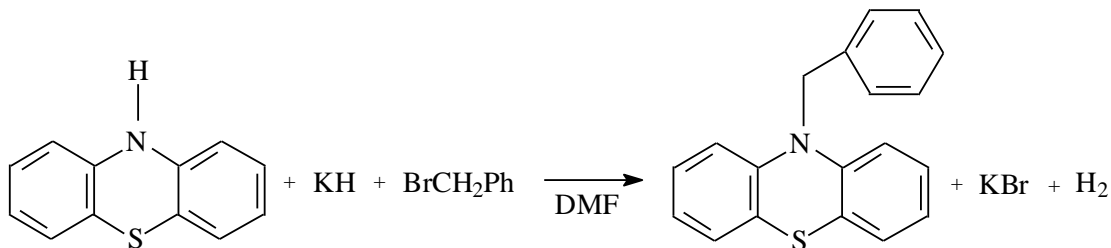
must be accomplished via intravenous injection in a vein near the tumor site, or intramuscular injection at a location near the tumor. Human serum albumin may be able to act as a carrier within the blood via intermolecular van der Waals attractions, which allows transport to the tumor site.

Internal organs may be treated by use of endoscopes and fiberoptic catheters to deliver the light to a photosensitizer. The major disadvantage of PDT is that the light which activates most photosensitizers is unable to penetrate through more than 1/3 inch (approximately 1 cm) of tissue, hence the development of a PS that can absorb light of longer wavelengths. Treatment by light which cannot penetrate deeper into the skin is limited to tumors on the skin or lining of some of the internal organs. PDT is also less effective for the treatment of large tumors and metastatic cancers due to the limitation discussed above (427).

**CHAPTER THREE**  
**EXPERIMENTAL RESEARCH & DEVELOPMENT**

**Experimental Description of Research**

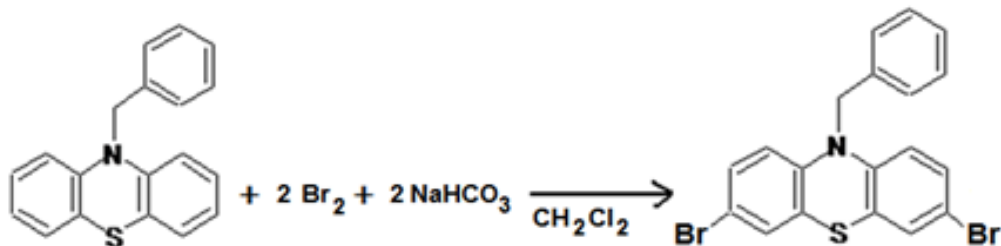
The synthesis of the photosensitizer consists of three reactions. The initial starting material is phenothiazine. Reaction 1 is protection of the N atom of phenothiazine (428). The compound used for this purpose is benzyl bromide. The final product is N-benzylphenothiazine. The reaction is shown below.



Scheme 1. Synthesis of N-benzylphenothiazine

The N atom of phenothiazine must be protected from bromination in the next phase of the synthesis, and also from oxidation. The purpose of the KH is to deprotonate the N-H, allowing N to attack the C attached to Br in benzyl bromide, forming a new C-N bond.

Reaction 2 consists of bromination of the N-benzylphenothiazine to form N-benzyl-3,7-dibromophenothiazine (429). The reaction is shown on the following page.



Scheme 2. Synthesis of N-benzyl-3,7-dibromophenothiazine

The purpose of the  $\text{NaHCO}_3$  is to neutralize any  $\text{HBr}$  that is produced after bromine replaces the H atoms on the two phenothiazine aromatic rings.

Reaction 3 consists of replacing the bromine atoms with the phenothiazine heterocycle. Other heterocycles that could replace the bromine atoms include carbazole, indole, or pyrrole. Structures of each of these compounds are shown below in Figure 7. Bromine could be replaced in order to increase the level of

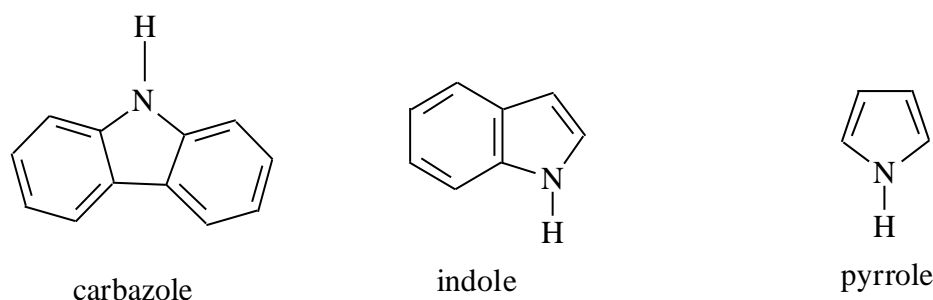
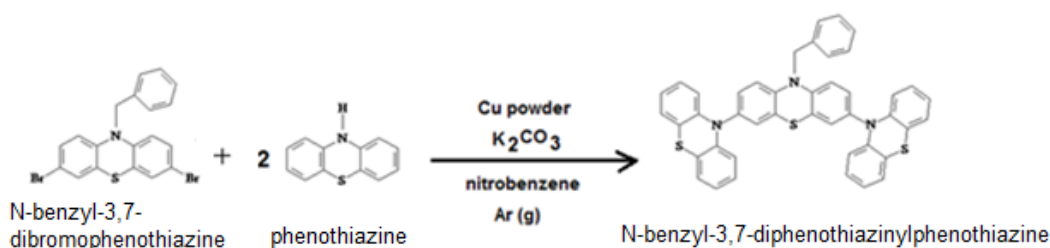


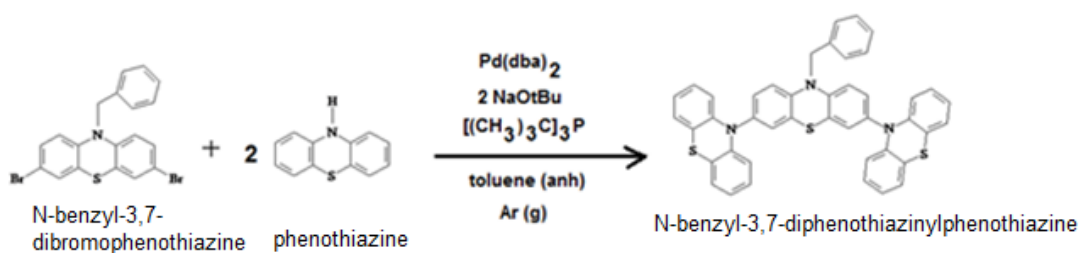
Figure 7. Other Heterocyclic Compounds to Replace Bromine

conjugation of the photosensitizer so that the absorption of light can be in the near IR range. Light of this range is better able to penetrate deeper tissues, so that cancers other than surface cancers can be treated more effectively using PDT. Initial research, however, was focused on replacing the bromine atoms with

phenothiazine to form N-benzyl-3,7-diphenothiazinylphenothiazine (phenothiazine trimer). Two approaches were used to synthesize the phenothiazine trimer. One reaction utilized Ullmann copper catalysts (Scheme 3)(430), and the other reaction utilized Buchwald-Hartwig palladium catalysts (Scheme 4) (431). Each reaction scheme is shown below.



Scheme 3. Ullmann Reaction Attempt to Produce Phenothiazine Trimer

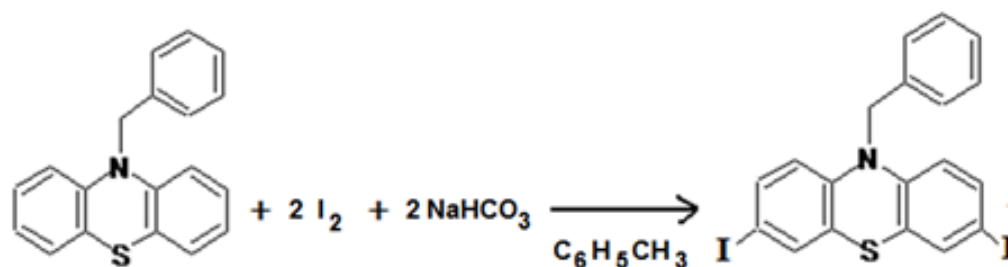


Scheme 4. Buchwald-Hartwig Reaction to Produce Phenothiazine Trimer

A TLC (mobile phase – 40 %  $\text{CH}_2\text{Cl}_2$  in hexane) of the Ullmann reaction products showed two new spots ( $R_f = 0.267$ ;  $R_f = 0.467$ ) that did not correspond to the starting materials of phenothiazine ( $R_f = 0.347$ ) or N-benzyl-3,7-dibromophenothiazine ( $R_f = 0.613$ ). A silica gel column using 10 % ethyl acetate in petroleum ether (432) was used for chromatography of the Ullmann products.

A total of 36 fractions were collected and TLC was run on all fractions, including a 37<sup>th</sup> fraction consisting of nitrobenzene solvent. Based on TLC results, fractions 25 – 36, 17 – 24, 13 – 16, and 11 – 12 were combined into pre-weighed 50 mL round bottom flasks. Approximately 1 mL of diethyl ether was added to each of the four round bottom flasks and rotary evaporation was used to remove solvent, followed by vacuum to dry the product. Solid from fractions 25 – 36 and 17 – 24 was combined and CDCl<sub>3</sub> was added to run proton NMRs of these combined fractions. This reaction yielded 19.6 mg (13 %) of expected product. NMR results showed one peak at 5.0 ppm, which is the CH<sub>2</sub> of the benzyl protection group, and indicates that the phenothiazine trimer was synthesized. However, the product was still impure, since a doublet found at 6.45 – 6.48 was indicative of some N-benzyl-3,7-dibromophenothiazine starting material.

The Ullmann reaction often works more effectively with iodides; therefore, iodination of N-benzylphenothiazine was attempted. Iodide is usually a more effective leaving group than bromide, due to its larger size and polarizability. The reaction for iodination of N-benzylphenothiazine is shown in Scheme 5.



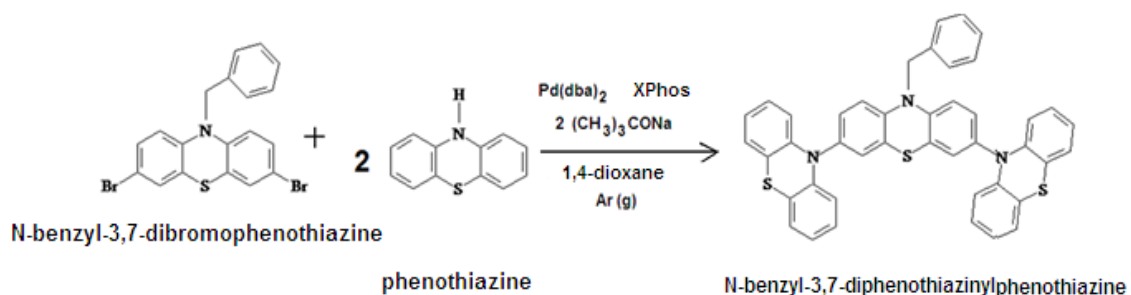
Scheme 5. Synthetic Approach to N-benzyl-3,7-diiodophenothiazine

Other iodination reactions have been attempted with  $\text{CH}_2\text{Cl}_2$  as solvent, and also using N-benzyl-3,7-dibromophenothiazine as the starting material with an  $\text{HIO}_3$  catalyst (433). An iodination reaction using N-benzyl-3,7-dibromophenothiazine, under Ullmann conditions, with KI as the iodine source,  $\text{K}_3\text{PO}_4$  as base, a Cu powder catalyst, and  $\text{CH}_3\text{CN}$  solvent was also attempted (434). These attempts suggested that iodination would be a low yield step, so it was decided to discontinue attempts to make N-benzyl-3,7-diiodophenothiazine. N-benzyl-3,7-dibromophenothiazine worked effectively in the the Buchwald-Hartwig Pd-catalyzed synthesis of the trimer, which was more effective than the Ullmann reactions.

The weight of the crude N-benzyl-3,7-diphenothiazinylphenothiazine product from the Buchwald-Hartwig reaction was 2.3 mg (1.4 % yield). TLC data (mobile phase - 10 % ether in hexane) for this reaction showed two new spots ( $R_f = 0.022$ ;  $R_f = 0.143$ ) that did not correspond to starting materials of phenothiazine ( $R_f = 0.077$ ) or N-benzyl-3,7-dibromophenothiazine ( $R_f = 0.198$ ). According to NMR data, the presence of four peaks at 5.0 ppm is indicative of impure product. Presence of peak closest to 5.0 ppm suggests the presence of the N-benzyl-3,7-dibromophenothiazine starting material.

Conditions were optimized by changing the solvent, ligand, and reaction temperature for the B-H Pd-catalyzed cross coupling of N-benzyl-3,7-dibromophenothiazine and phenothiazine to form the phenothiazine trimer as shown in Scheme 6. Structures of the ligand and catalyst are also shown in

Figure 8 (435). All future syntheses of the trimer utilized these conditions.



Scheme 6. Buchwald-Hartwig Synthesis of Phenothiazine Trimer

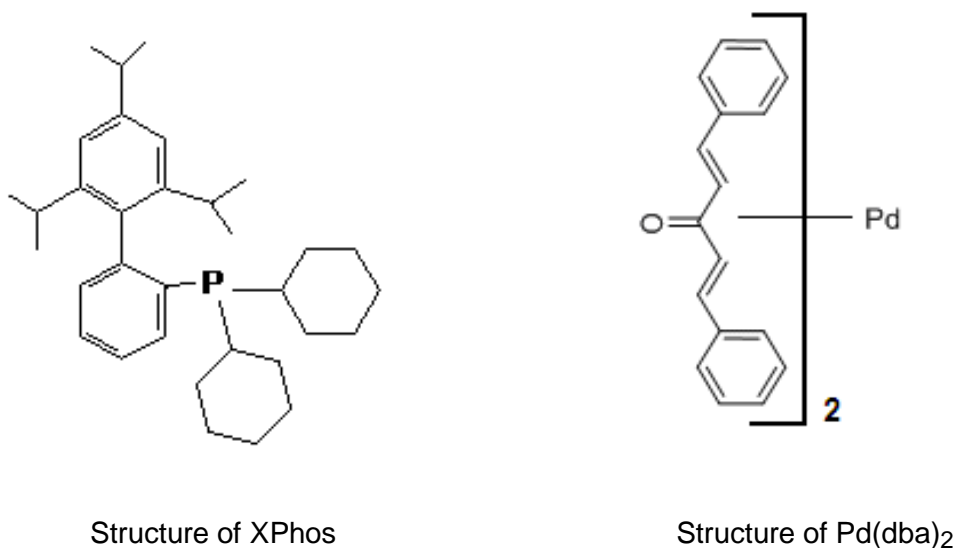


Figure 8. Structures of XPhos Ligand and Pd Catalyst

A sample of 41.4 mg of the product from the reaction using the optimized Buchwald-Hartwig conditions was purified via column chromatography using 230 - 400 mesh silica gel and gradient elution with mobile phases consisting of 10 % diethyl ether, 2 % triethylamine, 88 % hexane; 20 % diethyl ether, 2 % triethylamine, 78 % hexane; 30 % diethyl ether, 2 % triethylamine, 68 % hexane;

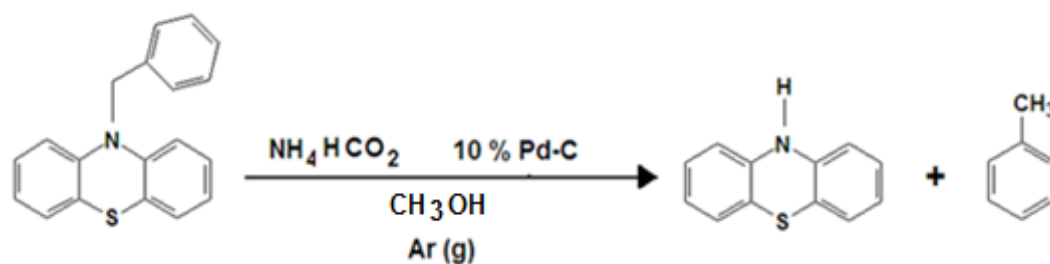
50 % diethyl ether, 2 % triethylamine, 48 % hexane; and 98 % diethyl ether, 2 % triethylamine. An NMR was taken of each set of combined fractions collected from the column.

A sample of 60.7 mg of the product from this same reaction was purified via column chromatography using an automated flash system with a 4 gram pre-packed column of silica gel and gradient elution with mobile phases consisting of 10 % diethyl ether, 1 % triethylamine, 89 % hexane; 20 % diethyl ether, 1 % triethylamine, 79 % hexane; and 50 % diethyl ether, 1 % triethylamine, 49 % hexane. An NMR was taken of each set of combined fractions collected from the column.

Subsequent reactions were purified via an automated flash system using a 4 g pre-packed silica gel column (column ht = 6.25 cm; column diam = 1.28 cm; column vol = 8 mL), and the best chromatographic conditions were determined to be a 6 % flow rate (1.33 mL/min) using a mobile phase of 10 % ether / 90 % hexane for the first 24 fractions, followed by a 20 % ether / 80 % hexane mobile phase for the next set of 12 fractions.

In order to attach a polyethylene glycol (PEG) linker to increase water solubility of the trimer, the benzyl protection group must be removed. Several deprotection reactions were attempted on a model reaction utilizing N-benzylphenothiazine (436-439). The reaction is shown in Scheme 7.





Scheme 7. Model Deprotection of N-benzylphenothiazine

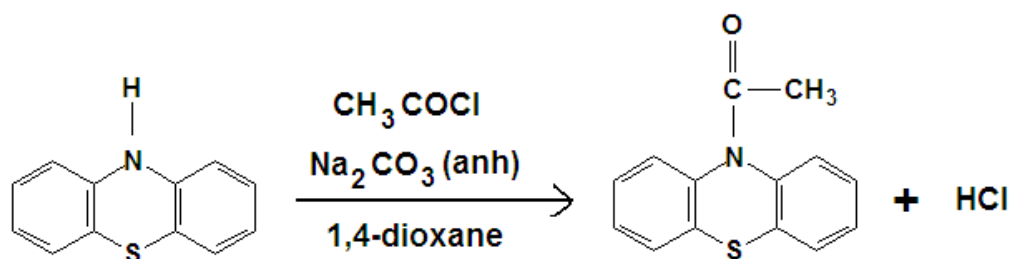
The next section will describe the variations on this procedure. Variations to the reactants in terms of the catalytic transfer hydrogen used include the following: increasing the equivalents of ammonium formate from 5 to 10 to 15; changing to 5 eq of 1,4-cyclohexadiene; changing to 4.4 % HCOOH (88 – 90 % reagent strength) and 10 % HCOOH; using both HCOOH and ammonium formate and varying the quantity of the HCOOH and the equivalents of ammonium formate. Variations to the solvent include the following: using  $\text{CH}_2\text{Cl}_2$ , tetrahydrofuran (THF), or 1,4-dioxane to dissolve the N-benzylphenothiazine; using methanol, ethanol, butanol, 1,4-dioxane, as well as combinations of butanol and  $\text{CH}_2\text{Cl}_2$  (1:1 and 3:1) as solvent. Variations to the catalyst include the following: using glacial acetic acid in 1:9 and 2:8 ratios with solvent for a total of 10 mL; using 10 mL glacial acetic acid without solvent. Temperature variations included: Room Temp; 60°C; 70°C; 80°C; 100°C; 112°C; 117°C. Variations to the reaction time include: a minimum of 39 h 15 min to ~ 10 days with variations in between these time ranges. Reaction vessel variations included: 25 mL RB; 50 mL RB; 15 mL PT; 30 mL PT.

Since TLC is very qualitative, NMR studies were completed to determine

the approximate percentages of phenothiazine (deprotected) and N-benzylphenothiazine (protected) present in the product. The results of this NMR study showed that the best deprotection reaction yielded 43.2 % phenothiazine and 56.8 % N-benzylphenothiazine. Since less than 50 % of the sample was deprotected in the best case, a new direction was taken for the synthesis of the phenothiazine trimer, which will be discussed later in this report.

Concurrent with the deprotection studies, studies on the acetylation of the phenothiazine N atom were completed in order to determine the type of PEG linker to be used if the deprotection studies had been successful. The next section will describe the two reactions used to acetylate the phenothiazine N atom.

The first reaction used acetyl chloride to acetylate phenothiazine (440). The reaction is shown below.



Scheme 8. Model Acetylation of Phenothiazine using Acetyl Chloride

NMR data show that the phenothiazine was successfully acetylated with this procedure; however, the type of PEG linker needed would be one with a protected amine group on one end and a  $\text{COOH}$  on the other end, which would

form an amide bond to the phenothiazine N as shown in Figure 9.

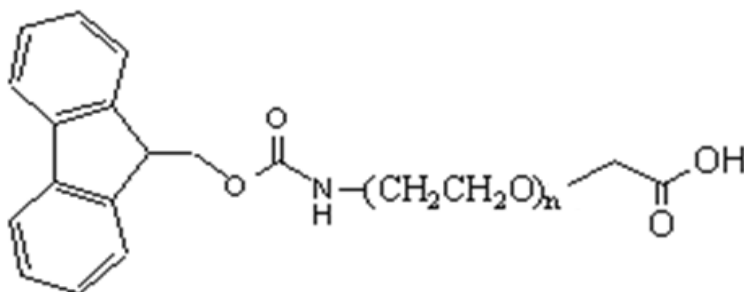


Figure 9. Structure of PEG linker with COOH group

However, for the amide bond to occur, the COOH end of the PEG would either need to be converted to COCl, which requires an extra step using SOCl<sub>2</sub>, or the phenothiazine could be acetylated using an NHS ester (440), since PEG linkers are available with a protected amine on one end and an NHS ester on the other, and, like Cl, an NHS ester is a good leaving group as shown in Figure 10.

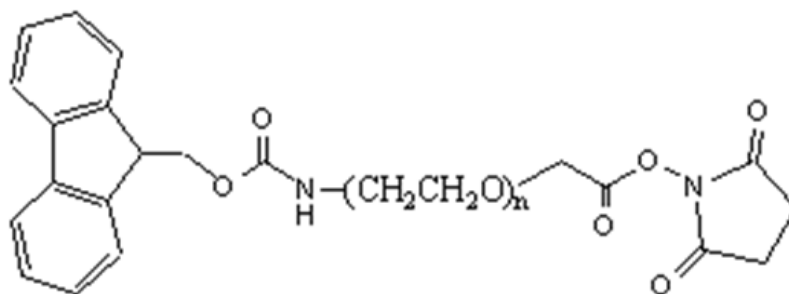
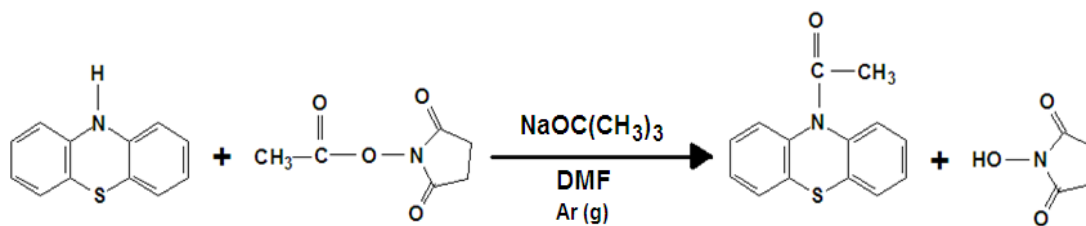


Figure 10. Structure of PEG linker with NHS ester group

The reaction of phenothiazine with acetic acid NHS ester is shown below.



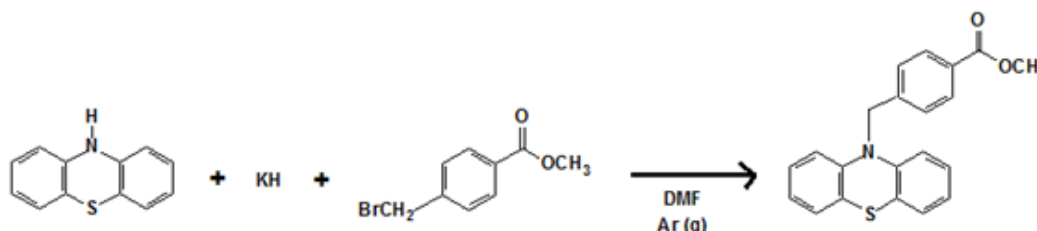
Scheme 9. Model Acetylation of Phenothiazine using Acetic Acid NHS Ester

TLC and NMR data showed that most of the product was still not acetylated; therefore, several variations on the procedure shown in Scheme 9 were attempted. This reaction was repeated 9 more times with some variations to the procedure. Variations to the reactants included the following: decrease in starting amount of phenothiazine to 50 mg and then 30 mg; making the acetic acid NHS ester the limiting reagent as opposed to phenothiazine and using 20 mg acetic acid NHS ester; using 2 equivalents of KH as the base; using 2 and 2.5 equivalents of NaOtBu as the base; using 2 and 4 equivalents of lithium diisopropyl amide (LDA) as the base. Variations to the solvent include the following: using toluene and 1-butanol (NHS ester and NaOtBu do not dissolve in toluene); using dimethylformamide (DMF); using tetrahydrofuran (THF); using a biphasic system of toluene and water. Variations in the temperature of the reaction include the following: increasing the temperature to 105°C, 110°C, 120°C, 135°C, 140°C; decreasing the temperature to 65°C. The length of time for the reaction varied from 48 h to 7 days.

NMR analysis showed that the best acetylation reaction by acetic acid

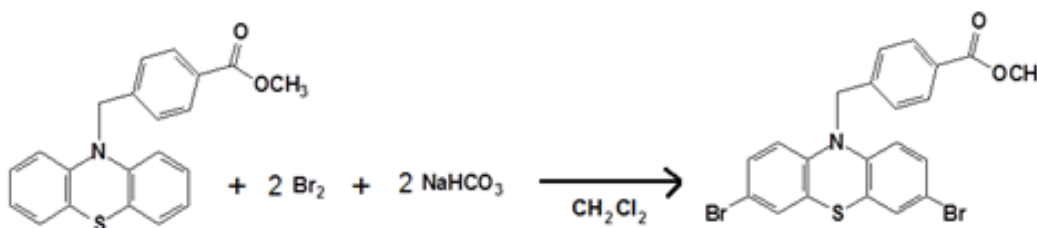
NHS ester yielded 31.5 % acetylphenothiazine and 68.5 % phenothiazine.

The low yields of benzyl deprotection and acylation in the model studies led to the choice of a new protection group, methyl 4-(bromomethyl)benzoate. Since an ester is attached to the aromatic ring, it will not be necessary to remove this protection group, since an amide bond can be directly made with an amine PEG and the carbonyl of the ester group. The first step in this 3 step synthesis is to protect phenothiazine shown in Scheme 10 (428).



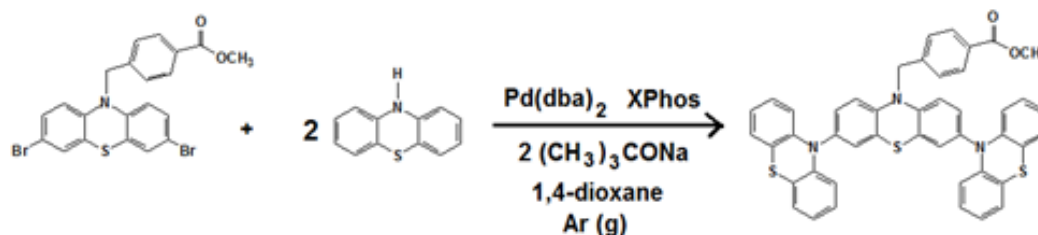
Scheme 10. Phenothiazine Protection using methyl 4-(bromomethyl)benzoate

The next step in the synthesis is the bromination of methyl 4-N-methylene phenothiazinylbenzoate (429) as shown in Scheme 11.



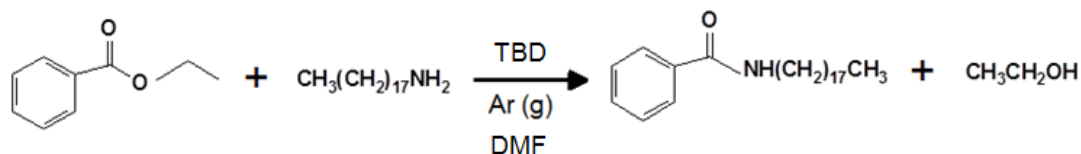
Scheme 11. Bromination of methyl 4-N-methylenephenothiazinylbenzoate

The third and final step in the synthesis is the replacement of the Br atoms by phenothiazine utilizing a Buchwald-Hartwig Pd-catalyzed cross coupling reaction (435) as shown in Scheme 12.



Scheme 12. Synthesis of methyl (3,7-diphenothiazinyl)-4-N-methylene-phenothiazinylbenzoate

Following synthesis of the benzoate protected phenothiazine trimer, an amine PEG attached to folic acid will be bonded to the carbonyl group of the benzoate portion of the trimer. A model aminolysis was set up with ethyl benzoate to represent the carbonyl group of the protecting group on the trimer and octadecylamine to represent the amine PEG, using a TBD (1,5,7-Triazabicyclo[4.4.0]dec-5-ene) catalyst (441). The reaction and mechanism are shown in Scheme 13. and Figure 11.



Scheme 13. Model Reaction Synthesis of N-octadecylbenzamide

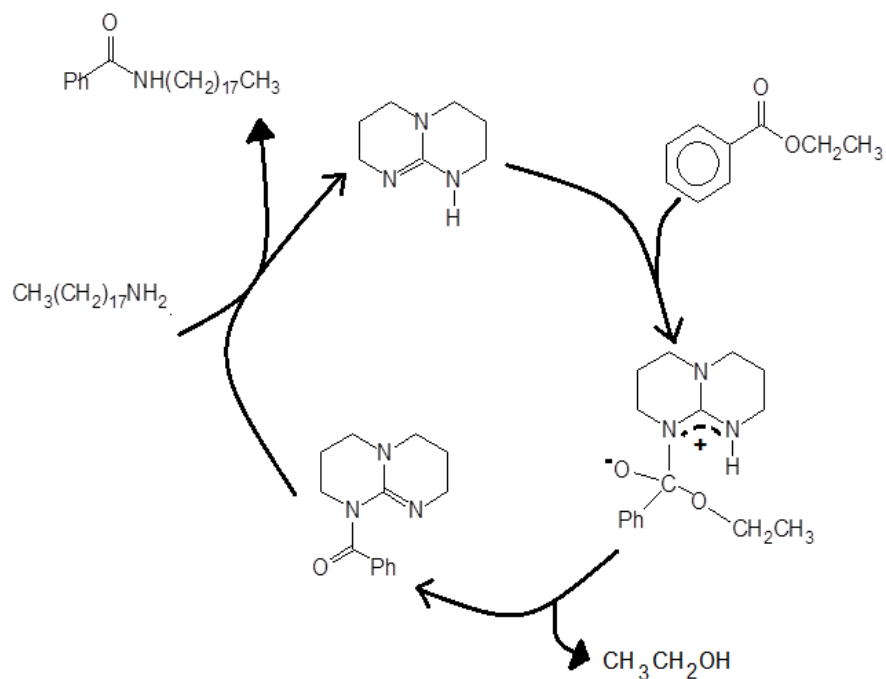
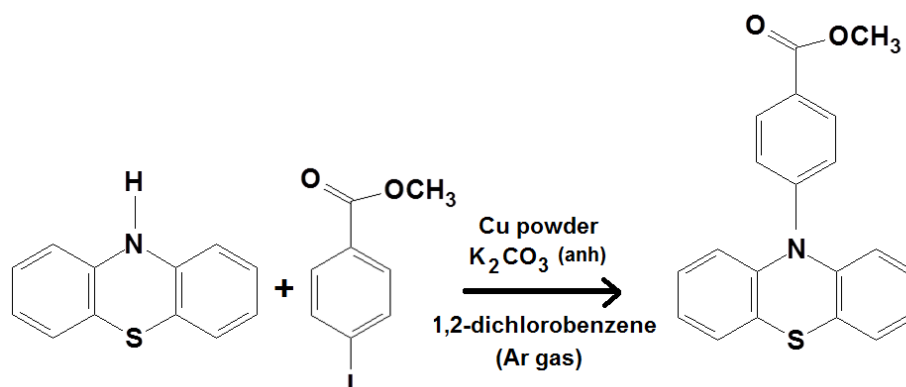


Figure 11. Mechanism of Aminolysis Using TBD Catalyst

Due to the lack of light absorption in the 600 – 900 nm UV-VIS region for both methyl (3,7-diphenothiazinyl)-4-N-methylenephenothiazinylbenzoate, and N-benzyl-3,7-diphenothiazinylphenothiazine (UV-VIS Spectra shown in Figures 27 and 28 in Appendix A), an Ullmann reaction, which gave a 68 % yield of methyl 4-N-phenothiazinylbenzoate, was completed. This reaction is shown in Scheme 14 (442).



Scheme 14. Ullmann Synthesis of methyl 4-N-phenothiazinylbenzoate

A UV spectrum taken of a 0.5405 mM sample dissolved in acetonitrile indicated that the product also did not absorb in the 600 – 900 nm range.

Since this compound and the previously synthesized phenothiazine trimers did not absorb light in the necessary range, a chlorin e6 derivative was chosen as the PS for cell killing studies. Chlorin e6 is a known PS that absorbs light at 660 nm (144). PEGylation of chlorin e6 utilized an NH<sub>2</sub>-PEG-Folate compound shown in Figure 12.

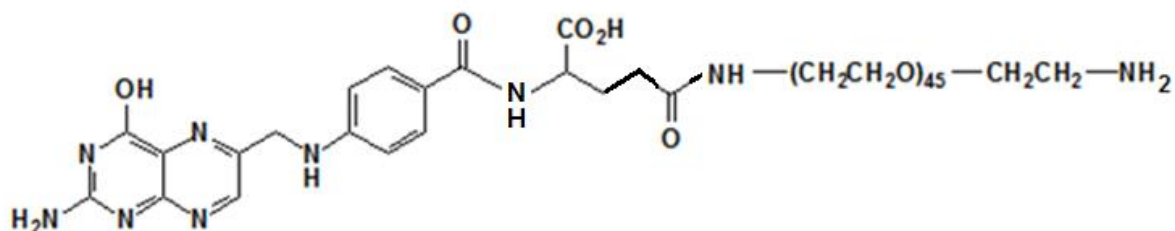
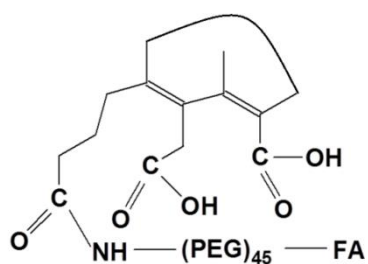
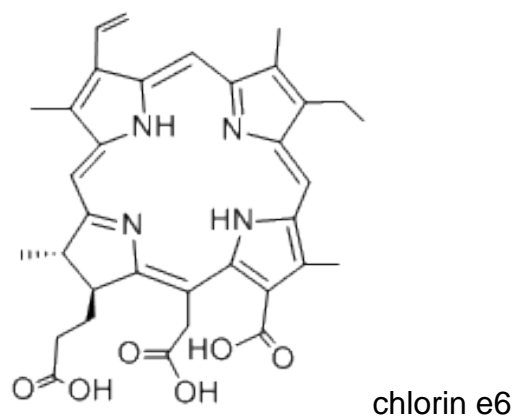


Figure 12. Structure of NH<sub>2</sub>-PEG-FA



The polyethylene glycol portion of the compound consists of ~45 PEG units with the  $\gamma$  C=O group of folic acid amide bonded to one end of the PEG and a free amine on the other end of the PEG. The  $\text{NH}_2$ -PEG-Folate was covalently bonded to the C-17 carboxylic acid group of the chlorin e6 as an amide (443). A 5:1 ratio of chlorin to  $\text{NH}_2$ -PEG-FA was used to maximize product formation. The reaction is shown in Scheme 15, and the mechanism of the reaction is shown in Figure 13.



Scheme 15. Synthesis of Chlorin e6-PEG-Folate

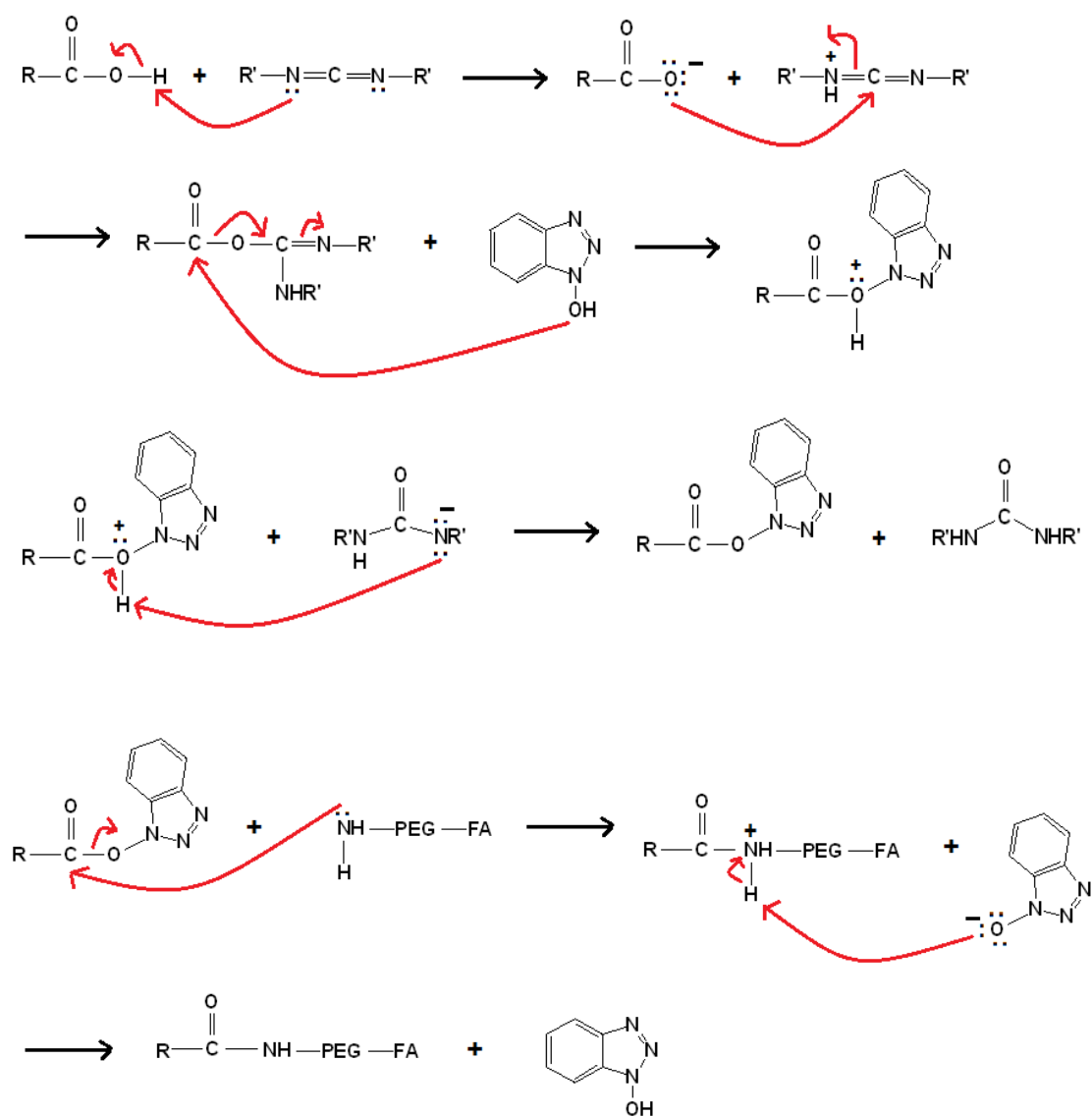


Figure 13. Mechanism of Amide Coupling of Chlorin e6 to  $NH_2$ -PEG-FA  
(Note –  $RCOOH$  indicates the carboxylic acid group at C-17 of Chlorin e6)

The product was purified by using a centrifugal filter with a molecular weight cutoff of 2000 Daltons. The approximate molecular weight of chlorin linked to PEG-FA is 3042.7 mg / mmol and the molecular weight of free chlorin is

596.7 mg / mmol; therefore, excess chlorin e6 will be removed from the product into the filtrate. The purified product was removed from the centrifuge filter by washing with PBS solution. A UV-VIS spectrum of the product in PBS is shown in Figure 14.

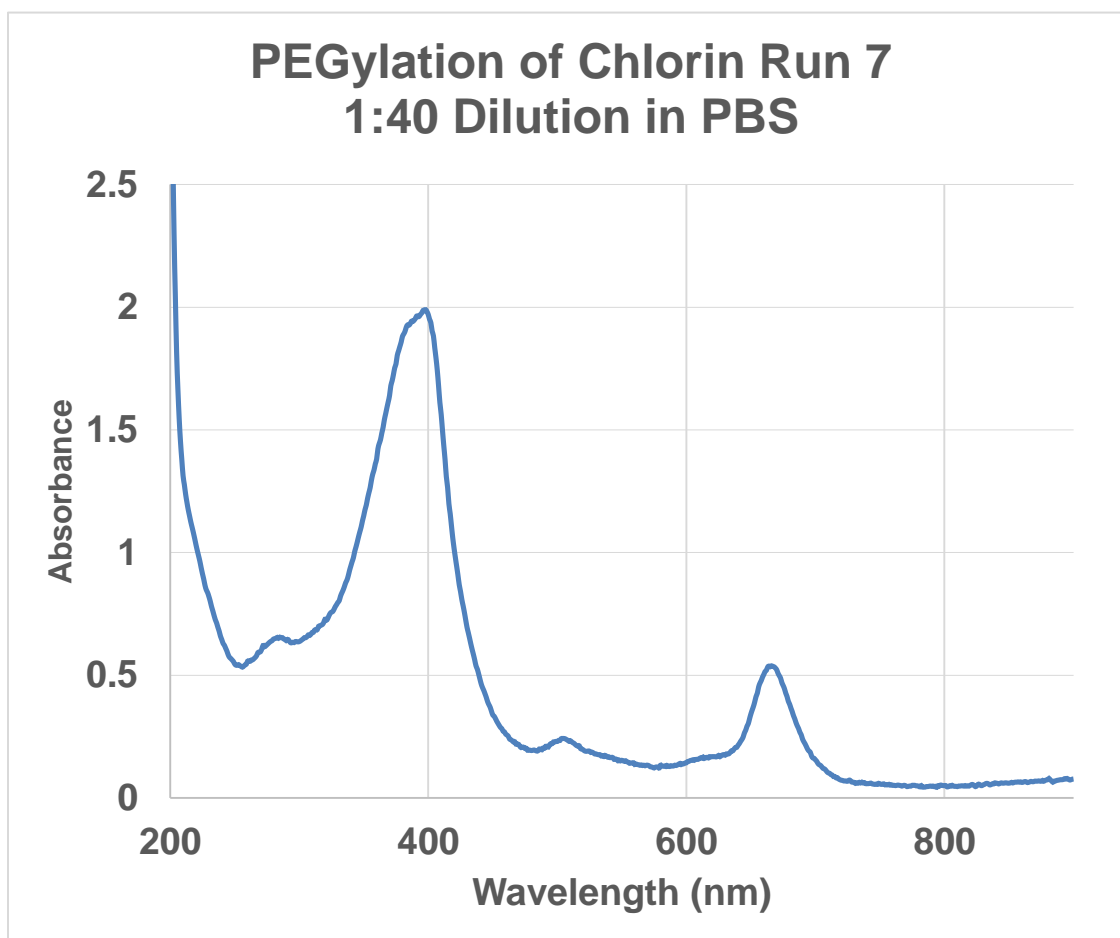


Figure 14. UV-VIS spectrum of Ce6-PEG-FA in PBS

Epsilon values were calculated for folate (283 nm) and for chlorin e6 (402 and 660 nm) from UV-VIS absorbance data for known concentrations of folate and chlorin e6. Excel charts of this data are shown in Table 1 on page 93, as well as graphs of the UV-VIS spectra (see Appendix A). Using Beer's Law, and the known epsilon values from the chlorin and folate standards, the concentrations of chlorin and folate were calculated using the UV data of the product. These calculated concentrations were then used to determine the ratio of folate to chlorin (see Tables 2 and 3, pp. 94 - 95). A 1:1 ratio indicates a successful reaction. The volume of the collected Ce6-PEG-FA product and the calculated chlorin concentration determined from the absorbance at 660 nm was used to calculate the percent yield.

<b>UV Data of Known Concentrations of Chlorin e6 and Folate</b>						
	Abs	Epsilon	Abs	Epsilon	Abs	Epsilon
	283 nm	283 nm	402 nm	402 nm	660 nm	660 nm
Chlorin 0.00523 mM	0.13	24,900	0.902	172,000	0.174	33,300
Chlorin 0.00525 mM	0.094	17,900	0.693	132,000	0.139	26,500
Chlorin 0.0105 mM	0.168	16,000	1.464	139,000	0.27	25,700
Chlorin 0.0105 mM	0.19	18,100	1.75	167,000	0.324	30,900
Folate 0.0296 mM	0.837	28,300				
Folate 0.0296 mM	0.809	27,300				
Folate 0.0592 mM	1.412	23,900				
Folate 0.0599 mM	1.516	25,300				
Average Epsilon Chlorin 283 nm	19,225					
St Dev Chlorin 283	3900					
Average Epsilon Folate 283 nm	26,200					
St Dev Folate 283	1977					
Average Epsilon Chlorin 402 nm	152,500					
St Dev Chlorin 402	19,942					
Average Epsilon Chlorin 660 nm	29,100					
St Dev Chlorin 660	3615					
Outlier Tests						
Chlorin Epsilon 283	0.8269	0.2885	0.3398	1.4552		No outliers
Folate Epsilon 283	0.4553	1.1637	0.5565	1.0625		No outliers
Chlorin Epsilon 402	0.6770	0.7271	1.0280	0.9779		No outliers
Chlorin Epsilon 660	1.1619	0.7193	0.9406	0.4980		No outliers
4 values = 1.4962						

Table 1. UV-VIS Data of Known Concentrations of Ce6 and Folate

Abs. Folate / Chlorin 283 nm 0.654	<b>1:40 Dilution in PBS</b>	
Abs. Folate ONLY 0.481	Epsilon Folate 283 nm 26,200	Concentration Folate 0.0184 mM x 40 = 0.736 mM
Abs. Chlorin 402 nm 1.937	Epsilon Chlorin 402 nm 153,000	Concentration Chlorin 0.0127 mM x 40 = 0.508 mM
Abs. Chlorin 660 nm 0.503	Epsilon Chlorin 660 nm 29,100	Concentration Chlorin 0.0173 mM x 40 = 0.692 mM

Table 2. Calculations of Concentration of Folate and Chlorin from UV-VIS Data and Epsilons of Known Concentrations (1:40 Dilution in PBS)

**Ratio to determine absorbance of folate at 283 nm if folate standard concentration = unknown concentration of 0.0173 mM**

$$0.823 / 0.0296 \text{ mM} = x / 0.0173 \text{ mM} \quad x = 0.481$$

Abs. Folate / Chlorin 283 nm 1.401	<b>1:20 Dilution in PBS</b>	
Abs. Folate ONLY 1.018	Epsilon Folate 283 nm 26,200	Concentration Folate 0.0389 mM x 20 = 0.778 mM
Abs. Chlorin 402 nm Peak off scale		
Abs. Chlorin 660 nm 1.066	Epsilon Chlorin 660 nm 29,100	Concentration Chlorin 0.0366 mM x 20 = 0.732 mM

Table 3. Calculations of Concentration of Folate and Chlorin from UV-VIS Data and Epsilons of Known Concentrations (1:20 Dilution in PBS)

**Ratio to determine absorbance of folate at 283 nm if folate standard concentration = unknown concentration of 0.0366 mM**

$$0.823 / 0.0296 \text{ mM} = x / 0.0366 \text{ mM} \quad x = 1.018$$

**Average concentration of Chlorin at 660 nm:**

$$0.692 \text{ mM} + 0.732 \text{ mM} / 2 = 0.712 \text{ mM}$$

**Percent Yield:**

$$3.0 \text{ mL} \times 0.712 \text{ mmol} / 1000 \text{ mL} \times 3042 \text{ mg} / \text{mmol} = 6.5 \text{ mg}$$

$$6.5 \text{ mg} / 6.9 \text{ mg} \times 100 = 94 \%$$

**Ratio of Folate : Chlorin**       $0.757 / 0.712 = 1.06 : 1$

## Experimental Materials

### Chemical Materials

Petroleum ether, diethyl ether, 1,4-cyclohexadiene, and acetyl chloride were purchased from Alfa Aesar. Methylene chloride was purchased from BDH. Carbazole was purchased from Eastman. Methanol was purchased from Fisher Scientific. Copper spheres were purchased from Flinn Scientific. Tetrahydrofuran was purchased from Fluka. Chlorin e6 was purchased from Frontier Scientific. Ethyl acetate was purchased from J. T. Baker. Silica gel (230 – 400 mesh), 4 gram pre-packed silica gel chromabond flash columns, and thin layer chromatography plates were purchased from Macherey Nagel. Nitrobenzene was purchased from Mallinckrodt. The NH<sub>2</sub>-PEG-Folate (MW 2463) compound was purchased from Nanocs, Inc. Acetic acid N-hydroxysuccinimide ester was purchased from Research Organics. Copper powder was purchased from Sargent Welch. The Vivaspin 2 centrifugal concentrator filter (MWCO 2000 Da) was purchased from Sartorius Corporation. XPhos was purchased from Strem Chemicals. All other chemicals were purchased from Sigma-Aldrich. <sup>1</sup>H and <sup>13</sup>C spectra were recorded in CDCl<sub>3</sub> solution on Varian INOVA 300 MHz and 500 MHz spectrometers. Chemical shifts were expressed downfield from internal tetramethylsilane (TMS, δ 0 ppm). <sup>1</sup>H NMR data were recorded stating the chemical shift, the number of protons and the multiplicity, which was noted as follows: (s, singlet; d, doublet; t, triplet; q, quartet; m, multiplet; dd doublet of doublets; td triplet of doublets). ESI-MS spectra were obtained on an Agilent



6460 Triple Quad and a ThermoFinnigan LCQ Advantage Ion Trap mass spectrometer. MALDI-MS were obtained from Washington University, St. Louis, MO. IR data were obtained on a Shimadzu IRAffinity-1S FTIR Spectrophotometer. UV-VIS data were obtained on an Ultrospec 2100 Pro Spectrophotometer.

### **Biological Materials**

RPMI cell culture media was purchased from Sigma Aldrich. Cell Star solid black 96 well tissue culture plates were purchased from VWR. LED lamp was purchased from Elixia, Ltd. The CellTiter-Blue Cell Viability Assay was purchased from Promega. HeLa cells were obtained from Professor Stefan Kanzok's research lab at Loyola University Chicago.

## **Experimental Procedures**

### **Synthesis of N-benzylphenothiazine**

A 2.79 g (20.9 mmol) sample of 30% potassium hydride suspension was placed in a 30 mL beaker in the hood and washed three times with 20 mL portions of petroleum ether. The solid was then carefully transferred to an oven dried 50 mL round bottom flask containing 10 mL of dry DMF, a stir bar and a rubber septum with a syringe needle connected to a bubbler and a syringe needle attached to a nitrogen line. Then, 2.05 g (10.3 mmol) of phenothiazine in 30 mL of DMF was added with a syringe while stirring. After 4 min, 4.0 mL (30 mmol) of benzyl bromide was added over 1 min via syringe. The mixture was flushed with nitrogen for approximately 10 min. After 4 hr of stirring, the reaction

was quenched by cautiously adding 40 mL of water over 15 min. The reaction mixture was transferred to a separatory funnel and was extracted 3 times with 20 mL portions of ethyl acetate. The combined organic layers were washed with three 20 mL volumes of water and one 20 mL volume of brine. The organic layer was dried over anhydrous sodium sulfate and then transferred to a weighed round bottom flask, concentrated and pumped to afford a viscous liquid which was analyzed by TLC. Crude weight of N-benzylphenothiazine was 2.08 g (70 % yield). Recrystallization from petroleum ether gave 1.72 g (58 % yield) of light pink crystalline solid N-benzylphenothiazine; mp 90–91°C [lit 90–91°C (425)].

$^1\text{H}$  NMR (300 MHz)  $\delta$  7.28 (m, 5 H), 7.07 (dd, 2 H,  $J = 9$  Hz, 3 Hz), 6.96 (td, 2 H,  $J = 8$  Hz, 7 Hz, 2 Hz), 6.85 (td, 2 H,  $J = 9$  Hz, 6 Hz, 2 Hz), 6.62 (dd, 2 H,  $J = 9$  Hz, 3 Hz), 5.08 (s, 2 H).  $^{13}\text{C}$  NMR (75 MHz)  $\delta$  144.5, 136.6, 128.7, 127.2, 127.0, 126.8, 126.6, 123.1, 122.5, 115.4, 52.7

### **Synthesis of N-benzyl-3,7-dibromophenothiazine**

A 300 mg (1.04 mmol) sample of N-benzylphenothiazine was added to a 10 mL round bottom flask, along with ~ 5 mL  $\text{CH}_2\text{Cl}_2$ , ~200 mg (2.38 mmol)  $\text{NaHCO}_3$  and a stir bar. A rubber septum with a syringe needle connected to a bubbler and a syringe needle attached to a nitrogen line was attached. A sample of 0.11 mL (2.1 mmol)  $\text{Br}_2$  was added slowly via syringe. The mixture was flushed with nitrogen for 10 min. The reaction was protected from light by covering the flask with aluminum foil. The reaction was allowed to proceed for 24 h. The

reaction mixture was transferred to a separatory funnel and was extracted 3 times with 10 mL portions of methylene chloride. The combined organic layers were washed with three 10 mL volumes of water and one 10 mL volume of brine. The organic layer was transferred to a weighed round bottom flask, concentrated and pumped to afford a crystalline solid, which was analyzed by TLC ( $R_f = 0.510$ ). Crude weight of N-benzyl-3,7-dibromophenothiazine was 375.1 mg (91%). Recrystallization from petroleum ether yielded 207.8 mg (51%) of a blue crystalline solid N-benzyl-3,7-dibromophenothiazine; mp 130–131°C

$^1\text{H NMR}$  (300 MHz)  $\delta$  7.29 (m, 5 H), 7.18 (d, 2 H,  $J = 3$  Hz), 7.05 (dd, 2 H,  $J = 9$  Hz, 3 Hz), 6.46 (d, 2 H,  $J = 9$  Hz), 5.01 (s, 2 H).  $^{13}\text{C NMR}$  (75 MHz)  $\delta$  143.3, 135.5, 130.1, 129.1, 128.9, 127.4, 126.5, 124.7, 116.7, 115.0, 52.7

#### **Attempted Ullmann Synthesis of N-benzyl-3,7-diphenothiazinyl-phenothiazine**

A 100 mg (0.224 mmol) sample of N-benzyl-3,7-dibromophenothiazine, 98.1 mg (0.492 mmol) phenothiazine, 61.8 mg (0.448 mmol) anh.  $\text{K}_2\text{CO}_3$ , 5.7 mg (0.089 mmol) Cu powder, 6.5 mL nitrobenzene, and a stir bar were added to a pressure tube. The solution and air space above solution were flushed with nitrogen, and the pressure tube was tightly capped and immersed in a 100°C oil bath. The reaction was run for 24 h. The cooled reaction mixture was transferred to a separatory funnel and extracted 2 times with 10 mL of methylene chloride. The combined organic layers were washed with two 10 mL volumes of water. The organic layer was transferred to a weighed round bottom flask, concentrated

and pumped to remove the solvent.

### **Buchwald-Hartwig Synthesis of N-benzyl-3,7-diphenothiazinyl-phenothiazine**

A 10.6 mg (0.0184 mmol; 0.1 eq) sample of Pd(dba)<sub>2</sub> catalyst was mixed with 82.5 mg (0.185 mmol; 1 eq) of N-benzyl-3,7-dibromophenothiazine and 17.8 mg (0.0373 mmol; 0.2 eq) XPhos ligand in a 15 mL pressure tube with a stir bar. A volume of 4 mL of dry 1,4-dioxane solvent was added to the pressure tube. An Ar atmosphere was delivered above the solution for 20 min. Then, 76.9 mg (0.386 mmol; 2.0 eq) phenothiazine and 60.4 mg (0.628 mmol; 3.4 eq) NaOC(CH<sub>3</sub>)<sub>3</sub> base was added to the pressure tube and an Ar atmosphere was delivered into the solution for 10 min. The pressure tube was placed in an oil bath at 130 °C and allowed to react for 48 h. A small amount of solution was withdrawn at 24 h to do a TLC (mobile phase 30 % ether /70 % hexane). An Ar atmosphere was delivered into the solution for 20 min before replacing the pressure tube in the oil bath. A final TLC was performed at the end of 48 h. The product mixture was extracted three times with diethyl ether and washed three times with water. The solvent was removed and the product dried under vacuum. Purification by column chromatography and automated flash chromatography yielded 59.2 mg (94.3 %) of cream colored crystals; mp = 148.1–149.3°C.

<sup>1</sup>H NMR (500 MHz) δ 7.44 (dd, 2 H, J = 8 Hz, 3 Hz), 7.40 (dd, 2 H, J = 9 Hz, 3 Hz), 7.34 (m, 1 H), 7.11 (d, 2 H, J = 3 Hz), 7.02 (dd, 2 H, J = 9 Hz, 2 Hz), 6.99 (dd, 4 H, J = 8 Hz, 2 Hz), 6.88 (td, 4 H, J = 8 Hz, 8 Hz, 1 Hz), 6.83 (d, 2 H, J = 9

Hz), 6.80 (td, 4 H, J = 8 Hz, 8 Hz, 1 Hz), 6.30 (dd, 4 H, J = 8 Hz, 2 Hz), 5.21 (s, 2 H).  $^{13}\text{C}$  NMR (125 MHz)  $\delta$  144.2, 143.9, 135.8, 135.7, 129.9, 129.0, 128.9, 127.4, 126.8, 126.7, 126.4, 125.0, 122.5, 120.3, 117.0, 116.0, 53.4; IR (KBr pellet) 3053 (C-H), 2951, 2920, 2846 (C-H), 1591 (C=C), 1303 (C-N), 742 (monosub. Ar ring); 2D NMR: COSY – correlations: 6.30 / 6.80 ortho coupling; 6.30 / 6.88 meta coupling; 6.80 / 6.88 ortho coupling; 6.80 / 6.99 meta coupling; 6.83 / 7.02 ortho coupling; 7.02 / 7.11 meta coupling; 7.34 / 7.40 ortho coupling; 7.34 / 7.44 meta coupling; 7.40 / 7.44 ortho coupling; HSQC – correlations: C 53.4 to H 5.21; C 116.0 to H 6.30; C 117.0 to H 6.83; C 120.3 (Quat.); C 122.5 to H 6.80; C 125.0 (Quat.); C 126.5 to H 7.40; C 126.7 to H 6.88; C 126.8 to H 6.99; C 127.4 to H 7.34; C 128.9 to H 7.11; C 129.0 to H 7.43; C 129.9 to H 7.02; C 135.8 (Quat.); C 135.9 (Quat.); C 143.9 (Quat.); C 144.2 (Quat.); MS:  $\text{M}^+$  peak at 683.2 m/z (N-benzyl-3,7-diphenothiazinylphenothiazine); no significant fragmentation peaks HRMS:  $\text{M}^+$  peak at 683.1529 m/z (N-benzyl-3,7-diphenothiazinylphenothiazine); HRMS calcd for  $\text{C}_{43}\text{H}_{29}\text{N}_3\text{S}_3$ , 683.1523; obsvd 683.1529.

### **Procedure for Deprotection of N-benzylphenothiazine**

A 20 mg (0.069 mmol) sample of N-benzylphenothiazine was placed in a 15 mL pressure tube containing a stir bar to which 2.0 mL  $\text{CH}_2\text{Cl}_2$  was added to dissolve the sample. Ar gas was added to remove any air from the system. A 25.5 mg sample of 10 % Pd on activated charcoal was added to a beaker along with 65.8 mg (1.04 mmol; 15 eq.) ammonium formate (used as the catalytic

transfer hydrogen) and 2 mL n-butanol. This solution was added to the pressure tube via syringe. The pressure tube was capped, placed in a 117°C oil bath, and allowed to react for ~5 d. TLC and NMR data showed that most of the material was still protected. NMR analysis showed that the best deprotection reaction yielded only 43.2 % phenothiazine and 56.8 % unreacted N-benzylphenothiazine.

### **Synthesis of Acetyl Phenothiazine Using Acetyl Chloride**

To a 100 mL RB flask with a stir bar, 2.8 g (26 mmol) anh.  $\text{Na}_2\text{CO}_3$ , 20 mL 1,4-dioxane, and 1.41 g (7.08 mmol) phenothiazine were added. Next, 1.5 mL (21 mmol; 3 eq.) of acetyl chloride was slowly added via syringe over a period of 5 min. Ar gas was blanketed over the solution for 10 min to expel air within the RB. The RB was placed in a 105°C oil bath and allowed to react for 48 h. The product was extracted with 3 – 10 mL portions of diethyl ether, and washed with 3 – 10 mL portions of water. Rotary evaporation and hyvac were used to remove the solvent.

Three additional reactions were run with slight variations of this procedure. The variations involved the mass of phenothiazine reactant, which was changed to 200 mg. The equivalents of acetyl chloride were changed from 3 to 2, and a 15 mL PT was used instead of a RB flask. The temperature was changed to 101°C, which is the boiling point of 1,4-dioxane. Finally, for the fourth reaction, to determine if product forms at lower temperatures, the oil bath temperature was set to 60°C. Crude yields of a cream colored solid ranged from 123.1–224.6 mg (50–93 %) with mps of 197–208°C. Purification was not completed.

### **Synthesis of Acetyl Phenothiazine Using Acetic Acid NHS Ester**

To a 15 mL PT with a stir bar, 200. mg (1.89 mmol) anh.  $\text{Na}_2\text{CO}_3$ , 6 mL 1,4-dioxane, and 100. mg (0.502 mmol) phenothiazine were added. Next, 118.2 mg (0.753 mmol; 1.5 eq.) acetic acid NHS ester was added to the PT. Ar gas was blanketed over the solution for 15 min to expel air. The PT was placed in a 102°C oil bath and allowed to react for ~ 8 days. The product was extracted with 3 – 10 mL portions of diethyl ether, and washed with 3 – 10 mL portions of water. The solvent was removed, and the product dried under vacuum. TLC and NMR data showed that most of the product was still not acetylated. The NMR analysis showed that the best acetylation reaction by acetic acid NHS ester yielded 31.5 % acetylphenothiazine and 68.5 % phenothiazine.

### **Synthesis of Methyl 4-N-methylenphenothiazinylbenzoate**

To a 50 mL RB flask, 277.6 mg (2.076 mmol) of KH mineral oil emulsion was added, and then washed three times with hexane. A stir bar and septum were added and the flask was blanketed with Ar gas. Then 203.3 mg; (1.020 mmol) of phenothiazine dissolved in 5 mL DMF was added via syringe. After waiting 30 min to allow for deprotonation, 308.1 mg (1.345 mmol) methyl 4-(bromomethyl)benzoate dissolved in 5 mL DMF was added via syringe. Ar gas from a balloon needle blanketed the reaction mixture. After 48 h, at room temp, the reaction was quenched with 1.0 mL (0.77 mmol) of a 50:50 mixture of glacial acetic acid and water. Approximately 10 mg of  $\text{NaHCO}_3$  was added to neutralize the acid. The reaction mixture was extracted with 3 – 10 mL volumes of diethyl

ether. The combined ether layers were washed with 3 – 10 mL volumes of brine, followed by 3 – 10 mL volumes of water, and then dried over MgSO<sub>4</sub>. The solvent was removed, and the product dried under vacuum to afford 926.3 mg (> 100 %) of crude methyl 4-N-methylenephenothiazinylbenzoate.

The crude product was purified via flash column chromatography utilizing a 4 g pre-packed column (column ht = 6.25 cm; column diam = 1.28 cm; column vol = 8 mL). The mobile phase consisted of 10 % diethyl ether / 90 % PET, and the flow rate was set at 3.45 mL/min. Purification yielded 253.3 mg (71.4 %) of a yellow orange crystalline solid; mp = 122 – 125°C. <sup>1</sup>H NMR (300 MHz) δ 8.00 (d, 2 H, J = 8 Hz), 7.40 (d, 2 H, J = 8 Hz), 7.06 (dd, 2 H, J = 9 Hz, 2 Hz), 6.97 (td, 2 H, J = 8 Hz, 7 Hz, 2 Hz), 6.87 (td, 2 H, J = 7 Hz, 8 Hz, 1 Hz), 6.58 (dd, 2 H, J = 8 Hz, 2 Hz), 5.13 (s, 2 H), 3.90 (s, 3 H). <sup>13</sup>C NMR (75 MHz) δ 166.8, 144.3, 142.3, 130.1, 129.1, 127.2, 127.0, 126.7, 123.5, 122.7, 115.3, 52.5, 52.2; HRMS calcd for C<sub>21</sub>H<sub>17</sub>NO<sub>2</sub>S, 347.0980; calcd. for C<sub>21</sub>H<sub>17</sub>NO<sub>2</sub>S+Na\*, 370.0878, obsvd 370.0879. NOTE: \*Sample was sent to Washington University in a screw capped glass vial, and the presence of Na is ubiquitous in glass.

### **Synthesis of Methyl (3,7-dibromo)-4-N-methylenephenothiazinylbenzoate**

To a 15 mL PT containing a stir bar and septum, 29.8 mg (0.355 mmol) of NaHCO<sub>3</sub> was added. Then, 61.4 mg (0.177 mmol) methyl 4-N-methylene-phenothiazinylbenzoate dissolved in 2.0 mL CH<sub>2</sub>Cl<sub>2</sub> was added. Next, a solution of 2.0 mL of CH<sub>2</sub>Cl<sub>2</sub> containing 18 μL (0.35 mmol) of Br<sub>2</sub> was added to the PT. Foil was placed around the PT and the reaction allowed to react for 72 h at RT.



The reaction mixture was extracted with 3 – 10 mL volumes of diethyl ether, then washed with 2 – 10 mL volumes of water, followed by 1 – 10 mL volume of brine. The solvent was removed, and the product dried under vacuum to yield 141.1 mg (78 %) of crude methyl (3,7-dibromo)-4-N-methylenephenothiazinylbenzoate.

The crude product was purified via flash column chromatography utilizing a 4 g pre-packed column (column ht = 6.25 cm; column diam = 1.28 cm; column vol = 8 mL). The mobile phase consisted of 10 % diethyl ether / 90 % PET, and the flow rate was set at 15 % (3.45 mL/min). Purification yielded 96.4 mg (53 %) of a blue crystalline solid; mp = 144–147°C. <sup>1</sup>H NMR (300 MHz) δ 8.00 (d, 2 H, J = 9 Hz), 7.35 (d, 2 H, J = 9 Hz), 7.20 (d, 2 H, J = 3 Hz), 7.07 (dd, 2 H, J = 8 Hz, 2 Hz), 6.42 (d, 2 H, J = 9 Hz), 5.04 (s, 2 H), 3.91 (s, 3 H). <sup>13</sup>C NMR (75 MHz) δ 166.6, 143.1, 141.1, 130.2, 130.2, 129.5, 129.4, 126.6, 125.1, 116.6, 115.3, 52.5, 52.2

### **Synthesis of Methyl (3,7-diphenothiazinyl)-4-N-methylenephenothiazinylbenzoate**

To an oven dried 15 mL pressure tube (PT) containing a stir bar, 13.6 mg (0.0238 mmol; 0.2 eq) of Pd(dba)<sub>2</sub> catalyst, 60.0 mg (0.119 mmol; 1 eq) of methyl (3,7-dibromo)-4-N-methylenephenothiazinylbenzoate, and 22.3 mg (0.0475 mmol; 0.4 eq) of XPhos ligand were added. Ar gas was added for 10 min to flush air from the PT. Then 4 mL of dry 1,4-dioxane was added via syringe. An Ar atmosphere was maintained above the solution for an additional 20 min. Then, 53.0 mg (0.261 mmol; 2.2 eq) phenothiazine and 34.8 mg (0.333 mmol; 2.8 eq)

NaOC(CH<sub>3</sub>)<sub>3</sub> base were added to the PT and Ar was bubbled into the solution for 10 min. The PT was placed in an oil bath at 130°C and reacted for 72 h. After cooling, 20 mL of diethyl ether was added and the organic layer washed with 4 – 10 mL volumes of water. The solvent was removed, and the product dried under vacuum to yield 87.0 mg (99 %) of crude methyl (3,7-diphenothiazinyl)-4-N-methylenephenothiazinylbenzoate as a brown solid. It was purified using a silica gel column to yield 14 mg (16 %) of methyl (3,7-diphenothiazinyl)-4-N-methylenephenothiazinylbenzoate as a yellow solid, mp = 168–174°C.

<sup>1</sup>H NMR (500 MHz) δ 8.10 (d, 2 H, J = 8 Hz), 7.51 (d, 2 H, J = 8 Hz), 7.14 (d, 2 H, J = 2 Hz), 7.03 (dd, 2 H, J = 9 Hz, 2 Hz), 7.00 (dd, 4 H, J = 8 Hz, 2 Hz), 6.89 (td, 4 H, J = 8 Hz, 8 Hz, 2 Hz), 6.84 (d, 2 H, J = 10 Hz), 6.79 (td, 4 H, J = 9 Hz, 9 Hz, 2 Hz), 6.30 (dd, 4 H, J = 8 Hz, 2 Hz), 5.25 (s, 2 H), 3.93 (s, 3 H). <sup>13</sup>C NMR (125 MHz) δ 166.7, 144.1, 143.6, 141.3, 136.0, 130.4, 129.9, 129.6, 129.1, 126.9, 126.8, 126.6, 125.3, 122.6, 120.4, 116.9, 116.0, 53.2, 52.2; IR (KBr pellet) 3088, 3049 (C-H), 2998, 2986 (C-H), 1721 (C=O), 1654 (C=C), 1300 (C-N), 1238, 1215 (C-O), 744 (p-disub. ring); HRMS calcd for C<sub>45</sub>H<sub>31</sub>N<sub>3</sub>S<sub>3</sub>O<sub>2</sub>, 741.1578; obsvd 741.1558.

### Synthesis of N-Octadecylbenzamide

To an oven dried 15 mL pressure tube with a stir bar, a septum was added, and air was evacuated by adding Ar gas for 10 min. Next, 157 mg (0.583 mmol) of octadecylamine and 2 mL DMF were added to the pressure tube. Then, 24.3 mg (0.175 mmol) TBD catalyst and 0.1 mL (0.7 mmol) ethyl benzoate were

added to the pressure tube. Air was evacuated again by adding Ar gas above the solution for 20 min. The reaction was warmed to 130°C in an oil bath and run for a minimum of 24 h. The product was extracted with 3 – 10 mL portions of diethyl ether, and washed with 3 – 10 mL portions of water. The solvent was removed and the product dried under vacuum. Crude yields of an off white crystalline solid ranged from 201–267 mg (88–96%); mp 66–78°C. Purification was not completed. NMR analysis indicated that the product was formed, as evidenced by peaks in the aromatic region as well as the peak for the CH<sub>2</sub> of the hydrocarbon chain bonded to the amide N, and the terminal CH<sub>3</sub> of the hydrocarbon chain. However, ethyl benzoate starting material remains, as is evidenced by the peaks at 4.4 ppm and 1.4 ppm which belong to the ethoxyl group. Peaks which belong to the TBD catalyst at ~2 and ~ 3 ppm were also present.

#### **Ullmann Synthesis of Methyl 4-N-phenothiazinylbenzoate**

To a 15 mL PT with stir bar that was oven dried overnight, was added 28.6 mg (0.447 mmol; 1.78 eq) Cu powder, 51.3 mg (0.258 mmol; 1 eq) phenothiazine, 44.3 mg (0.321 mmol; 1.28 eq) anh. K<sub>2</sub>CO<sub>3</sub>, and 100.8 mg (0.385 mmol; 1.53 eq) methyl 4-iodobenzoate. A septum was placed on the PT and Ar gas was added above the solids for 15 min. Then 1 mL of 1,2-dichlorobenzene solvent was added via syringe through the septum. Ar gas was added into the solution for 10 min. The PT was capped and heated to reflux for 72 h in a 180°C oil bath. After cooling, solids were filtered out of the solution. The product was

purified via a 4 gram pre-packed silica gel column (column ht = 6.25 cm; column diam = 1.28 cm; column vol = 8 mL) using a flash chromatography system. Flow rate was set to 3.45 mL/min and hexane was used to remove dichlorobenzene, followed by 3.3 % ether / 96.7 % hexane to elute the product. Purification yielded 58 mg (68 %) of the product as a yellow solid; mp = 130–136°C. <sup>1</sup>H NMR (500 MHz) δ 8.05 (d, 2 H, J = 8 Hz), 7.26 (dd, 2 H, J = 8 Hz, 2 Hz), 7.23 (d, 2 H, J = 8 Hz), 7.10 (td, 2 H, J = 8 Hz, 8 Hz, 2 Hz), 7.03 (td, 2 H, J = 8 Hz, 8 Hz, 2 Hz), 6.84 (dd, 2 H, J = 8 Hz, 1 Hz), 3.91 (s, 3 H)

### **Synthesis of Chlorin e6–PEG–Folate Conjugate**

To a 10 mL rb flask that was flushed with Ar gas for 3 min was added 5.6 mg (2.3 μmol) NH<sub>2</sub>–PEG–FA, followed by 1 mL CH<sub>2</sub>Cl<sub>2</sub>. Then, 7.1 mg (12 μmol) Chlorin e6 was added, followed by 2 μL of triethylamine. The solution was allowed to react for 5 min at RT. Then, 1.6 mg (12 μmol) of HOBt and 2.7 mg (13 μmol) of DCC were quickly added to the solution. The flask was stoppered, covered with foil, and allowed to react for 96 h at RT.

The CH<sub>2</sub>Cl<sub>2</sub> was removed by rotary evaporation and ~ 3 mL PBS was added to the flask. The contents were transferred, in increments, to a centrifuge filtration tube with a molecular weight cutoff of 2000 daltons to remove unreacted starting materials. The product was rinsed multiple times with ~1 mL of phosphate buffered saline (PBS) and centrifuged for 30 min until the filtrate was clear. The centrifuge filter with product was transferred to a 15 mL plastic conical tube and the centrifuge filter was soaked for 24 hr at 7°C with ~ 1 mL of PBS to

recover the product in 3.0 mL of solution. A UV-VIS spectrum of the solution was obtained and the chlorin e6 absorbance at 660 nm = 0.503 (1:40 dilution of product) and 1.066 (1:20 dilution of product); Epsilon = 29,100. The product yield was 6.5 mg (94%).  $^1\text{H}$  and  $^{13}\text{C}$  NMR spectra and a Mass spectrum were also obtained.  $^1\text{H}$  NMR clearly shows the peaks for the aminobenzoate portion of folate as well as the PEG [(500 MHz)  $\delta$  7.71 (dd, 2 H, J = 9 Hz, 3.5 Hz), 7.52 (dd, 2 H, J = 9.5 Hz, 3.5 Hz), 3.64 (s, 180 H)]; however, the concentration is too dilute to show peaks that are readily interpretable for both  $^1\text{H}$  and  $^{13}\text{C}$  NMR; UV-Vis (PBS)  $\lambda_{\text{max}}/\text{nm}$ : 283 ( $\epsilon$  Ce6 19,200; Folate 26,200), 402 ( $\epsilon$  Ce6 153,000), 503 ( $\epsilon$  Ce6 13,900), 601 ( $\epsilon$  Ce6 6700), 660 ( $\epsilon$  Ce6 29,100); UV-Vis ( $\text{CH}_3\text{OH}$ )  $\lambda_{\text{max}}/\text{nm}$ : 282 ( $\epsilon$  Folate 45,300), 286 ( $\epsilon$  Ce6 35,200) 400 ( $\epsilon$  Ce6 263,000), 503 ( $\epsilon$  Ce6 24,800), 530 ( $\epsilon$  Ce6 10,400), 608 ( $\epsilon$  Ce6 11,200), 661 ( $\epsilon$  Ce6 79,200). Negative ion mass spectrometry resulted in a molecular ion  $m/z$  595.00 for -1 charged Ce6, but the desired compound with a parent ion of 3042.7 MW was not observed, because the molecular weight limit of detection was 2000. The mass spectrum did not show a -2 (1521 MW) or -3 (1014 MW) charged ion. Further work on characterization is underway.

**CHAPTER FOUR**  
**EVALUATION OF A CHLORIN e6–PEG–FOLATE CONJUGATE AS A**  
**PHOTODYNAMIC THERAPY AGENT**

**Determination of the Phototoxicity of the Chlorin e6–PEG–FA Conjugate**

In an initial study to determine if the Ce6–PEG–FA conjugate could kill HeLa cells, 5,000 HeLa cells deprived of folic acid for 72 h, were seeded into 88 wells of two 96-well plates, inoculated with 2.65  $\mu\text{M}$  conjugate in 200  $\mu\text{L}$  of folate free RPMI media, and incubated at 37°C for 24 h. Eight wells were not seeded with cells to use as a blank for the cell viability assay. Following incubation, the media was removed, and cells were washed twice with HEPES buffer. Fresh media containing 4  $\mu\text{M}$  folic acid was added. Cells were irradiated with a halogen lamp, equipped with a filter to allow 600 – 900 nm light to pass through, at a distance of 45.72 cm (18 inches). Light was delivered for 30 min at an irradiance power of  $5.17 \times 10^{-6} \text{ W/cm}^2$  with a fluence of 9.3  $\text{mJ/cm}^2$ . Following irradiation, media was removed and cells were washed twice with complete media containing folate. A 100  $\mu\text{L}$  volume of complete media with folate was added, and the plates were incubated for 24 h. Plates were kept in a 37°C incubator with 5 %  $\text{CO}_2$  for the duration of the experiment except when irradiated with light.

The cell survival fraction was quantified using the CellTiter-Blue Cell Viability Assay by Promega. The assay is a fluorometric method for estimating

the number of living cells in multiwell plates by using the indicator dye resazurin to measure the metabolic activity of cells. Living cells will reduce resazurin to the highly fluorescent resorufin (Figure 15). Dying cells rapidly lose metabolic activity and will not reduce resazurin, and will not generate a fluorescent signal (444).

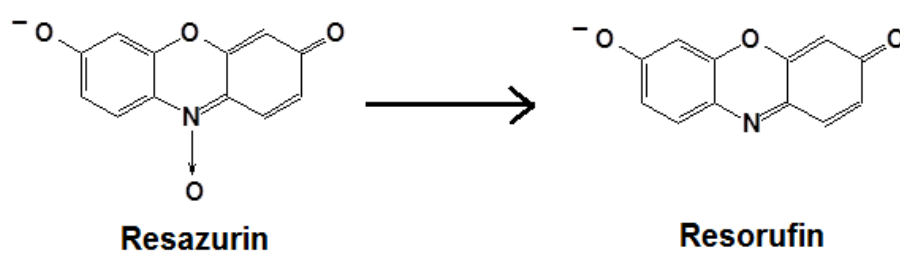
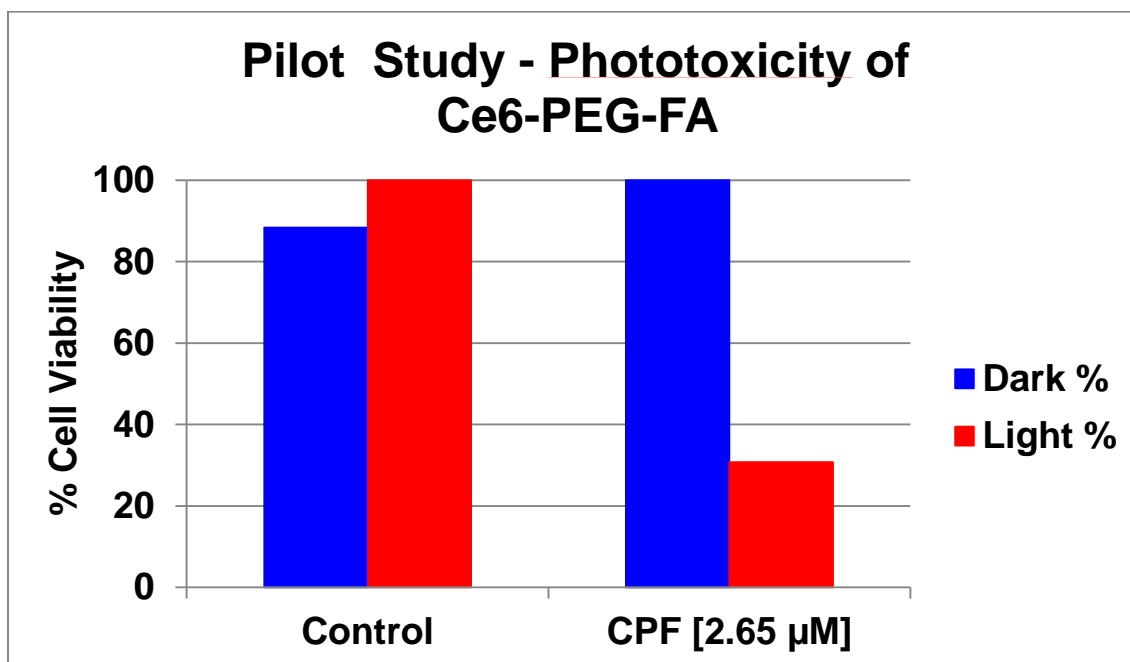


Figure 15. Reduction of Resazurin to Resorufin

A volume of 20  $\mu\text{L}$  of CellTiter-Blue reagent was added to all wells in the plate. After a 2 h incubation, cell viability was determined by reading fluorescence at 590 nm using a microplate reader.



Phototoxicity Data		
	Control	CPF [2.65 µM]
Dark %	88	100
Light %	100	31

Figure 16. Cytotoxicity / Phototoxicity of Ce6-PEG-FA. n = 8 (cells control), n = 2 (CPF 2.65 µM); incubation 24 h; light fluence 9.3 mJ/cm<sup>2</sup>

The cell viability results of the cells only control and the Ce6-PEG-FA conjugate, shows that the HeLa cells are not killed in the dark (Figure 16). The phototoxicity data shows that the Ce6-PEG-FA at 2.65 µM killed 69 % of HeLa cells.

In a more extensive study, the Ce6-PEG-FA conjugate at 5 and 10 µM concentrations, as well as a Ce6 control at 5 and 10 µM concentrations were inoculated in triplicate into two 96 well plates.



The cells were irradiated with an LED lamp (Elixa Ltd., Mega 120 LED) at 660 nm, which was equipped with a diffuser to allow a more even distribution of light across the entire plate, at a distance of 7.62 cm (3 in). The irradiance power of the lamp was  $9.37 \times 10^{-2} \text{ W/cm}^2$ . Light was delivered at varying fluences according to Table 4.

Irradiance Power $9.37 \times 10^{-2} \text{ W/cm}^2$				
Well Plate Rows	A/B	C/D	E/F	G/H
Exposure Time (sec)	60	120	240	360
Fluence ( $\text{J/cm}^2$ )	5.5	11	22	33

Table 4. Fluences of Irradiated Light Delivered to Various Cell Culture Plate Rows

## Results and Discussion

The goal of this study was to test the cell killing capacity of a Chlorin e6–PEG–FA conjugate using a HeLa cell line. The structure of the final compound is shown in Figure 17, along with a description of the interactions with the folate receptor. The structure of the folate receptor with bound folate is known (445). It shows that the hydrophobic interactions of the pterin and aminobenzoate groups with the protein are responsible for the binding (Figure 18). The carboxylate groups, particularly the  $\gamma$ -carboxylate, are pointed into the solution and should not effect the interactions of the folate with the receptor when the PEG chain is added. Molecular dynamics simulations of the Ce6–PEG–FA

conjugate with the receptor (*K.W. Olsen, personal communication*) indicate that the PEG modification will not disrupt this interaction. These computations and the X-ray structure suggest that the Ce6–PEG–FA conjugate should be functional in terms of bringing the dye into the cell.

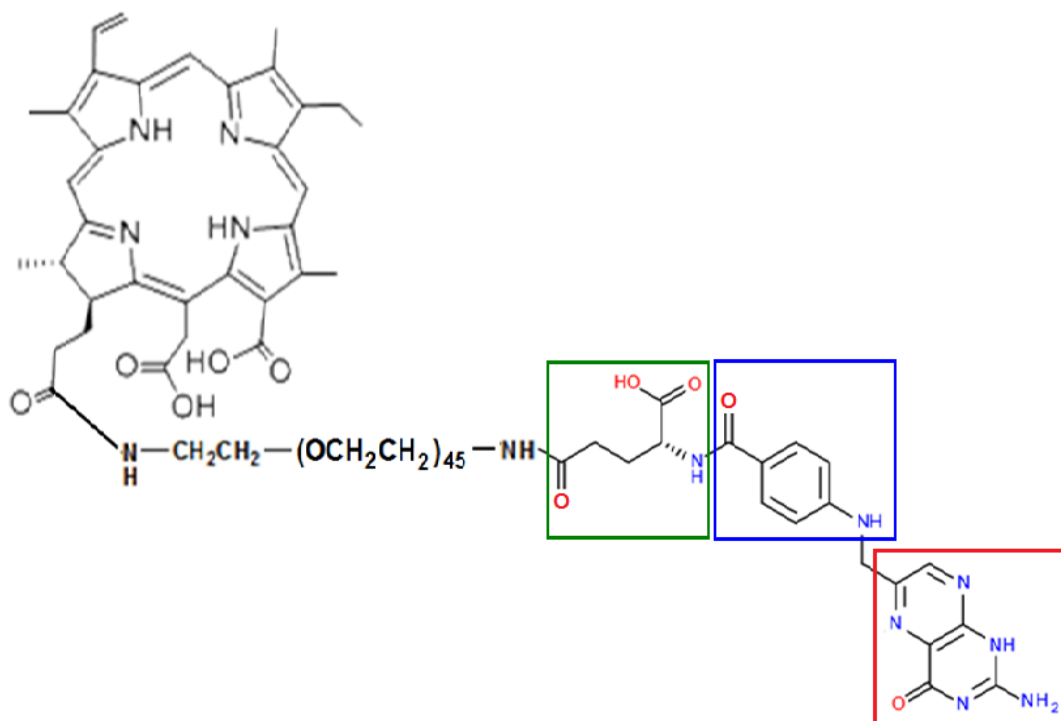


Figure 17. Chlorin e6–PEG–Folate Structure and FR Interactions

Interactions with the folate receptor are denoted as follows: pterin (shown in red box) anchors ligand in the binding pocket of FR by hydrophobic stacking between amino acids tyr and trp, and hydrophilic interactions between N and O atoms of pterin with amino acids asp, ser, arg, and his; aminobenzoate (shown in blue box) has hydrophobic interactions with amino acids tyr and trp located in the middle of the binding pocket. Glutamate (shown in green box) conjugates drugs (Ce6) without adversely affecting the ligand binding at the FR (445).

Additional diagrams showing the interaction of folate with the folate receptor are shown in Figure 18.

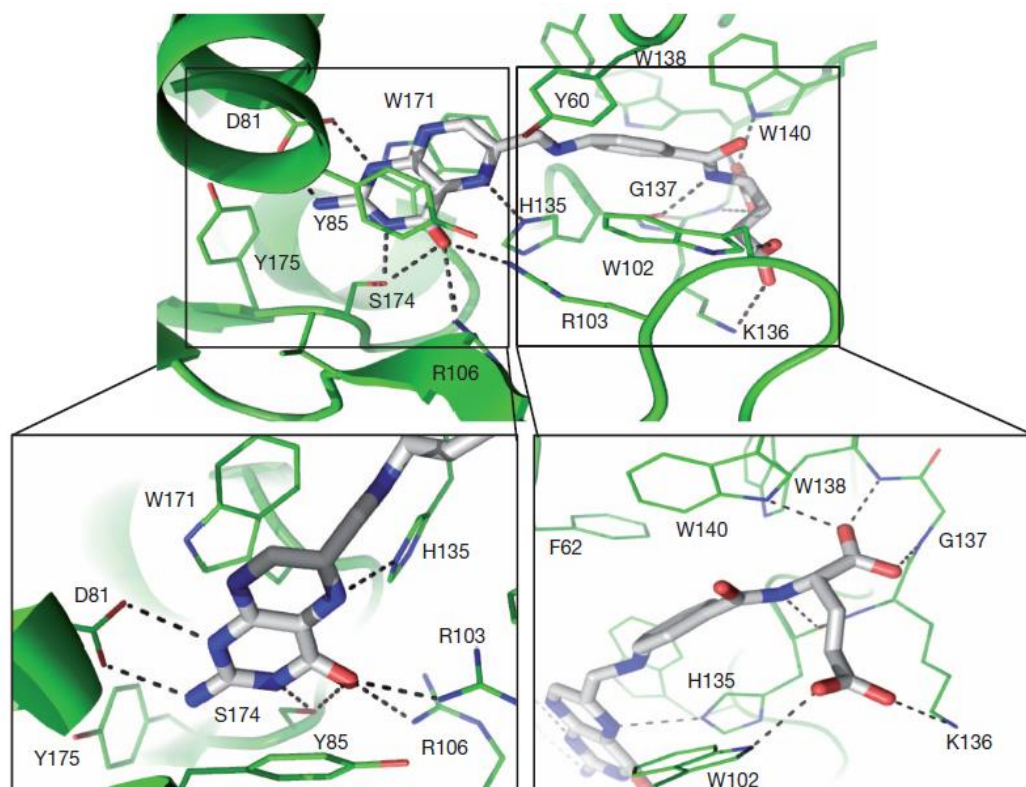
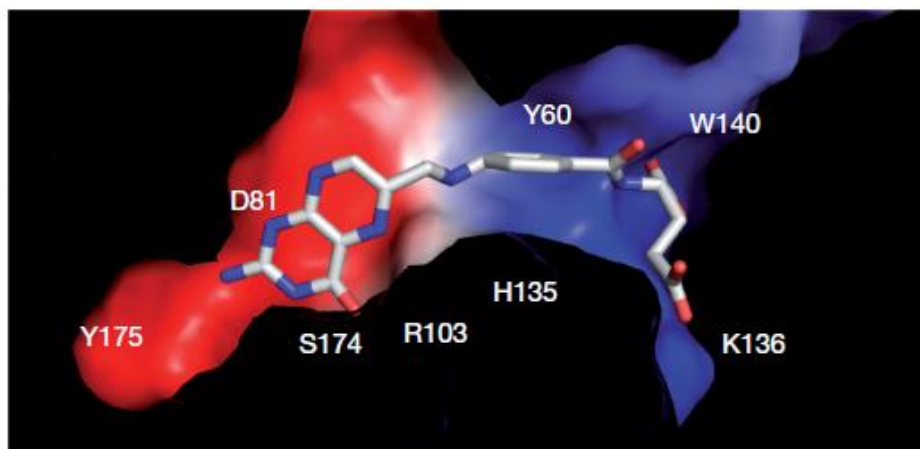
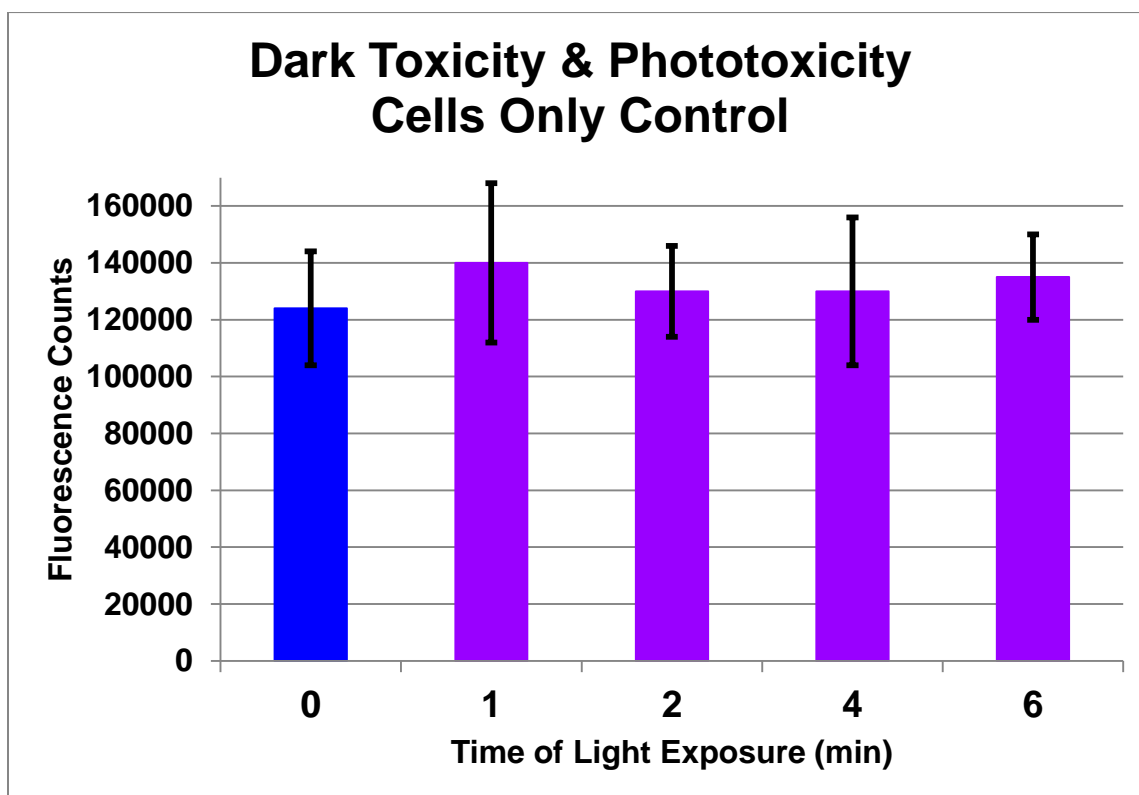


Figure 18. Structural Interactions of Folate with the Folate Receptor  
 Folate carbon atoms in grey, nitrogen atoms in blue, and oxygen atoms in red (top diagram). Close up representations of folate in the binding pocket with folate in grey and residues lining the binding pocket shown in green. Hydrogen bonds are indicated by dashed lines (bottom diagram). (445)

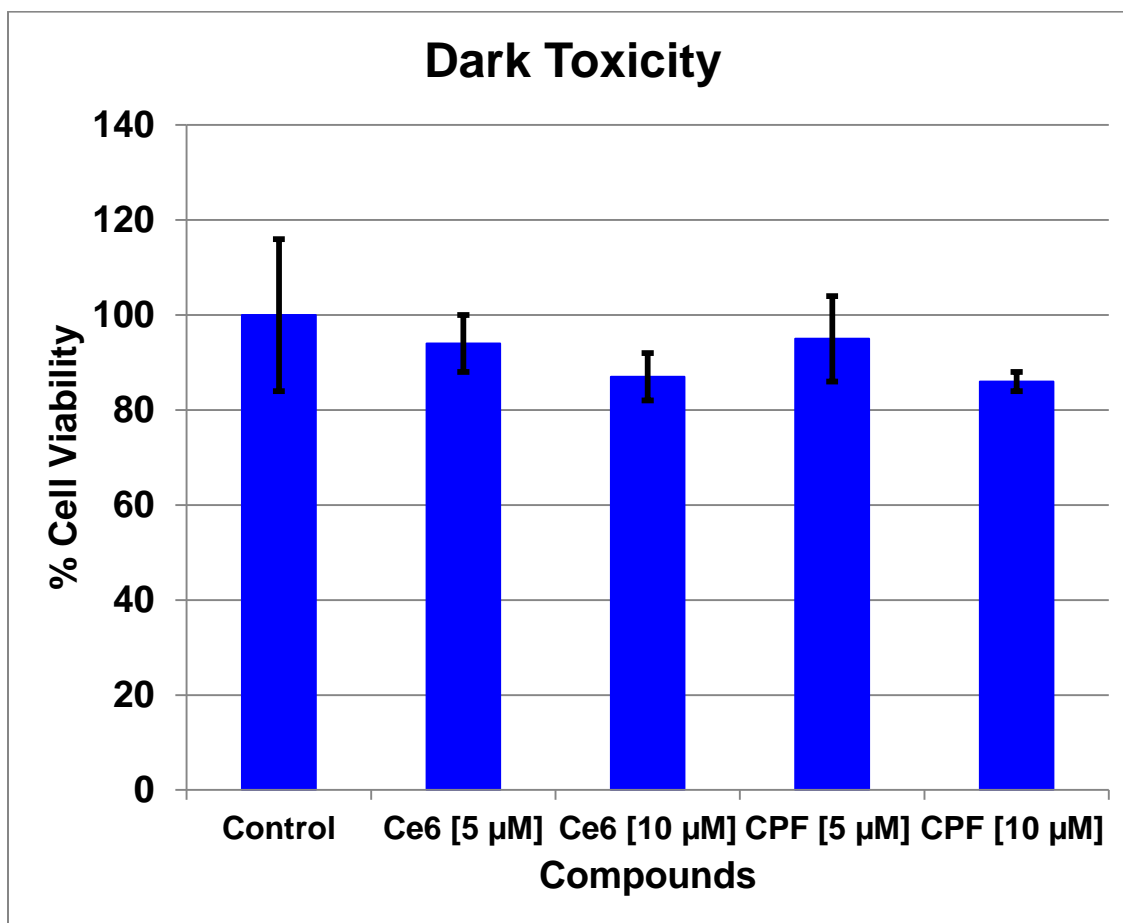
## Cytotoxicity / Phototoxicity Assays



Cells Only Control					
Dark and Light Data - 4 Expts.					
Time (min)	0	1	2	4	6
Ave. Fluor. Counts	124000	140000	130000	130000	135000
Std. Dev.	20000	28000	16000	26000	15000

Figure 19. Average Fluorescence Counts for Cells Only Control: 4 Expts. Std. Dev. (population) based on  $n = 49$  (0 min);  $n = 13$  (1 min);  $n = 12$  (2,4,& 6 min); incubation 24 h; light fluences 5.5, 11, 22, 33 J/cm<sup>2</sup>

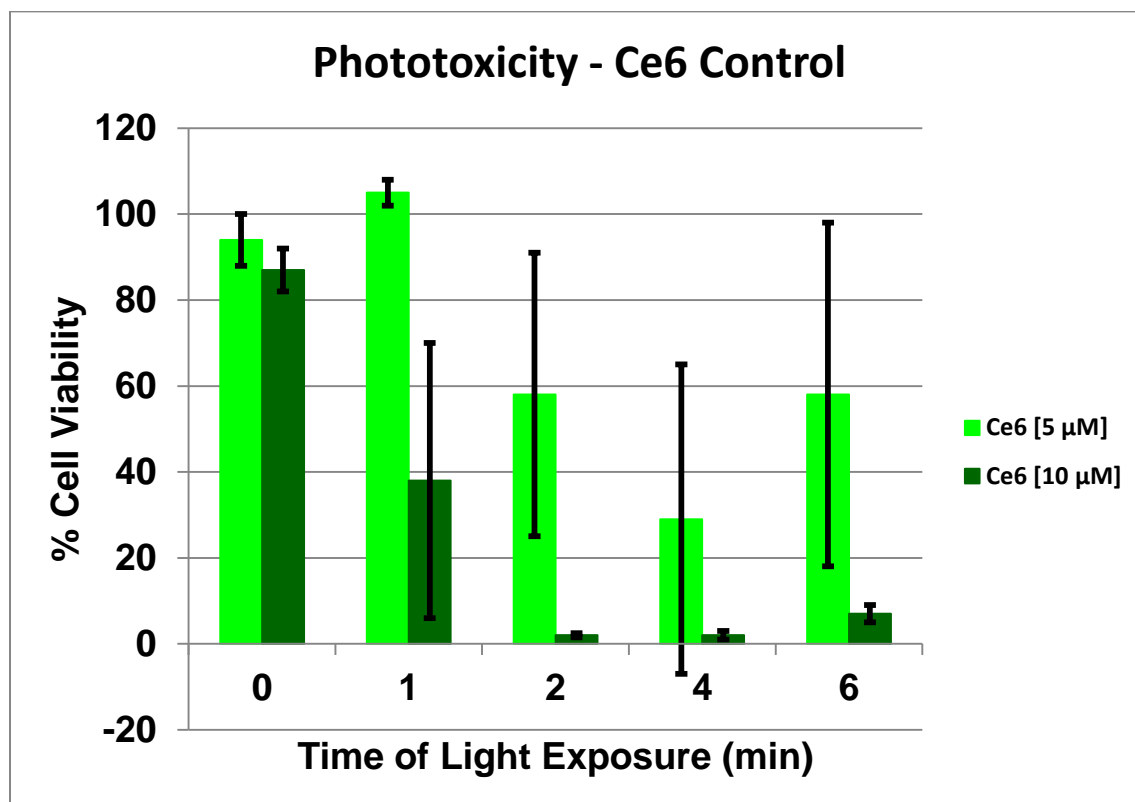
The cell viability results of the cells only control shows that the cells are not being killed in the dark or in the light, as the fluorescence counts are all above 120,000 (Figure 19). Therefore, any cell death can be attributable to the phototoxic effect of the compounds.



Dark Toxicity					
	Ave. % Viability				
Control	100	CPF = Ce6-PEG-FA			
Ce6 [5 μM]	94				
Ce6 [10 μM]	87				
CPF [5 μM]	95				
CPF [10 μM]	86				

Figure 20. Cytotoxicity Average % Viability for Cells Control, Ce6 Controls, and CPF: 4 Expts. Cytotoxicity Std. Dev. (population) based on  $n = 49$  (cells control),  $n = 35$  (Ce6 5  $\mu\text{M}$ ),  $n = 36$  (Ce6 10  $\mu\text{M}$ ),  $n = 48$  (CPF 5  $\mu\text{M}$ ),  $n = 45$  (CPF 10  $\mu\text{M}$ ); incubation 24 h

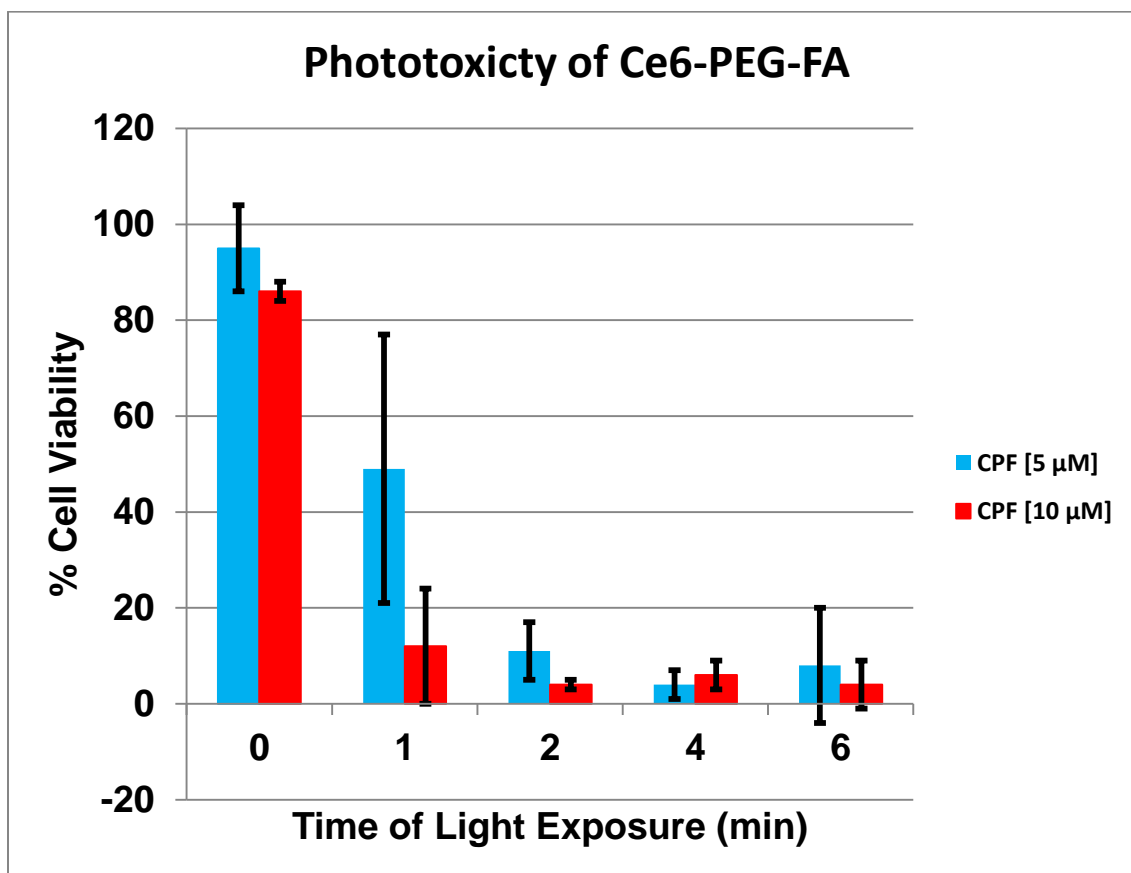
The cell viability results for all of the compounds in the dark shows that the cells-only controls, Ce6 controls, and conjugates are not cytotoxic to the cells in the dark, as all viabilities are greater than 85% (Figure 20).



	Ave. % Viability					Ce6 Control
Time (min)	0	1	2	4	6	
Ce6 [5 μM]	94	105	58	29	58	
Ce6 [10 μM]	87	38	2	2	7	

Figure 21. Average % Viability for Ce6 Control: 4 Expts. Cytotoxicity Std. Dev. (population) based on  $n = 35$  (Ce6 5 μM),  $n = 36$  (Ce6 10 μM). Phototoxicity Std. Dev. (population) based on  $n = 9$  (Ce6 5 μM - 1, 2, 4, 6 min; Ce6 10 μM - 1, 6 min),  $n = 8$  (Ce6 10 μM - 2, 4 min); incubation 24 h; light fluences 5.5, 11, 22, 33 J/cm<sup>2</sup>

At 1 min, the 5  $\mu\text{M}$  Ce6 killed no cells, and the 10  $\mu\text{M}$  Ce6 killed 62 % of the cells (Figure 21). At 2 min, the phototoxicity of the 5  $\mu\text{M}$  Ce6 is 42 %, and the 10  $\mu\text{M}$  Ce6 is 98 %. Similar results were seen at 6 min. At 4 min, the phototoxicity of the 5  $\mu\text{M}$  Ce6 is 71 %, and the 10  $\mu\text{M}$  Ce6 is 98 %. Error bars are large for the 5  $\mu\text{M}$  Ce6 at 2, 4, and 6 min, as well as for the 10  $\mu\text{M}$  Ce6 at 1 min, indicating variability in data. The results clearly show that the 10  $\mu\text{M}$  Ce6 is killing more cells at 1, 2, and 6 min, as the error bars do not overlap.



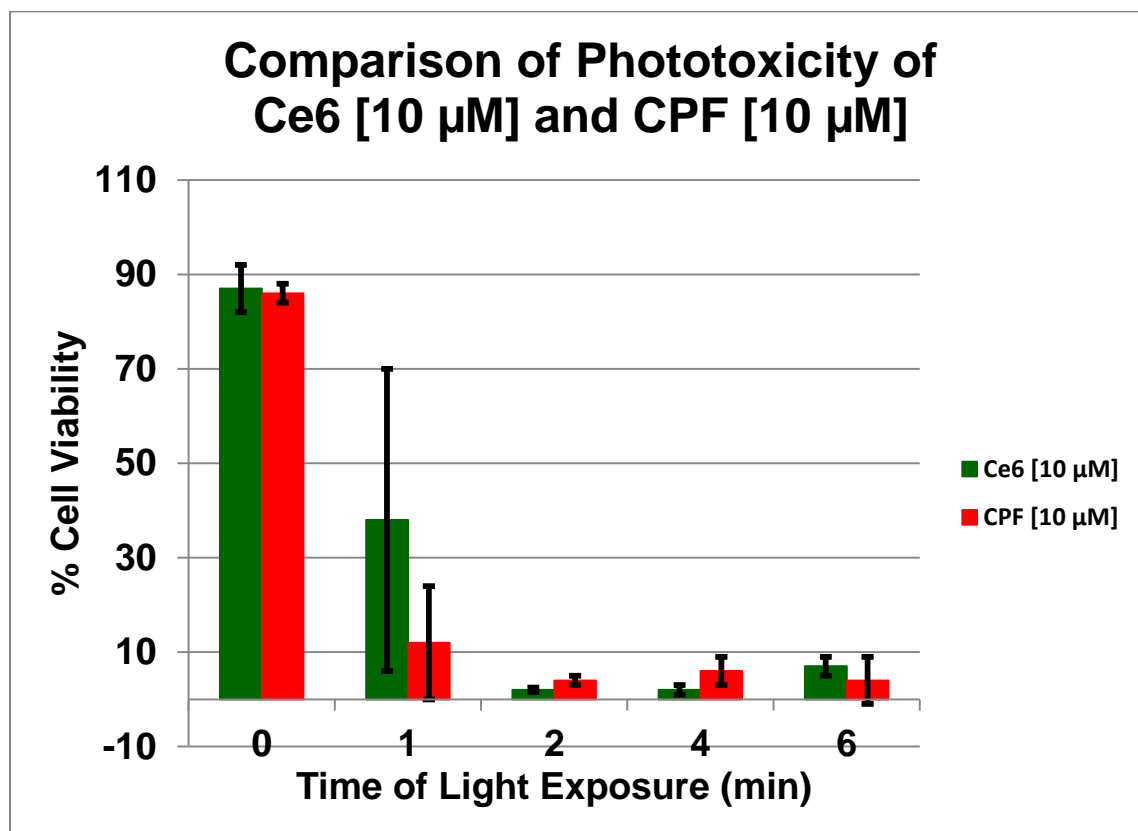
	Ave. % Viability Ce6-PEG-FA				
Time (min)	0	1	2	4	6
CPF [5 μM]	95	49	11	4	8
CPF [10 μM]	86	12	4	6	4

Figure 22. Average % Viability for Ce6-PEG-FA: 4 Expts. Cytotoxicity Std. Dev. (population) based on  $n = 48$  (CPF 5  $\mu\text{M}$ ),  $n = 45$  (CPF 10  $\mu\text{M}$ ); Phototoxicity Std. Dev. (population) based on  $n = 12$  (CPF 5  $\mu\text{M}$  - 1, 2 min; CPF 10  $\mu\text{M}$  - 1 min),  $n = 11$  (CPF 5  $\mu\text{M}$  - 4, 6 min; CPF 10  $\mu\text{M}$  - 2 min),  $n = 10$  (CPF 10  $\mu\text{M}$  - 4 min),  $n = 9$ ; CPF 10  $\mu\text{M}$  - 6 min); incubation 24 h; light fluences 5.5, 11, 22, 33  $\text{J}/\text{cm}^2$

At 1 min, the phototoxicity of the 5  $\mu\text{M}$  Ce6-PEG-FA is 51 %, and the 10  $\mu\text{M}$  Ce6-PEG-FA is 88 % (Figure 22). The error bars overlap, indicating no statistical differences; however, the errors are large, which means that the data is



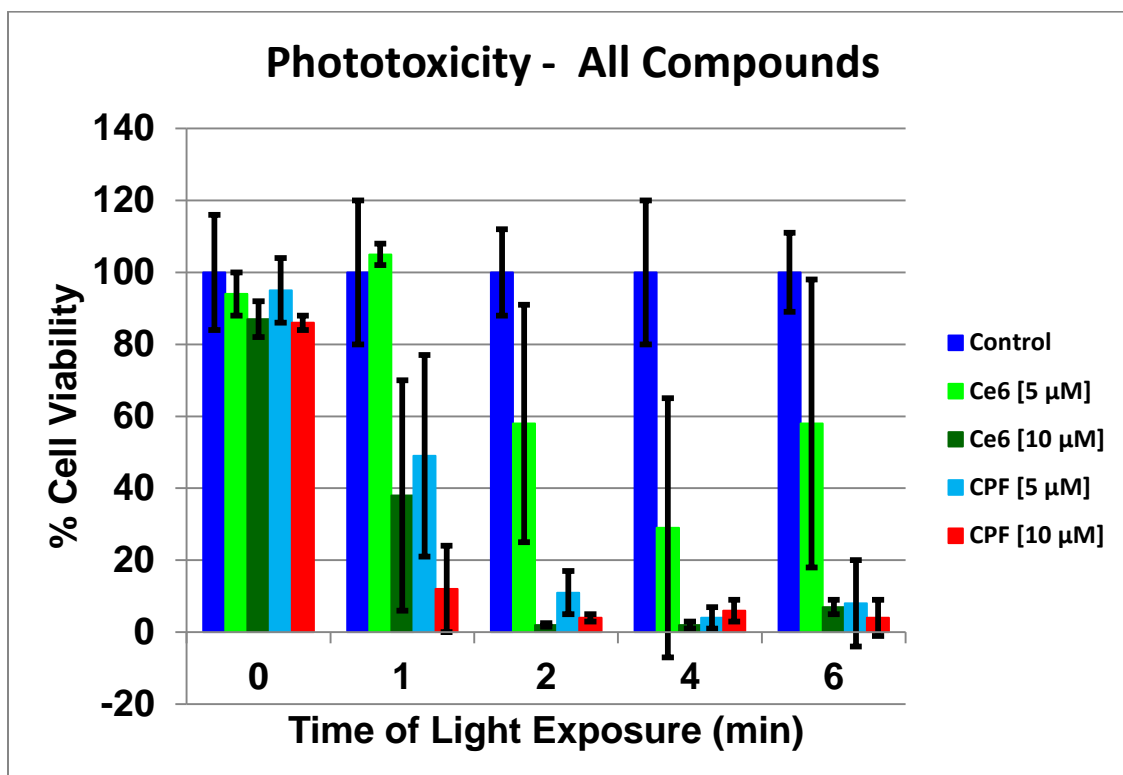
variable. Based on the percentages only, the results show that with an increase in concentration, more cells are killed. At 2, 4, and 6 min, nearly all of the cells are killed with both concentrations of the conjugate.



	Ave. % Viability		Ce6 / CPF [10 $\mu$ M]			
Time (min)	0	1	2	4	6	
Ce6 [10 $\mu$ M]	87	38	2	2	7	
CPF [10 $\mu$ M]	86	12	4	6	4	

Figure 23. Average % Viability for Ce6 / CPF 10  $\mu$ M: 4 Expts. Cytotoxicity Std. Dev. (population) based on n = 36 (Ce6 10  $\mu$ M), n = 45 (CPF 10  $\mu$ M); Phototoxicity Std. Dev. (population) based on n = 12 (CPF 10  $\mu$ M - 1 min), n = 11 (CPF 10  $\mu$ M - 2 min), n = 10 (CPF 10  $\mu$ M - 4 min), n = 9 (Ce6 10  $\mu$ M - 1, 6 min; CPF 10  $\mu$ M - 6 min), n = 8 (Ce6 10  $\mu$ M - 2, 4 min); incubation 24 h; light fluences 5.5, 11, 22, 33 J/cm<sup>2</sup>

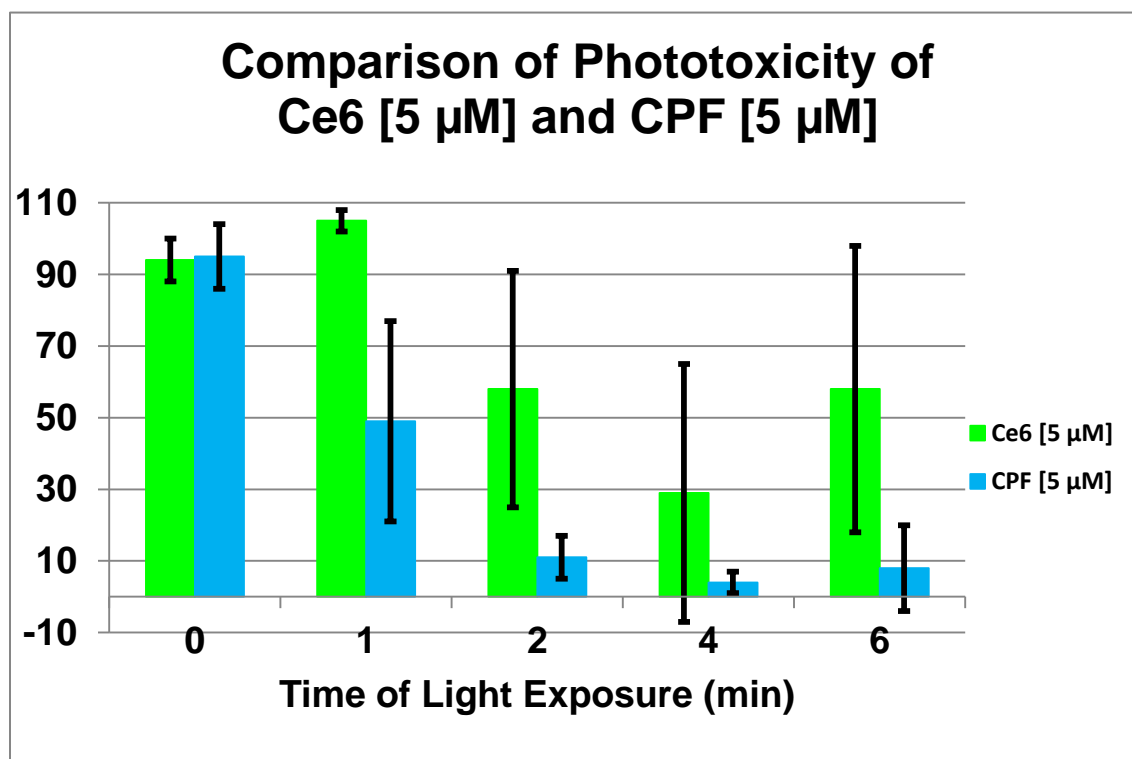
At 1 min, the phototoxicity of the 10  $\mu\text{M}$  Ce6 is 62 %, and the 10  $\mu\text{M}$  Ce6-PEG-FA is 88 % (Figure 23). Both error bars are large, and the bars overlap, indicating no statistical differences; however, according to the percentage data, it does appear that the Ce6-PEG-FA is killing better than the Ce6, but at this relatively high concentration, both are causing cellular damage. At 2 min and beyond, nearly all the cells are killed by both the 10  $\mu\text{M}$  Ce6 and Ce6-PEG-FA.



	Ave. % Viability	All Compounds				
Time (min)	0	1	2	4	6	
Control	100	100	100	100	100	
Ce6 [5 μM]	94	105	58	29	58	
Ce6 [10 μM]	87	38	2	2	7	
CPF [5 μM]	95	49	11	4	8	
CPF [10 μM]	86	12	4	6	4	

Figure 24. Average % Viability for All Compounds: 4 Expts. Cytotoxicity Std. Dev. (population) based on  $n = 49$  (cells control),  $n = 35$  (Ce6 5 μM),  $n = 36$  (Ce6 10 μM),  $n = 48$  (CPF 5 μM),  $n = 45$  (CPF 10 μM); Phototoxicity Std. Dev. (population) based on  $n = 13$  (cells control - 1 min),  $n = 12$  (cells control - 2, 4, 6 min; CPF 5 μM - 1, 2 min; CPF 10 μM - 1 min),  $n = 11$  (CPF 5 μM - 4, 6 min; CPF 10 μM - 2 min),  $n = 10$  (CPF 10 μM - 4 min),  $n = 9$  (Ce6 μM - 1, 2, 4, 6 min; Ce6 10 μM - 1, 6 min; CPF 10 μM - 6 min),  $n = 8$  (Ce6 10 μM - 2, 4 min); incubation 24 h; light fluences 5.5, 11, 22, 33 J/cm<sup>2</sup>

This graph is a summary of all the data for the cells control, Ce6, and Ce6-PEG-FA (Figure 24). At 1 min and 2 min, the phototoxicity of the 5  $\mu\text{M}$  Ce6-PEG-FA is clearly greater than that of the 5  $\mu\text{M}$  Ce6 only. At 2, 4, and 6 min, nearly all the cells are killed with all compounds, with the exception of the 5  $\mu\text{M}$  Ce6.



	Ave. % Viability	Ce6 / CPF [10 $\mu\text{M}$ ]				
Time (min)	0	1	2	4	6	
Ce6 [10 $\mu\text{M}$ ]	87	38	2	2	7	
CPF [10 $\mu\text{M}$ ]	86	12	4	6	4	

Figure 25. Average % Viability for Ce6 / CPF 5  $\mu\text{M}$ : 4 Expts. Cytotoxicity Std. Dev. (population) based on  $n = 35$  (Ce6 5  $\mu\text{M}$ ),  $n = 48$  (CPF 5  $\mu\text{M}$ ); Phototoxicity Std. Dev. (population) based on  $n = 12$  (CPF 5  $\mu\text{M}$  - 1, 2 min),  $n = 11$  (CPF 5  $\mu\text{M}$  - 4, 6 min);  $n = 9$  (Ce6 5  $\mu\text{M}$  - 1, 2, 4, 6 min); incubation 24 h; light fluences 5.5, 11, 22, 33  $\text{J}/\text{cm}^2$

At 1 min, no cells are killed with the 5  $\mu\text{M}$  Ce6, and the 5  $\mu\text{M}$  Ce6-PEG-FA is killing 51 % of the cells (Figure 25). At 2 min, the phototoxicity of the 5  $\mu\text{M}$  Ce6 is 42 %, and the 5  $\mu\text{M}$  Ce6-PEG-FA is 89 %. Although the error bars are large for the 5  $\mu\text{M}$  Ce6-PEG-FA at 1 min, and the 5  $\mu\text{M}$  Ce6 at 2 min, the bars do not overlap; therefore, it is clear that the Ce6-PEG-FA at 5  $\mu\text{M}$  is killing more cells at both 1 and 2 min. At 4 and 6 min, the error bars overlap indicating no statistical differences, which means that most of the cells were killed at this light exposure with both the 5  $\mu\text{M}$  Ce6 and Ce6-PEG-FA.

### **Conclusions**

Comparing the phototoxicity of the 5  $\mu\text{M}$  Ce6 and Ce6-PEG-FA at 1 and 2 min, clearly shows that the addition of the PEG-FA to the Ce6 increases the phototoxicity to the HeLa cells, and that an increase in light fluence kills more cells. The data also shows that an increase in concentration of the conjugate and Ce6 kills more cells. This data supports the hypothesis that the PEGylated Ce6 conjugate kills more HeLa cells than the Ce6 alone. The PEGylation with folate most likely allows the Ce6 conjugates to enter the cell by folate receptor mediated endocytosis, which increases the selectivity for the HeLa cancer cells. The free Ce6 may be adhering to the cell membrane, causing cell death. Consequently, free Ce6 could kill normal cells in addition to cancer cells, which causes more harm to the patient, hence the need for the PEGylation of Ce6 as a protective effect.

The data presented here (Figure 24) suggests that 5 and 10  $\mu\text{M}$  concentrations for the Ce6–PEG–FA conjugate were probably too high. It is likely that lower concentrations would show less mortality due to the Ce6 by itself, while still allowing the Ce6–PEG–FA conjugate to kill the cancer cells by irradiating them for somewhat longer times than used here. Since most of the cells were killed after 2 min, and 10  $\mu\text{M}$  concentrations, further studies can be done with lower light fluences, lower concentrations, and shorter incubation times.

Comparison of these data to that completed by Li, *et al.* (446) shows that the phototoxicity of this Ce6–PEG–FA conjugate is greater than the conjugate **1a** [5, 10, 15-tris (3-hydroxyphenyl)-20-(4-carboxyphenyl) chlorin-PEG-folate] synthesized by Li and his coworkers. The cell viability of Li's **1a** conjugate in HeLa cells was 35 % at a concentration of 17.5  $\mu\text{M}$ , with a light fluence of 18  $\text{J}/\text{cm}^2$  and an incubation time of 24 h (446). The approximate cell viability of the Ce6–PEG–FA conjugate in this research was 4 % and 6 % respectively for 5 and 10  $\mu\text{M}$  concentrations, with a light fluence of 22  $\text{J}/\text{cm}^2$  and an incubation time of 24 h. When adjusting for a linear response to light fluence, the cell viability of the 5  $\mu\text{M}$  Ce6–PEG–FA conjugate would be approximately 18 % at a light fluence of 18  $\text{J}/\text{cm}^2$  (~3.3 min light exposure time), and the cell viability of the 10  $\mu\text{M}$  Ce6–PEG–FA conjugate would be approximately 6 % at a light fluence of 18  $\text{J}/\text{cm}^2$ . These numbers clearly show the increase in phototoxicity of our Ce6–PEG–FA as compared to their conjugate **1a**. In addition, the concentrations

of our Ce6–PEG–FA conjugate are smaller. Also, compound **1a** synthesized by Li *et al.* (446) was PEGylated with a 75 unit PEG; whereas our Ce6–PEG–FA conjugate was PEGylated with a 45 unit PEG. Perhaps the longer PEG contributes to increased cell viability and decreased cell phototoxicity.

Comparison of our Ce6 compound (purchased from Frontier Scientific) used in this research with the **chlorin 4** synthesized by Li, *et al.* [5, 10, 15-tris (3-hydroxyphenyl)-20-(4-carboxyphenyl) chlorin] shows that the **chlorin 4** is phototoxic even in the dark, with a cell viability of ~ 49 % at a concentration of 9.2  $\mu\text{M}$ , and incubation time of 24 h (446). The Ce6 used in this research was not phototoxic in the dark, as the compound had a cell viability of 94 % (when compared to the cells only control) for Ce6 5  $\mu\text{M}$ , and 87 % at 10  $\mu\text{M}$ , with an incubation time of 24 h. Since the compound synthesized by Li, *et al.* (446) was structurally distinct from the Ce6 used in this research, apparently their compound was toxic in the dark. Comparisons cannot be made in the light, because Li and his coworkers did not use their **chlorin 4** compound in phototoxicity studies.

Since most of the cells were killed after 2 min, and 10  $\mu\text{M}$  concentrations, further studies can be done with lower light fluences, lower concentrations, and shorter incubation times.

To fully ascertain the role of PEGylation of Ce6, further studies must be completed with these compounds on normal cellular tissues that do not overexpress folate receptors. Also, competitive assays could be completed using

varying concentrations of folate in the media along with inoculation with the conjugates. Further studies can also be completed *in vivo* to determine the optimum light exposure and dosage needed for an LD<sub>50</sub>.

This study allowed the experimenter to determine a good protocol for cell culturing and determining controls. In addition, a good technique was determined to irradiate the cells using an LED lamp, and subsequently to assay for cell viability.

Targeting a Ce6 photosensitizer to HeLa cell folate receptors by PEGylation with an NH<sub>2</sub>-PEG-FA clearly increases the phototoxic potential of the conjugate at a 5 μM concentration.



## CHAPTER FIVE

### CONCLUSION

This research involves synthesis of two photosensitizers, both of which contain the compound phenothiazine, and a targeted photodynamic therapy agent containing chlorin e6. The two phenothiazine based photosensitizers are N-benzyl-3,7-diphenothiazinylphenothiazine, and methyl (3,7-diphenothiazinyl)-4-N-methylenephenothiazinylbenzoate. Both of these photosensitizers contain phenothiazine substituents at the 3 and 7 position on the central phenothiazine molecule to create a phenothiazine trimer. The difference between these two phenothiazine compounds is the protection group attached to the N of the phenothiazine base. In order to attach a PEGylated folic acid compound, needed to target the photosensitizer to enter the cancer cells via receptor mediated endocytosis, the benzyl group of N-benzyl-3,7-diphenothiazinylphenothiazine needed to be removed, or deprotected. The deprotection was unsuccessful after numerous attempts; therefore, a second phenothiazine trimer was synthesized with a methyl benzoate protection group. Due to the presence of the carbomethoxy group ( $\text{COOCH}_3$ ) attached to the benzyl group, there was no need to deprotect this newer compound, as an amine PEGylated folic acid compound could be directly attached via an amide bond to the carbomethoxy protection group. However, when both of these compounds were analyzed via UV

spectrophotometry, neither compound was found to have a  $\lambda_{\max}$  absorption in the be successful for deeper tissue cancers. Subsequently, the N-benzyl-3,7-diphenothiazinylphenothiazine was oxidized with HCl catalysis using 12 M HCl. This reaction showed a  $\lambda_{\max}$  absorption at approximately 670 nm. The following data was recorded by UV-VIS analysis of this trimer:  $\lambda_{\max}$  665 nm absorption of 1.479 in  $\text{CH}_3\text{CN}$ ,  $\lambda_{\max}$  679 nm absorption of 2.194 in DCM, and  $\lambda_{\max}$  670 nm absorption of 0.867 in  $\text{CH}_3\text{CN}$ . An electron paramagnetic resonance (EPR) spectrum exhibited a signal, which indicates that a radical species was formed. The EPR spectrum of the sample was completed over 6 months from the time that the compound was originally made; therefore, the radical formed was stable in PBS solvent. Subsequent analysis by UV-VIS verified the high absorbance at  $\lambda_{\max}$  670 nm several months after the radical was made. The stability of this radical can be attributed to the delocalization of the lone electron around the conjugation of the phenothiazine aromatic ring. Also, a multiple radical species could have been formed on each of the three N atoms in each of the three phenothiazines, each with resonance delocalization, which allows further stabilization, as shown in Figure 26.

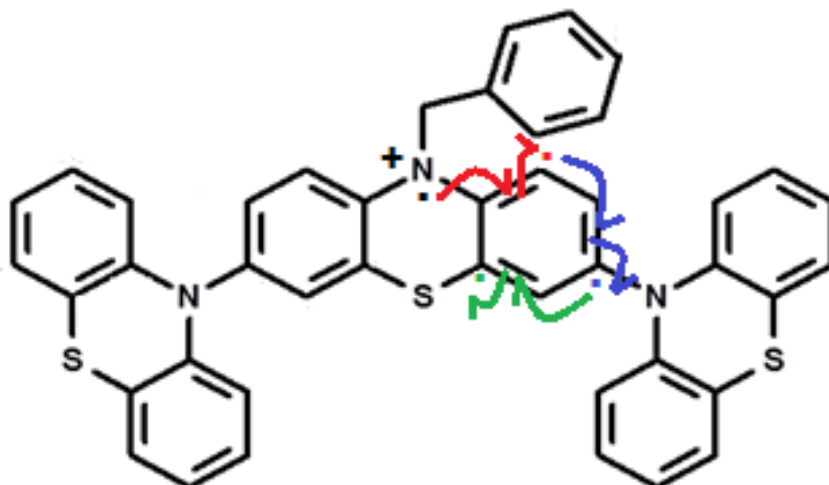


Figure 26. Diagram of N-benzyl-3,7-diphenothiazinylphenothiazine Showing Delocalization of a Lone Electron

The possibility of a multiple radical could explain the large absorbance values at 670 nm. Further work must be completed to determine if this compound could act as a photosensitizer in cancer cell killing studies. The oxidation of the second photosensitizer, methyl (3,7-diphenothiazinyl)-4-N-methylenephenothiazinylbenzoate, was not studied. Further work must be done to optimize the synthesis and purification of this compound. If the oxidation is subsequently successful, a PEGylated folic acid molecule can be attached via an amide bond, and cell killing studies can be completed to test for cancer cell killing potential.

The PDT agent that was synthesized was Ce6-PEG-FA. Since Chlorin e6 is a known photosensitizer, it was hypothesized that by attaching a PEGylated folic acid compound to the C-17 atom of Chlorin e6 via an amide bond, the cancer cell killing potential would be greater due to the ability of the folic acid

portion to enter the cell via receptor mediated endocytosis. Also, since cancer cells express more folate receptors as compared to normal cells, the compound could target cancer cells more effectively, minimizing the destruction of normal cells. To ensure that the HeLa cells were taking up folic acid attached to the Ce6 photosensitizer, the cells were given folate free media for 3 days prior to exposure to the Ce6-PEG-FA compound.

The results of cell mortality studies with the Ce6-PEG-FA conjugates supported the hypothesis that PEGylation of Ce6 has more phototoxic potential than a Ce6 compound without PEGylation. The results also indicate that the conjugates are most likely entering the cell via FR mediated endocytosis, which increases the selectivity for HeLa cells. Increases in light fluence or the concentration of the conjugate and Ce6 killed more HeLa cells. Because Ce6 may be adhering to the cell membrane and causing cell death through phototoxicity, this process could also happen with non-cancerous cells, potentially causing more harm to the patient. Decreasing the concentration of Ce6 should decrease this effect. Because of its specific targeting of cancer cells, Ce6-PEG-FA would be concentrated in the target cells. The PEGylation of Ce6 should decrease its hydrophobicity, providing a protective effect because it may be less likely to stick to the membranes of normal cells. Connecting a Ce6 photosensitizer to folate by PEGylation with an  $\text{NH}_2$ -PEG-FA clearly increases the phototoxic potential of a Ce6 conjugate to HeLa cells.

APPENDIX A  
LIST OF FIGURES

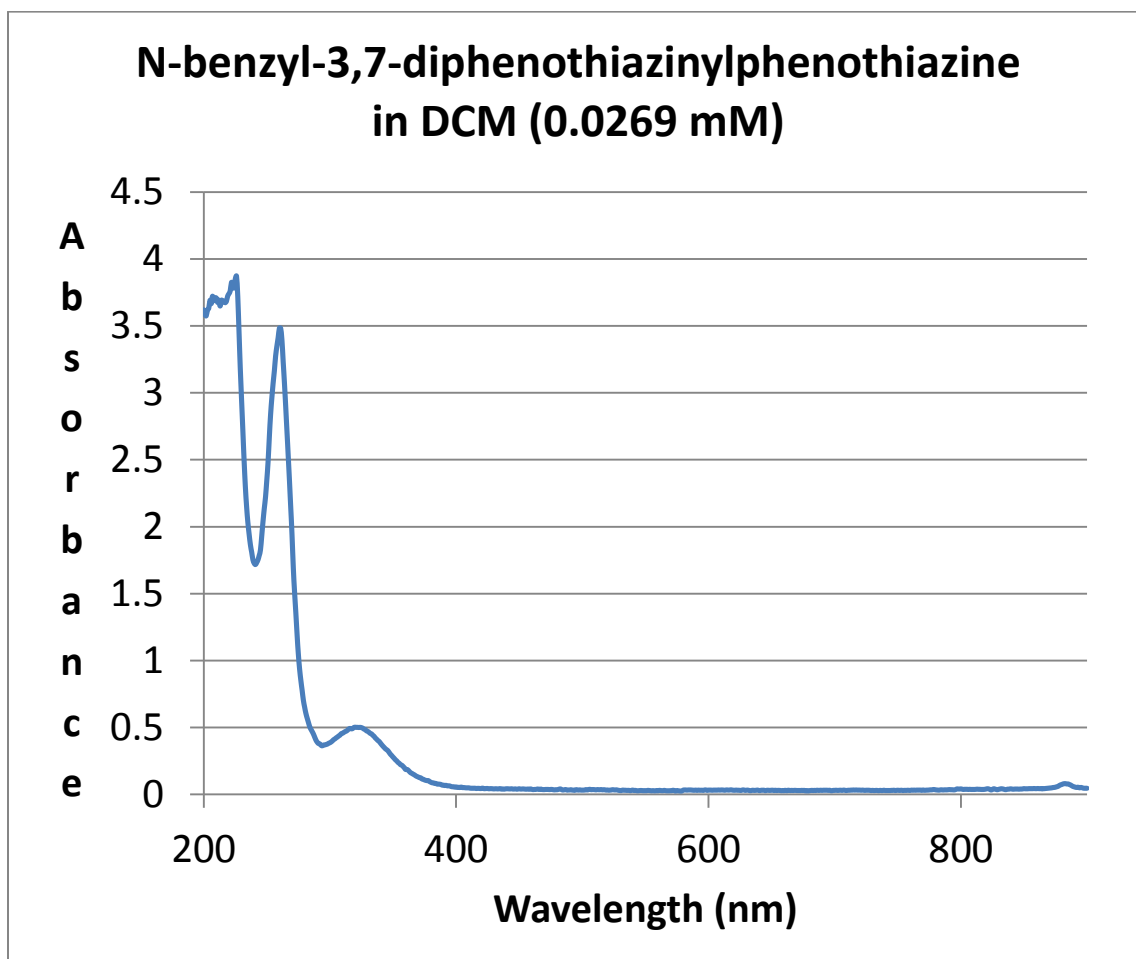


Figure 27. UV-VIS Spectrum of N-benzyl-3,7-diphenothiazinyphenothiazine

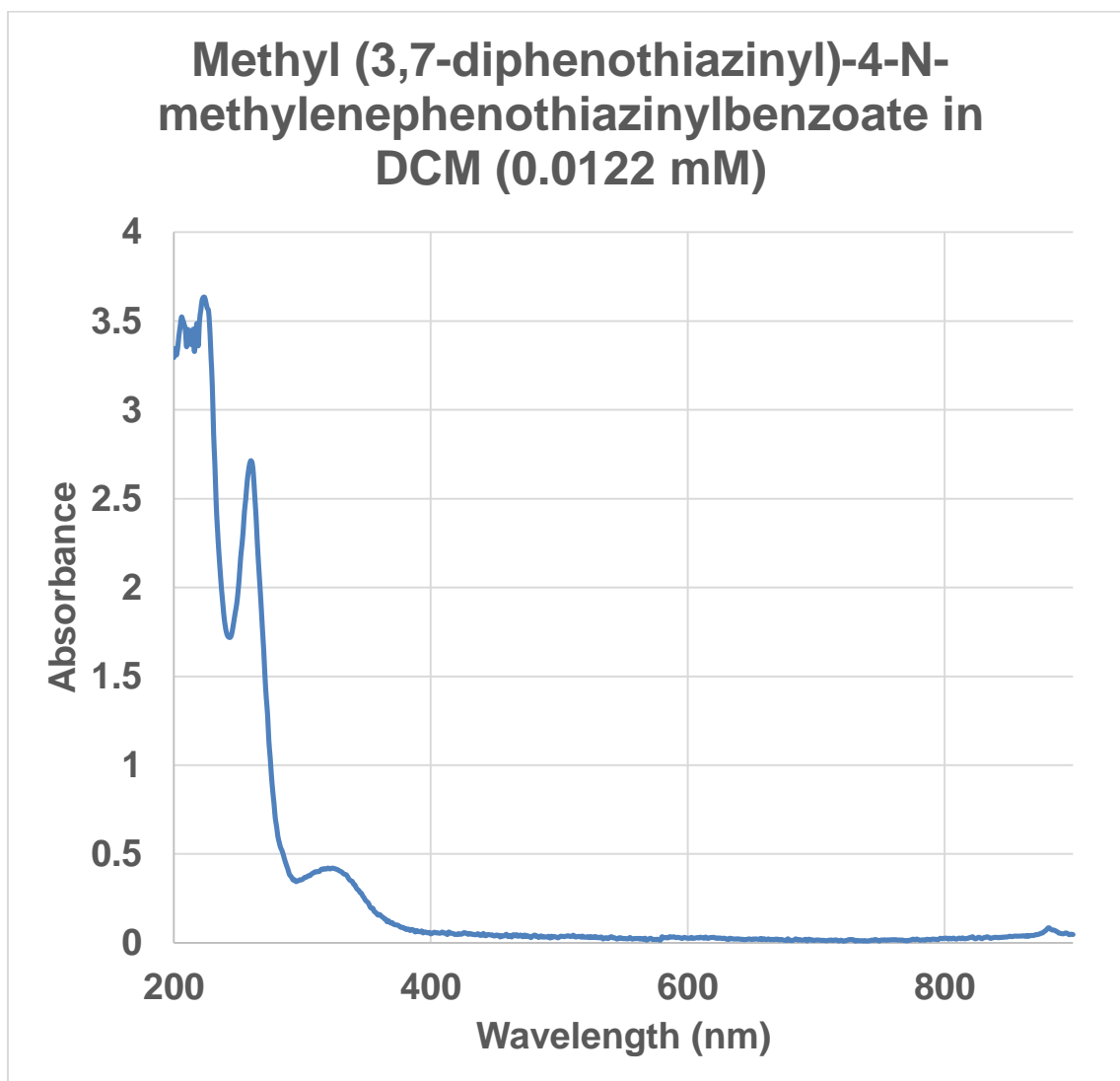


Figure 28. UV-VIS Spectrum of methyl (3,7-diphenothiazinyl)-4-N-methylenephenothiazinylbenzoate

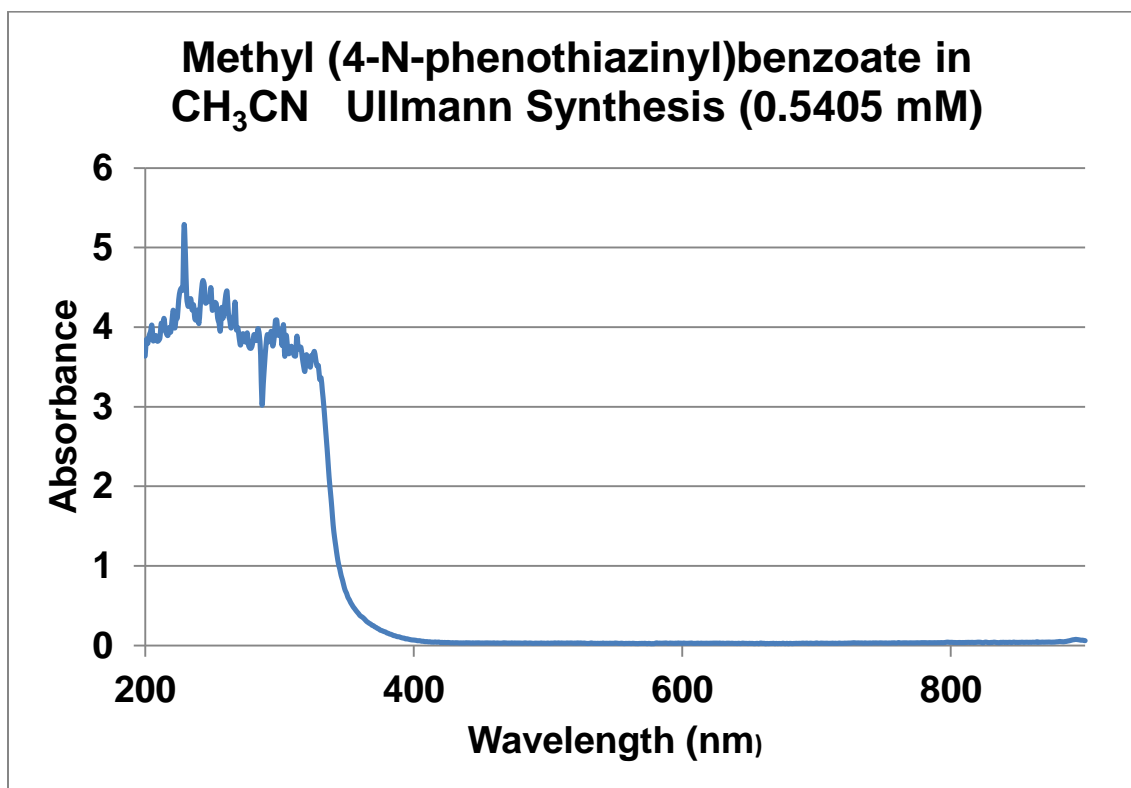


Figure 29. UV-VIS Spectrum of Ullmann methyl 4-N-phenothiazinylbenzoate



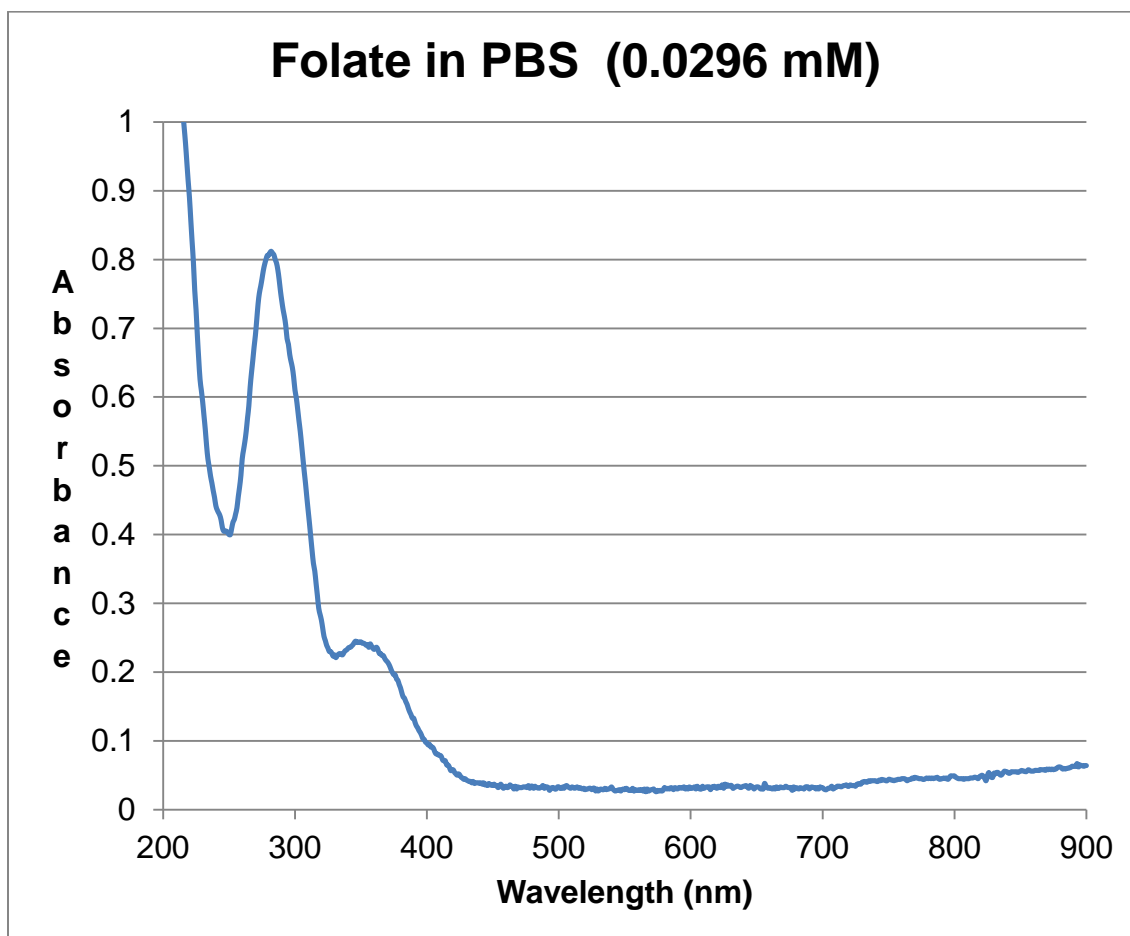


Figure 30. UV-VIS Spectrum of Folic Acid Dihydrate Standard

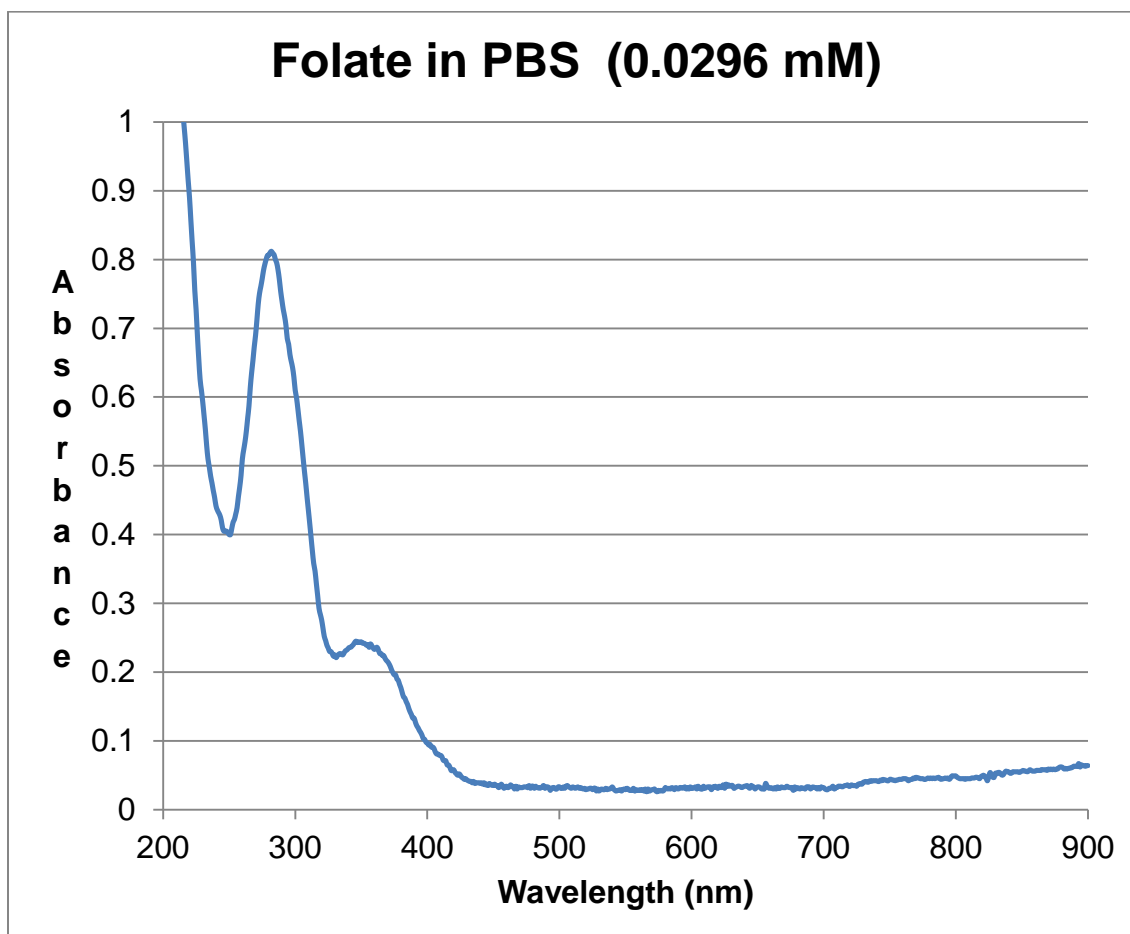


Figure 31. UV-VIS Spectrum of Folic Acid Dihydrate Standard

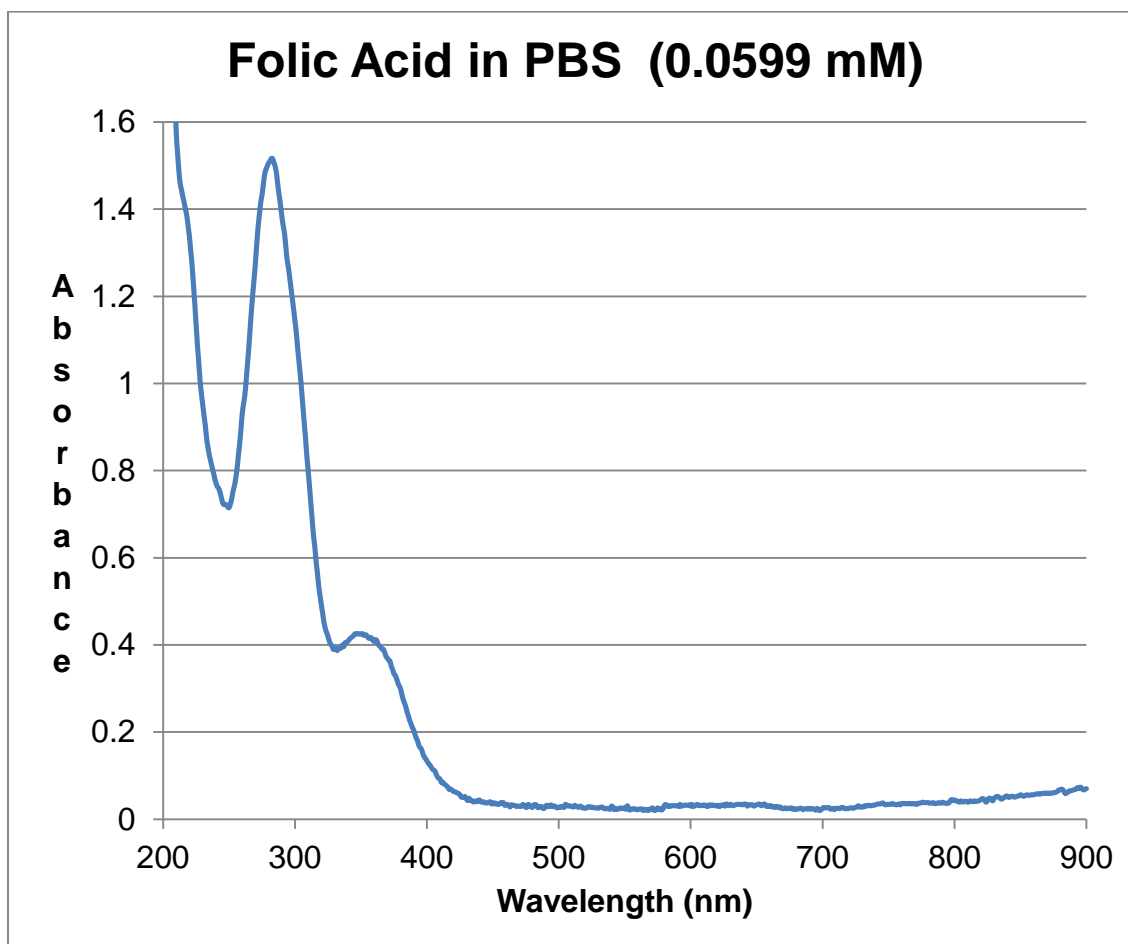


Figure 32. UV-VIS Spectrum of Folic Acid Dihydrate Standard

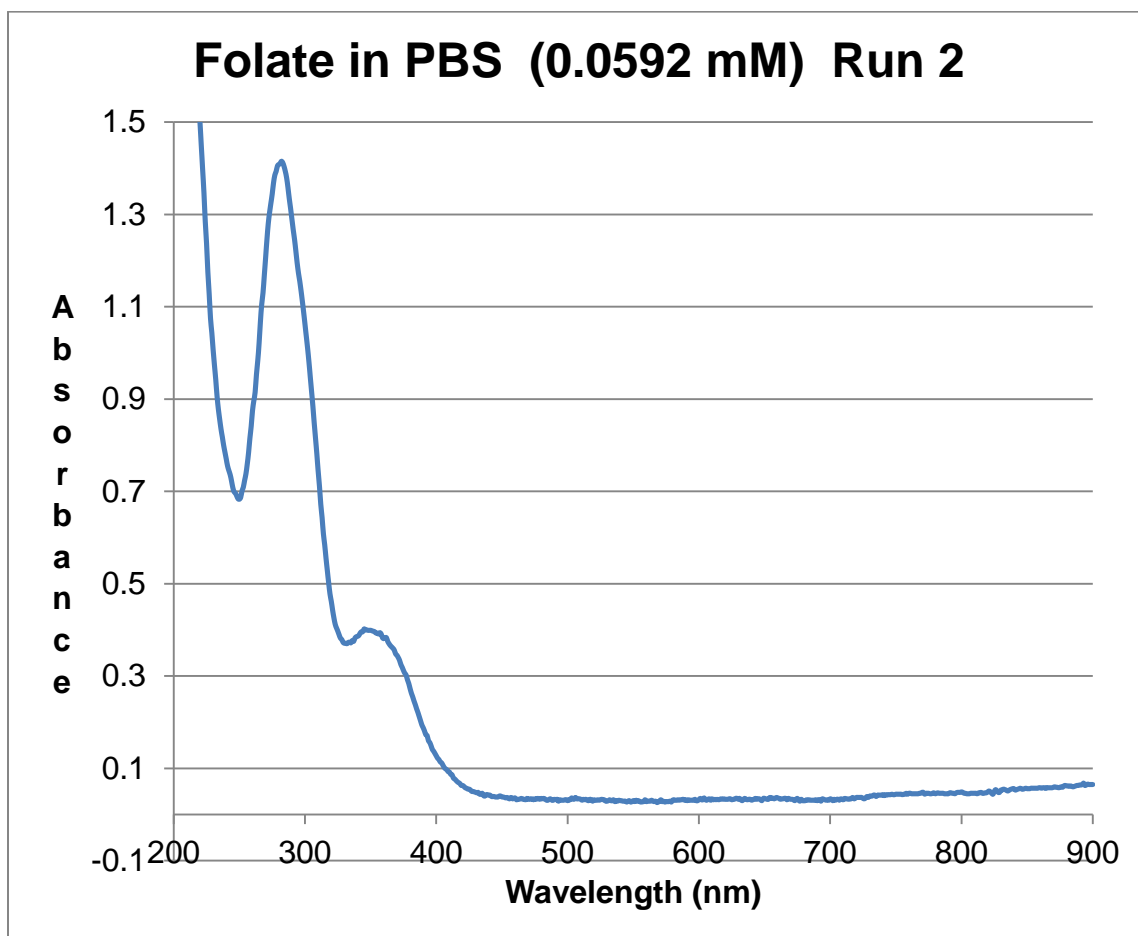


Figure 33. UV-VIS Spectrum of Folic Acid Dihydrate Standard

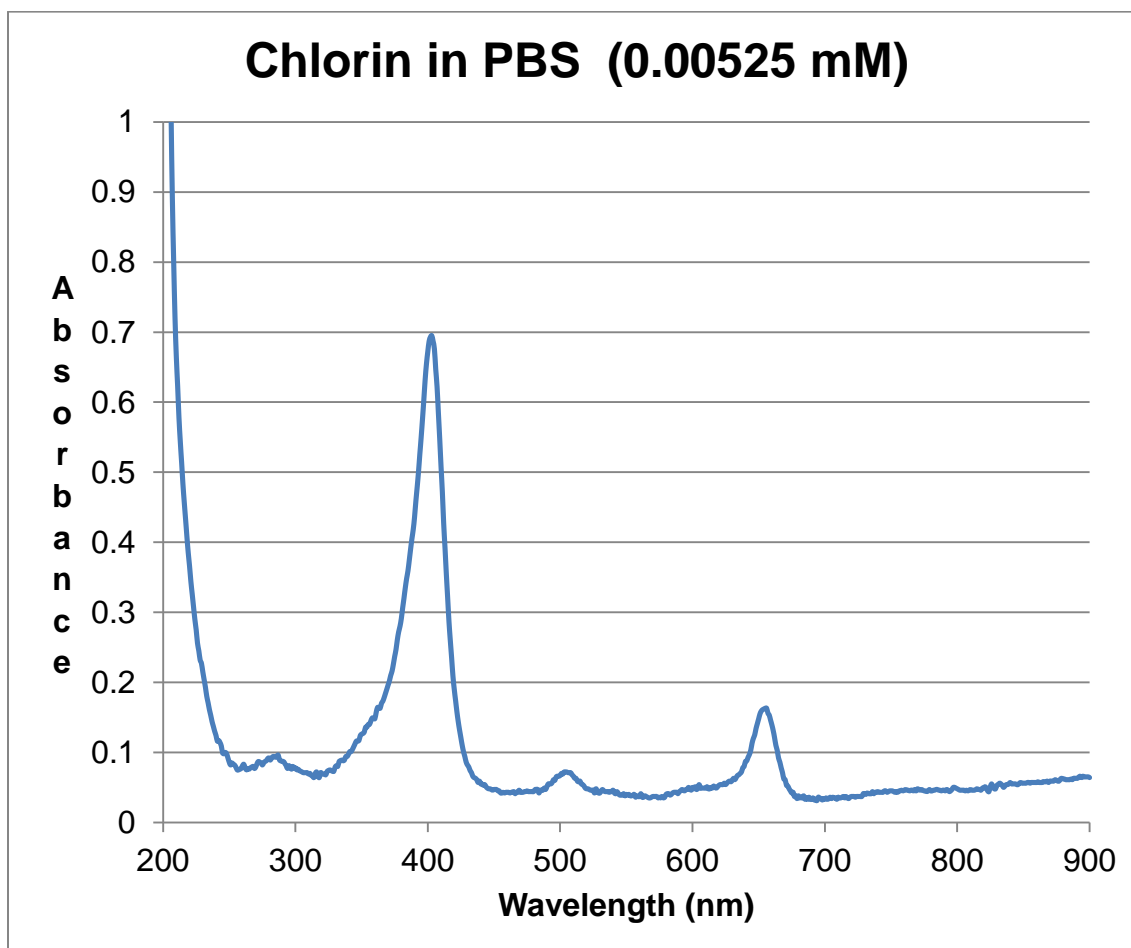


Figure 34. UV-VIS Spectrum of Ce6 Standard

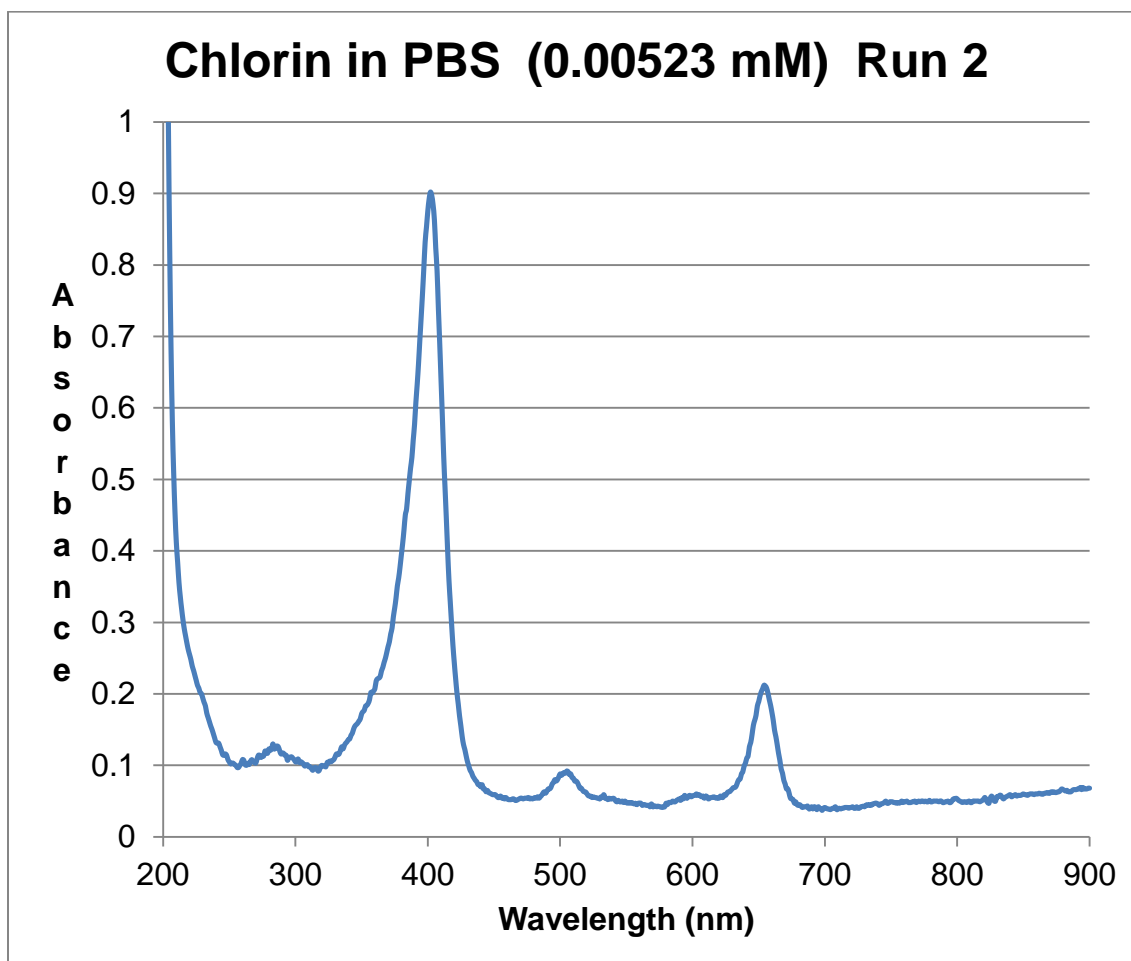


Figure 35. UV-VIS Spectrum of Ce6 Standard

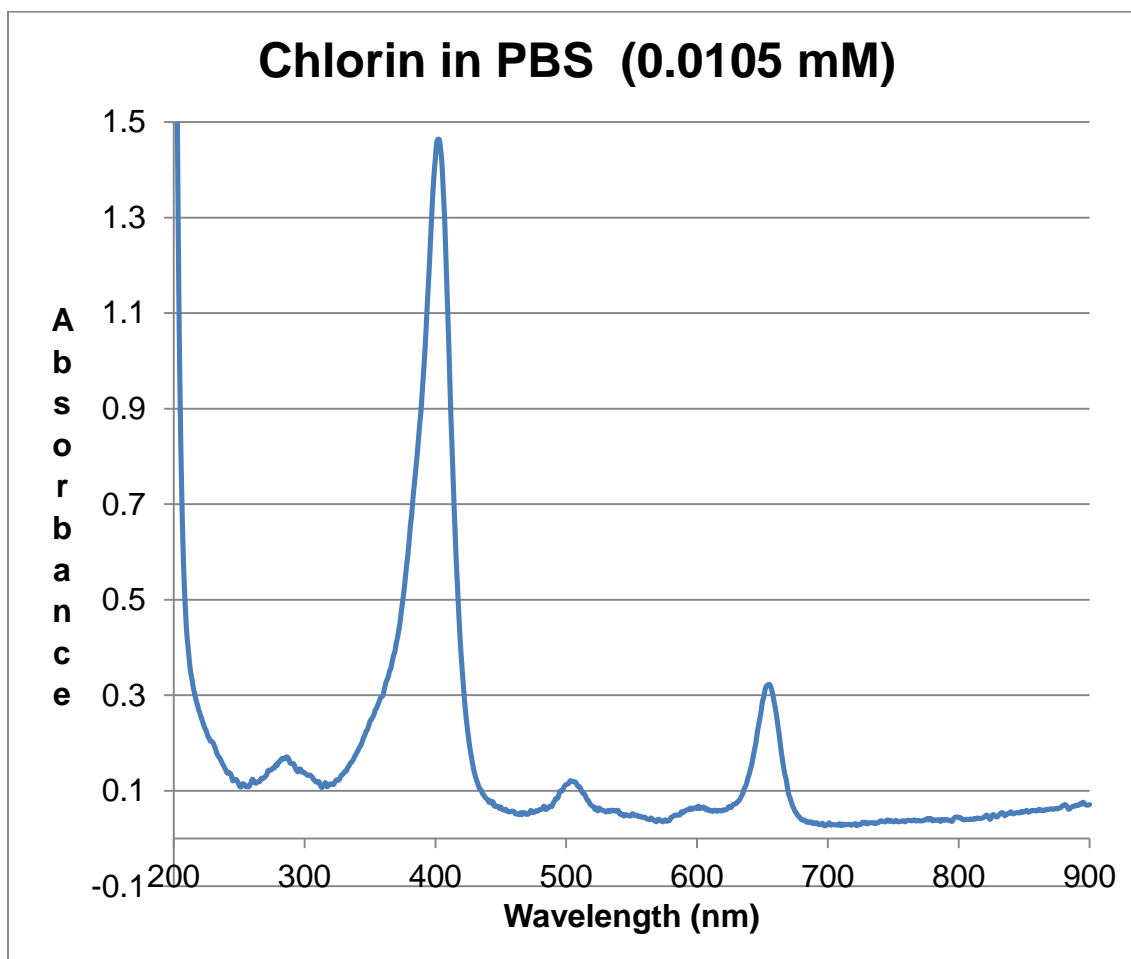


Figure 36. UV-VIS Spectrum of Ce6 Standard

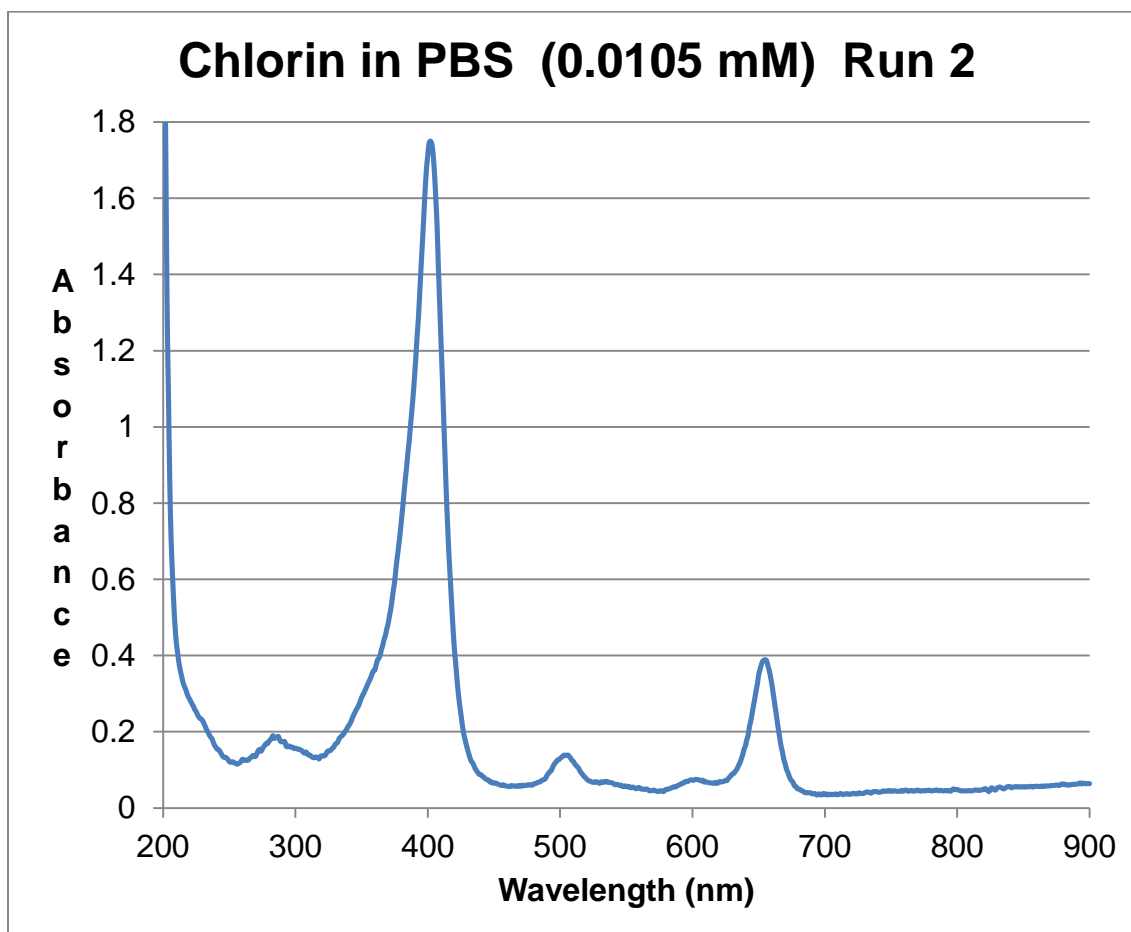
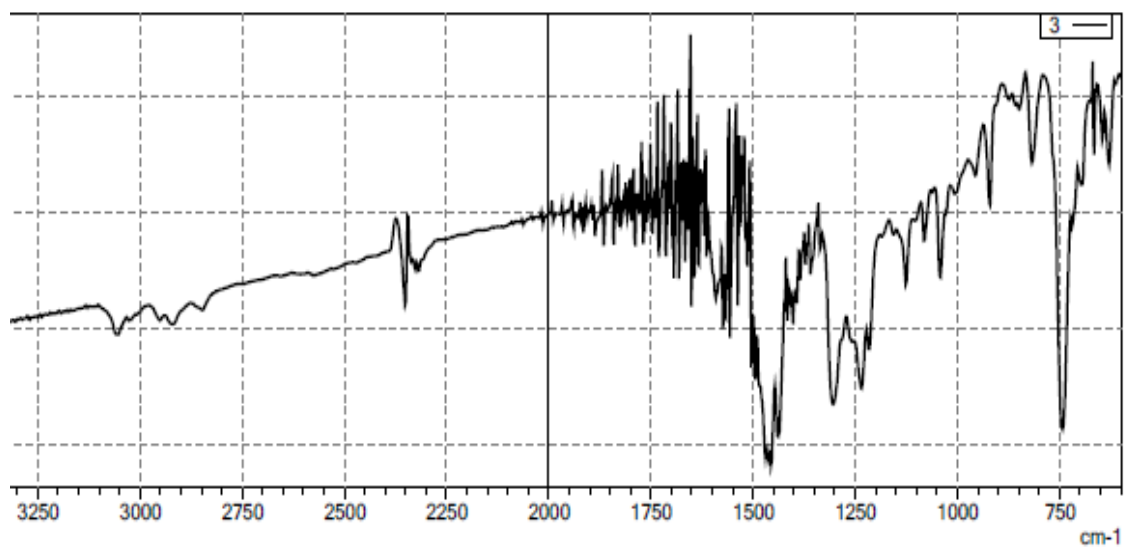


Figure 37. UV-VIS Spectrum of Ce6 Standard

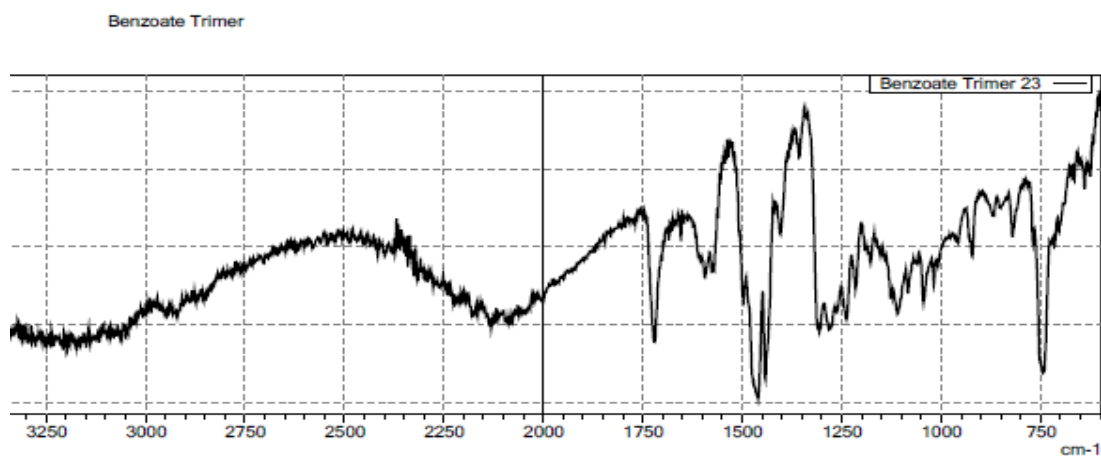


Benzyl Trimer



Functional Group	Frequency (cm <sup>-1</sup> )
C-H stretch (sp <sup>2</sup> )	3053
C-H stretch (sp <sup>3</sup> )	2951, 2920, 2846
C=C stretch (aromatic ring)	1591
C-N stretch	1303
monosubstituted aromatic ring bend	742

Figure 38. IR Spectrum of N-benzyl-3,7-diphenothiazinylphenothiazine



Functional Group	Frequency (cm <sup>-1</sup> )
C-H stretch (sp <sup>2</sup> )	3088, 3049
C-H stretch (sp <sup>3</sup> )	2998, 2986
C=O stretch (ester)	1721
C=C stretch (aromatic ring)	1654
C-N stretch	1300
C-O stretch	1238, 1215
p-disubstituted aromatic ring bend	744

Figure 39. IR Spectrum of methyl (3,7-diphenothiazinyl)-4-N-methylenephenothiazinylbenzoate

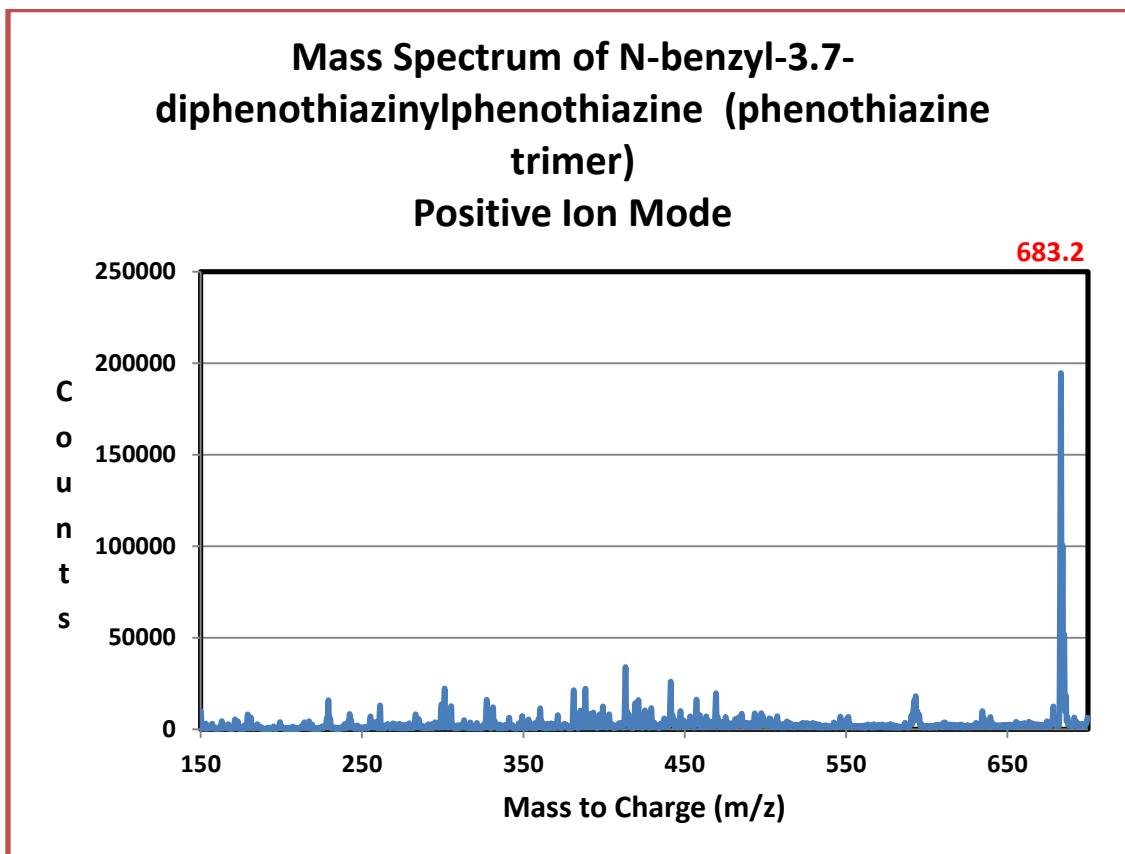


Figure 40. Mass Spectrum of N-benzyl-3,7-diphenothiazinylphenothiazine

### Interpretation of Mass Spectral Data

The product molecular mass is 683.2 g/mol. A high abundance is seen at this weight in the spectrum. This indicates a good purity in this particular fraction. Also, since the instrument was run in positive ion mode, the molecular ion peak is represented as a radical cation, since the mass remains identical to the actual product mass. If the sample had become protonated, as is often seen in positive ion mode, the mass would be represented as 684.2 g/mol.

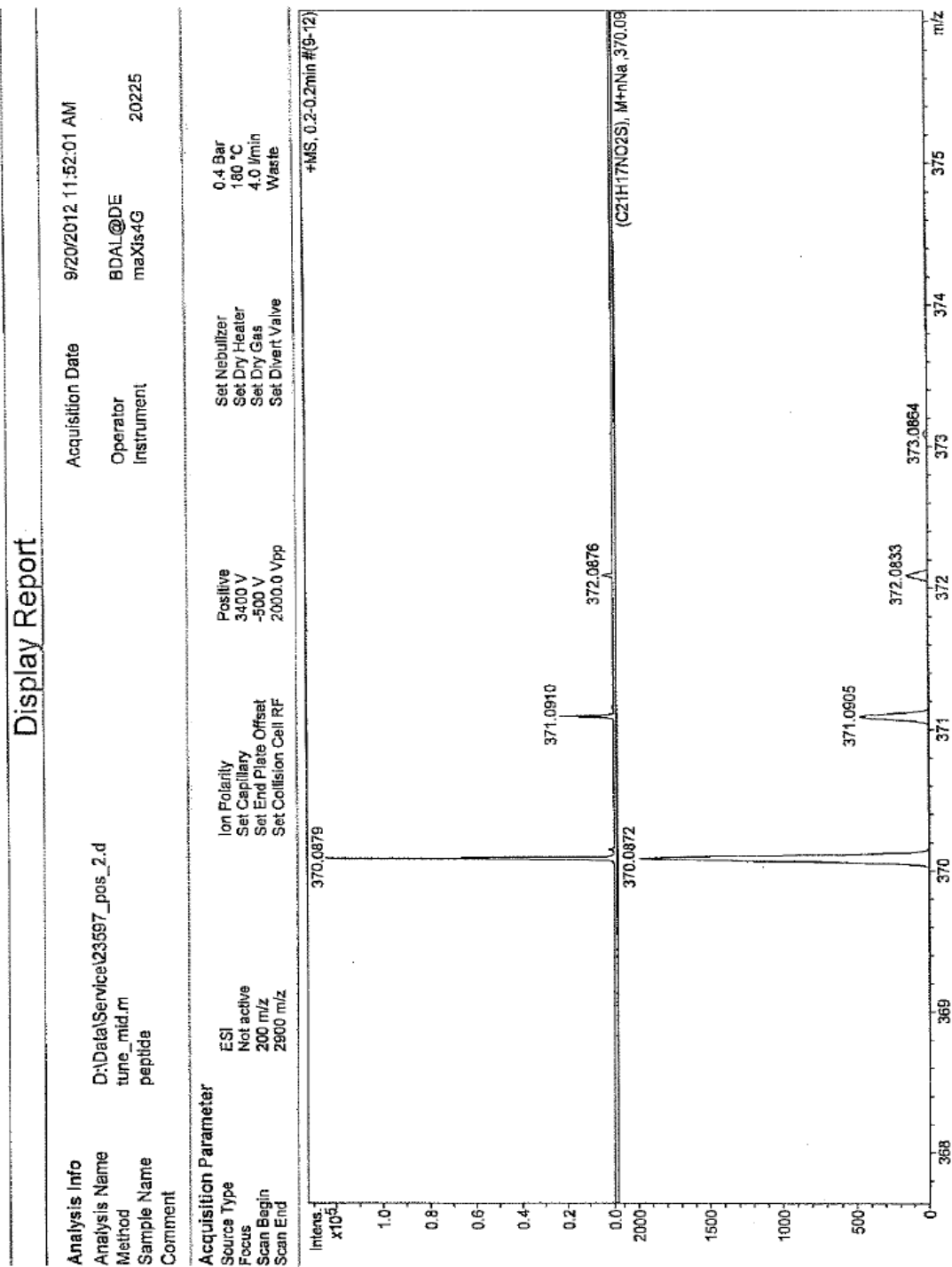
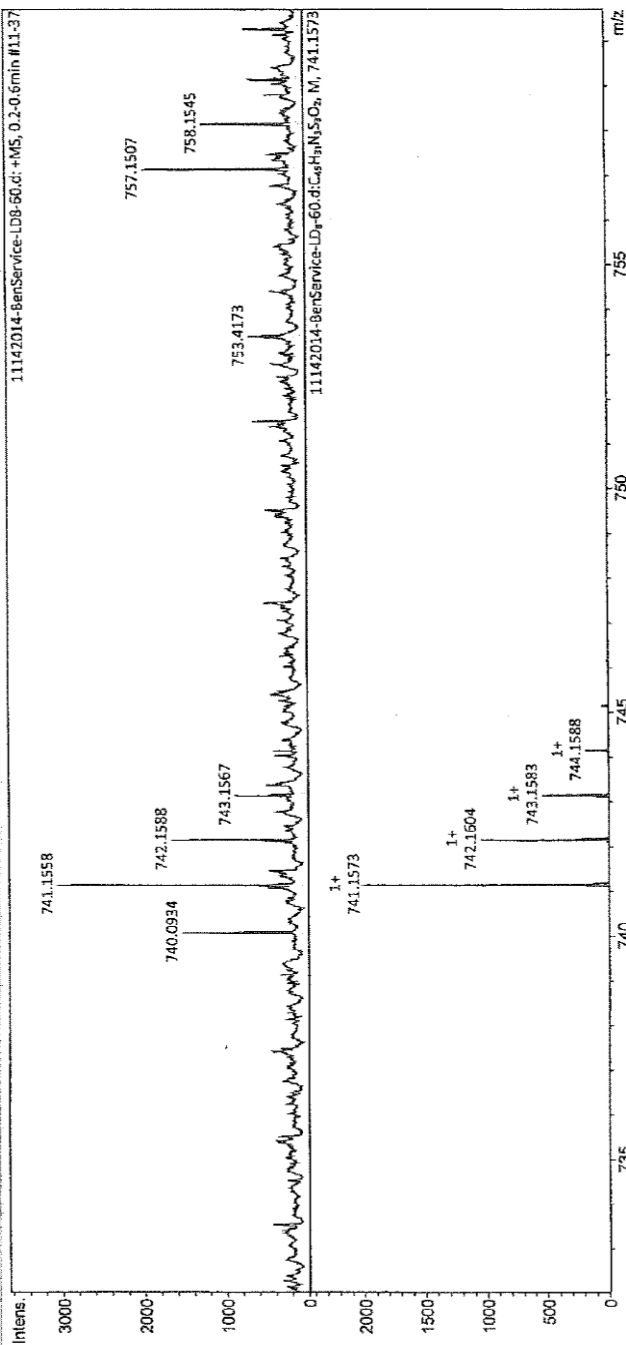


Figure 41. Mass Spectrum of methyl 4-N-methylenephenthiazinylbenzoate

## Display Report

**Analysis Info**  
 Analysis Name: D:\Data\Ben\11142014-BenService-LD8-60.d  
 Method: Tune\_mid\_pos.m  
 Sample Name:   
 Comment:   
 Acquisition Date: 11/14/2014 3:35:30 PM  
 Operator: BDAL@DE  
 Instrument: maXis  
 288882.20225

**Acquisition Parameter**  
 Source Type: ESI  
 Focus: Not active  
 Scan Begin: 150 m/z  
 Scan End: 3000 m/z  
 Ion Polarity: Positive  
 Set Capillary: 3800 V  
 Set End Plate Offset: -500 V  
 Set Charging Voltage: 0 V  
 Set Corona: 0 nA  
 Set Nebulizer: 0.3 Bar  
 Set Dry Heater: 180 °C  
 Set Dry Gas: 4.0 l/min  
 Set Divert Valve: Waste  
 Set APCI Heater: 0 °C



11142014-BenService-LD8-60.d  
 Bruker Compass DataAnalysis 4.2  
 printed: 11/14/2014 3:39:05 PM  
 by: BDAL@DE  
 Page 1 of 1

Figure 42. Mass Spectrum of methyl (3,7-diphenothiazinyl)-4-N-methylene phenothiazinylbenzoate

Chlorin e6 for Laura #1-84 RT: 0.00-1.01 AV: 84 NL: 7.71E5  
T: - p ESI Full ms [50.00-650.00]

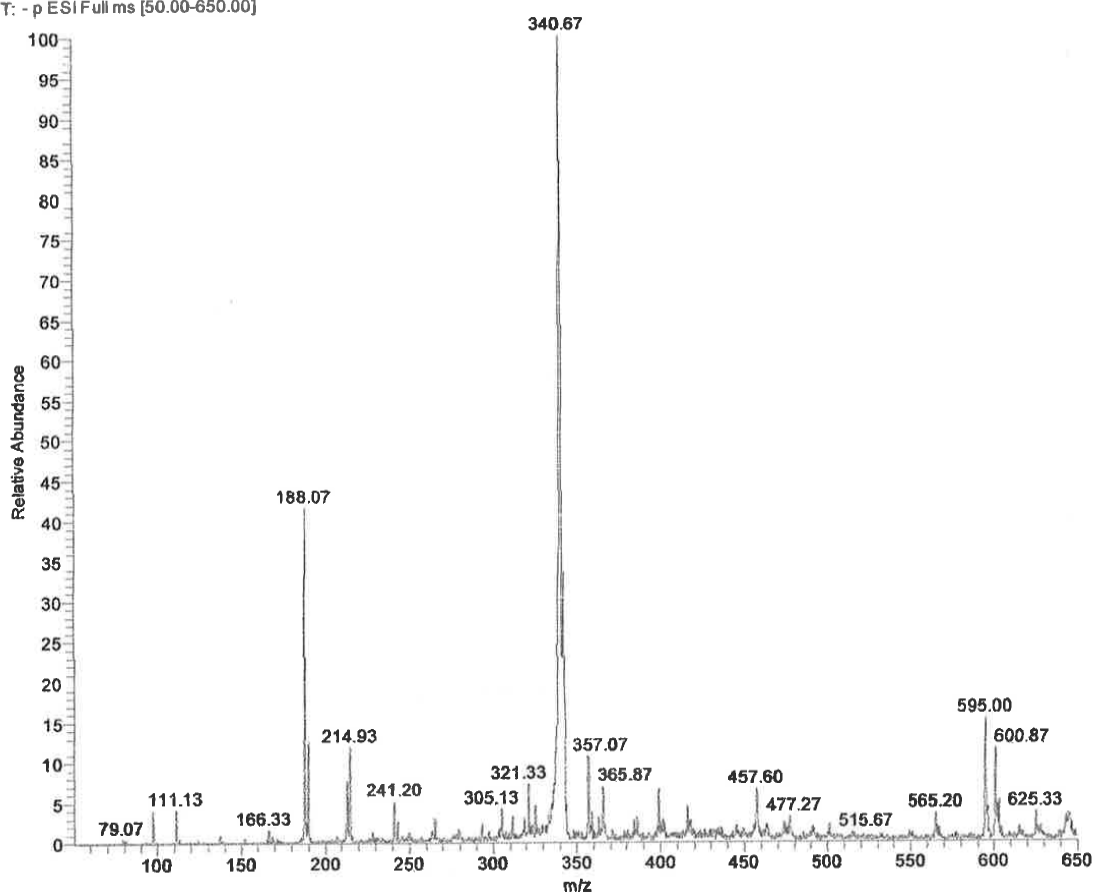


Figure 43. Mass Spectrum of Chlorin e6

Chlorin PEG folic acid neg mode 800-1200 Daltons #1-220 RT: 0.01-2.00 AV: 220 NL: 5.68E5  
T: - p ESI Full ms [800.00-1200.00]

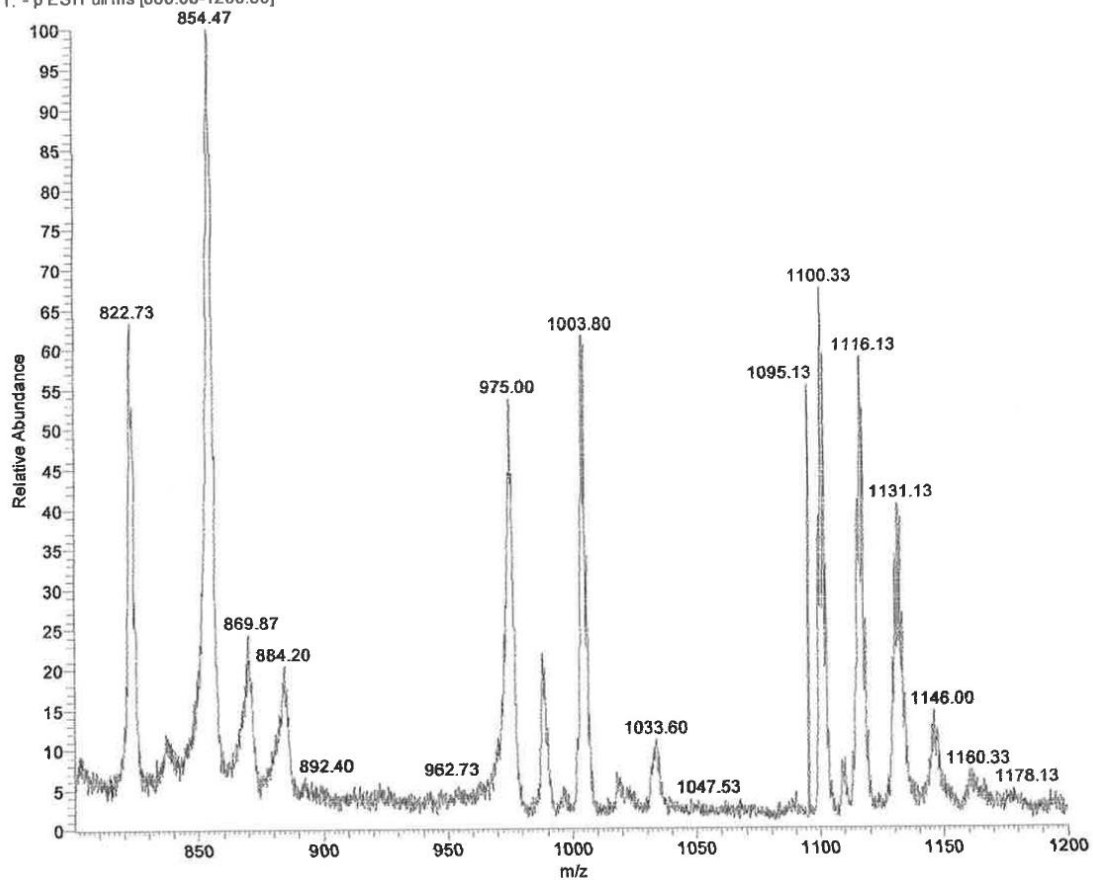


Figure 44. Mass Spectrum of Ce6-PEG-FA

Chlorin PEG Folic Acid #1-36 RT: 0.02-1.00 AV: 36 NL: 1.26E6  
T: - p ESI Full ms [100.00-2000.00]

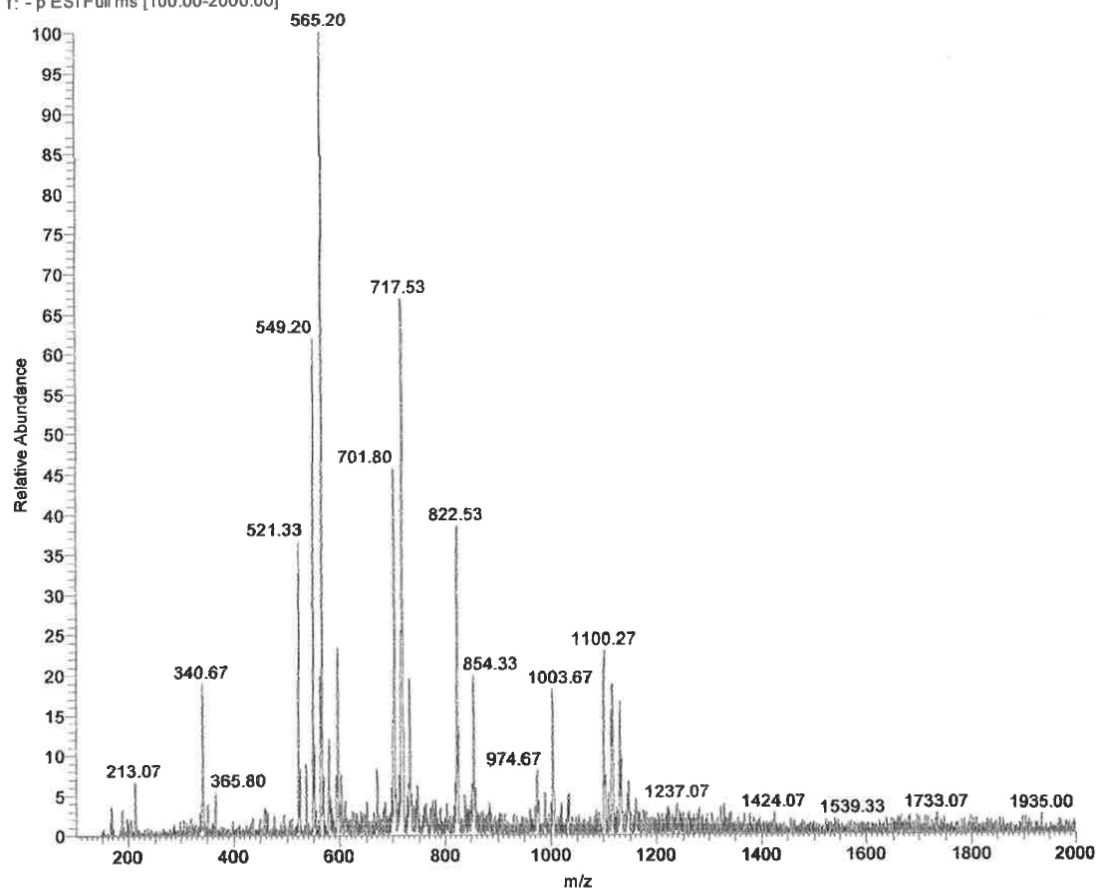


Figure 45. Mass Spectrum of Ce6-PEG-FA





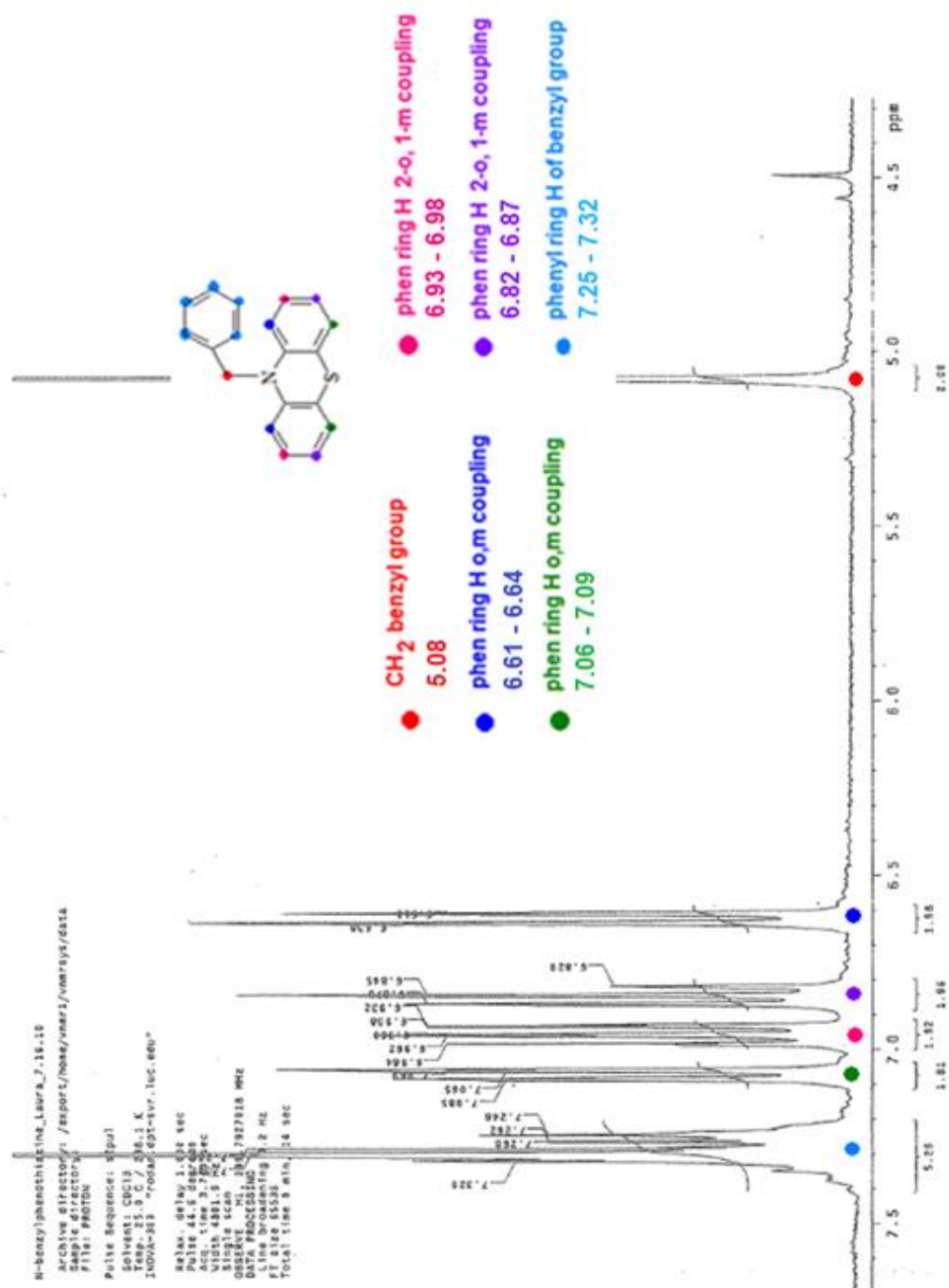


Figure 47. <sup>1</sup>H NMR Expansion of N-benzylphenothiazine

**Interpretation of  $^1\text{H}$  NMRs in Figures 46. and 47.**

- Peak at 1.54 = H from  $\text{H}_2\text{O}$
- Peak at 4.5 = H from  $\text{CH}_2\text{Cl}_2$  used in extraction
- Peak at 5.08 = H from  $\text{CH}_2$  (benzyl group)
- Peaks at 6.61 / 6.64 = phenothiazine ring H with ortho and meta coupling (doublet of doublets);  $J = 9 \text{ Hz}, 3 \text{ Hz}$
- Peaks at 6.82 / 6.84 / 6.87 = phenothiazine ring H with 2 ortho and 1 meta coupling (triplet of doublets);  $J = 9 \text{ Hz}, 6 \text{ Hz}, 2 \text{ Hz}$
- Peaks at 6.93 / 6.94 / 6.96 / 6.98 = phenothiazine ring H with 2 ortho and 1 meta coupling (triplet of doublets);  $J = 8 \text{ Hz}, 7 \text{ Hz}, 2 \text{ Hz}$
- Peaks at 7.06 / 7.09 = phenothiazine ring H with ortho and meta coupling (doublet of doublets);  $J = 9 \text{ Hz}, 3 \text{ Hz}$
- Peaks at 7.25 / 7.26 / 7.27 / 7.32 = phenyl H atoms from benzyl protection group on N
- Peak at 7.29 =  $\text{CHCl}_3$  peak

**C-13 NMR**  
**N-benzylphenothiazine**

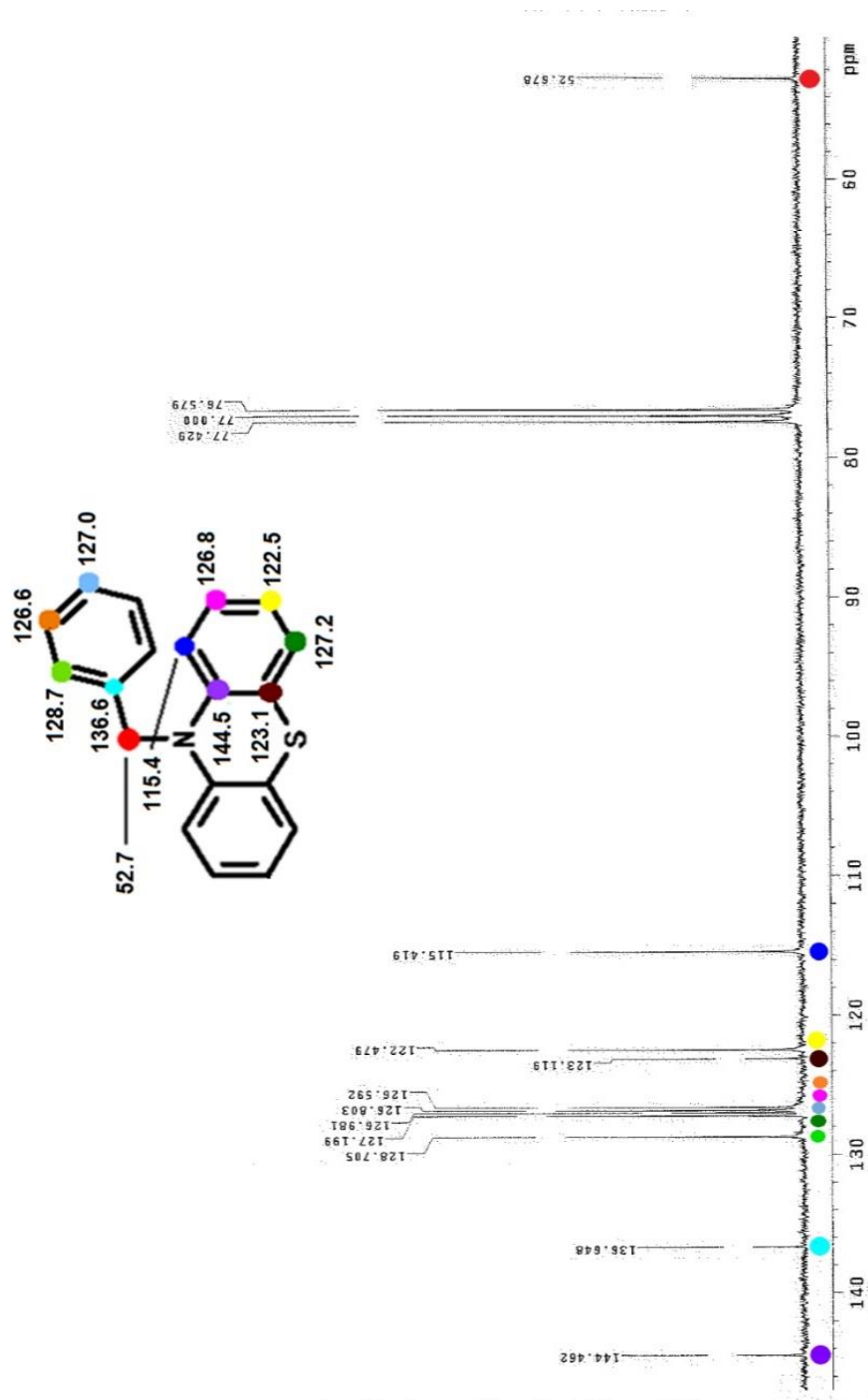


Figure 48.  $^{13}\text{C}$  NMR Expansion of N-benzylphenothiazine

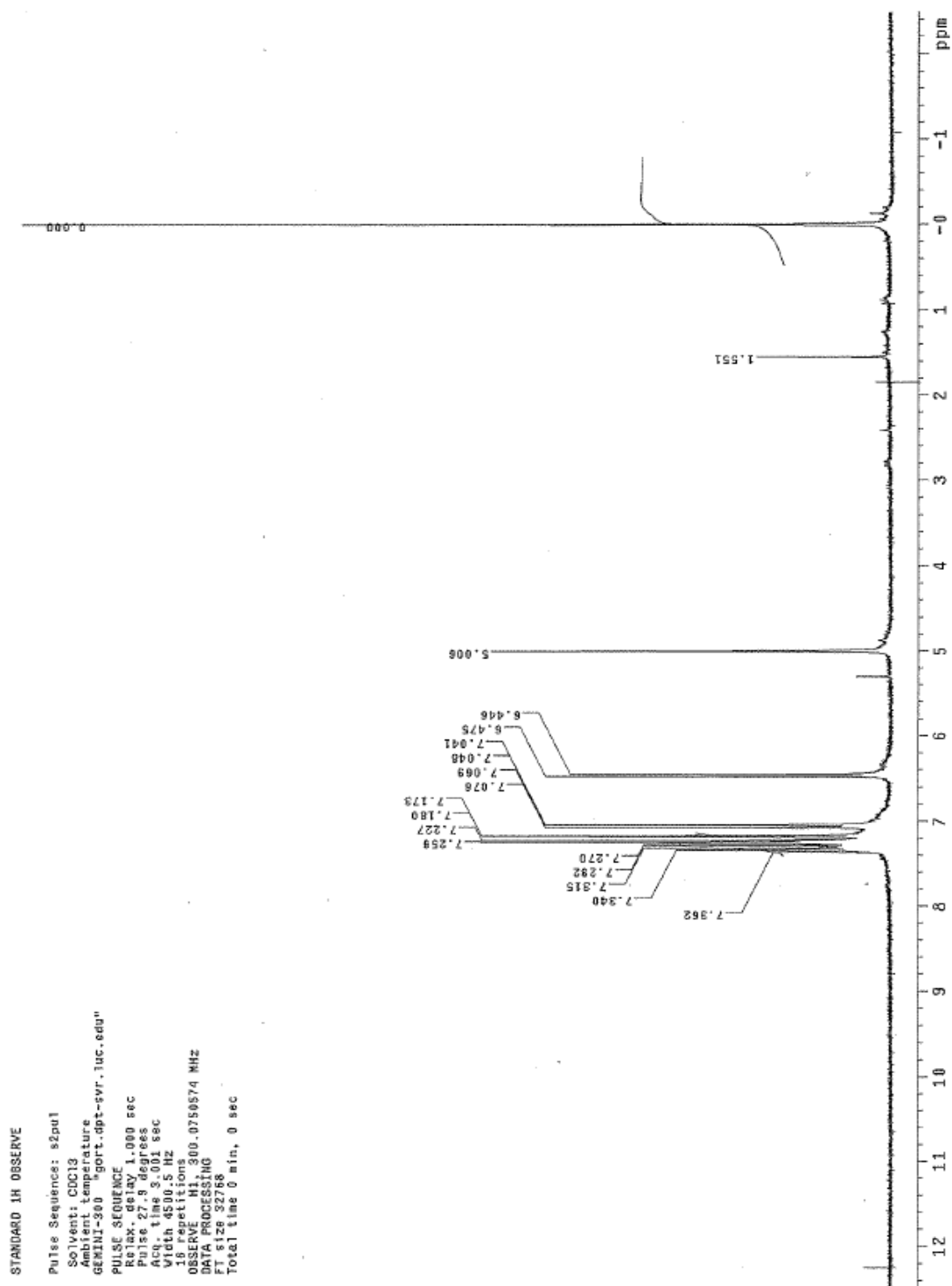


Figure 49.  $^1\text{H}$  NMR of N-benzyl-3,7-dibromophenothiazine

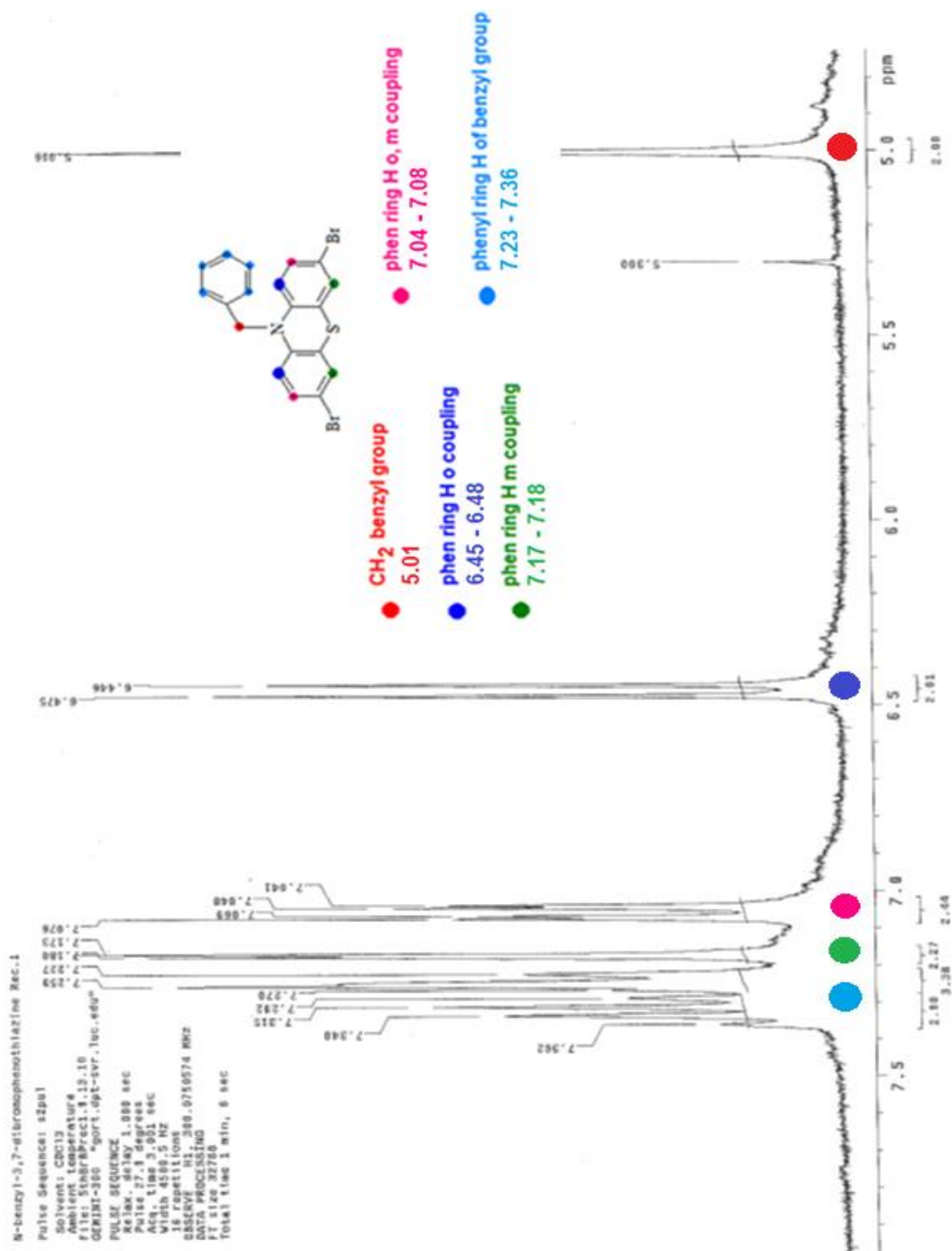
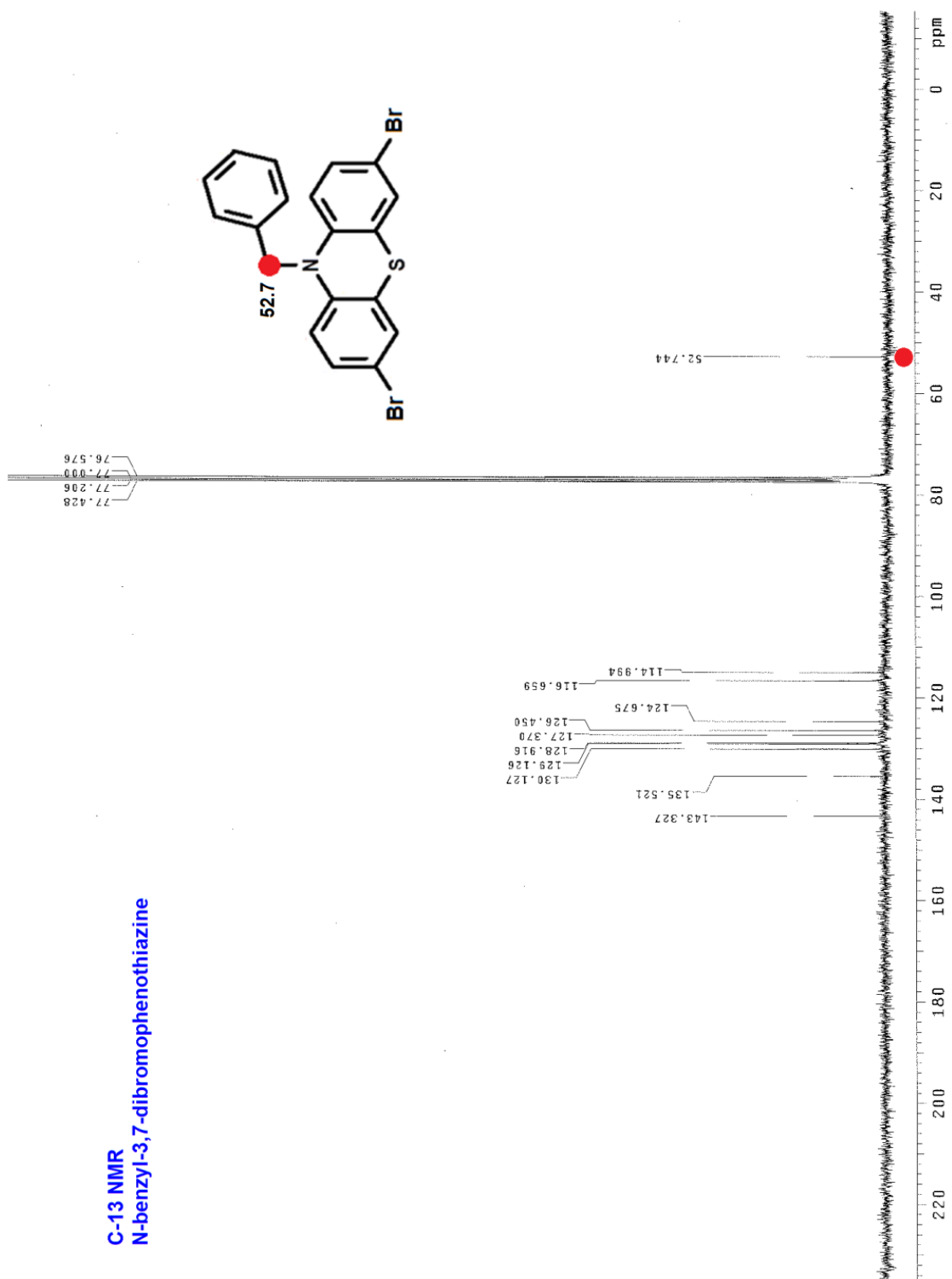


Figure 50. <sup>1</sup>H NMR Expansion of N-benzyl-3,7-dibromophenothiazine

**Interpretation of  $^1\text{H}$  NMRs in Figures 49. and 50.**

- Peak at 1.55 = H from  $\text{H}_2\text{O}$
- Peak at 5.01 = H from  $\text{CH}_2$  (benzyl group)
- Peaks at 6.45 / 6.48 = phenothiazine ring H with ortho coupling (doublet;  $J = 9$  Hz)
- Peaks at 7.04 / 7.05 / 7.07 / 7.08 = phenothiazine ring H with ortho and meta coupling (doublet of doublets;  $J = 9$  Hz, 3 Hz)
- Peaks at 7.17 / 7.18 = phenothiazine ring H with meta coupling (doublet;  $J = 3$  Hz)
- Peaks at 7.23 / 7.26 / 7.27 / 7.29 / 7.32 / 7.34 / 7.36 phenyl H atoms from benzyl protection group on N

Figure 51.  $^{13}\text{C}$  NMR of N-benzyl-3,7-dibromophenothiazine



**C-13 NMR**  
**N-benzyl-3,7-dibromophenothiazine**

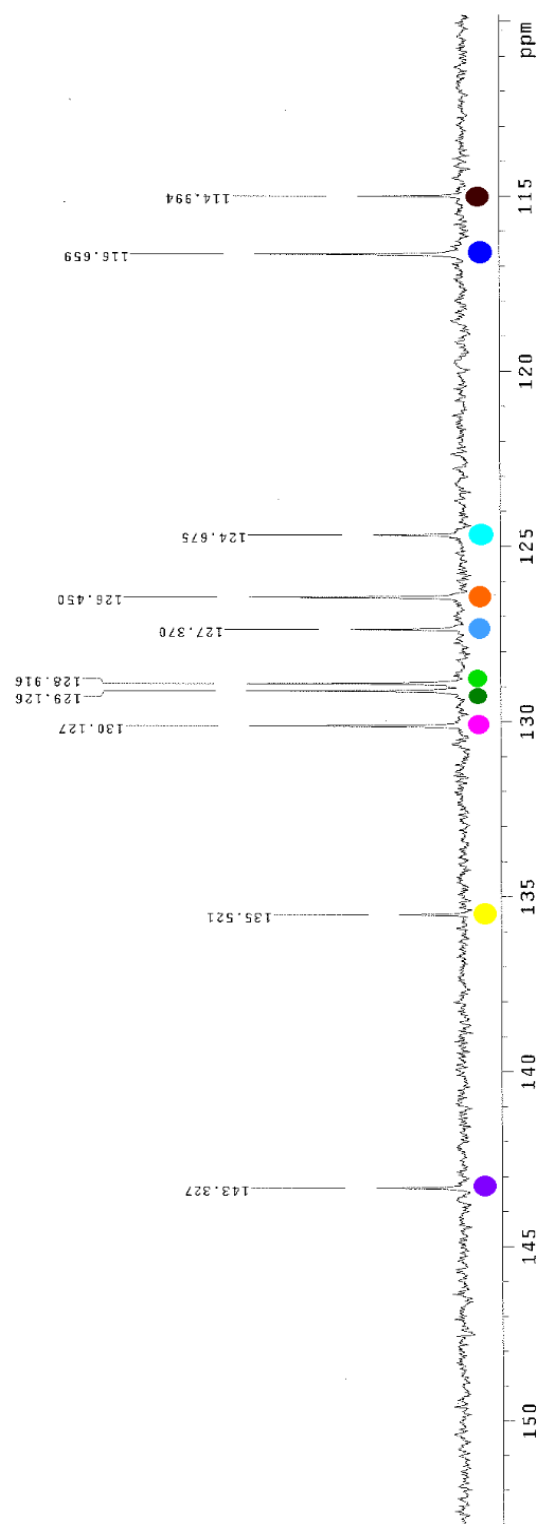
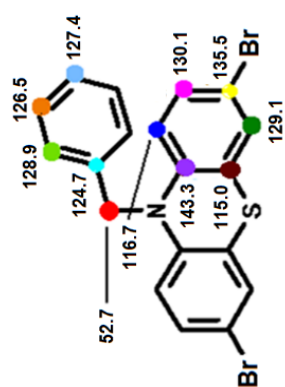


Figure 52. <sup>13</sup>C NMR Expansion of N-benzyl-3,7-dibromophenothiazine

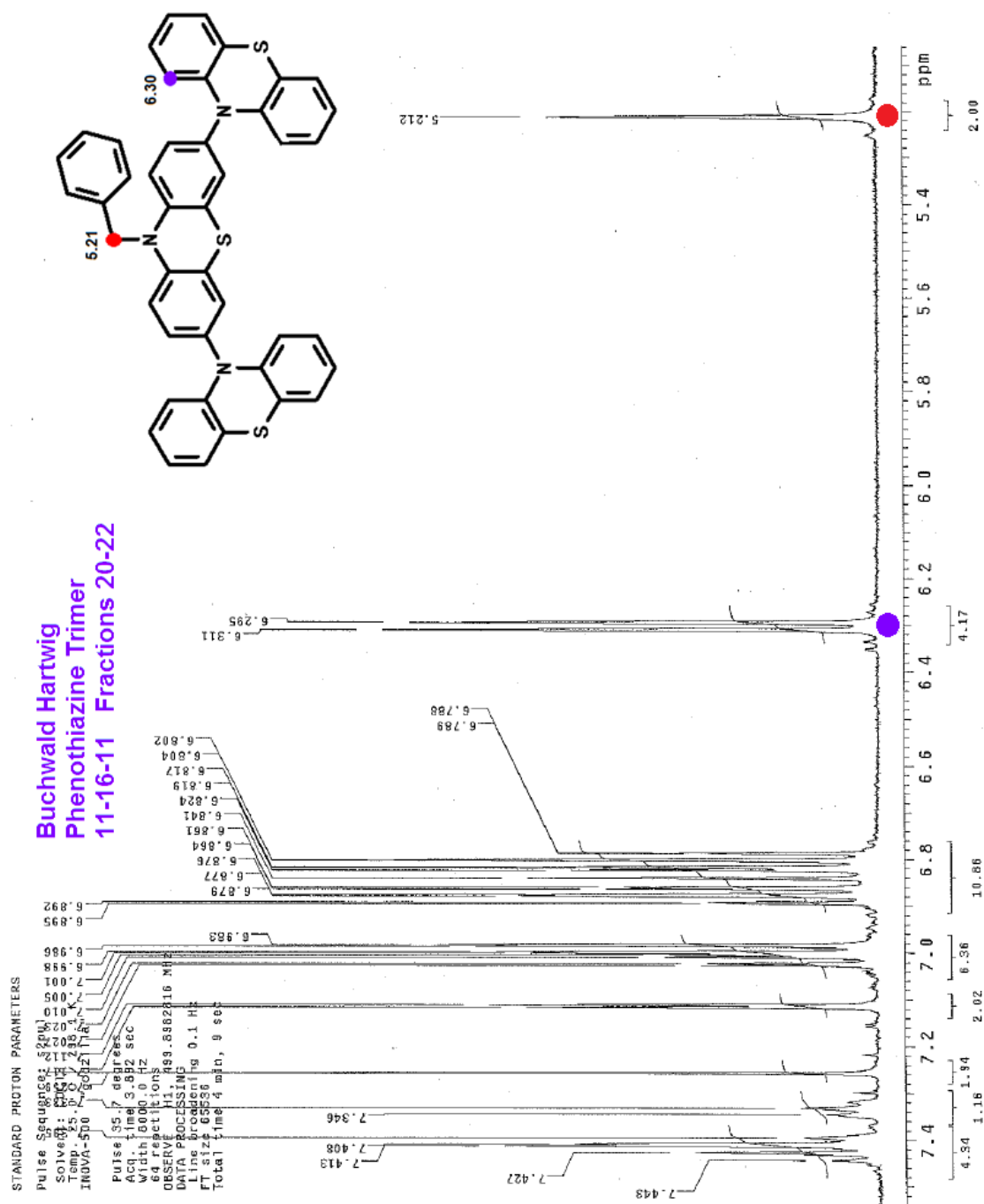


Figure 53. <sup>1</sup>H NMR Expansion of N-benzyl-3,7-diphenothiazinylphenothiazine

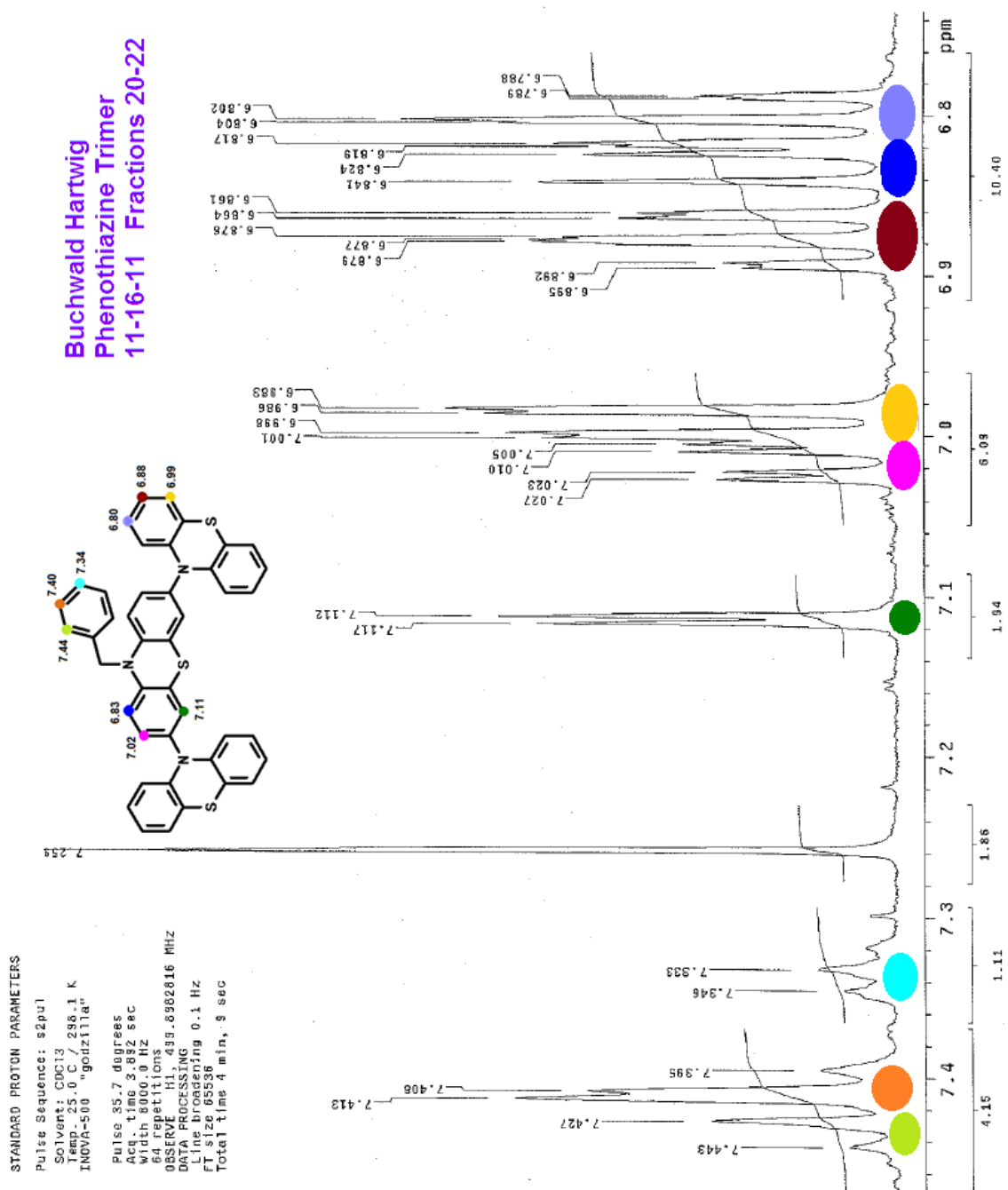
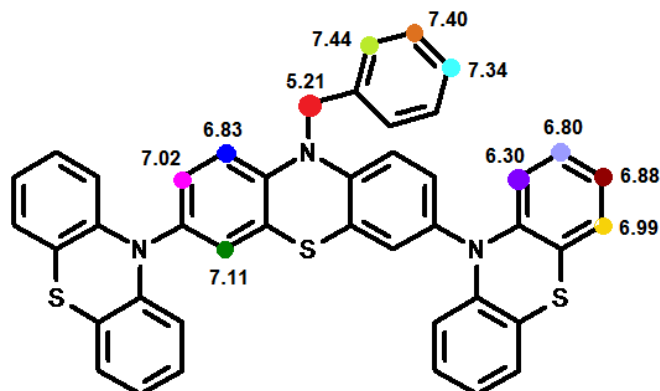


Figure 54. <sup>1</sup>H NMR Expansion of N-benzyl-3,7-diphenothiazinylphenothiazine

### Interpretation of $^1\text{H}$ NMRs in Figures 53. and 54.

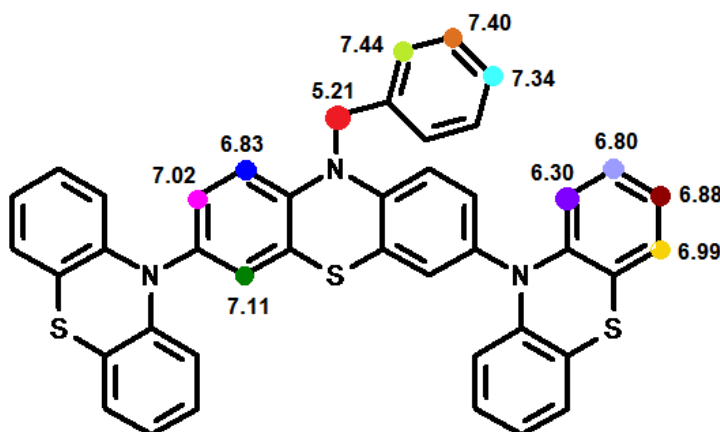


**Peak at 5.21** – integrates at 2 H atoms; H on  $\text{CH}_2$  of protection group is non-aromatic and is farther upfield

**Peaks at 6.30 – 6.31 (6.30)** – integrates at 4 H atoms; H on phenthiazine substituents; peak is a doublet of doublets due to ortho and meta coupling; it is in close proximity to the N atom, and since N lone pairs interact with the ring system, this provides a shielding effect and shifts peak farther upfield;  $J = 8 \text{ Hz}, 2 \text{ Hz}$

**Peaks at 6.79 – 6.90** – integrates at 10 H atoms

- **Peaks at 6.79 – 6.82 (6.80)** – integrates at 4 H atoms; H on phenthiazine substituents; peak is a triplet of doublets due to two ortho and one meta coupling; it is closer to the N atom and farther upfield;  $J = 8 \text{ Hz}, 8 \text{ Hz}, 1 \text{ Hz}$
- **Peaks at 6.86 – 6.90 (6.88)** – integrates at 4 H atoms; H on phenthiazine substituents; peak is a triplet of doublets due to two ortho and one meta coupling; it is closer to the S atom and farther downfield;  $J = 8 \text{ Hz}, 8 \text{ Hz}, 1 \text{ Hz}$
- Both peaks in the 6.79 – 6.90 range show a similar pattern as the H atoms in the same positions on phenthiazine
- **Peaks at 6.82 – 6.84 (6.83)** – integrates at 2 H atoms; H on phenthiazine base; peak is a doublet due to ortho coupling; it is in close proximity to the N atom and farther upfield;  $J = 9 \text{ Hz}$



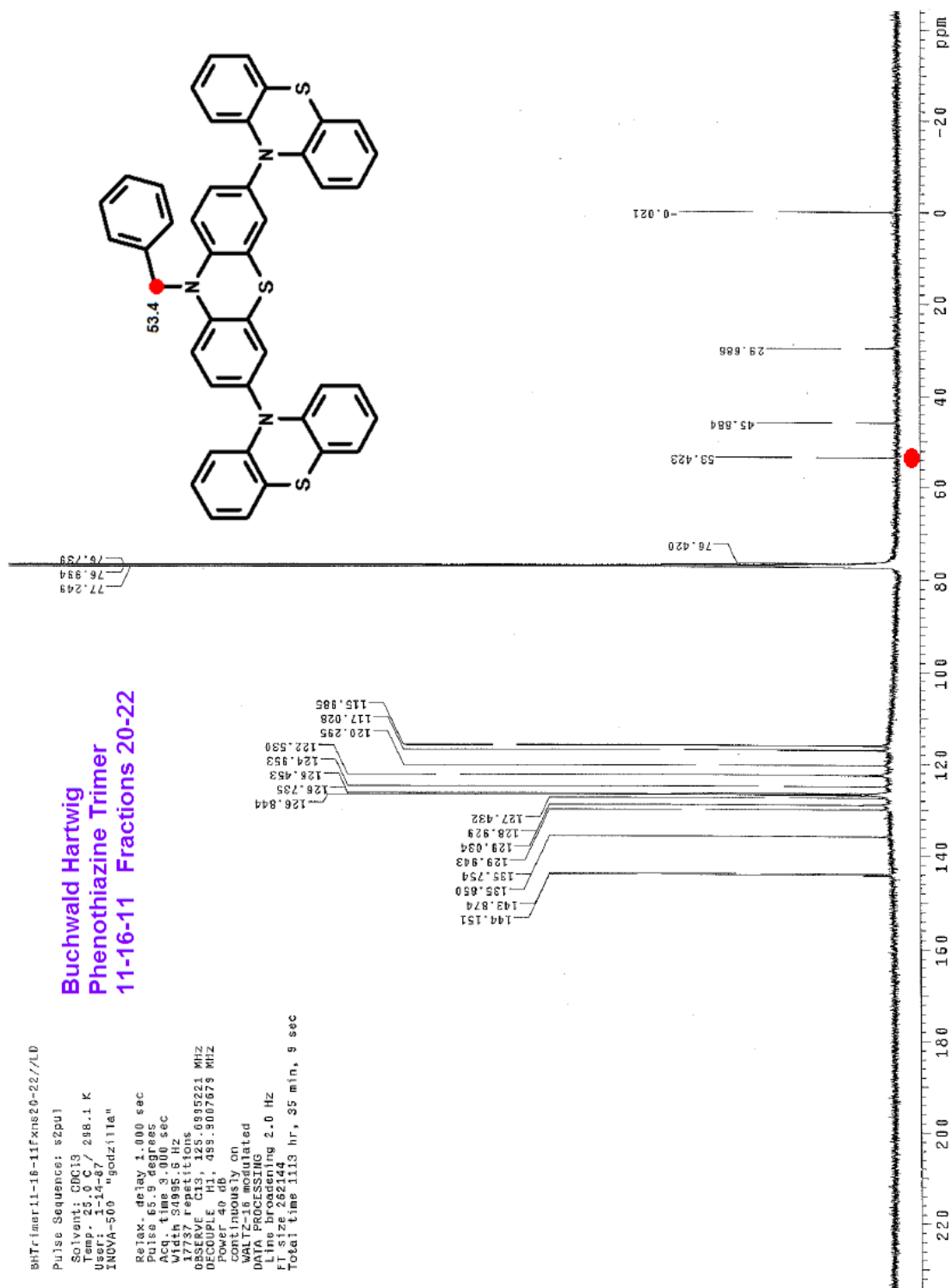
**Peaks at 6.98 – 7.03** – integrates at 6 H atoms

- **Peaks at 6.98 – 7.00 (6.99)** – integrates at 4 H; H on phenothiazine substituents; peak is a doublet of doublets due to ortho and meta coupling; it is in close proximity to the S atom and farther downfield;  $J = 8 \text{ Hz}, 2 \text{ Hz}$
- **Peaks at 7.01 – 7.03 (7.02)** – integrates at 2 H atoms; H on phenothiazine base; peak is a doublet of doublets due to ortho and meta coupling; it is closer to the N atom and farther upfield;  $J = 9 \text{ Hz}, 2 \text{ Hz}$

**Peaks at 7.11 – 7.12 (7.11)** – integrates at 2 H atoms; H on phenothiazine base; peak is a doublet due to meta coupling; it is in close proximity to the S atom and farther downfield;  $J = 3 \text{ Hz}$

**Peaks at 7.33 – 7.44** – integrates at 5 H atoms; H atoms of the aromatic ring of the benzyl protection group

- **Peaks at 7.33 – 7.35 (7.34)** – integrates at 1 H atom; ring H that is para to the area of the ring which is connected to the  $\text{CH}_2$  group; peak is a triplet of triplets (multiplet of peaks) due to two ortho and two meta couplings
- **Peaks at 7.40 – 7.41 (7.40)** – integrates at 2 H atoms; ring H atoms closest to the one H atom that is described in the preceding section; peak is a triplet of doublets due to two ortho and one meta coupling;  $J = 9 \text{ Hz}, 3 \text{ Hz}$
- **Peaks at 7.43 – 7.44 (7.44)** – integrates at 2 H atoms, ring H atoms adjacent to the point of  $\text{CH}_2$  attachment; peak is a doublet of doublets due to ortho and meta coupling;  $J = 8 \text{ Hz}, 3 \text{ Hz}$

Figure 55.  $^{13}\text{C}$  NMR of N-benzyl-3,7-diphenothiazinylphenothiazine

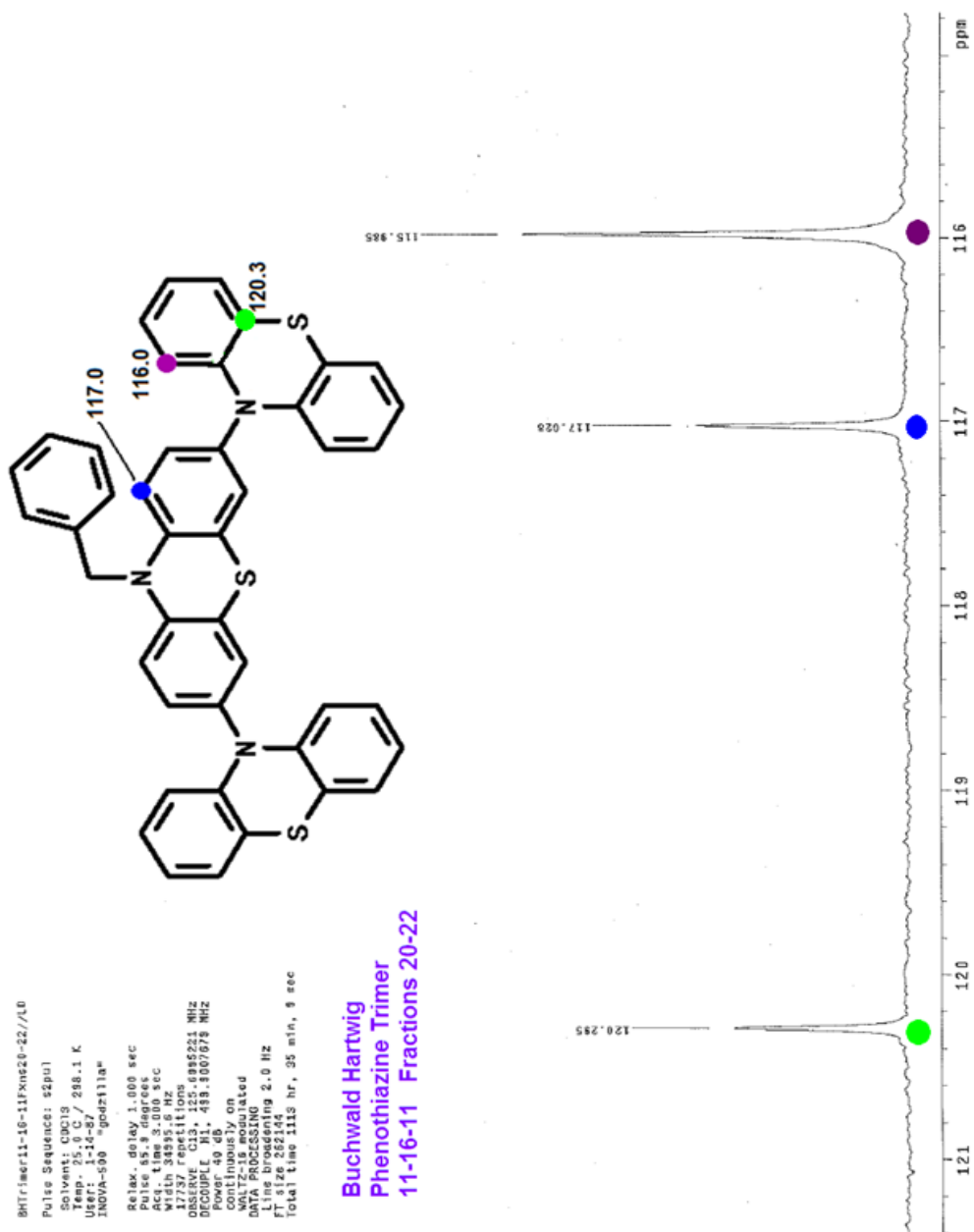


Figure 56.  $^{13}\text{C}$  NMR Expansion of N-benzyl-3,7-diphenothiazinylphenothiazine

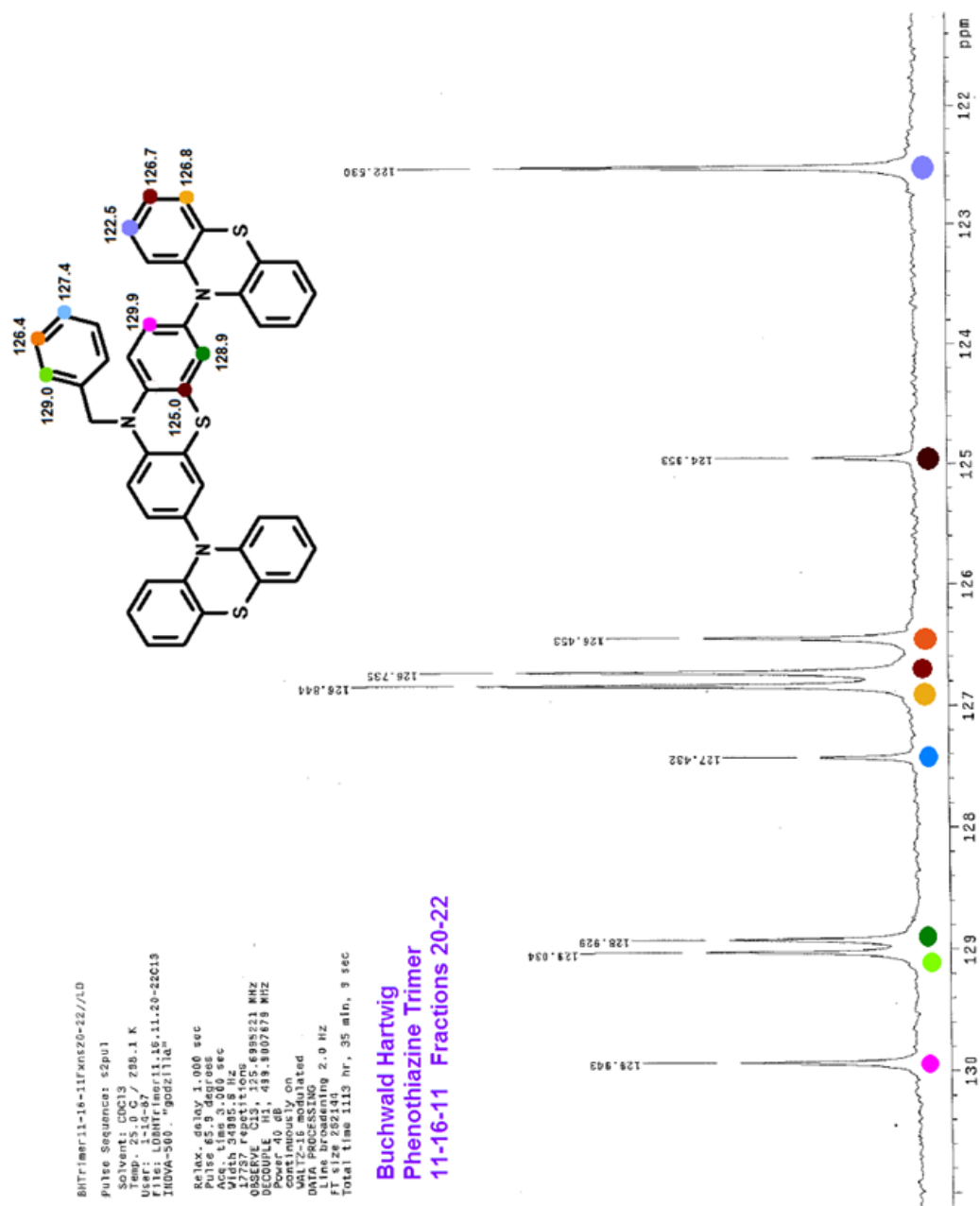


Figure 57.  $^{13}\text{C}$  NMR Expansion of N-benzyl-3,7-diphenothiazinylphenothiazine



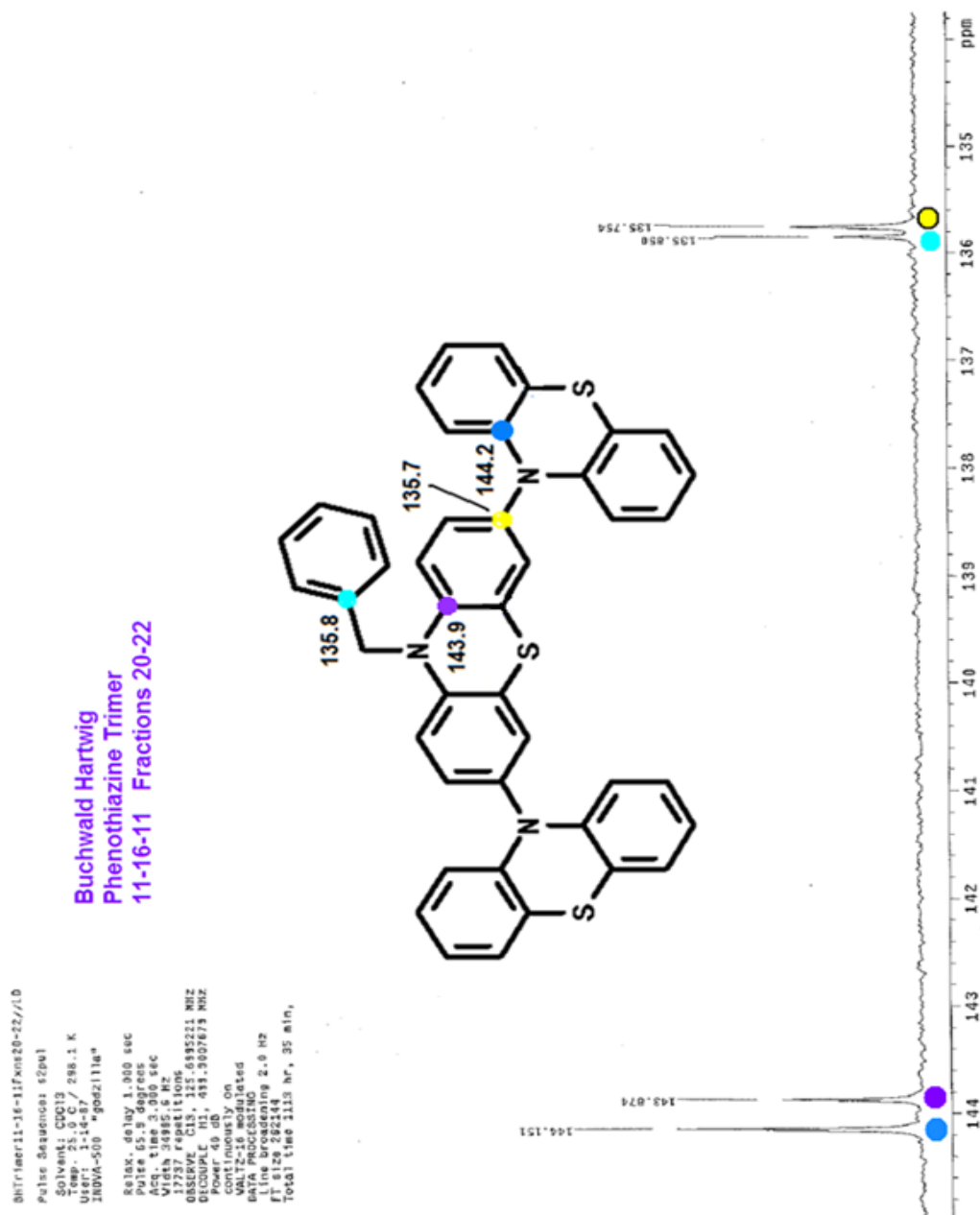
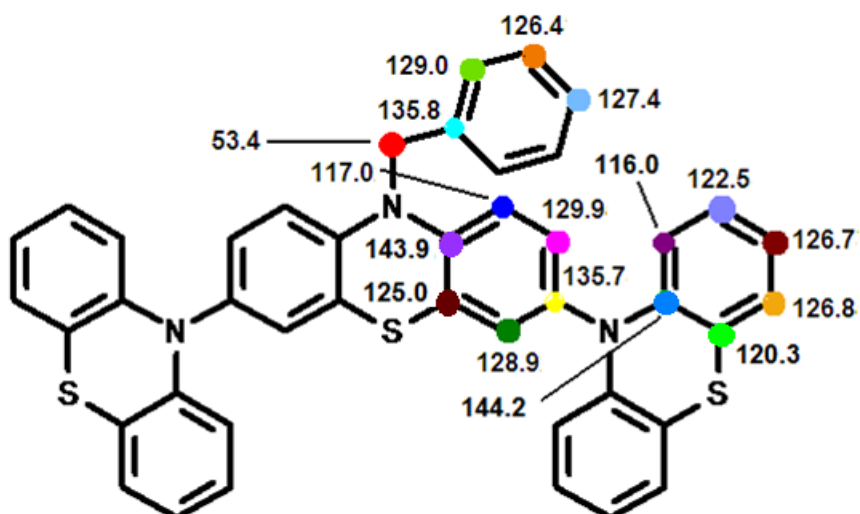


Figure 58.  $^{13}\text{C}$  NMR Expansion of N-benzyl-3,7-diphenothiazinylphenothiazine

### Interpretation of $^{13}\text{C}$ NMRs in Figures 55. to 58.

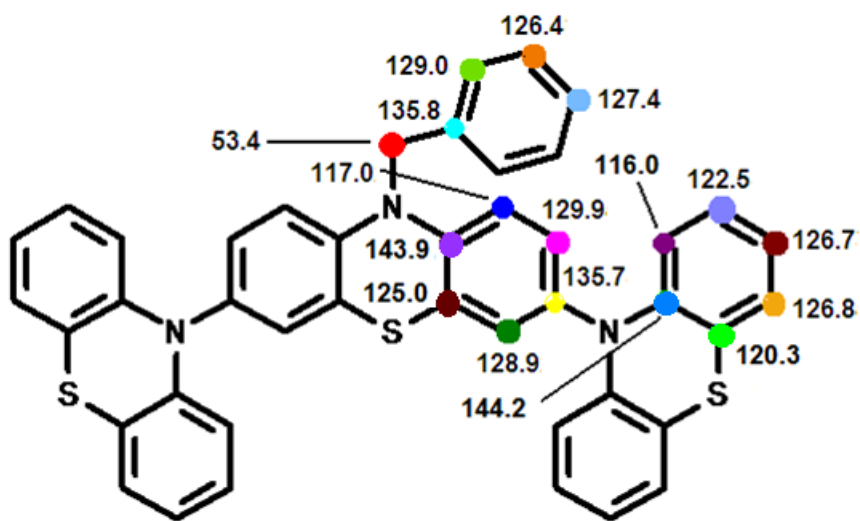


**53.4** – C of the  $\text{CH}_2$  benzyl protection group; it is non-aromatic and farther upfield; this C also corresponds by a factor of approximately 10 to the peak for the H atoms

The smallest peaks belong to quaternary carbon atoms – since no H atoms are attached, the peak heights are smaller due to lack of the Nuclear Overhauser Effect (NOE).

There are 6 unique quaternary carbons, which are all in aromatic rings, and are found in the aromatic region of 110 – 160 ppm

- **135.8** – C of protection group; correlates to the position of this C in N-benzylphenothiazine; smallest quaternary C peak, since it is attributed to only 1 C atom
- **125.0** – C in phenothiazine base; farther upfield due to its proximity to the S atom; correlates to the position of this C in N-benzylphenothiazine
- **143.9** – C in phenothiazine base; farther downfield due to its proximity to the N atom; correlates to the position of this C in N-benzylphenothiazine
- **135.7** – C in phenothiazine base; this C has a similar arrangement as quaternary C from the protection group, since this C is bonded to two carbons in the aromatic ring and 1 N atom external to the ring system; farther upfield than quaternary C from protection group due to its proximity to the N atom



Carbons discussed below are the largest of the quaternary C peaks, since they are attributed to 4 C atoms on the phenothiazine substituents

- **120.3** – farther upfield due to its proximity to the S atom
- **144.2** – farther downfield due to its proximity to the N atom

#### There are 10 unique aromatic carbon atoms

- Carbons attributed to 2 C atoms have the smaller peaks
- Carbons attributed to 4 C atoms have the largest peaks
- **117.0** – C on phenothiazine base; farther upfield due to its close proximity to the N atom; correlates to the position of this C in N-benzylphenothiazine
- **129.9** – C on phenothiazine base; farther downfield since it is farther away from the N atom; correlates to the position of this C in N-benzylphenothiazine
- **128.9** – C on phenothiazine base; farther downfield due to its close proximity to the S atom
- **116.0** – C on phenothiazine substituents; farthest upfield due to its close proximity to the N atom
- **122.5** – C on phenothiazine substituents; a little farther downfield since it is farther away from the N atom
- **126.7** – C on phenothiazine substituents; a little farther downfield than previous C since it is closer to the S atom

- **126.8** – C on phenothiazine substituents; farthest downfield since it is in close proximity to the S atom
- **129.0** – C of protection group adjacent to the C attached to the CH<sub>2</sub> group; correlates to the position of this C in N-benzylphenothiazine
- **126.4** – C of protection group adjacent to C above; correlates to the position of this C in N-benzylphenothiazine
- **127.4** – C of protection group para to the C attached to the CH<sub>2</sub> group

Two dimensional spectra were also taken of the N-benzyl-3,7-diphenothiazinylphenothiazine product. A COSY (Correlation Spectroscopy) and HSQC, also known as a HetCor spectrum, were the two types of 2D NMR utilized. A COSY NMR spectrum correlates protons with other protons that are up to 4 bonds away, which allows determination of proton coupling. The HSQC NMR spectrum correlates <sup>13</sup>C carbons on the x axis with <sup>1</sup>H hydrogens on the y axis. The intersection of the two spectra allows the determination of which H atoms are attached to the specific C atoms. The spectra as well as the interpretation are shown in Figures 59. – 64. on the following pages.

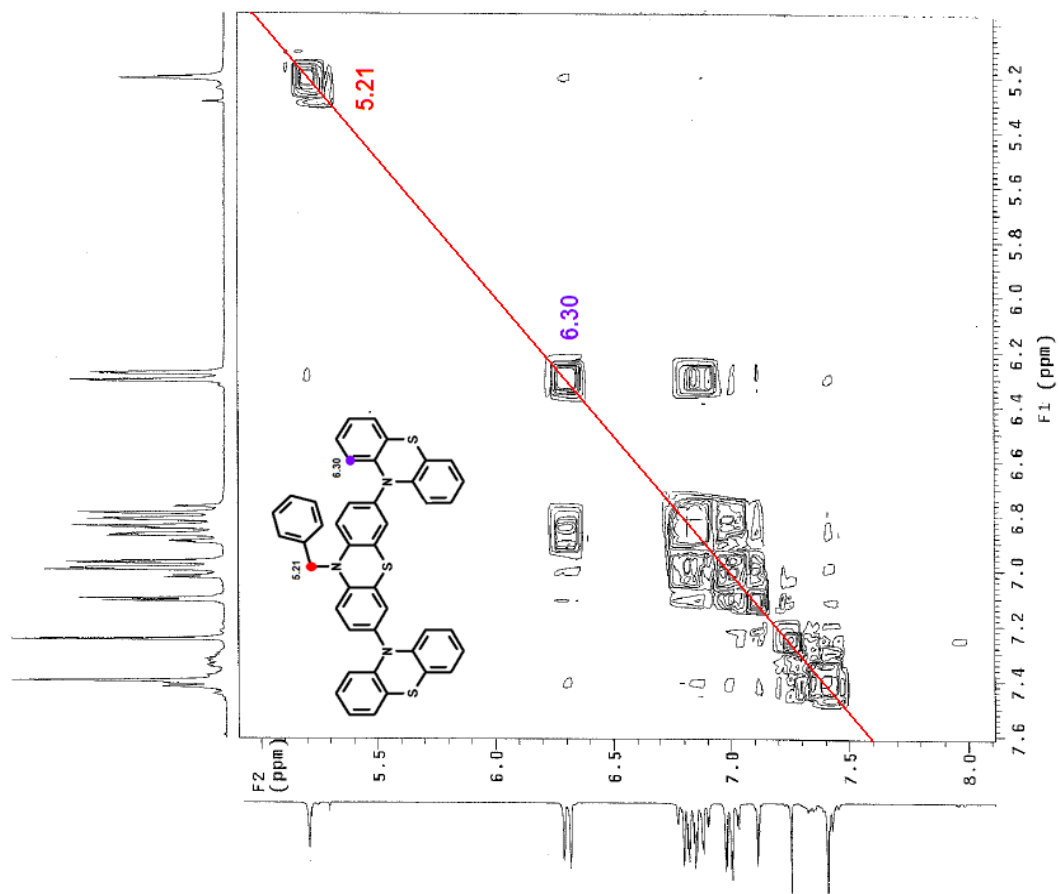


Figure 59. 2D COSY Spectrum of N-benzyl-3,7-diphenothiazinylphenothiazine

**Interpretation of Figure 59.**

The H in the CH<sub>2</sub> of the benzyl protection group at 5.21 is not correlated to any other proton, since it is next to a quaternary C atom in the protection group aromatic ring with no attached protons and also bonded to a N atom with no attached protons.

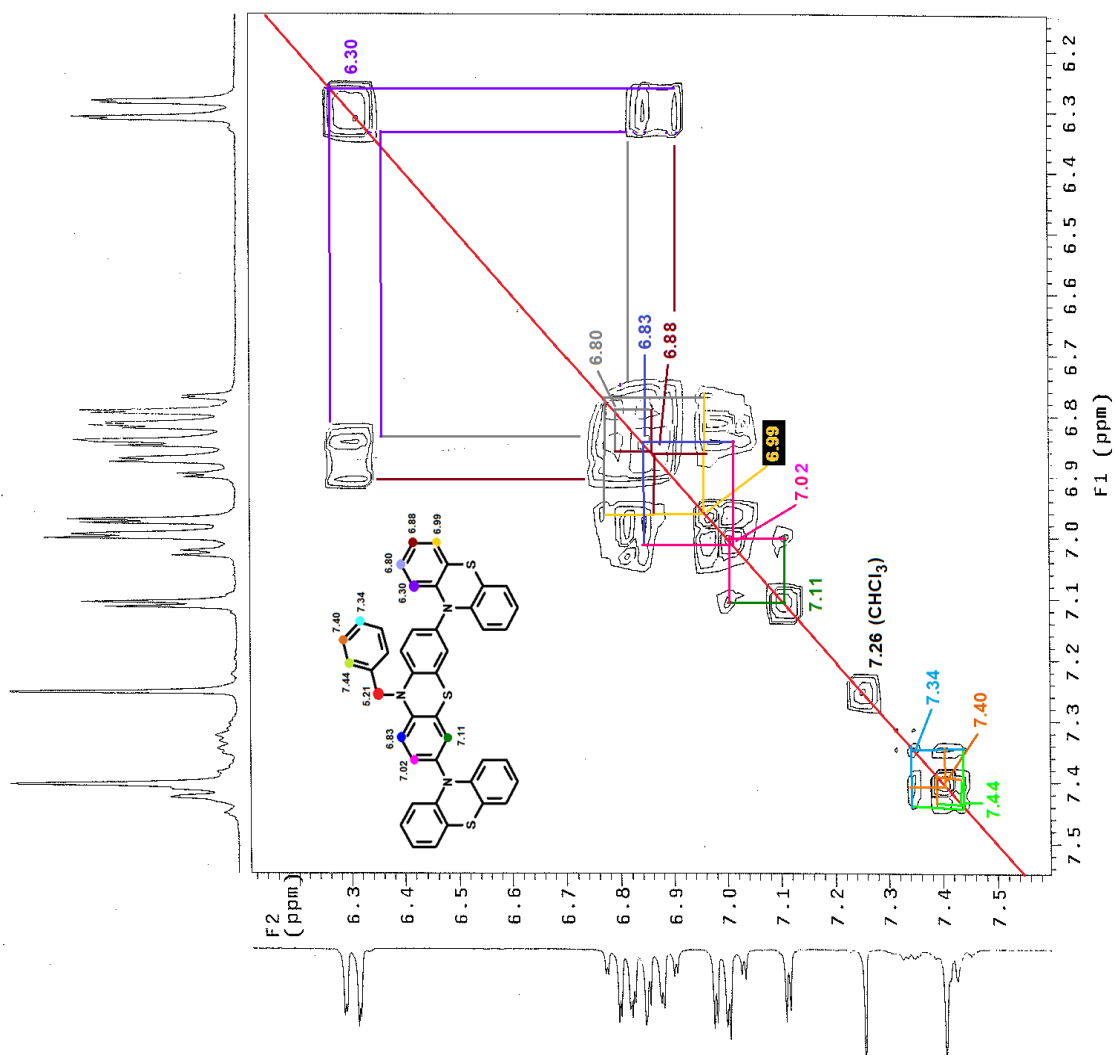


Figure 60. 2D COSY Spectrum Expansion of N-benzyl-3,7-diphenothiazinyphenothiazine

The H at 6.30 has an ortho coupling to the H at 6.80, and a meta coupling to the H at 6.88. These protons are part of the phenothiazine substituents. Other couplings shown on this COSY will be described on more magnified COSY spectra.

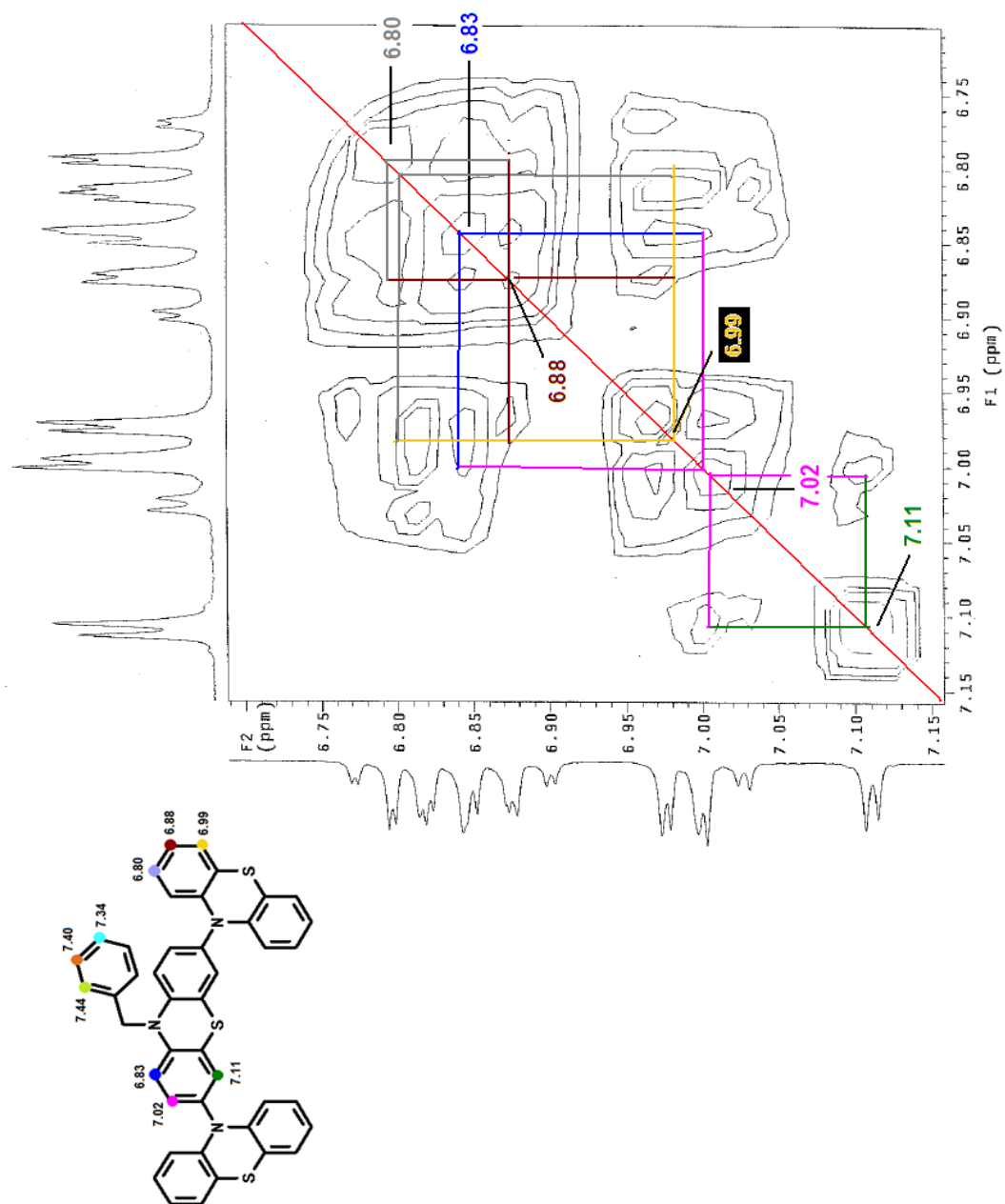


Figure 61. 2D COSY Spectrum Expansion of N-benzyl-3,7-diphenothiazinylphenothiazine



**Interpretation of Figure 61.**

The H at 6.80 has an ortho coupling to the H at 6.88 and a meta coupling to the H at 6.99. These protons are part of the phenothiazine substituents. The H at 6.83 has an ortho coupling to the H at 7.02. These protons are on the phenothiazine base. The H at 7.02 has a meta coupling to the H at 7.11. These protons are on the phenothiazine base.

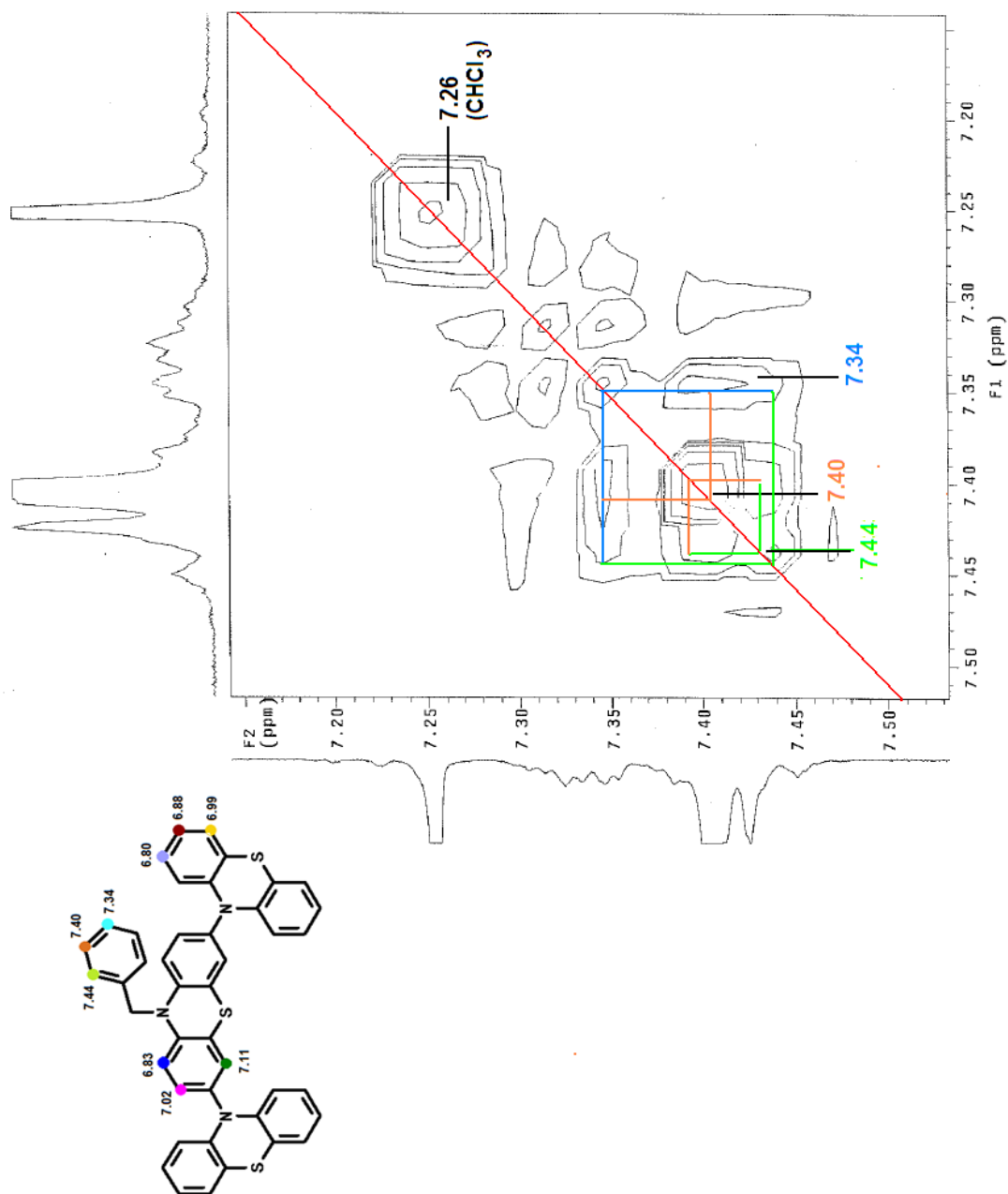


Figure 62. 2D COSY Spectrum Expansion of N-benzyl-3,7-diphenothiazinyphenothiazine

**Interpretation of Figure 62.**

The H belonging to the chloroform is not coupled to any other H since it is another molecule in the spectra separate from the phenothiazine trimer and has only one H atom so no coupling is possible. The H at 7.34 has an ortho coupling to the H at 7.40, and a meta coupling to the H at 7.44. The H at 7.40 has an ortho coupling to the H at 7.44. These three different H atoms are part of the aromatic ring of the benzyl protection group.

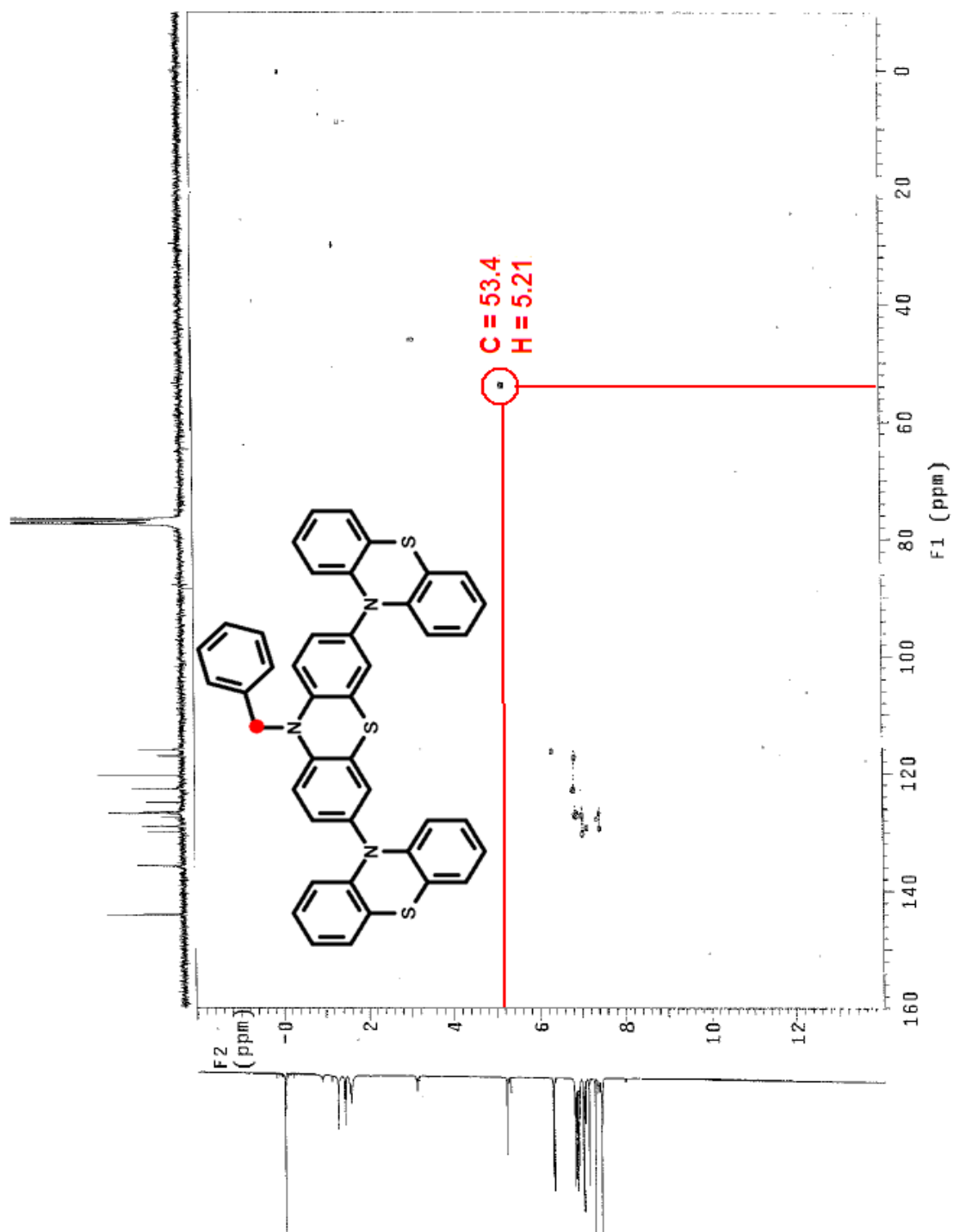


Figure 63. 2D HSQC Spectrum of N-benzyl-3,7-diphenothiazinylphenothiazine

**Interpretation of Figure 63.**

The spectra shows that the CH<sub>2</sub> carbon and hydrogen atoms are correlated in the benzyl protection group.

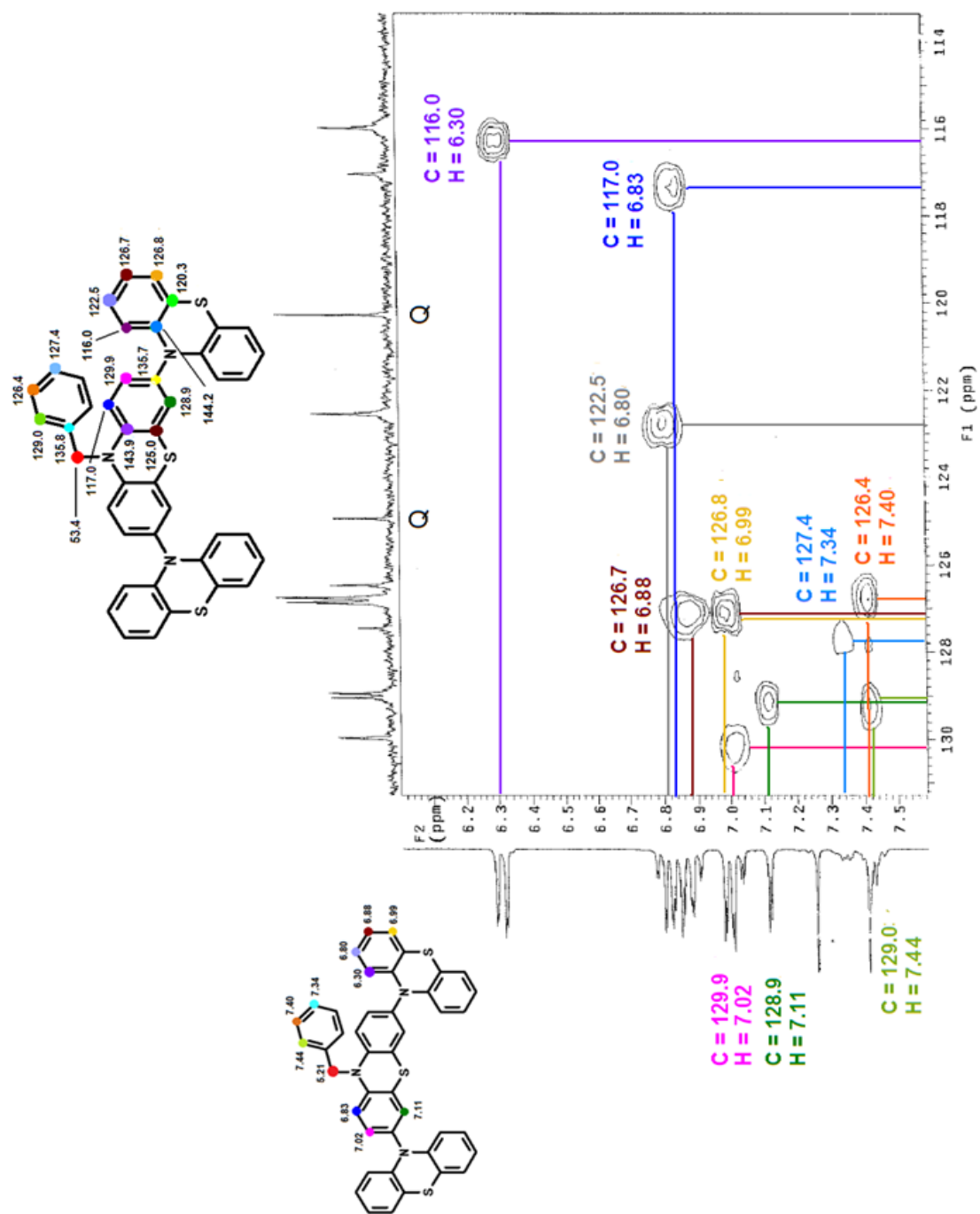


Figure 64. 2D HSQC Spectrum Expansion of N-benzyl-3,7-diphenothiazinyphenothiazine

**Interpretation of Figure 64.**

This enlargement of the aromatic region shows the proton and carbon correlations of the 10 unique aromatic carbon atoms. Note that the carbon peaks shown at approximately 120 ppm and 125 ppm have no hydrogen atom correlations because these peaks are attributed to quaternary carbon atoms.

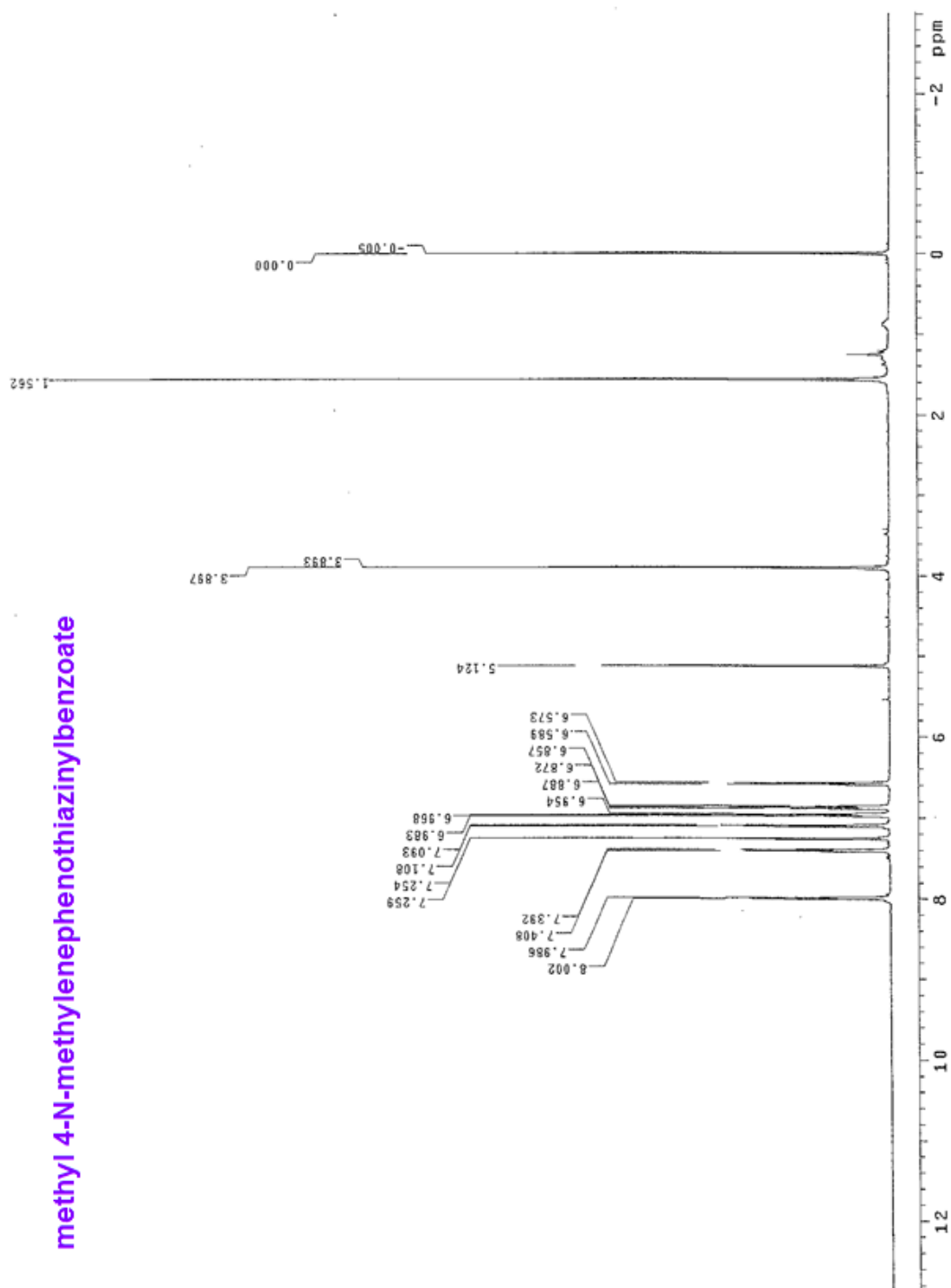


Figure 65.  $^1\text{H}$  NMR of methyl 4-N-methylenephenothiazinylbenzoate



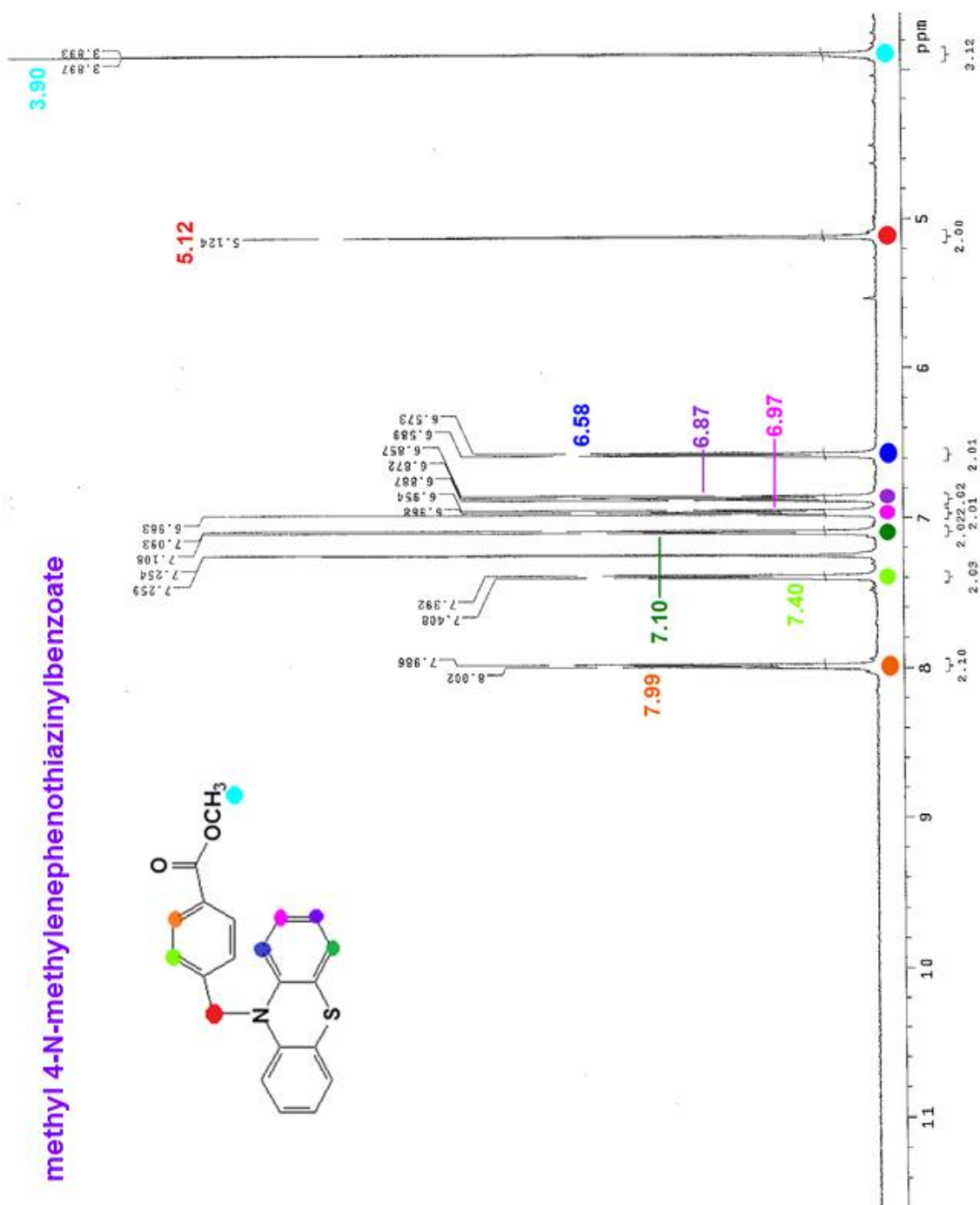


Figure 66. <sup>1</sup>H NMR Expansion of methyl 4-N-methylenphenothiazinybenzoate

**Interpretation of  $^1\text{H}$  NMR in Figure 66.**

- Peak at 3.90 = H from  $\text{OCH}_3$  (benzoate group)
- Peak at 5.12 = H from  $\text{CH}_2$  (benzoate group)
- Peak at 6.58 = phenothiazine ring H with ortho and meta coupling (doublet of doublets);  $J = 8 \text{ Hz}, 2 \text{ Hz}$
- Peak at 6.87 = phenothiazine ring H with 2 ortho and 1 meta coupling (triplet of doublets);  $J = 7 \text{ Hz}, 8 \text{ Hz}, 1 \text{ Hz}$
- Peak at 6.97 = phenothiazine ring H with 2 ortho and 1 meta coupling (triplet of doublets);  $J = 8 \text{ Hz}, 7 \text{ Hz}, 2 \text{ Hz}$
- Peak at 7.10 = phenothiazine ring H with ortho and meta coupling (doublet of doublets);  $J = 9 \text{ Hz}, 2 \text{ Hz}$
- Peaks at 7.40 / 7.99 = phenyl H atoms from benzoate protection group on N

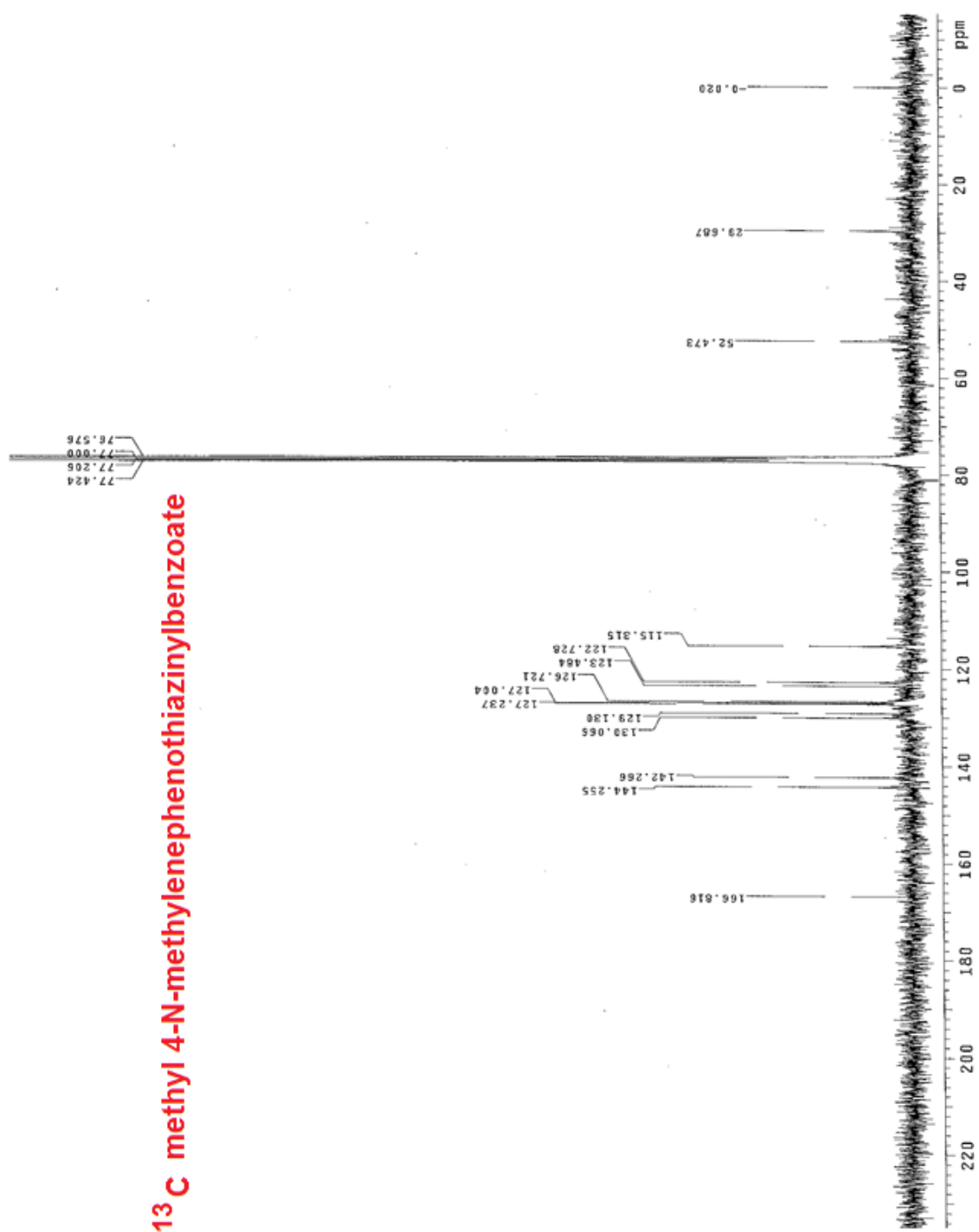


Figure 67. <sup>13</sup>C NMR of methyl 4-N-methylenephenothiazinylbenzoate

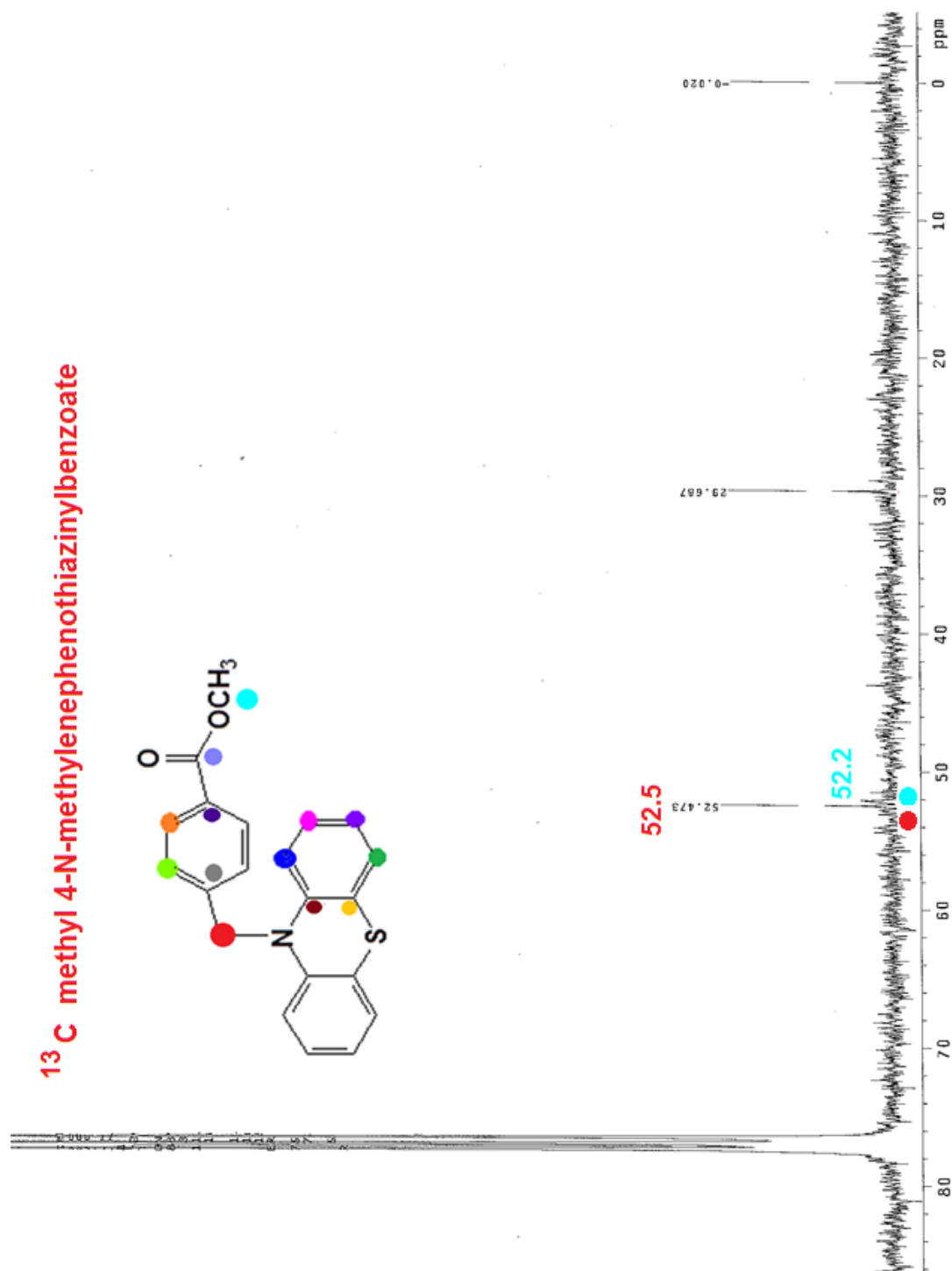


Figure 68. <sup>13</sup>C NMR Expansion of methyl 4-N-methylenphenothiazinybenzoate

**Interpretation of  $^{13}\text{C}$  NMR in Figure 68.**

- Peak at 52.2 – aliphatic C from methoxy group of benzoate protection group shifted downfield due to presence of O atom
- Peak at 52.5 – aliphatic C from methenyl group of benzoate protection group

**<sup>13</sup>C methyl 4-N-methylenphenothiazinylbenzoate**

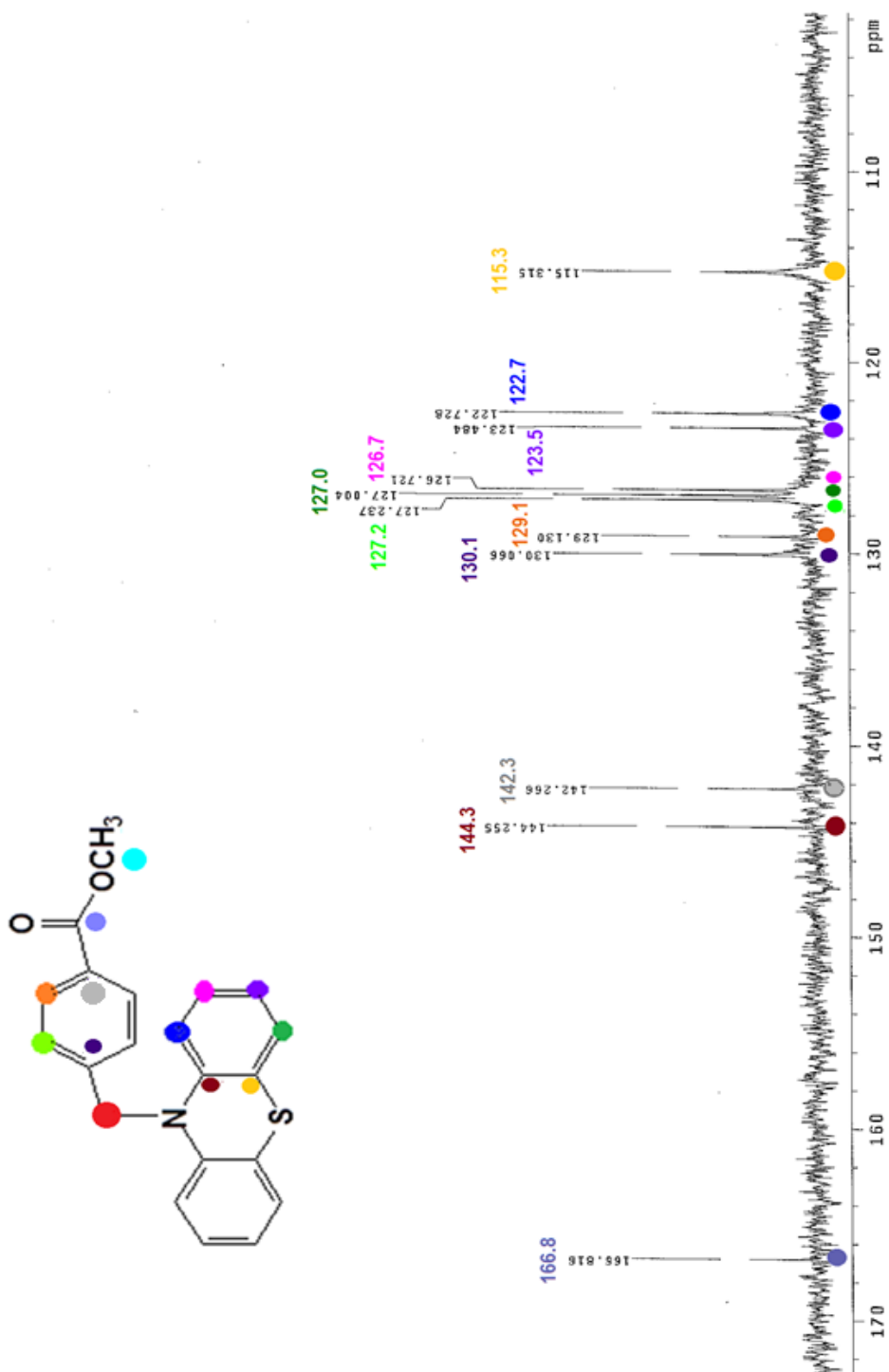


Figure 69. <sup>13</sup>C NMR Expansion of methyl 4-N-methylenphenothiazinylbenzoate

**Intrepretation of  $^{13}\text{C}$  NMR in Figure 69.**

- Peak at 115.3 – aromatic quaternary C atom in phenothiazine ring
- Peak at 122.7 – aromatic C atom of phenothiazine ring ortho to N atom
- Peak at 123.5 – aromatic C atom of phenothiazine ring para to N atom
- Peak at 126.7 – aromatic C atom of phenothiazine ring meta to N atom
- Peak at 127.0 – aromatic C atom of phenothiazine ring ortho to S atom
- Peak at 127.2 – aromatic C atom of phenyl ring of benzoate protection group
- Peak at 129.1 – aromatic C atom of phenyl ring of benzoate protection group shifted downfield due to closer proximity to carbonyl group O
- Peak at 130.1 – aromatic quaternary C atom para to benzoate protection group
- Peak at 142.3 – aromatic quaternary C atom ipso to benzoate protection group
- Peak at 144.3 - aromatic quaternary C atom in phenothiazine ring
- Peak at 166.8 – C atom of carbonyl group shifted downfield due to O atoms

## methyl (3,7-dibromo)-4-N-methylenphenothiazinylbenzoate

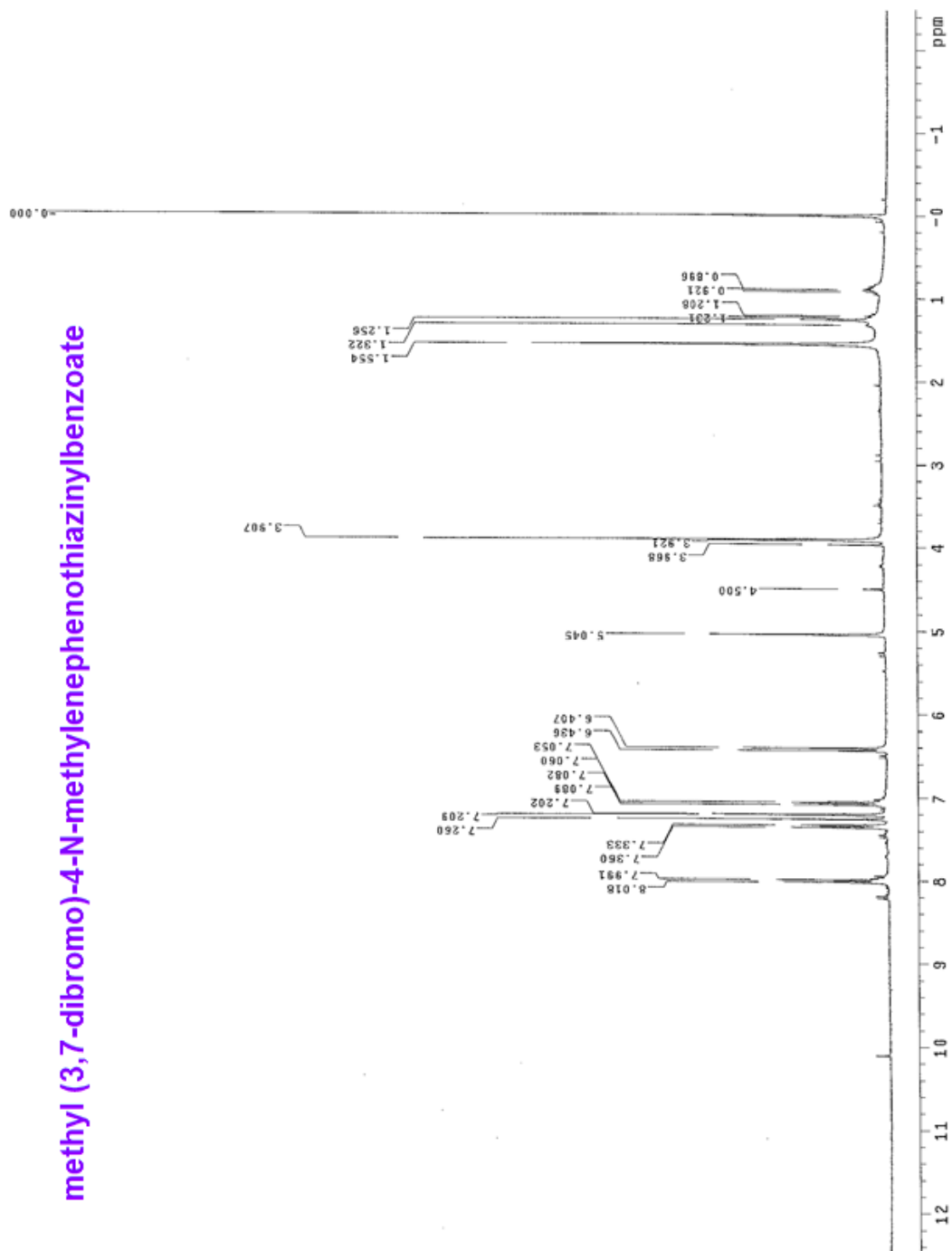


Figure 70.  $^1\text{H}$  NMR of methyl (3,7-dibromo)-4-N-methylenphenothiazinylbenzoate



methyl (3,7-dibromo)-4-N-methylenphenothiazinybenzoate

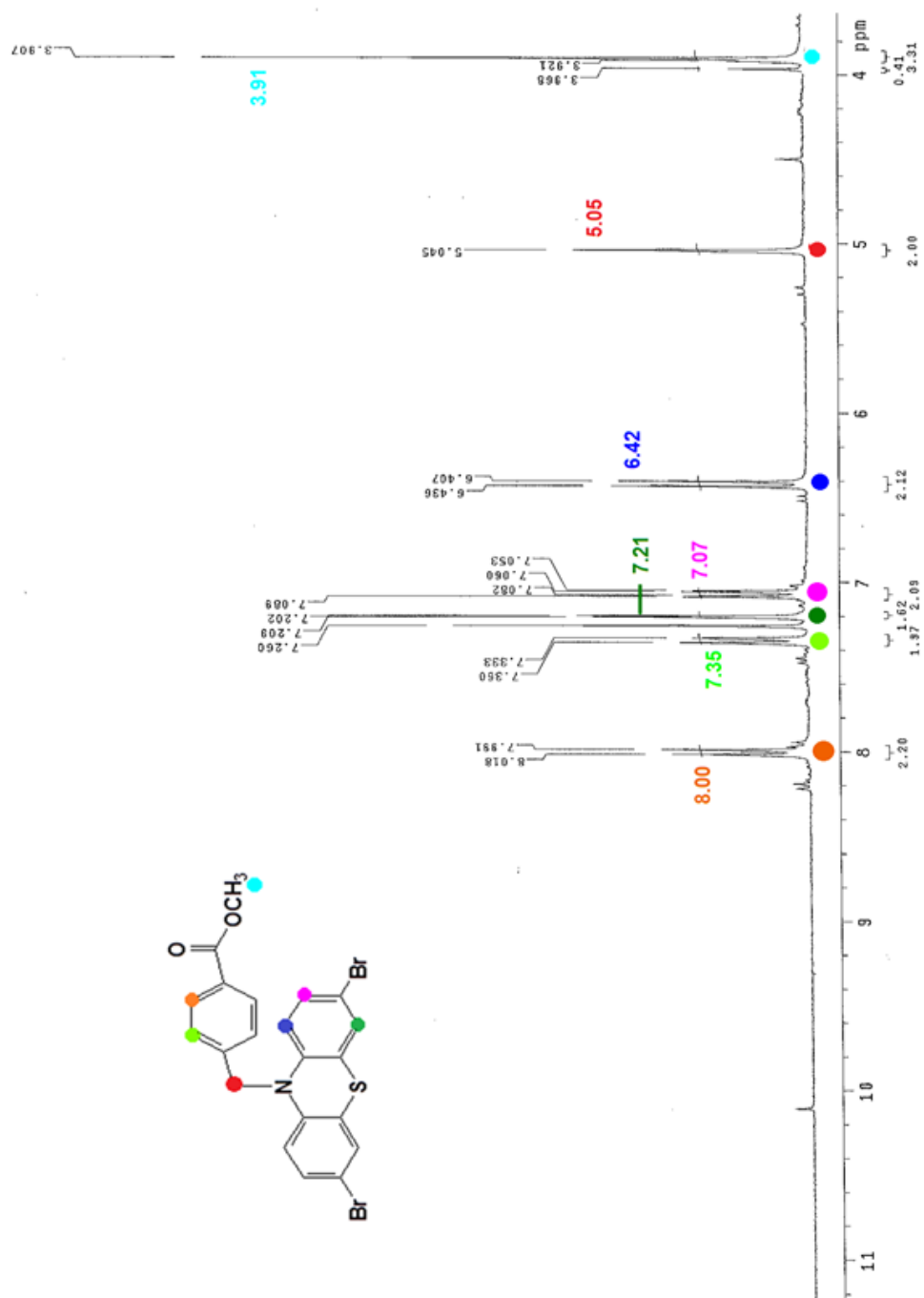


Figure 71.  $^1\text{H}$  NMR Expansion of methyl (3,7-dibromo)-4-N-methylenphenothiazinybenzoate

**Interpretation of  $^1\text{H}$  NMR in Figure 71.**

- Peak at 3.91 = H from  $\text{OCH}_3$  (benzoate group)
- Peak at 5.05 = H from  $\text{CH}_2$  (methylene group)
- Peak at 6.42 = phenothiazine ring H with ortho coupling (doublet);  $J = 9$  Hz
- Peak at 7.07 = phenothiazine ring H with ortho and meta coupling (doublet of doublets);  $J = 8$  Hz, 2 Hz
- Peak at 7.21 = phenothiazine ring H with meta coupling (doublet);  $J = 3$  Hz
- Peaks at 7.35 / 8.00 = phenyl H atoms from benzoate protection group on N

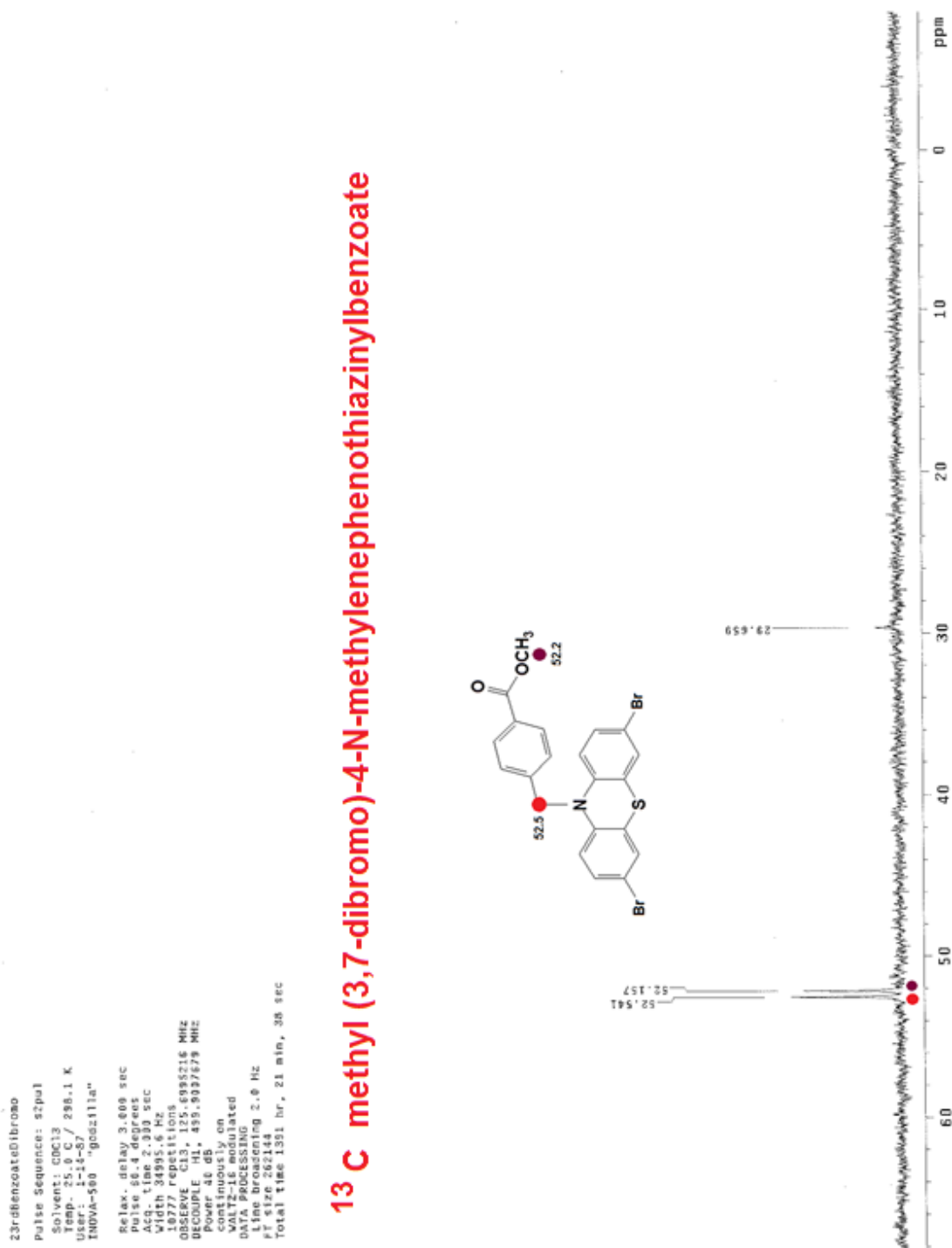


Figure 72. <sup>13</sup>C NMR Expansion of methyl (3,7-dibromo)-4-N-methylenphenothiazinylbenzoate

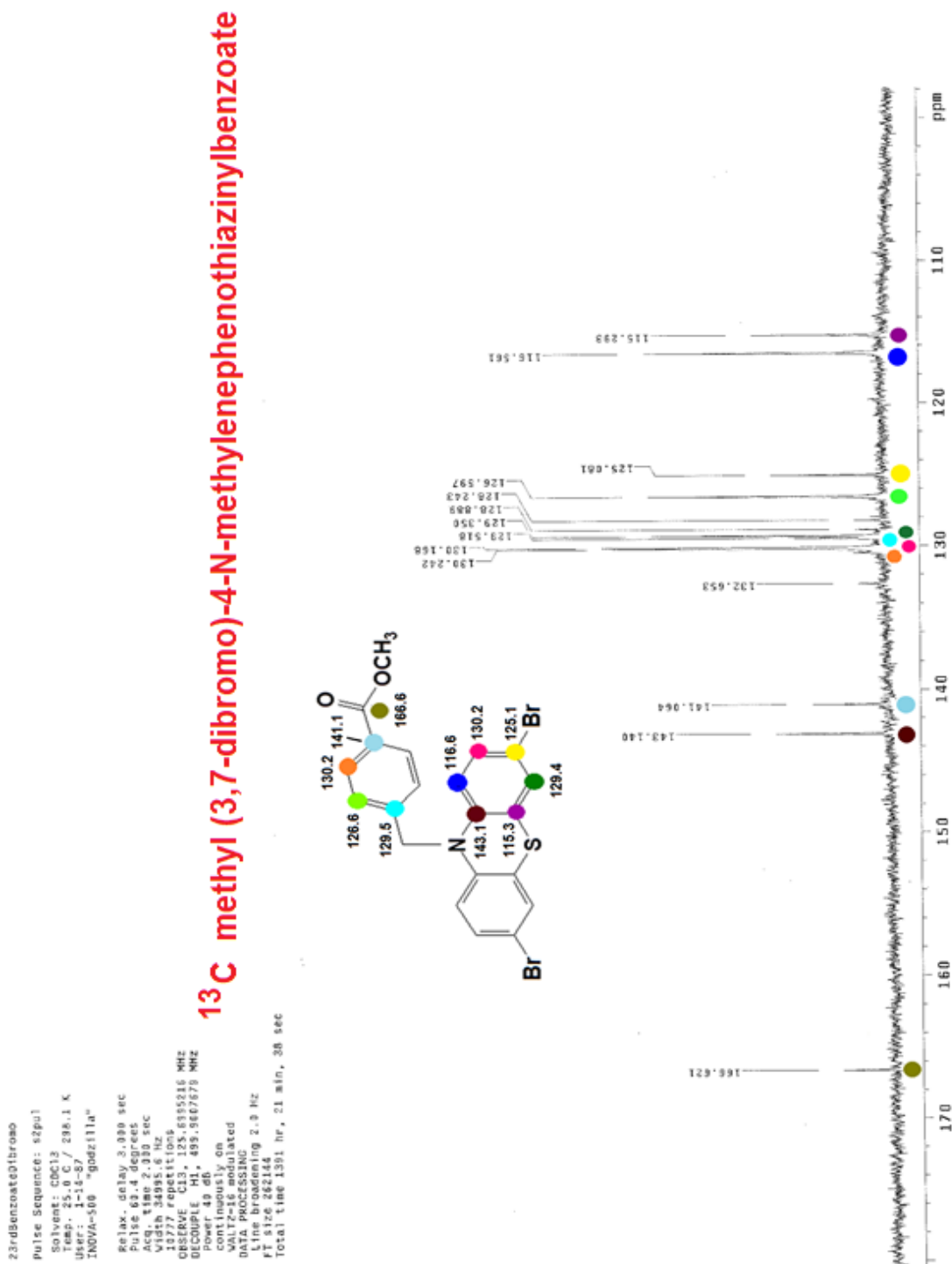


Figure 73. <sup>13</sup>C NMR Expansion of methyl (3,7-dibromo)-4-N-methylenphenothiazinylbenzoate

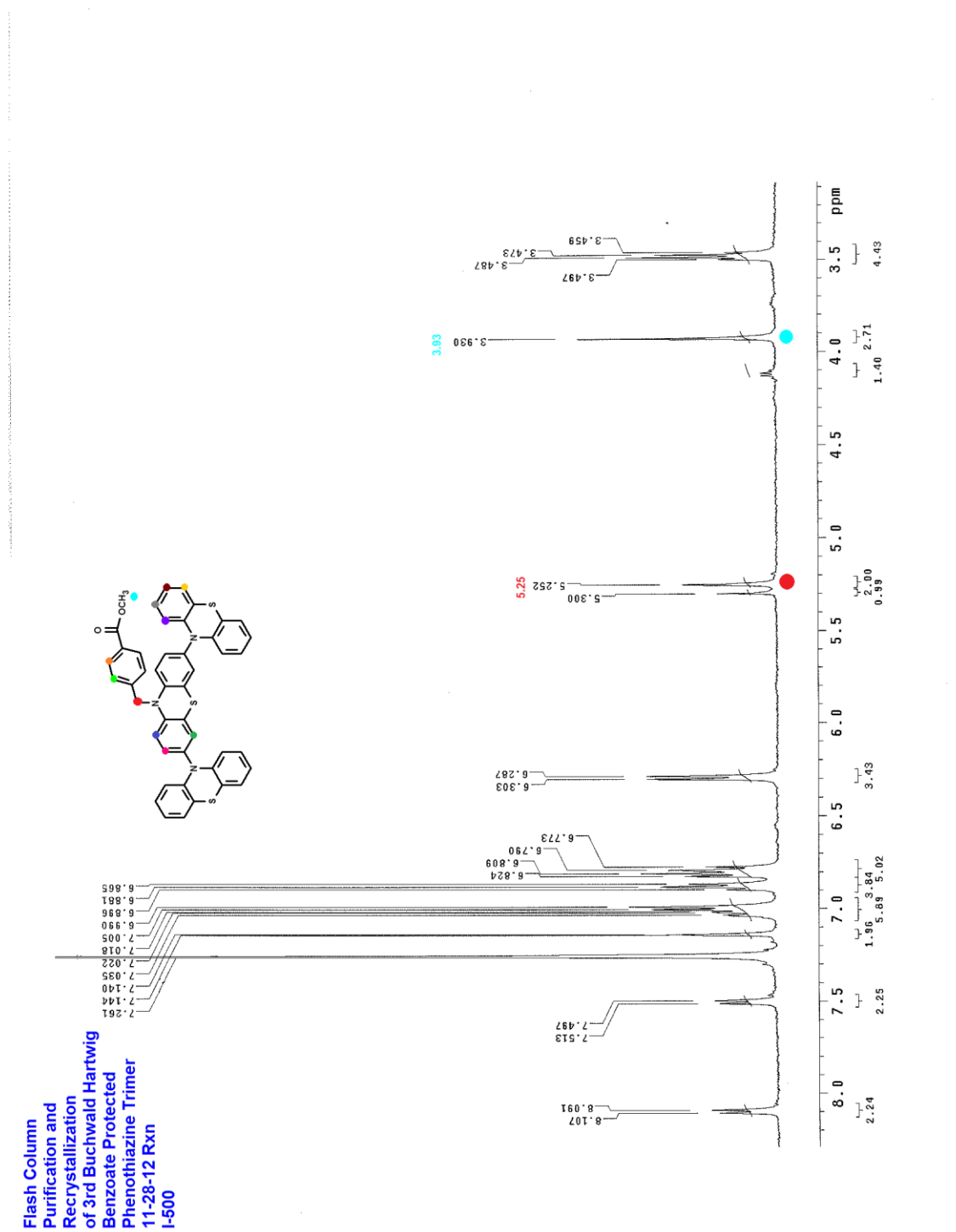


Figure 74. <sup>1</sup>H NMR Expansion of methyl (3,7-diphenothiazinyl)-4-N-methylenephenothiazinylbenzoate

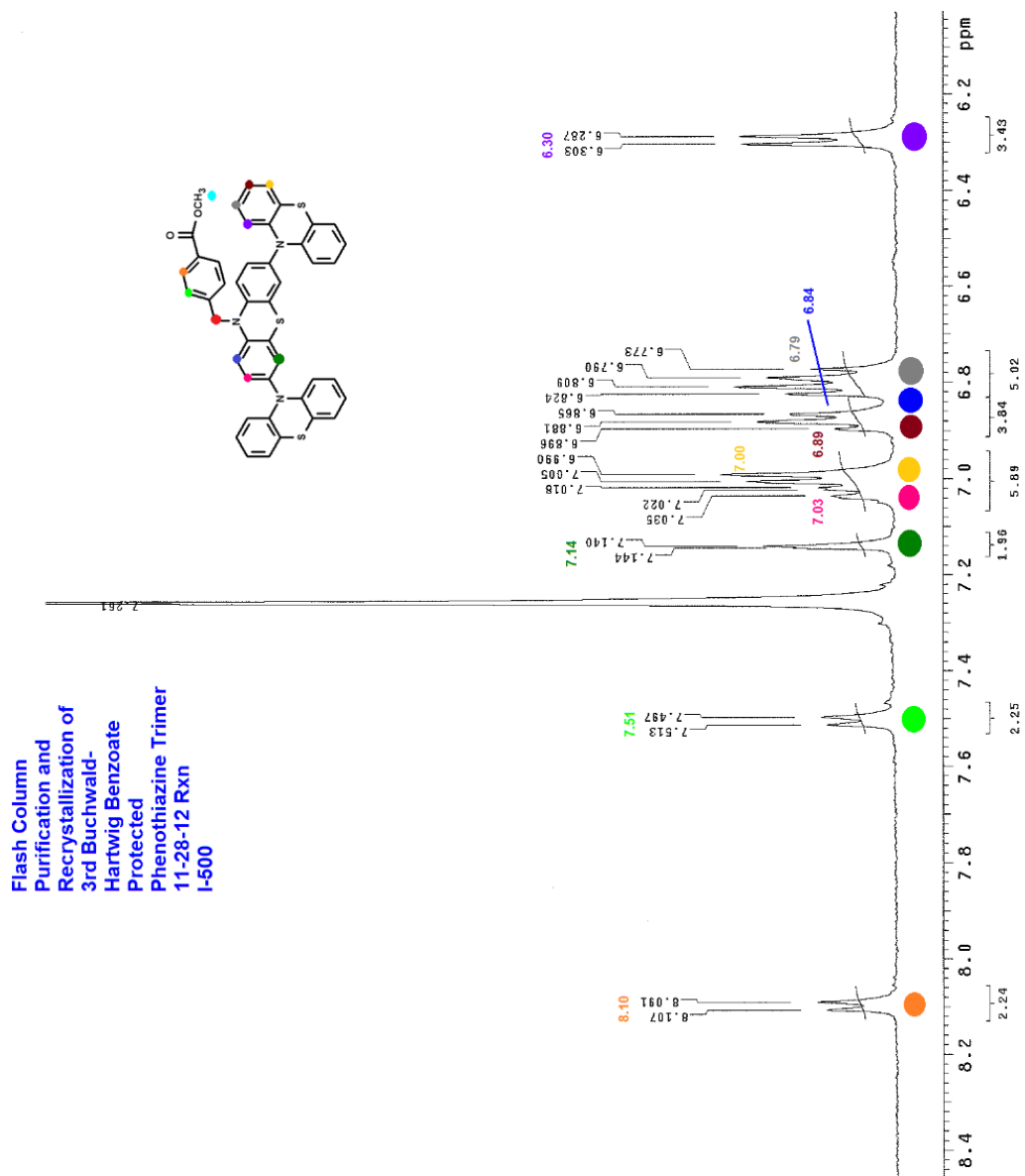


Figure 75.  $^1\text{H}$  NMR Expansion of methyl (3,7-diphenothiazinyl)-4-N-methylenphenothiazinylbenzoate

3rd Buchwald-Hartwig  
Benzoate Trimer  
Fractions 3 - 16  
Recrystallization 1  
11-28-12 Reaction

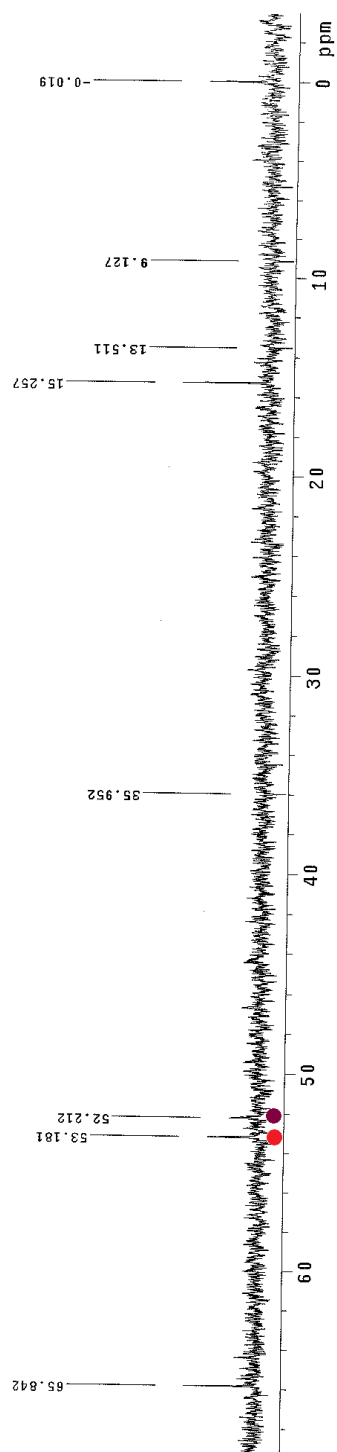
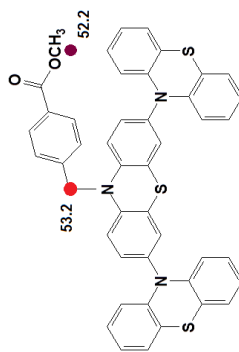


Figure 76. <sup>13</sup>C NMR Expansion of methyl (3,7-diphenothiazinyl)-4-N-methylenphenothiazinylbenzoate

3rd Buchwald-Hartwig  
Benzoate Trimer  
Fractions 3-16  
Recrystallization 1  
11-28-12 Reaction

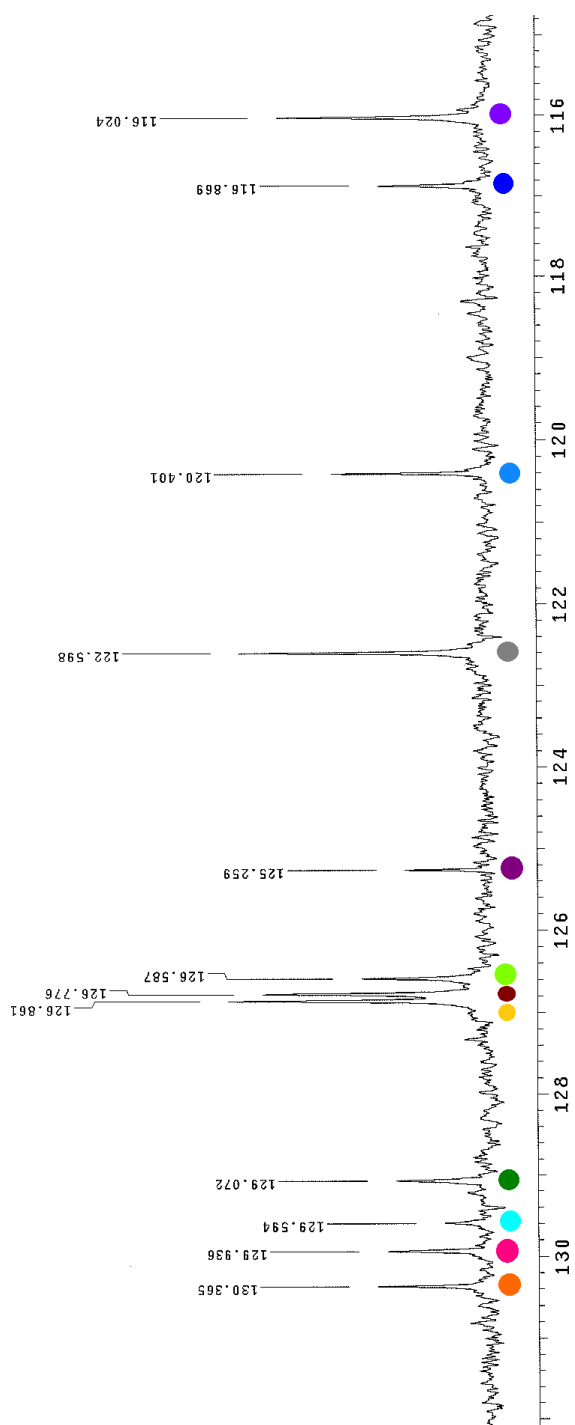


Figure 77.  $^{13}\text{C}$  NMR Expansion of methyl (3,7-diphenothiazinyl)-4-N-methylenphenothiazinylbenzoate



3rd Buchwald-Hartwig  
Benzoate Trimer  
Fractions 3-16  
Recrystallization 1  
11-28-12 Reaction

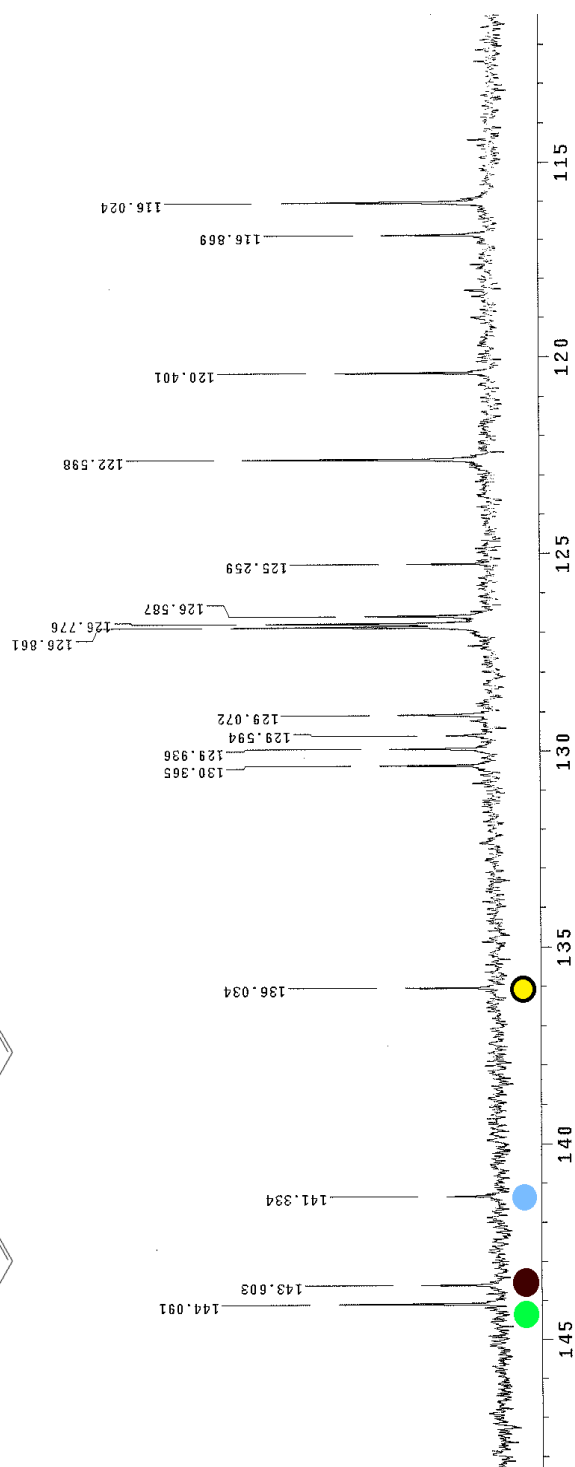
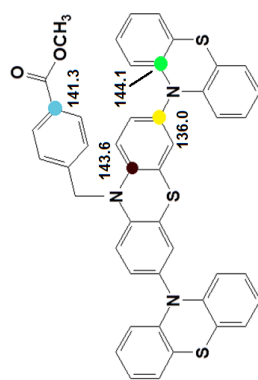


Figure 78. <sup>13</sup>C NMR Expansion of methyl (3,7-diphenothiazinyl)-4-N-methylenphenothiazinylbenzoate

3rd Buchwald-Hartwig  
Benzoate Trimer  
Fractions 3-16  
Recrystallization 1  
11-28-12 Reaction

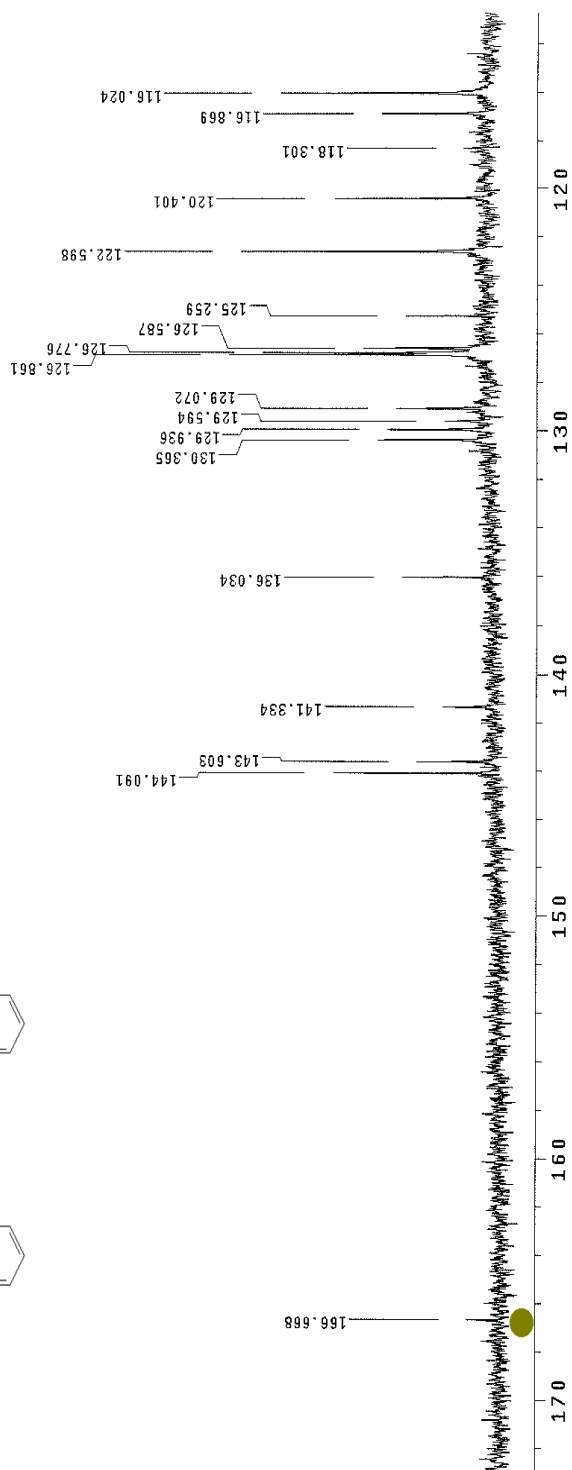
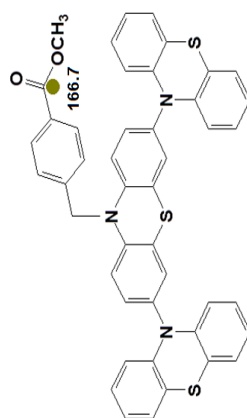


Figure 79.  $^{13}\text{C}$  NMR Expansion of methyl (3,7-diphenothiazinyl)-4-N-methylenephenothiazinylbenzoate

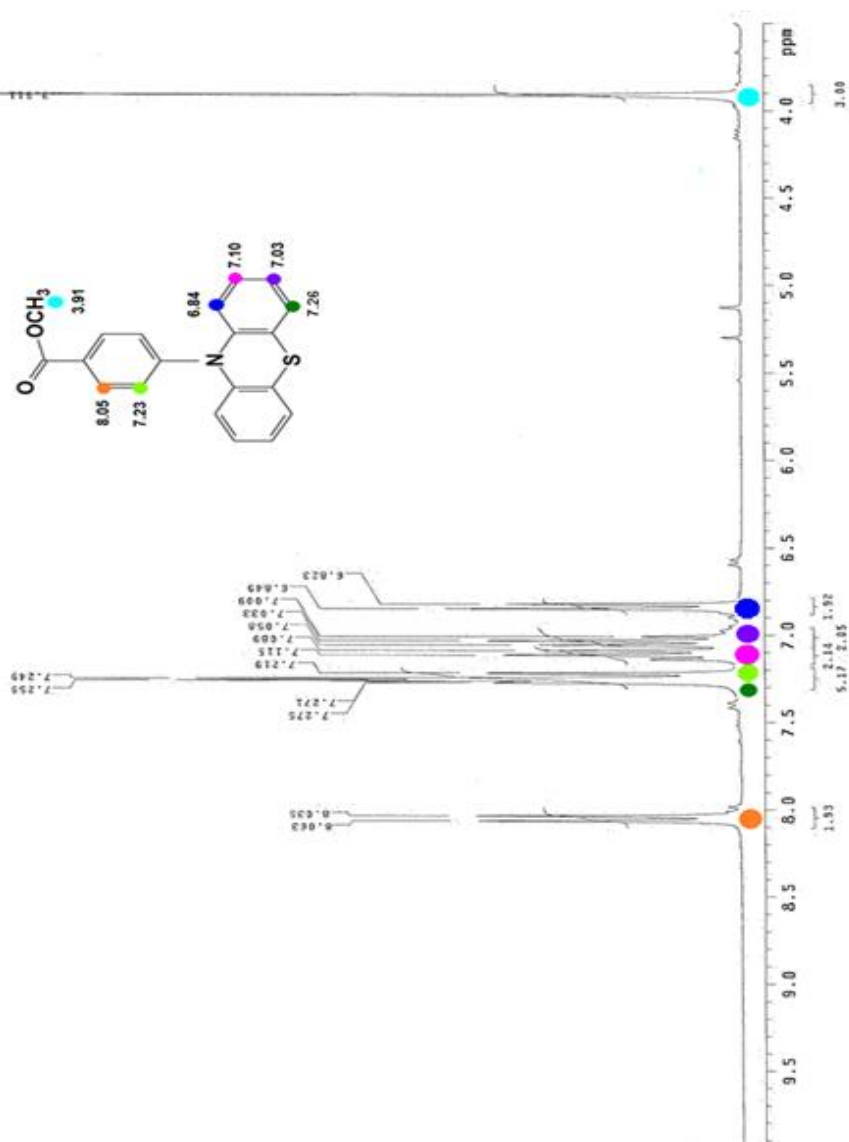
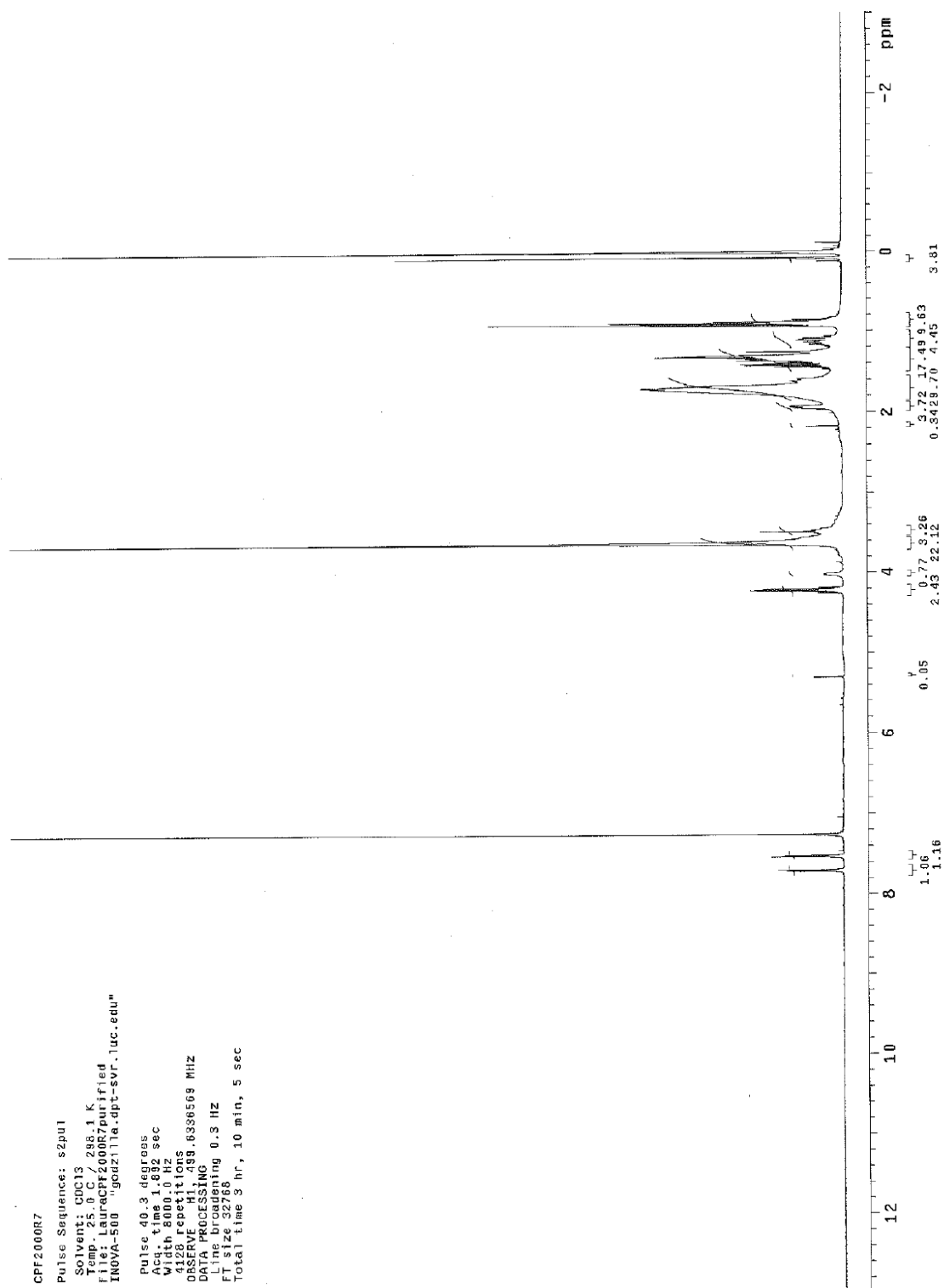
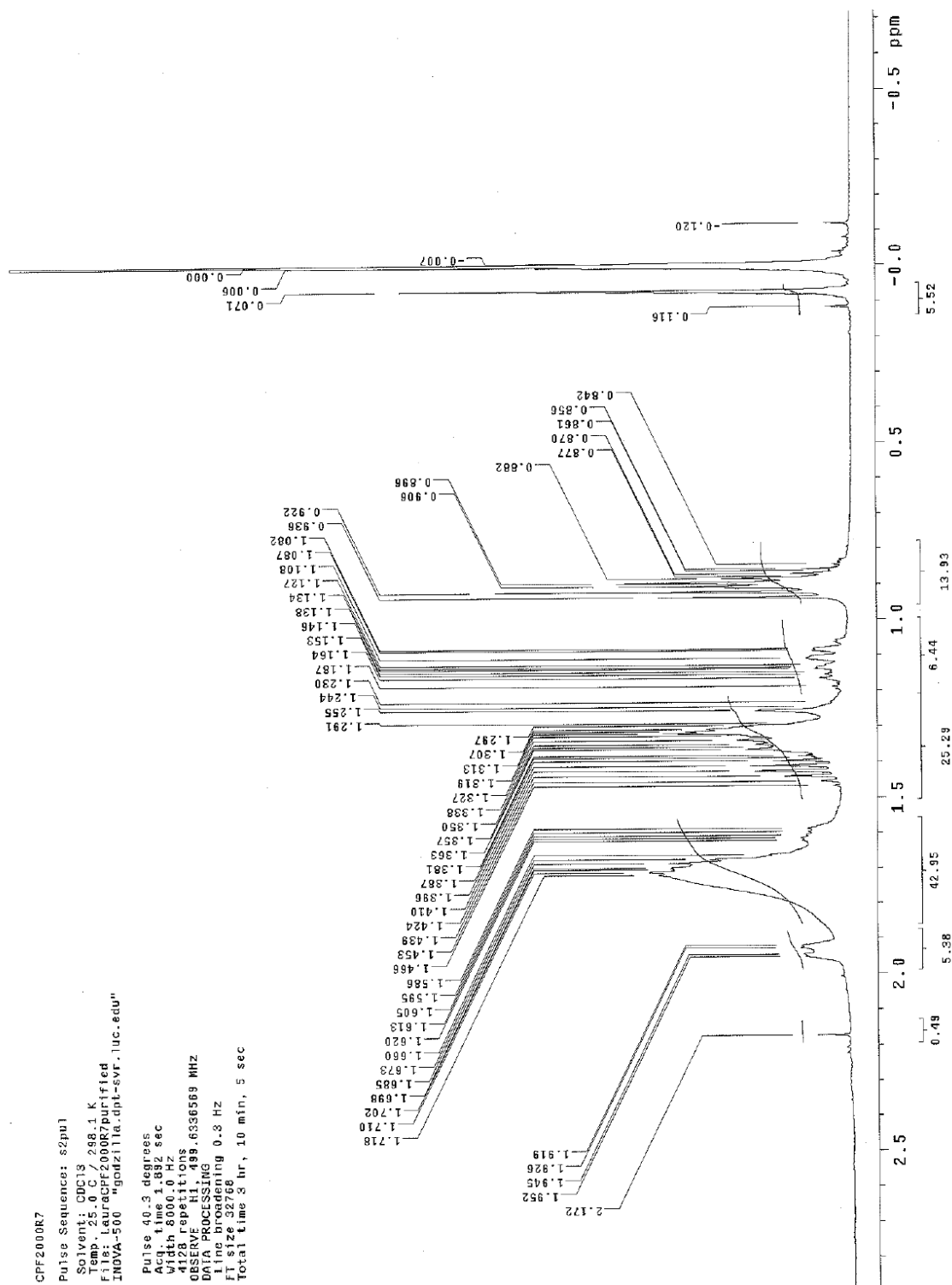
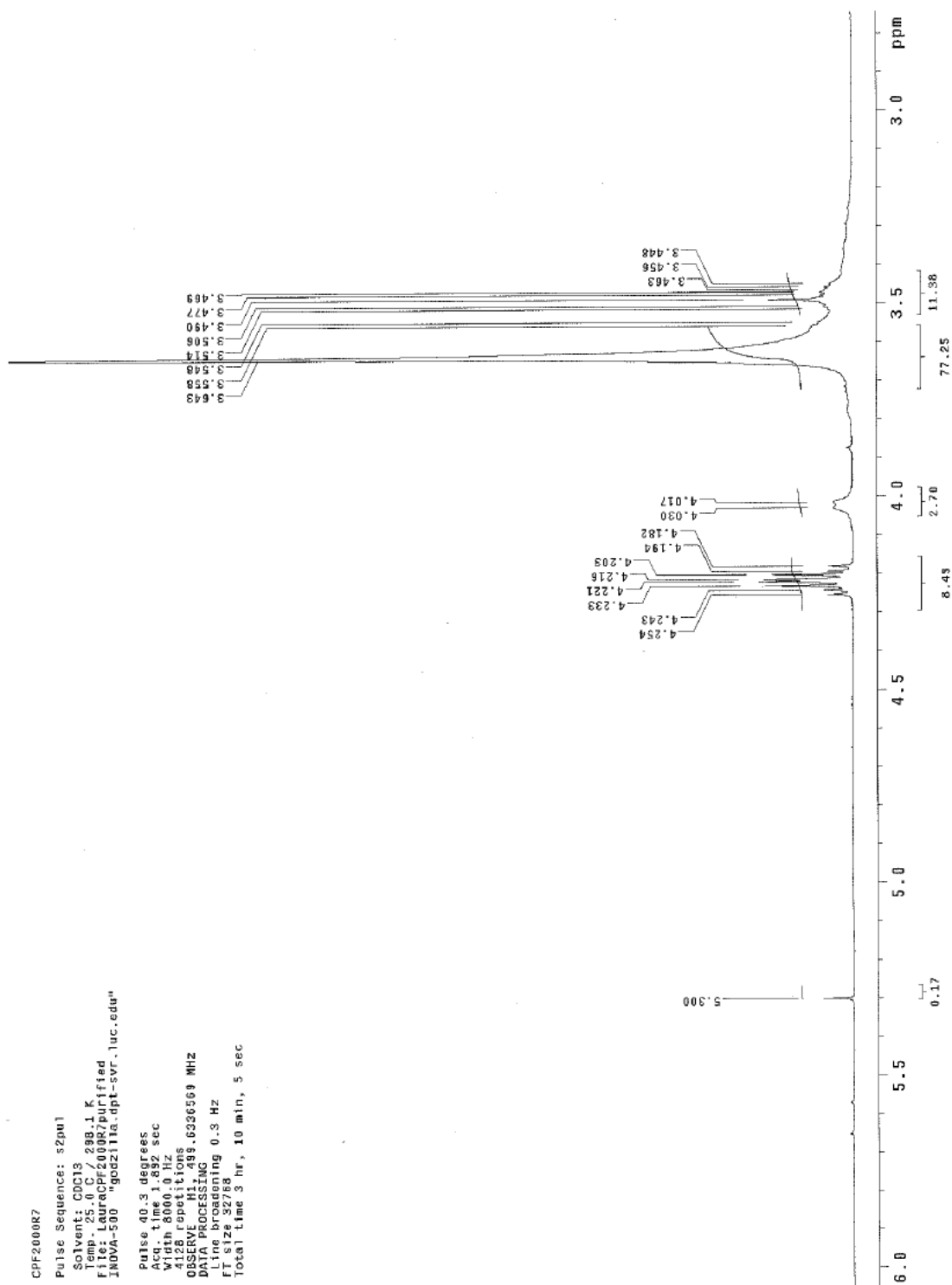
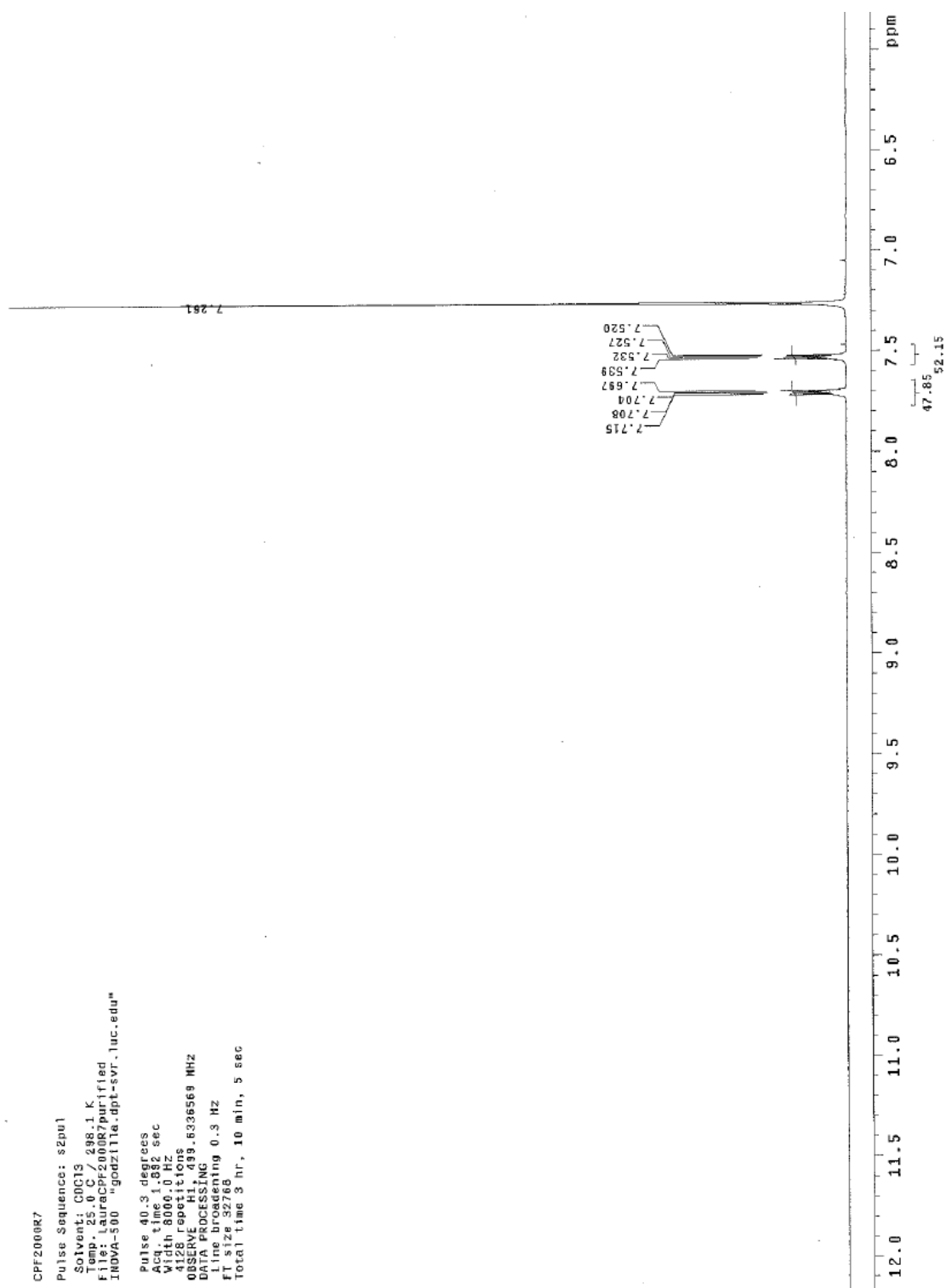
**methyl 4-N-phenothiazinylbenzoate**

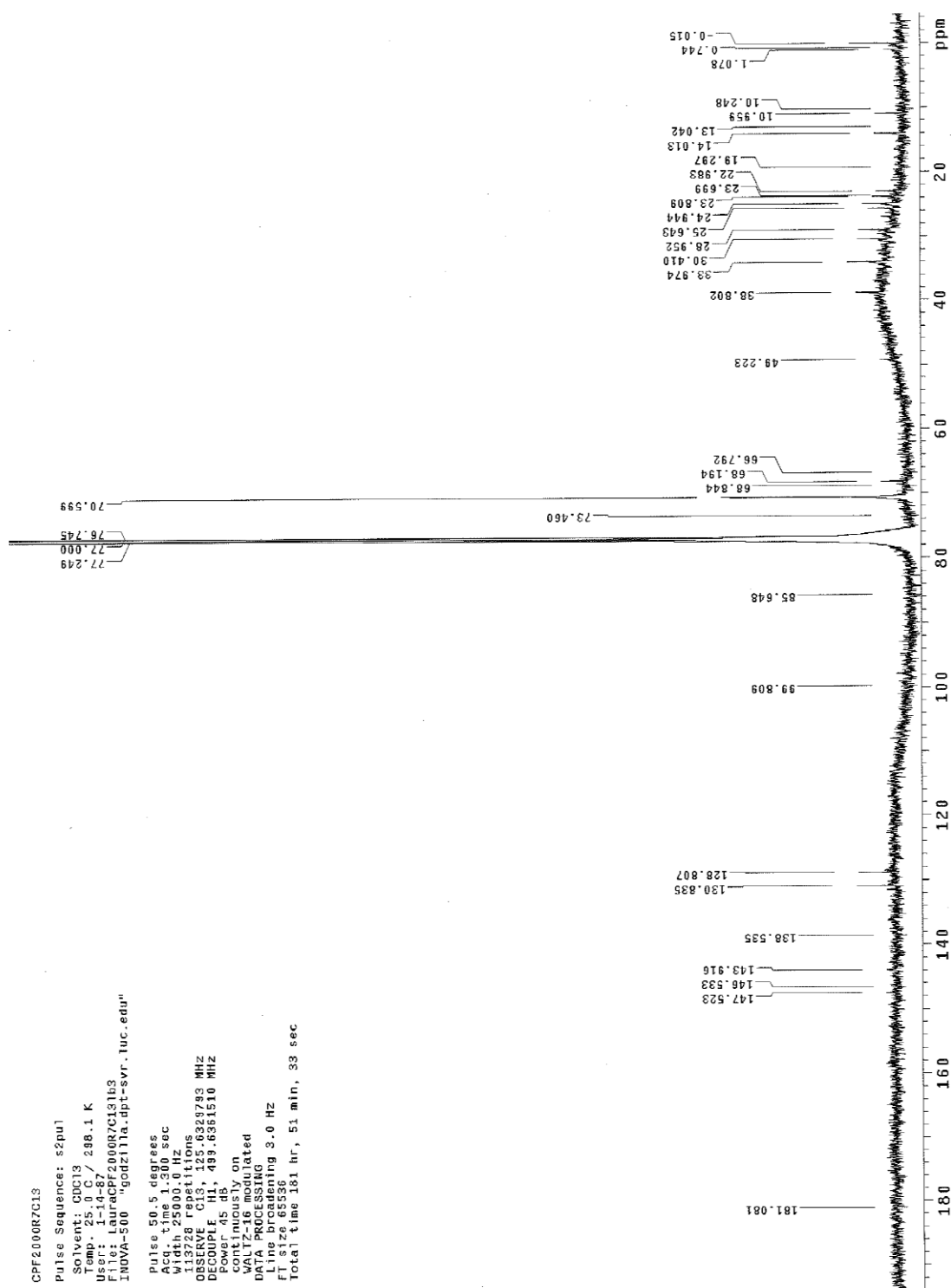
Figure 80. <sup>1</sup>H NMR Expansion of methyl 4-N-phenothiazinylbenzoate (Ullmann Synthesis)

Figure 81. <sup>1</sup>H NMR of Ce6-PEG-FA

Figure 82.  $^1\text{H}$  NMR Expansion of Ce6-PEG-FA

Figure 83.  $^1\text{H}$  NMR Expansion of Ce6-PEG-FA

Figure 84. <sup>1</sup>H NMR Expansion of Ce6-PEG-FA

Figure 85.  $^{13}\text{C}$  NMR of Ce6-PEG-FA



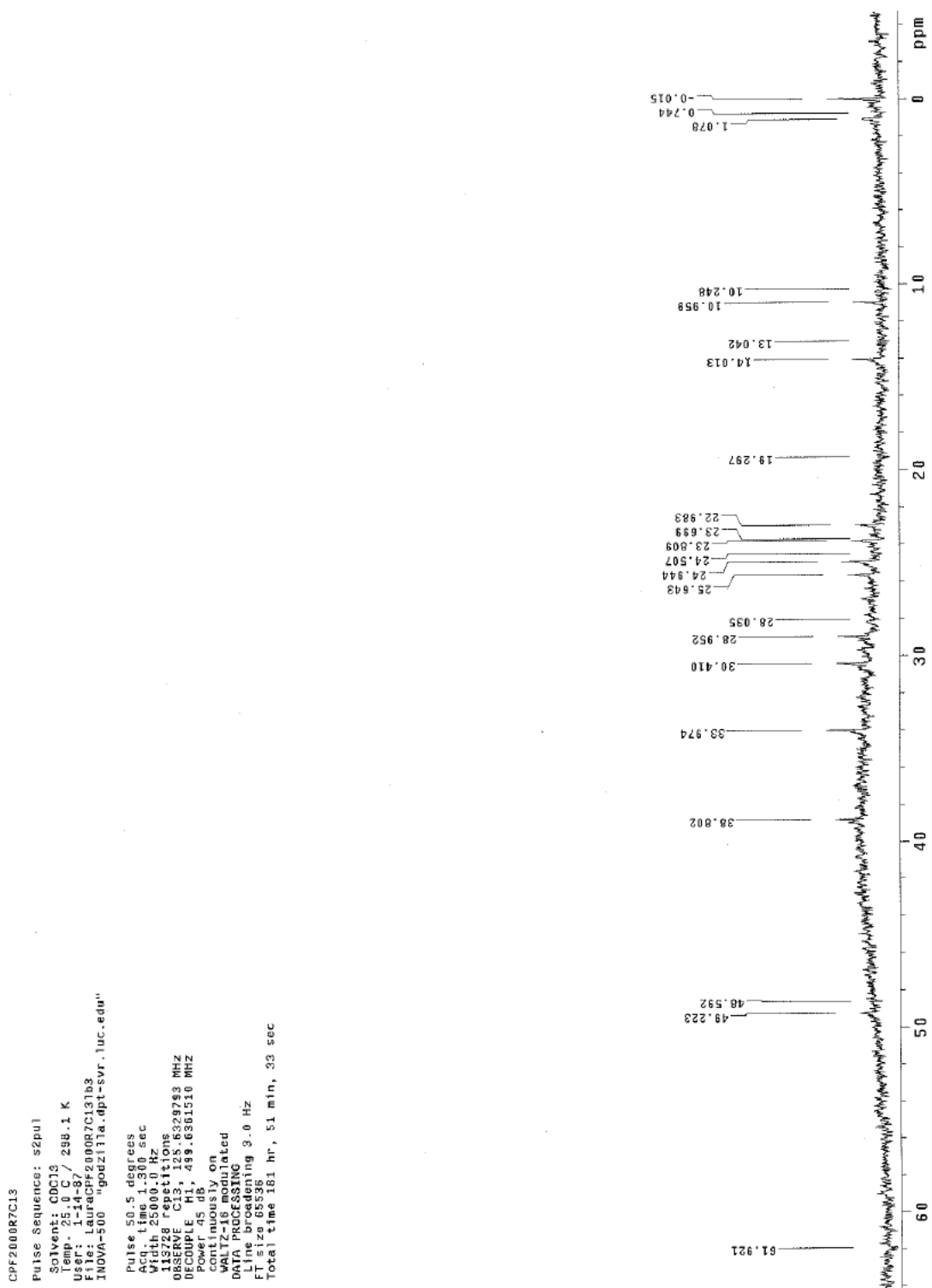
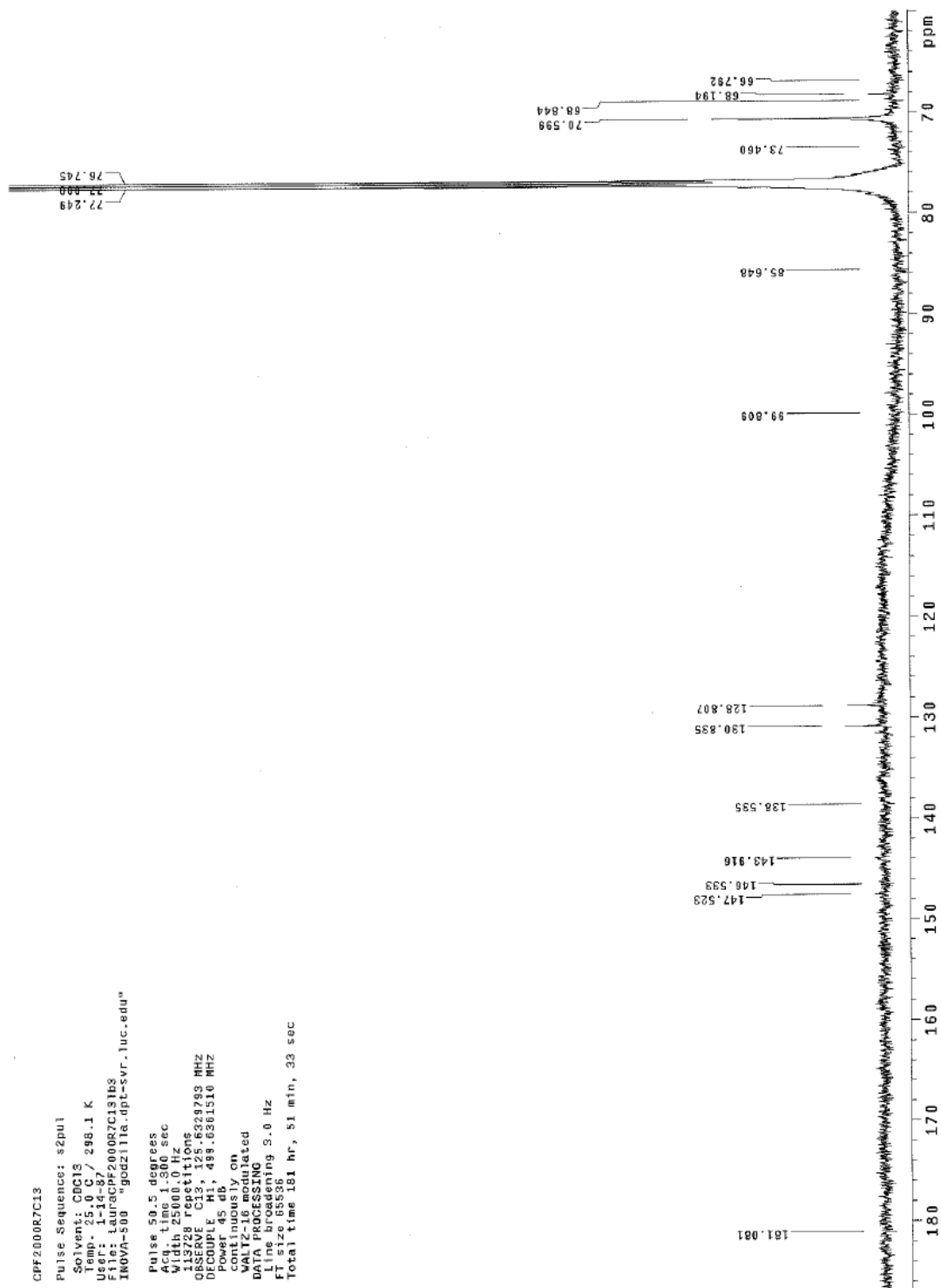


Figure 86.  $^{13}\text{C}$  NMR Expansion of Ce6-PEG-FA

Figure 87.  $^{13}\text{C}$  NMR Expansion of Ce6-PEG-FA

APPENDIX B  
LIST OF TABLES

Row	Column	Content	Blank Corrected Raw Data 544 nm; 590 nm	Average
E	4	Control C1	71018	142906
E	5	Control C2	128270	
E	6	Control C3	157541	
F	4	Control C4	137407	130374
F	5	Control C5	130933	
F	6	Control C6	129815	
G	4	Control C7	134570	133775
G	5	Control C8	140067	
G	6	Control C9	132979	
H	4	Control C10	135777	138038
H	5	Control C11	140299	
H	6	Control C12	129893	
D	4	Sample X34	152281	154166
D	5	Sample X35	197096	
D	6	Sample X36	156051	
		Control	Average	136000

Table 5. Cytotoxicity Data: August 1, 2014

Row	Column	Content	Blank Corrected Raw Data 544 nm; 590 nm	Average
E	4	Control C1	151020	150561
E	5	Control C2	150101	
E	6	Control C3	162601	
F	4	Control C4	176618	177729
F	5	Control C5	146999	
F	6	Control C6	178839	
G	4	Control C7	158791	170431
G	5	Control C8	230336	
G	6	Control C9	182071	
H	4	Control C10	159270	155778
H	5	Control C11	176942	
H	6	Control C12	152285	
D	4	Sample X34	62939	50262
D	5	Sample X35	52669	
D	6	Sample X36	47855	
		Control	Average	164000

Table 6. Phototoxicity Data: August 1, 2014

Cytotoxicity Data - November 21, 2014					
Row	Column	Content	Exposure Time (min)	Blank Corrected Raw Data ( $\lambda_{\text{ex}} 544/\lambda_{\text{em}} 590$ )	Average
A	5	Control C9	1	136351	117891
B	5	Control C10	1	127255	
A	12	Control C1	1	159421	
B	12	Control C2	1	97687	
C	5	Control C11	2	111965	
D	5	Control C12	2	138811	
C	12	Control C3	2	119594	
D	12	Control C4	2	116229	
E	5	Control C13	4	105970	
F	5	Control C14	4	105364	
E	12	Control C5	4	123758	
F	12	Control C6	4	109619	
G	5	Control C15	6	120397	
H	5	Control C16	6	107507	
G	12	Control C7	6	93159	
H	12	Control C8	6	113174	
A	2	Ce6-PEG-FA [5 $\mu\text{M}$ ]	1	157255	119508
A	3	Ce6-PEG-FA [5 $\mu\text{M}$ ]	1	147507	
A	4	Ce6-PEG-FA [5 $\mu\text{M}$ ]	1	155367	
C	2	Ce6-PEG-FA [5 $\mu\text{M}$ ]	2	110504	
C	3	Ce6-PEG-FA [5 $\mu\text{M}$ ]	2	129372	
C	4	Ce6-PEG-FA [5 $\mu\text{M}$ ]	2	95058	
E	2	Ce6-PEG-FA [5 $\mu\text{M}$ ]	4	123549	
E	3	Ce6-PEG-FA [5 $\mu\text{M}$ ]	4	86738	
E	4	Ce6-PEG-FA [5 $\mu\text{M}$ ]	4	90585	
G	2	Ce6-PEG-FA [5 $\mu\text{M}$ ]	6	121739	
G	3	Ce6-PEG-FA [5 $\mu\text{M}$ ]	6	106476	
G	4	Ce6-PEG-FA [5 $\mu\text{M}$ ]	6	109951	

Table 7. Cytotoxicity Data: November 21, 2014

Cytotoxicity Data - November 21, 2014					
Row	Column	Content	Exposure Time (min)	Blank Corrected Raw Data ( $\lambda_{ex}$ 544/ $\lambda_{em}$ 590)	Average
B	2	Ce6-PEG-FA [10 $\mu$ M]	1	100573	105440
B	3	Ce6-PEG-FA [10 $\mu$ M]	1	91668	
B	4	Ce6-PEG-FA [10 $\mu$ M]	1	107277	
D	2	Ce6-PEG-FA [10 $\mu$ M]	2	103967	
D	3	Ce6-PEG-FA [10 $\mu$ M]	2	94803	
D	4	Ce6-PEG-FA [10 $\mu$ M]	2	104514	
F	2	Ce6-PEG-FA [10 $\mu$ M]	4	120801	
F	3	Ce6-PEG-FA [10 $\mu$ M]	4	117852	
F	4	Ce6-PEG-FA [10 $\mu$ M]	4	96317	
H	2	Ce6-PEG-FA [10 $\mu$ M]	6	108747	
H	3	Ce6-PEG-FA [10 $\mu$ M]	6	100614	
H	4	Ce6-PEG-FA [10 $\mu$ M]	6	118144	
			% Viability		
		Control	100		
		Ce6-PEG-FA [5 $\mu$ M]	101		
		Ce6-PEG-FA [10 $\mu$ M]	89		

Table 8. Cytotoxicity Data (cont.): November 21, 2014

Phototoxicity Data - November 21, 2014					
Row	Column	Content	Exposure Time (min)	Blank Corrected Raw Data ( $\lambda_{ex}$ 544/ $\lambda_{em}$ 590)	Average
A	5	Control C9	1	173966	138725
B	5	Control C10	1	123266	
A	12	Control C1	1	171042	
B	12	Control C2	1	169747	
C	5	Control C11	2	129123	
D	5	Control C12	2	122504	
C	12	Control C3	2	143087	
D	12	Control C4	2	137829	
E	5	Control C13	4	100799	
F	5	Control C14	4	101039	
E	12	Control C5	4	147236	
F	12	Control C6	4	154285	
G	5	Control C15	6	117320	
H	5	Control C16	6	145846	
G	12	Control C7	6	143326	
H	12	Control C8	6	139182	
A	2	Ce6-PEG-FA [5 $\mu$ M]	1	108990	110246
A	3	Ce6-PEG-FA [5 $\mu$ M]	1	111502	
A	4	Ce6-PEG-FA [5 $\mu$ M]	1	93112	
B	2	Ce6-PEG-FA [10 $\mu$ M]	1	597	356
B	3	Ce6-PEG-FA [10 $\mu$ M]	1	15	
B	4	Ce6-PEG-FA [10 $\mu$ M]	1	114	
C	2	Ce6-PEG-FA [5 $\mu$ M]	2	17573	16300
C	3	Ce6-PEG-FA [5 $\mu$ M]	2	15027	
C	4	Ce6-PEG-FA [5 $\mu$ M]	2	11798	
D	2	Ce6-PEG-FA [10 $\mu$ M]	2	3611	3553
D	3	Ce6-PEG-FA [10 $\mu$ M]	2	3494	
D	4	Ce6-PEG-FA [10 $\mu$ M]	2	11603	

Table 9. Phototoxicity Data: November 21, 2014





Cytotoxicity Data - December 5, 2014					
Row	Column	Content	Exposure Time (min)	Blank Corrected Raw Data ( $\lambda_{ex}$ 544/ $\lambda_{em}$ 590)	Average
A	5	Control C9	1	139319	144222
B	5	Control C10	1	127024	
A	12	Control C1	1	160185	
B	12	Control C2	1	168356	
C	5	Control C11	2	122778	
D	5	Control C12	2	127415	
C	12	Control C3	2	149766	
D	12	Control C4	2	159358	
E	5	Control C13	4	124038	
F	5	Control C14	4	137134	
E	12	Control C5	4	150768	
F	12	Control C6	4	156226	
G	5	Control C15	6	137002	
H	5	Control C16	6	130937	
G	12	Control C7	6	158977	
H	12	Control C8	6	158272	
A	2	Ce6-PEG-FA [5 $\mu$ M]	1	143367	133377
A	3	Ce6-PEG-FA [5 $\mu$ M]	1	134162	
A	4	Ce6-PEG-FA [5 $\mu$ M]	1	137930	
C	2	Ce6-PEG-FA [5 $\mu$ M]	2	124733	
C	3	Ce6-PEG-FA [5 $\mu$ M]	2	128739	
C	4	Ce6-PEG-FA [5 $\mu$ M]	2	119926	
E	2	Ce6-PEG-FA [5 $\mu$ M]	4	131401	
E	3	Ce6-PEG-FA [5 $\mu$ M]	4	124251	
E	4	Ce6-PEG-FA [5 $\mu$ M]	4	145814	
G	2	Ce6-PEG-FA [5 $\mu$ M]	6	142974	
G	3	Ce6-PEG-FA [5 $\mu$ M]	6	143643	
G	4	Ce6-PEG-FA [5 $\mu$ M]	6	123588	

Table 11. Cytotoxicity Data: December 5, 2014

Cytotoxicity Data - December 5, 2014					
Row	Column	Content	Exposure Time (min)	Blank Corrected Raw Data ( $\lambda_{ex}$ 544/ $\lambda_{em}$ 590)	Average
B	2	Ce6-PEG-FA [10 $\mu$ M]	1	112553	121905
B	3	Ce6-PEG-FA [10 $\mu$ M]	1	125934	
B	4	Ce6-PEG-FA [10 $\mu$ M]	1	130164	
D	2	Ce6-PEG-FA [10 $\mu$ M]	2	127190	
D	3	Ce6-PEG-FA [10 $\mu$ M]	2	122069	
D	4	Ce6-PEG-FA [10 $\mu$ M]	2	114706	
F	2	Ce6-PEG-FA [10 $\mu$ M]	4	117201	
F	3	Ce6-PEG-FA [10 $\mu$ M]	4	114327	
F	4	Ce6-PEG-FA [10 $\mu$ M]	4	113438	
H	2	Ce6-PEG-FA [10 $\mu$ M]	6	130009	
H	3	Ce6-PEG-FA [10 $\mu$ M]	6	131269	
H	4	Ce6-PEG-FA [10 $\mu$ M]	6	124002	
			% Viability		
		Control	100		
		Ce6-PEG-FA [5 $\mu$ M]	92		
		Ce6-PEG-FA [10 $\mu$ M]	85		

Table 12. Cytotoxicity Data (cont.): December 5, 2014

Phototoxicity Data - December 5, 2014					
Row	Column	Content	Exposure Time (min)	Blank Corrected Raw Data ( $\lambda_{ex}$ 544/ $\lambda_{em}$ 590)	Average
A	5	Control C9	1	161914	150582
B	5	Control C10	1	133921	
A	12	Control C1	1	176624	
B	12	Control C2	1	159597	
C	5	Control C11	2	121245	
D	5	Control C12	2	137578	
C	12	Control C3	2	164381	
D	12	Control C4	2	145108	
E	5	Control C13	4	134025	
F	5	Control C14	4	140855	
E	12	Control C5	4	168871	
F	12	Control C6	4	176068	
G	5	Control C15	6	145444	
H	5	Control C16	6	158572	
G	12	Control C7	6	146726	
H	12	Control C8	6	138384	
A	2	Ce6-PEG-FA [5 $\mu$ M]	1	112180	109571
A	3	Ce6-PEG-FA [5 $\mu$ M]	1	106962	
A	4	Ce6-PEG-FA [5 $\mu$ M]	1	93028	
B	2	Ce6-PEG-FA [10 $\mu$ M]	1	50708	8916
B	3	Ce6-PEG-FA [10 $\mu$ M]	1	10156	
B	4	Ce6-PEG-FA [10 $\mu$ M]	1	7676	
C	2	Ce6-PEG-FA [5 $\mu$ M]	2	100316	9552
C	3	Ce6-PEG-FA [5 $\mu$ M]	2	3158	
C	4	Ce6-PEG-FA [5 $\mu$ M]	2	15945	
D	2	Ce6-PEG-FA [10 $\mu$ M]	2	3863	3985
D	3	Ce6-PEG-FA [10 $\mu$ M]	2	4106	
D	4	Ce6-PEG-FA [10 $\mu$ M]	2	12942	

Table 13. Phototoxicity Data: December 5, 2014

Phototoxicity Data - December 5, 2014					
Row	Column	Content	Exposure Time (min)	Blank Corrected Raw Data ( $\lambda_{ex}$ 544/ $\lambda_{em}$ 590)	Average
E	2	Ce6-PEG-FA [5 $\mu$ M]	4	3308	2405
E	3	Ce6-PEG-FA [5 $\mu$ M]	4	1501	
E	4	Ce6-PEG-FA [5 $\mu$ M]	4	14073	
F	2	Ce6-PEG-FA [10 $\mu$ M]	4	1196	2622
F	3	Ce6-PEG-FA [10 $\mu$ M]	4	15768	
F	4	Ce6-PEG-FA [10 $\mu$ M]	4	4047	
G	2	Ce6-PEG-FA [5 $\mu$ M]	6	574	591
G	3	Ce6-PEG-FA [5 $\mu$ M]	6	179	
G	4	Ce6-PEG-FA [5 $\mu$ M]	6	607	
H	2	Ce6-PEG-FA [10 $\mu$ M]	6	1675	512
H	3	Ce6-PEG-FA [10 $\mu$ M]	6	33	
H	4	Ce6-PEG-FA [10 $\mu$ M]	6	990	
	Time (min)		% Viability		
		Control	100		
	1	Ce6-PEG-FA [5 $\mu$ M]	72.8		
	1	Ce6-PEG-FA [10 $\mu$ M]	5.9		
	2	Ce6-PEG-FA [5 $\mu$ M]	6.3		
	2	Ce6-PEG-FA [10 $\mu$ M]	2.6		
	4	Ce6-PEG-FA [5 $\mu$ M]	1.6		
	4	Ce6-PEG-FA [10 $\mu$ M]	1.7		
	6	Ce6-PEG-FA [5 $\mu$ M]	0.4		
	6	Ce6-PEG-FA [10 $\mu$ M]	0.3		

Table 14. Phototoxicity Data (cont.): December 5, 2014

Cytotoxicity Data - Feb. 6, 2015						
Row	Column	Content	Exposure Time (min)	Blank Corrected Raw Data (544/590)	Average	
B	2	Control 1	1	119907	114447	
B	3	Control 2	1	107483		
B	4	Control 3	1	125396		
B	5	Control 4	1	96506		
D	2	Control 1	2	112866		
D	3	Control 2	2	102257		
D	4	Control 3	2	117746		
F	2	Control 1	4	110414		
F	3	Control 2	4	107281		
F	4	Control 3	4	119238		
H	2	Control 1	6	115677		
H	3	Control 2	6	126056		
H	4	Control 3	6	126978		
A	2	Ce6 [5 $\mu$ M]	1	136755		117956
A	3	Ce6 [5 $\mu$ M]	1	149673		
A	4	Ce6 [5 $\mu$ M]	1	127840		
C	2	Ce6 [5 $\mu$ M]	2	109498		
C	3	Ce6 [5 $\mu$ M]	2	108286		
C	4	Ce6 [5 $\mu$ M]	2	99426		
E	2	Ce6 [5 $\mu$ M]	4	121713		
E	3	Ce6 [5 $\mu$ M]	4	105892		
E	4	Ce6 [5 $\mu$ M]	4	103633		
G	2	Ce6 [5 $\mu$ M]	6	122196		
G	3	Ce6 [5 $\mu$ M]	6	116855		
G	4	Ce6 [5 $\mu$ M]	6	113699		

Table 15. Cytotoxicity Data: February 6, 2015



Cytotoxicity Data - Feb. 6, 2015						
Content	St. Dev.	Outliers		New Ave.	Std. Dev.	
Ce6-PEG-FA [5 $\mu$ M]	16386	0.3142		119098	11417	0.7733
Ce6-PEG-FA [5 $\mu$ M]		2.4708				
Ce6-PEG-FA [5 $\mu$ M]		-0.2203				0.0062
Ce6-PEG-FA [5 $\mu$ M]		-1.4957				-1.8243
Ce6-PEG-FA [5 $\mu$ M]		0.8323				1.5170
Ce6-PEG-FA [5 $\mu$ M]		0.5787				1.1529
Ce6-PEG-FA [5 $\mu$ M]		-0.6109				-0.5544
Ce6-PEG-FA [5 $\mu$ M]		-1.1438				-1.3192
Ce6-PEG-FA [5 $\mu$ M]		-0.0056				0.3144
Ce6-PEG-FA [5 $\mu$ M]		-0.5128				-0.4136
Ce6-PEG-FA [5 $\mu$ M]		-0.6120				-0.5559
Ce6-PEG-FA [5 $\mu$ M]		0.4050				0.9037
Ce6-PEG-FA [10 $\mu$ M]	7325	-0.8825	<b>G for 9</b>			
Ce6-PEG-FA [10 $\mu$ M]		-0.1655	<b>2.2150</b>			
Ce6-PEG-FA [10 $\mu$ M]		-0.6490				
Ce6-PEG-FA [10 $\mu$ M]		0.3541				
Ce6-PEG-FA [10 $\mu$ M]		-1.6744				
Ce6-PEG-FA [10 $\mu$ M]		-0.5430				
Ce6-PEG-FA [10 $\mu$ M]		1.6188				
Ce6-PEG-FA [10 $\mu$ M]		1.1182				
Ce6-PEG-FA [10 $\mu$ M]		0.8232				

Table 17. Cytotoxicity Data (cont.): February 6, 2015



Phototoxicity Data - Feb. 6, 2015					
Row	Column	Content	Exposure Time (min)	Blank Corrected Raw Data (544/590)	Average
B	2	Control 1	1	119723	117476
B	3	Control 2	1	111350	
B	4	Control 3	1	107133	
B	5	Control 4	1	97819	
D	2	Control 1	2	123864	
D	3	Control 2	2	122045	
D	4	Control 3	2	112034	
F	2	Control 1	4	118449	
F	3	Control 2	4	114336	
F	4	Control 3	4	114057	
H	2	Control 1	6	136083	
H	3	Control 2	6	128654	
H	4	Control 3	6	121645	
A	2	Ce6 [5 $\mu$ M]	1	137861	121457
A	3	Ce6 [5 $\mu$ M]	1	120811	
A	4	Ce6 [5 $\mu$ M]	1	122103	
A	5	PEG-FA [5 $\mu$ M]	1	125288	114890
A	6	PEG-FA [5 $\mu$ M]	1	104492	
A	7	PEG-FA [5 $\mu$ M]	1	99049	
A	8	Ce6-PEG-FA [5 $\mu$ M]	1	7821	19682
A	9	Ce6-PEG-FA [5 $\mu$ M]	1	15853	
B	9	Ce6-PEG-FA [5 $\mu$ M]	1	23510	
B	6	Ce6-PEG-FA [10 $\mu$ M]	1	2734	12653
B	7	Ce6-PEG-FA [10 $\mu$ M]	1	14523	
B	8	Ce6-PEG-FA [10 $\mu$ M]	1	10783	

Table 18. Phototoxicity Data: February 6, 2015

Phototoxicity Data - Feb. 6, 2015			Exposure		
Row	Column	Content	Time (min)	Blank Corrected	Average
				Raw Data (544/590)	
C	2	Ce6 [5 $\mu$ M]	2	110189	94972
C	3	Ce6 [5 $\mu$ M]	2	94754	
C	4	Ce6 [5 $\mu$ M]	2	95189	
C	5	PEG-FA [5 $\mu$ M]	2	93959	97060
C	6	PEG-FA [5 $\mu$ M]	2	100160	
C	7	PEG-FA [5 $\mu$ M]	2	1500	
C	8	Ce6-PEG-FA [5 $\mu$ M]	2	99309	7546
D	7	Ce6-PEG-FA [5 $\mu$ M]	2	4431	
D	8	Ce6-PEG-FA [5 $\mu$ M]	2	10661	
D	5	Ce6-PEG-FA [10 $\mu$ M]	2	97435	6746
D	6	Ce6-PEG-FA [10 $\mu$ M]	2	6746	
E	2	Ce6 [5 $\mu$ M]	4	82769	93779
E	3	Ce6 [5 $\mu$ M]	4	59360	
E	4	Ce6 [5 $\mu$ M]	4	104788	
E	5	PEG-FA [5 $\mu$ M]	4	32962	75324
E	6	PEG-FA [5 $\mu$ M]	4	117685	
E	7	PEG-FA [5 $\mu$ M]	4	1765	
E	8	Ce6-PEG-FA [5 $\mu$ M]	4	110125	2168
F	7	Ce6-PEG-FA [5 $\mu$ M]	4	1669	
F	8	Ce6-PEG-FA [5 $\mu$ M]	4	2667	
F	5	Ce6-PEG-FA [10 $\mu$ M]	4	112778	3129
F	6	Ce6-PEG-FA [10 $\mu$ M]	4	3129	

Table 19. Phototoxicity Data (cont.): February 6, 2015



Cytotoxicity Data - Apr. 3, 2015						
Row	Column	Content	Exposure Time (min)	Blank Corrected Raw Data (544/590)	Average	St. Dev.
B	12	Control 1	1	110647	102633	
D	12	Control 2	2	106823		
F	12	Control 3	4	107848		
H	12	Control 4	6	85212		
A	2	Ce6 [5 $\mu$ M]	1	102968	97246	32417
A	3	Ce6 [5 $\mu$ M]	1	90220		
A	4	Ce6 [5 $\mu$ M]	1	88788		
A	5	Ce6 [5 $\mu$ M]	1	140733		
A	6	Ce6 [5 $\mu$ M]	1	227458		
A	7	Ce6 [5 $\mu$ M]	1	168527		
C	2	Ce6 [5 $\mu$ M]	2	111222		
C	3	Ce6 [5 $\mu$ M]	2	93031		
C	4	Ce6 [5 $\mu$ M]	2	95093	87682	
C	5	Ce6 [5 $\mu$ M]	2	87111		
C	6	Ce6 [5 $\mu$ M]	2	80816		
C	7	Ce6 [5 $\mu$ M]	2	83810		
E	2	Ce6 [5 $\mu$ M]	4	84566		
E	3	Ce6 [5 $\mu$ M]	4	96824		
E	4	Ce6 [5 $\mu$ M]	4	100708		
E	5	Ce6 [5 $\mu$ M]	4	72528		
E	6	Ce6 [5 $\mu$ M]	4	91620	95777	
E	7	Ce6 [5 $\mu$ M]	4	86761		
G	2	Ce6 [5 $\mu$ M]	6	98517		
G	3	Ce6 [5 $\mu$ M]	6	105140		
G	4	Ce6 [5 $\mu$ M]	6	98705		
G	5	Ce6 [5 $\mu$ M]	6	89776		
G	6	Ce6 [5 $\mu$ M]	6	110952		
G	7	Ce6 [5 $\mu$ M]	6	84745		

Table 21. Cytotoxicity Data: April 3, 2015

Cytotoxicity Data - Apr. 3, 2015							
Content	Outliers	G for 24					
		Between					
		2.7082					
		and					
		2.8217					
			<b>New Ave.</b>	<b>Std. Dev.</b>	<b>Outliers</b>	<b>Outliers</b>	<b>Outliers</b>
Ce6 [5 µM]	0.1765		98398	20063	0.2278	0.5671	1.0313
Ce6 [5 µM]	-0.2167				-0.4076	-0.3649	-0.2933
Ce6 [5 µM]	-0.2609				-0.4790	-0.4696	-0.4421
Ce6 [5 µM]	1.3415		<b>G for 23,22,21</b>		2.1101	<b>3.3281</b>	
Ce6 [5 µM]	4.0168	<b>outlier</b>	Between				
Ce6 [5 µM]	2.1989		2.7082		<b>3.4955</b>		
Ce6 [5 µM]	0.4311		and		0.6392	1.1706	1.8889
Ce6 [5 µM]	-0.1300		2.8217		-0.2675	-0.1594	-0.0012
Ce6 [5 µM]	-0.0664				-0.1648	-0.0086	0.2130
Ce6 [5 µM]	-0.3126		<b>2nd New Ave.</b>	<b>St. Dev.</b>	-0.5626	-0.5922	-0.6164
Ce6 [5 µM]	-0.5068		95211	13678	-0.8764	-1.0524	-1.2704
Ce6 [5 µM]	-0.4145				-0.7271	-0.8335	-0.9594
Ce6 [5 µM]	-0.3912		<b>3rd New Ave.</b>	<b>St. Dev.</b>	-0.6895	-0.7782	-0.8808
Ce6 [5 µM]	-0.0130		93043	9624	-0.0785	0.1180	0.3929
Ce6 [5 µM]	0.1068				0.1151	0.4019	0.7965
Ce6 [5 µM]	-0.7625				-1.2895	-1.6583	-2.1316
Ce6 [5 µM]	-0.1735				-0.3379	-0.2625	-0.1478
Ce6 [5 µM]	-0.3234				-0.5801	-0.6177	-0.6527
Ce6 [5 µM]	0.0392				0.0059	0.2417	0.5688
Ce6 [5 µM]	0.2435				0.3360	0.7259	1.2570
Ce6 [5 µM]	0.0450				0.0153	0.2555	0.5883
Ce6 [5 µM]	-0.2304				-0.4298	-0.3973	-0.3395
Ce6 [5 µM]	0.4228				0.6257	1.1508	1.8609
Ce6 [5 µM]	-0.3856				-0.6805	-0.7651	-0.8622

Table 22. Cytotoxicity Data (cont.): April 3, 2015

Cytotoxicity Data - Apr. 3, 2015					
Row	Column	Content	Light Exp. (min)	Blank Corrected Raw Data (544/590)	Average
B	2	Ce6 [10 µM]	1	98929	88444
B	3	Ce6 [10 µM]	1	106479	
B	4	Ce6 [10 µM]	1	95980	
B	5	Ce6 [10 µM]	1	94244	
B	6	Ce6 [10 µM]	1	78368	
B	7	Ce6 [10 µM]	1	82069	
B	8	Ce6 [10 µM]	1	82950	
B	9	Ce6 [10 µM]	1	83201	
B	10	Ce6 [10 µM]	1	73777	
D	2	Ce6 [10 µM]	2	86274	83210
D	3	Ce6 [10 µM]	2	91578	
D	4	Ce6 [10 µM]	2	91000	
D	5	Ce6 [10 µM]	2	77420	
D	6	Ce6 [10 µM]	2	76392	
D	7	Ce6 [10 µM]	2	77744	
D	8	Ce6 [10 µM]	2	81584	
D	9	Ce6 [10 µM]	2	83212	
D	10	Ce6 [10 µM]	2	83689	
F	2	Ce6 [10 µM]	4	85213	90214
F	3	Ce6 [10 µM]	4	93083	
F	4	Ce6 [10 µM]	4	90240	
F	5	Ce6 [10 µM]	4	81368	
F	6	Ce6 [10 µM]	4	102578	
F	7	Ce6 [10 µM]	4	90426	
F	8	Ce6 [10 µM]	4	97268	
F	9	Ce6 [10 µM]	4	88108	
F	10	Ce6 [10 µM]	4	83642	
H	2	Ce6 [10 µM]	6	99825	96608
H	3	Ce6 [10 µM]	6	103928	
H	4	Ce6 [10 µM]	6	99176	
H	5	Ce6 [10 µM]	6	92867	
H	6	Ce6 [10 µM]	6	103785	
H	7	Ce6 [10 µM]	6	98532	
H	8	Ce6 [10 µM]	6	95921	
H	9	Ce6 [10 µM]	6	100532	
H	10	Ce6 [10 µM]	6	74906	

Table 23. Cytotoxicity Data (cont.): April 3, 2015



Cytotoxicity Data - Apr. 3, 2015					
Content	Outliers				
			New Ave.	Std. Dev.	Outliers
Ce6-PEG-FA [10 $\mu$ M]	-0.0747	<b>G for 12</b>	65857	4458	0.2124
Ce6-PEG-FA [10 $\mu$ M]	0.2337	<b>2.4116</b>			0.6522
Ce6-PEG-FA [10 $\mu$ M]	0.8936	<b>G for 11</b>			1.5936
Ce6-PEG-FA [10 $\mu$ M]	<b>2.4587</b>		<b>2.3547</b>		
Ce6-PEG-FA [10 $\mu$ M]	-0.0231				0.2859
Ce6-PEG-FA [10 $\mu$ M]	-0.8443				-0.8856
Ce6-PEG-FA [10 $\mu$ M]	-1.1321				-1.2961
Ce6-PEG-FA [10 $\mu$ M]	-0.2803				-0.0810
Ce6-PEG-FA [10 $\mu$ M]	0.1379				0.5156
Ce6-PEG-FA [10 $\mu$ M]	-1.1541				-1.3275
Ce6-PEG-FA [10 $\mu$ M]	0.8002				1.4604
Ce6-PEG-FA [10 $\mu$ M]	-1.0156				-1.1299

Table 25. Cytotoxicity Data (cont.): April 3, 2015



Phototoxicity Data - April 3, 2015					
Row	Column	Content	Exposure Time (min)	Blank Corrected Raw Data (544/590)	Average
B	12	Control	1	115617	99159
D	12	Control	2	100660	
F	12	Control	4	95428	
H	12	Control	6	101390	
A	2	Ce6 [5 $\mu$ M]	1	121575	107689
A	3	Ce6 [5 $\mu$ M]	1	106913	
A	4	Ce6 [5 $\mu$ M]	1	108464	
A	5	Ce6 [5 $\mu$ M]	1	101548	101742
A	6	Ce6 [5 $\mu$ M]	1	100347	
A	7	Ce6 [5 $\mu$ M]	1	103331	
B	2	Ce6 [10 $\mu$ M]	1	100689	82691
B	3	Ce6 [10 $\mu$ M]	1	64692	
B	4	Ce6 [10 $\mu$ M]	1	24404	
B	5	Ce6 [10 $\mu$ M]	1	13554	14305
B	6	Ce6 [10 $\mu$ M]	1	17178	
B	7	Ce6 [10 $\mu$ M]	1	12182	
B	8	Ce6 [10 $\mu$ M]	1	11813	16996
B	9	Ce6 [10 $\mu$ M]	1	16777	
B	10	Ce6 [10 $\mu$ M]	1	22397	
A	8	Ce6-PEG-FA [5 $\mu$ M]	1	34251	26931
A	9	Ce6-PEG-FA [5 $\mu$ M]	1	107573	
A	10	Ce6-PEG-FA [5 $\mu$ M]	1	19610	
A	11	Ce6-PEG-FA [10 $\mu$ M]	1	40292	31661
A	12	Ce6-PEG-FA [10 $\mu$ M]	1	23029	
B	11	Ce6-PEG-FA [10 $\mu$ M]	1	2779	

Table 26. Phototoxicity Data: April 3, 2015

Phototoxicity Data - April 3, 2015					
Row	Column	Content	Exposure Time (min)	Blank Corrected Raw Data (544/590)	Average
C	2	Ce6 [5 $\mu$ M]	2	103686	80805
C	3	Ce6 [5 $\mu$ M]	2	57923	
C	4	Ce6 [5 $\mu$ M]	2	11016	
C	5	Ce6 [5 $\mu$ M]	2	10525	11523
C	6	Ce6 [5 $\mu$ M]	2	47039	
C	7	Ce6 [5 $\mu$ M]	2	12521	
D	2	Ce6 [10 $\mu$ M]	2	98008	2063
D	3	Ce6 [10 $\mu$ M]	2	2720	
D	4	Ce6 [10 $\mu$ M]	2	1406	
D	5	Ce6 [10 $\mu$ M]	2	2725	2223
D	6	Ce6 [10 $\mu$ M]	2	4238	
D	7	Ce6 [10 $\mu$ M]	2	1720	
D	8	Ce6 [10 $\mu$ M]	2	1342	1159
D	9	Ce6 [10 $\mu$ M]	2	976	
D	10	Ce6 [10 $\mu$ M]	2	3127	
C	8	Ce6-PEG-FA [5 $\mu$ M]	2	12218	21237
C	9	Ce6-PEG-FA [5 $\mu$ M]	2	5173	
C	10	Ce6-PEG-FA [5 $\mu$ M]	2	9019	
C	11	Ce6-PEG-FA [10 $\mu$ M]	2	6338	4508
C	12	Ce6-PEG-FA [10 $\mu$ M]	2	11612	
D	11	Ce6-PEG-FA [10 $\mu$ M]	2	2677	

Table 27. Phototoxicity Data (cont.): April 3, 2015

Phototoxicity Data - April 3, 2015					
Row	Column	Content	Exposure Time (min)	Blank Corrected Raw Data (544/590)	Average
E	2	Ce6 [5 $\mu$ M]	4	97368	6372
E	3	Ce6 [5 $\mu$ M]	4	9655	
E	4	Ce6 [5 $\mu$ M]	4	3088	
E	5	Ce6 [5 $\mu$ M]	4	1491	1052
E	6	Ce6 [5 $\mu$ M]	4	2422	
E	7	Ce6 [5 $\mu$ M]	4	613	
F	2	Ce6 [10 $\mu$ M]	4	57572	3417
F	3	Ce6 [10 $\mu$ M]	4	6247	
F	4	Ce6 [10 $\mu$ M]	4	587	
F	5	Ce6 [10 $\mu$ M]	4	636	790
F	6	Ce6 [10 $\mu$ M]	4	1739	
F	7	Ce6 [10 $\mu$ M]	4	943	
F	8	Ce6 [10 $\mu$ M]	4	467	1074
F	9	Ce6 [10 $\mu$ M]	4	1680	
F	10	Ce6 [10 $\mu$ M]	4	3421	
E	8	Ce6-PEG-FA [5 $\mu$ M]	4	1823	1817
E	9	Ce6-PEG-FA [5 $\mu$ M]	4	15184	
E	10	Ce6-PEG-FA [5 $\mu$ M]	4	1810	
E	11	Ce6-PEG-FA [10 $\mu$ M]	4	5006	9386
E	12	Ce6-PEG-FA [10 $\mu$ M]	4	9950	
F	11	Ce6-PEG-FA [10 $\mu$ M]	4	8821	

Table 28. Phototoxicity Data (cont.): April 3, 2015

Phototoxicity Data - April 3, 2015					
Row	Column	Content	Exposure Time (min)	Blank Corrected Raw Data (544/590)	Average
G	2	Ce6 [5 $\mu$ M]	6	75760	70766
G	3	Ce6 [5 $\mu$ M]	6	65771	
G	4	Ce6 [5 $\mu$ M]	6	3747	
G	5	Ce6 [5 $\mu$ M]	6	4970	4201
G	6	Ce6 [5 $\mu$ M]	6	7664	
G	7	Ce6 [5 $\mu$ M]	6	3432	
H	2	Ce6 [10 $\mu$ M]	6	60694	7905
H	3	Ce6 [10 $\mu$ M]	6	11843	
H	4	Ce6 [10 $\mu$ M]	6	3967	
H	5	Ce6 [10 $\mu$ M]	6	5513	5124
H	6	Ce6 [10 $\mu$ M]	6	7658	
H	7	Ce6 [10 $\mu$ M]	6	4735	
H	8	Ce6 [10 $\mu$ M]	6	7517	9260
H	9	Ce6 [10 $\mu$ M]	6	11002	
H	10	Ce6 [10 $\mu$ M]	6	42476	
G	8	Ce6-PEG-FA [5 $\mu$ M]	6	1327	1484
G	9	Ce6-PEG-FA [5 $\mu$ M]	6	676	
G	10	Ce6-PEG-FA [5 $\mu$ M]	6	1640	
G	11	Ce6-PEG-FA [10 $\mu$ M]	6	3075	2256
G	12	Ce6-PEG-FA [10 $\mu$ M]	6	4905	
H	11	Ce6-PEG-FA [10 $\mu$ M]	6	1436	

Table 29. Phototoxicity Data (cont.): April 3, 2015

<b>Phototoxicity Data - April 3, 2015</b>		
	Time (min)	% Viability
	Control	100
	1 Ce6 [5 $\mu$ M]	109
	1 Ce6 [5 $\mu$ M]	103
	1 Ce6 [10 $\mu$ M]	83
	1 Ce6 [10 $\mu$ M]	14
	1 Ce6 [10 $\mu$ M]	17
	1 Ce6-PEG-FA [5 $\mu$ M]	27
	1 Ce6-PEG-FA [10 $\mu$ M]	32
	2 Ce6 [5 $\mu$ M]	81
	2 Ce6 [5 $\mu$ M]	12
	2 Ce6 [10 $\mu$ M]	2
	2 Ce6 [10 $\mu$ M]	2
	2 Ce6 [10 $\mu$ M]	1
	2 Ce6-PEG-FA [5 $\mu$ M]	21
	2 Ce6-PEG-FA [10 $\mu$ M]	5

Table 30. Phototoxicity Data (cont.): April 3, 2015

<b>Phototoxicity Data - April 3, 2015</b>		
	Time (min)	% Viability
	4 Ce6 [5 $\mu$ M]	6
	4 Ce6 [5 $\mu$ M]	1
	4 Ce6 [10 $\mu$ M]	3
	4 Ce6 [10 $\mu$ M]	0.8
	4 Ce6 [10 $\mu$ M]	1
	4 Ce6-PEG-FA [5 $\mu$ M]	2
	4 Ce6-PEG-FA [10 $\mu$ M]	9
	6 Ce6 [5 $\mu$ M]	71
	6 Ce6 [5 $\mu$ M]	4
	6 Ce6 [10 $\mu$ M]	8
	6 Ce6 [10 $\mu$ M]	5
	6 Ce6 [10 $\mu$ M]	9
	6 Ce6-PEG-FA [5 $\mu$ M]	1
	6 Ce6-PEG-FA [10 $\mu$ M]	2

Table 31. Phototoxicity Data (cont.): April 3, 2015

<b>Compiled</b>						
<b>Dark Data</b>						
	<b>Ave % Viab.</b>	<b>Ave % Viab.</b>	<b>Ave % Viab.</b>	<b>Ave % Viab.</b>	<b>Compiled</b>	<b>Std. Dev.</b>
	<b>Exp. 1</b>	<b>Exp. 2</b>	<b>Exp. 3</b>	<b>Exp. 4</b>	<b>Ave</b>	
Control	100	100	100	100	100	
Ce6 [5 µM]	103	95	85	93	94	6
Ce6 [10 µM]	86	81	88	94	87	5
CPF [5 µM]	101	92	104	81	95	9
CPF [10 µM]	89	85	84	64	81	10
			<b>Outliers</b>			
<b>Dark</b>				<b>New Ave</b>	<b>Std. Dev.</b>	
	<b>Ave % Viab.</b>					
Control	100		<b>G for 4</b>	86	2	
Ce6 [5 µM]	94		<b>1.4812</b>			
Ce6 [10 µM]	87					
CPF [5 µM]	95		0.8755	0.4635	0.3605	-1.6996
CPF [10 µM]	86					

Table 32. Compiled Cytotoxicity Data: 4 Experiments

Compiled							
Light Data							
		Ave % Viab.	Ave % Viab.	Ave % Viab.	Ave % Viab.	Compiled	Std. Dev.
Time		Exp. 1	Exp. 2	Exp. 3	Exp. 4	Average	
	Control	100	100	100	100		
1	Ce6 [5 $\mu$ M]		103	109	103	105	3
1	Ce6 [10 $\mu$ M]		83	14	17	38	32
1	CPF [5 $\mu$ M]	80	73	17	27	49	28
1	CPF [10 $\mu$ M]	0.3	6	11	32	12	12
2	Ce6 [5 $\mu$ M]		81	81	12	58	33
2	Ce6 [10 $\mu$ M]		2	2	1	2	0.5
2	CPF [5 $\mu$ M]	12	6	6	21	11	6
2	CPF [10 $\mu$ M]	3	3	6	5	4	1
4	Ce6 [5 $\mu$ M]		80	6	1	29	36
4	Ce6 [10 $\mu$ M]		3	1	1	2	1
4	CPF [5 $\mu$ M]	9	2	2	2	4	3
4	CPF [10 $\mu$ M]	9	2	3	9	6	3
6	Ce6 [5 $\mu$ M]		98	71	4	58	40
6	Ce6 [10 $\mu$ M]		8	5	9	7	2
6	CPF [5 $\mu$ M]	28	0.4	2	1	8	12
6	CPF [10 $\mu$ M]	12	0.3	1	2	4	5

Table 33. Compiled Phototoxicity Data: 4 Experiments



## REFERENCE LIST

1. Allison, L., Ed.; *Fundamental Molecular Biology*; Blackwell Publishing: Massachusetts, 2008.
2. Lovell, J. F.; Liu, T. W. B.; Chen, J.; Zheng, G. Activatable photosensitizers for imaging and therapy. *Chem. Rev.* **2010**, *110*, 2839 - 2857.
3. Dougherty, T. J.; Henderson, B. W.; Gomer, C. J.; Jori, G.; Kessel, D.; Korbelik, M.; Moan, J.; Peng, Q. Photodynamic therapy. *J. Natl. Cancer Inst.* **1998**, *90*, 889 - 905.
4. Wilson, B. C.; Patterson, M. S. The physics, biophysics and technology of photodynamic therapy. *Phys. Med. Biol.* **2008**, *53*, R61.
5. Triesscheijn, M.; Baas, P.; Schellens, J. H.; Stewart, F. A. Photodynamic therapy in oncology. *Oncologist* **2006**, *11*, 1034 - 1044.
6. Sharman, W. M.; Allen, C. M.; van Lier, J. E. Photodynamic therapeutics: basic principles and clinical applications. *Drug Discov. Today* **1999**, *4*, 507-517.
7. Huang, Z. A review of progress in clinical photodynamic therapy. *Technology in cancer research & treatment* **2005**, *4*, 283.
8. Hamblin, M. R.; Hasan, T. Photodynamic therapy: a new antimicrobial approach to infectious disease? *Photochem. Photobiol. Sci.* **2004**, *3*, 436 - 450.
9. Ethirajan, M.; Chen, Y.; Joshi, P.; Pandey, R. K. The role of porphyrin chemistry in tumor imaging and photodynamic therapy. *Chem. Soc. Rev.* **2011**, *40*, 340 - 362.
10. Josefsen, L. B.; Boyle, R. W. *Met. Based Drugs* **2008**, 2008, 276109.
11. Hamblin, M. R.; Mroz, P., Eds.; *Advances in Photodynamic Therapy: Basic, Translational, and Clinical*; Artech House: Norwood, MA, 2008.

12. Pervaiz, S.; Olivo, M. Art and science of photodynamic therapy. *Clinical and experimental pharmacology and physiology* **2006**, *33*, 551 - 556.
13. Otake, M.; Nishiwaki, M.; Kobayashi, Y.; Baba, S.; Kohno, E.; Kawasaki, T.; Fujise, Y.; Nakamura, H. Selective accumulation of ALA-induced PpIX and photodynamic effect in chemically induced hepatocellular carcinoma. *Br. J. Cancer* **2003**, *89*, 730 - 736.
14. Oleinick, N. L.; Morris, R. L.; Belichenko, I. The role of apoptosis in response to photodynamic therapy: what, where, why, and how. *Photochem. Photobiol. Sci.* **2002**, *1*, 1 - 21.
15. Sharman, W. M.; Allen, C. M.; van Lier, J. E. Role of activated oxygen species in photodynamic therapy. *Meth. Enzymol.* **2000**, *319*, 376 - 400.
16. Girotti, A. W. Photosensitized oxidation of membrane lipids: reaction pathways, cytotoxic effects, and cytoprotective mechanisms. *J. Photochem. Photobiol. B.* **2001**, *63*, 103 - 113.
17. Davies, M. J. Singlet oxygen-mediated damage to proteins and its consequences. *Biochem. Biophys. Res. Commun.* **2003**, *305*, 761 - 770.
18. Cadet, J.; et al. Singlet oxygen oxidation of isolated and cellular DNA: product formation and mechanistic insights. *Photochem. Photobiol.* **2006**, *82*, 1219 - 1225.
19. Agostinis, P.; et al. Photodynamic therapy of cancer: an update. *CA: A Cancer Journal for Clinicians* **2011**, *61*, 250 - 281.
20. Castano, A. P.; Mroz, P.; Hamblin, M. R. Photodynamic therapy and anti-tumour immunity. *Nature Reviews Cancer* **2006**, *6*, 535 - 545.
21. Halliwell, B.; Gutteridge, J. M. C., Eds.; *Free Radicals in Biology and Medicine*; Oxford University Press: New York, 2007.
22. Bedard, K.; Krause, K. H. The NOX family of ROS-generating NADPH oxidases: physiology and pathophysiology. *Physiol. Rev.* **2007**, *87*, 245 - 313.
23. Redmond, R. W.; Kochevar, I. E. Spatially resolved cellular responses to singlet oxygen. *Photochem. Photobiol.* **2006**, *82*, 1178 - 1186.

24. Dahle, J.; et al. Bystander effects in cell death induced by photodynamic treatment UVA radiation and inhibitors of ATP synthesis. *Photochem. Photobiol.* **2001**, *73*, 378 - 387.
25. Moan, J.; Sommer, S. Oxygen dependence of the photosensitizing effect of hematoporphyrin derivative in NHIK 3025 cells. *Cancer Res.* **1985**, *45*, 1608 - 1610.
26. Chapman, J.; Stobbe, C.; Arnfield, M.; Santus, R.; Lee, J.; McPhee, M. Oxygen dependency of tumor cell killing in vitro by light-activated Photofrin II. *Radiat. Res.* **1991**, *126*, 73 - 79.
27. Mitchell, J. B.; et al. Oxygen dependence of hematoporphyrin derivative-induced photoinactivation of Chinese hamster cells. *Cancer Res.* **1985**, *45*, 2008 - 2011.
28. Freitas, I. Role of hypoxia in photodynamic therapy of tumors. *Tumori* **1985**, *71*, 251 - 259.
29. Henderson, B. W.; Fingar, V. H. Relationship of tumor hypoxia and response to photodynamic treatment in an experimental mouse tumor. *Cancer Res.* **1987**, *47*, 3110 - 3114.
30. Bonnett, R. Photosensitizers of the porphyrin and phthalocyanine series for photodynamic therapy. *Chem. Soc. Rev.* **1995**, *24*, 19 - 33.
31. Roeder, B.; et al. Photophysical properties and photodynamic activity in vivo of some tetrapyrroles. *Biophys. Chem.* **1990**, *35*, 303 - 312.
32. Wilkinson, F.; Helman, W. P.; Ross, A. B. Quantum yields for the photosensitized formation of the lowest electronically excited singlet state of molecular oxygen in solution. *J. Phys. Chem. Ref. Data.* **1993**, *22*, 113 - 262.
33. DeRosa, M. C.; Crutchley, R. J. Photosensitized singlet oxygen and its applications. *Coord. Chem. Rev.* **2002**, *233 - 234*, 351 - 371.
34. Lang, K.; Mosinger, J.; Wagnerova, D. M. Photophysical properties of porphyrinoid sensitizers non-covalently bound to host molecules; models for photodynamic therapy. *Coord. Chem. Rev.* **2004**, *248*, 321 - 350.
35. Redmond, R. W.; Gamlin, J. N. A compilation of singlet oxygen yields from biologically relevant molecules. *Photochem. Photobiol.* **1999**, *70*, 391 - 475.

36. Moan, J. On the diffusion length of singlet oxygen in cells and tissues. *J. Photochem. Photobiol. B.* **1990**, *6*, 343 - 344.
37. Moan, J.; Berg, K. The photodegradation of porphyrins in cells can be used to estimate the lifetime of singlet oxygen. *Photochem. Photobiol.* **1991**, *53*, 549 - 553.
38. Peng, Q.; Moan, J.; Nesland, J. M. Correlation of subcellular and intratumoral photosensitizer localization with ultrastructural features after photodynamic therapy. *Ultrastruct. Pathol.* **1996**, *20*, 109 - 129.
39. Juzeniene, A.; Moan, J. The history of PDT in Norway: Part one: identification of basic mechanisms of general PDT. *Photodiagn. Photodyn. Ther.* **2007**, *4*, 3 - 11.
40. Moan, J.; et al. Intracellular localization of photosensitizers. *Ciba found. Symp.* **1989**, *146*, 95 - 107.
41. Oleinick, N. L.; Evans, H. H. The photobiology of photodynamic therapy: cellular targets and mechanisms. *Radiat. Res.* **1998**, *150*, S146 - S156.
42. Fiel, R. J.; et al. Induction of DNA damage by porphyrin photosensitizers. *Cancer Res.* **1981**, *41*, 3543 - 3545.
43. Boye, E.; Moan, J. The photodynamic effect of hematoporphyrin on DNA. *Photochem. Photobiol.* **1980**, *31*, 223 - 228.
44. Moan, J.; Waksvik, H.; Christensen, T. DNA single-strand breaks and sister chromatid exchanges induced by treatment with hematoporphyrin and light or by x-rays in human NHIK 3025 cells. *Cancer Res.* **1980**, *40*, 2915 - 2918.
45. Moan, J.; Christensen, T. Photodynamic effects on human cells exposed to light in the presence of hematoporphyrin. Localization of the active dye. *Cancer Lett.* **1981**, *11*, 209 - 214.
46. Moan, J.; Boye, E. Photodynamic effect on DNA and cell survival of human cells sensitized by hematoporphyrin. *Photochem. Photobiophys.* **1981**, *2*, 301 - 307.
47. Lafleur, M. V.; Loman, H. Influence of anoxic sensitizers on the radiation damage in biologically active DNA in aqueous solution. *Int. J. Radiat. Biol. Relat. Stud. Phys. Chem. Med.* **1982**, *41*, 295 - 302.

48. Kvam, E.; Moan, J. A comparison of three photosensitizers with respect to efficiency of cell inactivation, fluorescence quantum yield and DNA strand breaks. *Photochem. Photobiol.* **1990**, *52*, 769 - 773.
49. Kvam, E.; Stokke, T.; Moan, J. The lengths of DNA fragments light-induced in the presence of a photosensitizer localized at the nuclear membrane of human cells. *Biochem. Biophys. Acta.* **1990**, *1049*, 33 - 37.
50. Moan, J.; Berg, K.; Kvam, E. Effects of photodynamic treatment on DNA and DNA-related cell functions; Kessel, D., Ed.; In *Photodynamic Therapy of Neoplastic Disease*; CRC Press: Boca Raton, Ann Arbor, Boston, 1990; pp 197 - 209.
51. Moan, J.; et al. In Effects of PDT on DNA and chromosomes; Riklis, E., Ed.; In *Photobiology*; Plenum Press: New York, 1991; pp 821 - 829.
52. Kvam, E.; et al. Plateau distributions of DNA fragment lengths produced by extended light exposure of extranuclear photosensitizers in human cells. *Nucleic Acids Res.* **1992**, *20*, 6687 - 6693.
53. Niedre, M.; Patterson, M. S.; Wilson, B. C. Direct near-infrared luminescence detection of singlet oxygen generated by photodynamic therapy in cells in vitro and tissues in vivo. *Photochem. Photobiol.* **2002**, *75*, 382 - 391.
54. Barr, H.; et al. Comparison of lasers for photodynamic therapy with a phthalocyanine photosensitizer. *Lasers Med. Sci.* **1989**, *4*, 7 - 12.
55. Gomer, C. J.; Razum, N. J. Acute skin response in albino mice following porphyrin photosensitization under oxic and anoxic conditions. *Photochem. Photobiol.* **1984**, *40*, 435 - 439.
56. Anholt, H.; Peng, Q.; Moan, J. Pressure against the tumor can reduce the efficiency of photochemotherapy. *Cancer Lett.* **1994**, *82*, 73 - 80.
57. Whipp, B. J.; Ward, S. A. Pulmonary gas exchange dynamics and the tolerance to muscular exercise: effects of fitness and training. *Ann. Physiol. Anthropol.* **1992**, *11*, 207 - 214.
58. Zhou, J.; et al. Tumor hypoxia and cancer progression. *Cancer Lett.* **2006**, *237*, 10 - 21.

59. Al-Waili, N. S.; et al. Hyperbaric oxygen and malignancies: a potential role in radiotherapy, chemotherapy, tumor surgery and phototherapy. *Med. Sci. Monit.* **2005**, *11*, RA279 - RA289.
60. Moan, J.; Christensen, T. Photodynamic inactivation of cancer cells in vitro. Effect of irradiation temperature and dose fractionation. *Cancer Lett.* **1979**, *6*, 331 - 335.
61. Qiu, K.; S., F. Merocyanine 540-sensitized photoinactivation of leukemia cells: effects of dose fractionation. *Photochem. Photobiol.* **1992**, *56*, 489 - 493.
62. Gomer, C. J.; et al. Expression of potentially lethal damage in Chinese hamster cells exposed to hematoporphyrin derivative photodynamic therapy. *Cancer Res.* **1986**, *46*, 3348 - 3352.
63. Dereski, M. O.; Madigan, L.; Chopp, M. The effect of hypothermia and hyperthermia on photodynamic therapy of normal brain. *Neurosurgery* **1995**, *36*, 141 - 145.
64. Devlin, T. M., Ed.; *Textbook of Biochemistry with Clinical Correlations*; Wiley & Sons, Inc.: New York, 1992.
65. Foster, T. H.; et al. Oxygen consumption and diffusion effects in photodynamic therapy. *Radiat. Res.* **1991**, *126*, 296 - 303.
66. Veenhuizen, R. B.; Stewart, F. A. The importance of fluence rate in photodynamic therapy: is there a parallel with ionizing radiation dose-rate effects? *Radiother. Oncol.* **1995**, *37*, 131 - 135.
67. Henderson, B. W.; et al. Photofrin photodynamic therapy can significantly deplete or preserve oxygenation in human basal cell carcinomas during treatment, depending on fluence rate. *Cancer Res.* **2000**, *60*, 525 - 529.
68. Henderson, B. W.; Busch, T. M.; Snyder, J. W. Fluence rate as a modulator of PDT mechanisms. *Lasers Surg. Med.* **2006**, *38*, 489 - 493.
69. Fingar, V. H. Vascular effects of photodynamic therapy. *J. Clin. Laser Med. Surg.* **1996**, *14*, 323 - 328.
70. Fingar, V. H.; et al. Vascular damage after photodynamic therapy of solid tumors: a view and comparison of effect in pre-clinical and clinical models at the University of Louisville. *In Vivo* **2000**, *14*, 93 - 100.

71. Krammer, B. Vascular effects of photodynamic therapy. *Anticancer Res.* **2001**, 21, 4271 - 4277.
72. Abels, C. Targeting of the vascular system of solid tumors by photodynamic therapy (PDT). *Photochem. Photobiol. Sci.* **2004**, 3, 765 - 771.
73. Chen, B.; Pogue, B. W.; Hoopes, P. J.; Hasan, T. Vascular and cellular targeting for photodynamic therapy. *Crit. Rev. Eukaryot. Gene Expr.* **2006**, 16, 279 - 305.
74. Henderson, B. W.; Fingar, V. H. Oxygen limitation of direct tumor cell kill during photodynamic treatment of a murine tumor model. *Photochem. Photobiol.* **1989**, 49, 299 - 304.
75. Engbrecht, B. W.; et al. Photofrin-mediated photodynamic therapy induces vascular occlusion and apoptosis in a human sarcoma xenograft model. *Cancer Res.* **1999**, 59, 4334 - 4342.
76. Ferrario, A.; et al. Antiangiogenic treatment enhances photodynamic therapy responsiveness in a mouse mammary carcinoma. *Cancer Res.* **2000**, 60, 4066 - 4069.
77. Yu, G.; et al. Noninvasive monitoring of murine tumor blood flow during and after photodynamic therapy provides early assessment of therapeutic efficacy. *Clin. Cancer Res.* **2005**, 11, 3543 - 3552.
78. Kunzi-Rapp, K.; et al. In vivo uptake and biodistribution of lipophilic and hydrophilic photosensitizers. *Proc. SPIE* **1996**, 2924, 176 - 180.
79. Peng, Q.; et al. Localization of potent photosensitizers in human tumor LOX by means of laser scanning microscopy. *Cancer Lett.* **1990**, 53, 129 - 139.
80. Peng, Q.; et al. Aluminum phthalocyanines with asymmetrical lower sulfonation and with symmetrical higher sulfonation: a comparison of localizing and photosensitizing mechanism in human tumor LOX xenografts. *Int. J. Cancer* **1990**, 46, 719 - 726.
81. Peng, Q.; Nesland, J. M. Effects of photodynamic therapy on tumor stroma. *Ultrastruct. Pathol.* **2004**, 28, 333 - 340.

82. Brooke, R. C.; et al. Histamine is released following aminolevulinic acid photodynamic therapy of human skin and mediates an aminolevulinic acid dose related immediate inflammatory response. *J. Invest. Dermatol.* **2006**, *126*, 2296 - 2301.
83. Ormrod, D.; Jarvis, B. Topical aminolevulinic acid HCl photodynamic therapy. *Am. J. Clin. Dermatol.* **2000**, *1*, 133 - 139.
84. Lober, B. A.; Fenske, N. A. Optimum treatment strategies for actinic keratosis (intraepidermal squamous cell carcinoma). *Am. J. Clin. Dermatol.* **2004**, *5*, 395 - 401.
85. Alexiades-Amenakas, M. Laser-mediated photodynamic therapy. *Clin. Dermatol.* **2006**, *24*, 16 - 25.
86. Pålsson, S.; Gustafsson, L.; Bendsoe, N.; Soto Thompson, M.; Andersson-Engels, S.; Svanberg, K. Kinetics of the superficial perfusion and temperature in connection with photodynamic therapy of basal cell carcinomas using esterified and non-esterified 5-aminolaevulinic acid. *Br. J. Dermatol.* **2003**, *148*, 1179 - 1188.
87. Pogue, B. W.; O'Hara, J. A.; Goodwin, I. A.; Wilmot, C. J.; Fournier, G. P.; Akay, A. R.; Swartz, H. Tumor Po<sub>2</sub> changes during photodynamic therapy depend upon photosensitizer type and time after injection. *Comparative Biochemistry and Physiology Part A: Molecular & Integrative Physiology* **2002**, *132*, 177 - 184.
88. Mattiello, J.; Hetzel, F.; Vandenheede, L. Intratumor temperature measurements during photodynamic therapy. *Photochem. Photobiol.* **1987**, *46*, 873 - 879.
89. Orenstein, A.; Kostenich, G.; Tsur, H.; Kogan, L.; Malik, Z. Temperature monitoring during photodynamic therapy of skin tumors with topical 5-aminolevulinic acid application. *Cancer Lett.* **1995**, *93*, 227 - 232.
90. Tsutsui, H.; MacRobert, A.; Curnow, A.; Rogowska, A.; Buonaccorsi, G.; Kato, H.; Bown, S. Optimisation of illumination for photodynamic therapy with mTHPC on normal colon and a transplantable tumour in rats. *Lasers in medical science* **2002**, *17*, 101 - 109.
91. Xu, T.; Li, Y.; Wu, X. Application of lower fluence rate for less microvasculature damage and greater cell-killing during photodynamic therapy. *Lasers in medical science* **2005**, *19*, 257 - 262.



92. Coutier, S.; Bezdetnaya, L. N.; Foster, T. H.; Parache, R.; Guillemin, F. Effect of Irradiation Fluence Rate on the Efficacy of Photodynamic Therapy and Tumor Oxygenation in Meta-Tetra (Hydroxyphenyl) Chlorin (m THPC)-Sensitized HT29 Xenografts in Nude Mice 1. *Radiat. Res.* **2002**, *158*, 339 - 345.
93. Ericson, M. B.; Sandberg, C.; Stenquist, B.; Gudmundson, F.; Karlsson, M.; Ros, A.; Rosén, A.; Larkö, O.; Wennberg, A.; Rosdahl, I. Photodynamic therapy of actinic keratosis at varying fluence rates: assessment of photobleaching, pain and primary clinical outcome. *Br. J. Dermatol.* **2004**, *151*, 1204 - 1212.
94. Sitnik, T.; Hampton, J.; Henderson, B. Reduction of tumour oxygenation during and after photodynamic therapy in vivo: effects of fluence rate. *Br. J. Cancer* **1998**, *77*, 1386 - 1394.
95. Wilson, B.; Patterson, M.; Lilge, L. Implicit and explicit dosimetry in photodynamic therapy: a new paradigm. *Lasers in medical science* **1997**, *12*, 182 - 199.
96. Juzeniene, A.; Juzenas, P.; Ma, L.; Iani, V.; Moan, J. Effectiveness of different light sources for 5-aminolevulinic acid photodynamic therapy. *Lasers in medical science* **2004**, *19*, 139 - 149.
97. Szeimies, R.; Morton, C. A.; Sidoroff, A.; Braathen, L. R. Photodynamic therapy for non-melanoma skin cancer. *Acta Dermatovenereologica-Stockholm* **2005**, *85*, 483.
98. Beyer, W. Systems for light application and dosimetry in photodynamic therapy. *Journal of Photochemistry and Photobiology B: Biology* **1996**, *36*, 153 - 156.
99. Pandey, R. K.; Zheng, G. In Kadish, K. M., Smith, K. M. and Guillard, R., Eds.; *The Porphyrin Handbook*; Academic Press: Boston, 2000; Vol. 6, pp 157 - 230.
100. Bonnett, R. *Chemical Aspects of Photodynamic Therapy*; Gordon and Breach Science Publishers: Canada, 2000; Vol. 1., pp. 3-4, 6-11, 129-130, 237-238.
101. Finsen, N.R.; *Phototherapy*; Arnold Publishing: London, 1901.

102. Parrish, J.A.; Fitzpatrick, T. B.; Tanenbaum, L.; Pathak, M.A. Photochemotherapy of psoriasis with oral methoxsalen and longwave ultraviolet light. *N. Engl. J. Med.* **1974**, *291*, 1207 - 1222.
103. Cremer, R.J.; Perryman, P.W.; Richards, D. H. Influence of light on the hyperbilirubinemia of infants. *Lancet* **1958**, (*i*), 1094 - 1097.
104. Auler, H.; Banzer, G. Untersuchungen über die Rolle der Porphyrine bei geschwulstkranken Menschen und Tieren. *Journal of Cancer Research and Clinical Oncology* **1942**, *53*, 65 - 68.
105. Kelly, J. F.; Snell, M. E. Hematoporphyrin derivative: a possible aid in the diagnosis and therapy of carcinoma of the bladder. *The Journal of Urology* **1976**, *115*, 150 - 151.
106. Houle, J.; Strong, A. Clinical pharmacokinetics of verteporfin. *The Journal of Clinical Pharmacology* **2002**, *42*, 547 - 557.
107. Houle, J.; Strong, H. A. Duration of skin photosensitivity and incidence of photosensitivity reactions after administration of verteporfin. *Retina* **2002**, *22*, 691 - 697.
108. Levy, J. G. Photosensitizers in photodynamic therapy. *Semin. Oncol.* **1994**, *21*, 4 - 10.
109. Richter, A. M.; Kelly, B.; Chow, J.; Liu, D. J.; Towers, G. N.; Dolphin, D.; Levy, J. G. Preliminary studies on a more effective phototoxic agent than hematoporphyrin, 2. *J. Natl. Cancer Inst.* **1987**, *79*, 1327 - 1332.
110. Gragoudas, E.; Schmidt-Erfurth, U.; Sickenkey, M. Results and preliminary dosimetry of photodynamic therapy for choroidal neovascularization in age-related macular degeneration in a phase I/II study. *Assoc Res Vision Ophthalmol* **1997**, *38*, 73.
111. Young, L.; Howard, M. A.; Hu, L. K.; Kim, R. Y.; Gragoudas, E. S. Photodynamic therapy of pigmented choroidal melanomas using a liposomal preparation of benzoporphyrin derivative. *Arch. Ophthalmol.* **1996**, *114*, 186.
112. Barbazetto, I. A.; Lee, T. C.; Rollins, I. S.; Chang, S.; Abramson, D. H. Treatment of choroidal melanoma using photodynamic therapy. *Am. J. Ophthalmol.* **2003**, *135*, 898 - 899.

113. Sessler, J. L.; Miller, R. A. Texaphyrins: new drugs with diverse clinical applications in radiation and photodynamic therapy. *Biochem. Pharmacol.* **2000**, *59*, 733 - 739.
114. Young, S. W.; Woodburn, K. W.; Wright, M.; Mody, T. D.; Fan, Q.; Sessler, J. L.; Dow, W. C.; Miller, R. A. Lutetium texaphyrin (PCI-0123): a near-infrared, water-soluble photosensitizer. *Photochem. Photobiol.* **1996**, *63*, 892 - 897.
115. Sessler, J. L.; Hemmi, G.; Mody, T. D.; Murai, T.; Burrell, A.; Young, S. W. Texaphyrins: synthesis and applications. *Acc. Chem. Res.* **1994**, *27*, 43 - 50.
116. Renschler, M. F.; Yuen, A.; Panella, T. J.; et al. Photodynamic therapy trials with lutetium texaphyrin PCI-0123 (Lu-Tex); In *25th Annual Meeting for Photobiology*; St. Louis, MO: The American Society for Photobiology, 1997.
117. Renschler, M.; Yuen, A.; Panella, T.; Wieman, T.; Julius, C.; Panjehpour, M.; Taber, S.; Fingar, V.; Horning, S.; Miller, R. Photodynamic therapy trials with lutetium texaphyrin. *Photochem. Photobiol.* **1997**, *65*, 47S.
118. Kübler, A. C.; Haase, T.; Staff, C.; Kahle, B.; Rheinwald, M.; Mühlhng, J. Photodynamic therapy of primary nonmelanomatous skin tumours of the head and neck. *Lasers Surg. Med.* **1999**, *25*, 60 - 68.
119. Baas, P.; Saarnak, A.; Oppelaar, H.; Neering, H.; Stewart, F. Photodynamic therapy with meta-tetrahydroxyphenylchlorin for basal cell carcinoma: a phase I/II study. *Br. J. Dermatol.* **2001**, *145*, 75 - 78.
120. Kubler, A.; De Carpentier, J.; Hopper, C.; Leonard, A.; Putnam, G. Treatment of squamous cell carcinoma of the lip using Foscan-mediated photodynamic therapy. *Int. J. Oral Maxillofac. Surg.* **2001**, *30*, 504 - 509.
121. Grosjean, P.; Wagnieres, G.; Fontolliet, C.; Van Den Bergh, H.; Monnier, P. Clinical photodynamic therapy for superficial cancer in the oesophagus and the bronchi: 514 nm compared with 630 nm light irradiation after sensitization with Photofrin II. *Br. J. Cancer* **1998**, *77*, 1989 - 1995.
122. Grosjean, P.; Savary, J.; Mizeret, J.; Wagnieres, G.; Woodtli, A.; Theumann, J.; Fontolliet, C.; Vandenberg, H.; Monnier, P. Photodynamic therapy for cancer of the upper aerodigestive tract using tetra (m-hydroxyphenyl) chlorin. *J. Clin. Laser Med. Surg.* **1996**, *14*, 281 - 287.

123. Friedberg, J. S.; Mick, R.; Stevenson, J.; Metz, J.; Zhu, T.; Buyske, J.; Sterman, D. H.; Pass, H. I.; Glatstein, E.; Hahn, S. M. A phase I study of Foscan-mediated photodynamic therapy and surgery in patients with mesothelioma. *Ann. Thorac. Surg.* **2003**, *75*, 952 - 959.
124. Schouwink, H.; Rutgers, E. T.; van der Sijp, J.; Oppelaar, H.; van Zandwijk, N.; van Veen, R.; Burgers, S.; Stewart, F. A.; Zoetmulder, F.; Baas, P. Intraoperative photodynamic therapy after pleuropneumonectomy in patients with malignant pleural mesothelioma; dose finding and toxicity results. *CHEST Journal* **2001**, *120*, 1167 - 1174.
125. Ris, H.; Altermatt, H. J.; Nachbur, B.; Stewart, C. M.; Wang, Q.; Lim, C. K.; Bonnett, R.; Althaus, U. Intraoperative photodynamic therapy with m-tetrahydroxyphenylchlorin for chest malignancies. *Lasers Surg. Med.* **1996**, *18*, 39 - 45.
126. Savary, J.; Monnier, P.; Fontolliet, C.; Mizeret, J.; Wagnieres, G.; Braichotte, D.; van den Bergh, H. Photodynamic therapy for early squamous cell carcinomas of the esophagus, bronchi, and mouth with m-tetra (hydroxyphenyl) chlorin. *Arch. Otolaryngol. Head. Neck.* **1997**, *123*, 162 - 168.
127. Savary, J.; Grosjean, P.; Monnier, P.; Fontolliet, C.; Wagnieres, G.; Braichotte, D.; Van Den Bergh, H. Photodynamic therapy of early squamous cell carcinomas of the esophagus: a review of 31 cases. *Endoscopy* **1998**, *30*, 258 - 265.
128. Etienne, J.; Dorme, N.; Bourg-Heckly, G.; Raimbert, P.; Fekete, F. Local curative treatment of superficial adenocarcinoma in Barrett's esophagus. First results of photodynamic therapy with a new photosensitizer. *Bull. Acad. Natl. Med.* **2000**, *184*, 1731 - 1744; discussion 1744 - 1747.
129. Grant, W.; MacRobert, A.; Bown, S.; Hopper, C.; Speight, P. Photodynamic therapy of oral cancer: photosensitisation with systemic aminolaevulinic acid. *The Lancet* **1993**, *342*, 147 - 148.
130. Dilkes, M.; Benjamin, E.; Ovaisi, S.; Banerjee, A. Treatment of primary mucosal head and neck squamous cell carcinoma using photodynamic therapy: results after 25 treated cases. *The Journal of Laryngology & Otology* **2003**, *117*, 713 - 717.

131. Fan, K. F.; Hopper, C.; Speight, P. M.; Buonaccorsi, G. A.; Bown, S. G. Photodynamic therapy using mTHPC for malignant disease in the oral cavity. *International Journal of Cancer* **1997**, *73*, 25 - 32.
132. Wenig, B.; D'Cruz, A.; Iqbal, A.; Bryce, R. P. Foscan-mediated photodynamic therapy in the palliative treatment of advanced head and neck cancer; In *Proceedings of the 39th American Society of Clinical Oncology*; 2000.
133. Hornung, R.; Fehr, M. K.; Tromberg, B. J.; Krasieva, T. B.; Berns, M. W.; Tadir, Y. Uptake of the photosensitizer benzoporphyrin derivative in human endometrium after topical application in vivo. *J. Am. Assoc. Gynecol. Laparosc.* **1998**, *5*, 367 - 374.
134. Suhr, M. A.; Hopper, C.; MacRobert, A. J.; Speight, P. M.; Kubler, A. C.; Kunz, L. Clinical pilot study of interstitial photodynamic therapy for treatment of advanced head and neck tumors. *Mund Kiefer Gesichtschir.* **2001**, *5*, 277 - 282.
135. Copper, M. P.; Tan, I. B.; Oppelaar, H.; Ruevekamp, M. C.; Stewart, F. A. Meta-tetra (hydroxyphenyl) chlorin photodynamic therapy in early-stage squamous cell carcinoma of the head and neck. *Archives of Otolaryngology—Head & Neck Surgery* **2003**, *129*, 709 - 711.
136. Allison, R. R.; Downie, G. H.; Cuenca, R.; Hu, X.; Childs, C. J.; Sibata, C. H. Photosensitizers in clinical PDT. *Photodiagnosis and photodynamic therapy* **2004**, *1*, 27 - 42.
137. Patterson, M.; Wilson, B. Photodynamic therapy; Dyh, J. V., Ed.; In *The modern technology of radiation oncology*; Medical Physics Publishing; **1999**; pp. 941 - 980.
138. Grekin, R.; Razun, N.; Trommer, R.; et al. Tin ethyl etiopurpurin (SnET2) photodynamic therapy (PDT): results of a phase I / II clinical study conducted at UCSF for the treatment of AIDS-associated cutaneous Kaposi's sarcomas. In *International Conference on AIDS*, 1996.
139. Mang, T. S.; Allison, R.; Hewson, G.; Snider, W.; Moskowitz, R. A phase II/III clinical study of tin ethyl etiopurpurin (Purlytin)-induced photodynamic therapy for the treatment of recurrent cutaneous metastatic breast cancer. *Cancer J. Sci. Am.* **1998**, *4*, 378 - 384.

140. Kaplan, M. J.; Somers, R. G.; Greenberg, R. H.; Ackler, J. Photodynamic therapy in the management of metastatic cutaneous adenocarcinomas: case reports from phase 1/2 studies using tin ethyl etiopurpurin (SnET2). *J. Surg. Oncol.* **1998**, *67*, 121 - 125.
141. Razum, N.; Snyder, A.; Doiron, D. SnET2: clinical update. *Proc. Soc. Photo-Opt. Instrum. Eng.* **1996**, *2675*, 43 - 46.
142. Spikes, J. D. New trends in photobiology: chlorins as photosensitizers in biology and medicine. *Journal of Photochemistry and Photobiology B: Biology* **1990**, *6*, 259 - 274.
143. Kreimer-Birnbaum, M. Modified porphyrins, chlorins, phthalocyanines, and purpurins: second-generation photosensitizers for photodynamic therapy. *Semin. Hematol.* **1989**, *26*, 157 - 173.
144. Taber, S. W.; Fingar, V. H.; Coots, C. T.; Wieman, T. J. Photodynamic therapy using mono-L-aspartyl chlorin e6 (Npe6) for the treatment of cutaneous disease: a Phase I clinical study. *Clinical cancer research* **1998**, *4*, 2741 - 2746.
145. Lim, J. I. Photodynamic therapy for choroidal neovascular disease: photosensitizers and clinical trials. *Ophthalmol. Clin. North Am.* **2002**, *15*, 473.
146. Pandey, R. K.; Bellnier, D. A.; Smith, K. M.; Dougherty, T. J. Chlorin and porphyrin derivatives as potential photosensitizers in photodynamic therapy. *Photochem. Photobiol.* **1991**, *53*, 65 - 72.
147. Magne, M. L.; Rodriguez, C. O.; Autry, S. A.; Edwards, B. F.; Theon, A. P.; Madewell, B. R. Photodynamic therapy of facial squamous cell carcinoma in cats using a new photosensitizer. *Lasers Surg. Med.* **1998**, *20*, 202 - 209.
148. McCaw, D.; Pope, E.; Payne, J.; West, M.; Tompson, R.; Tate, D. Treatment of canine oral squamous cell carcinomas with photodynamic therapy. *Br. J. Cancer* **2000**, *82*, 1297.
149. Bellnier, D. A.; Greco, W. R.; Loewen, G. M.; Nava, H.; Oseroff, A. R.; Pandey, R. K.; Tsuchida, T.; Dougherty, T. J. Population pharmacokinetics of the photodynamic therapy agent 2-[1-hexyloxyethyl]-2-devinyl pyropheophorbide-a in cancer patients. *Cancer Res.* **2003**, *63*, 1806 - 1813.

150. Ben-Hur, E.; Rosenthal, I. The phthalocyanines: a new class of mammalian cells photosensitizers with a potential for cancer phototherapy. *Int. J. Radiat. Biol.* **1985**, *47*, 145 - 147.
151. Allen, C. M.; Sharman, W. M.; Van Lier, J. E. Current status of phthalocyanines in the photodynamic therapy of cancer. *Journal of Porphyrins and Phthalocyanines* **2001**, *5*, 161 - 169.
152. Peaston, A.; Leach, M.; Higgins, R. Photodynamic therapy for nasal and aural squamous cell carcinoma in cats. *J. Am. Vet. Med. Assoc.* **1993**, *202*, 1261.
153. Van Leengoed, H.; Van Der Veen, N.; Versteeg, A.; Van Der Berg-Blok, A.; Marijnissen, J.; Star, W. Tumour tissue imaging using the localizing properties and fluorescence of some phthalocyanines. *Int. J. Radiat. Biol.* **1991**, *60*, 121 - 124.
154. Uspenskii, L. V.; Chistov, L. V.; Kogan, E. A.; Loshchenov, V. B.; Ablitsov, I.; Rybin, V. K.; Zavodnov, V. I.; Shiktorov, D. I.; Serbinenko, N. F.; Semenova, I. G. Endobronchial laser therapy in complex preoperative preparation of patients with lung diseases. *Khirurgiia (Mosk)* **2000**, (2), 38 - 40.
155. Sokolov, V. V.; Stranadko, E. F.; Zharkova, N. N.; Iakubovskaia, R. I.; Filonenko, E. V.; Astrakhankina, T. A. The photodynamic therapy of malignant tumors in basic sites with the preparations photohem and photosens (the results of 3 years of observations). *Vopr. Onkol.* **1995**, *41*, 134 - 138.
156. Stranadko, E. F.; Garbuzov, M. I.; Zenger, V. G.; Nasedkin, A. N.; Markichev, N. A.; Riabov, M. V.; Leskov, I. V. Photodynamic therapy of recurrent and residual oropharyngeal and laryngeal tumors. *Vestn. Otorinolaringol.* **2001**, (3), 36 - 39.
157. Ben-Hur, E.; Kol, R.; Marko, R.; Riklis, E.; Rosenthal, I. Combined action of phthalocyanine photosensitization and gamma-radiation on mammalian cells. *Int. J. Radiat. Biol.* **1988**, *54*, 21 - 30.
158. Sharman, W. M.; van Lier, J. E.; Allen, C. M. Targeted photodynamic therapy via receptor mediated delivery systems. *Adv. Drug Deliv. Rev.* **2004**, *56*, 53 - 76.

159. Foley, M. S. C.; Beeby, A.; Parker, A. W.; Bishop, S. M.; Phillips, D. Excited triplet state photophysics of the sulfonated aluminum phthalocyanine bound to human serum albumin. *Photochem. Photobiol. B.* **1997**, *38*, 10 - 17.
160. Gantchev, T. G.; Ouellet, R.; van Lier, J. E. Binding interactions and conformational changes induced by sulfonated aluminum phthalocyanines in human serum albumin. *Arch. Biochem. Biophys.* **1999**, *366*, 21 - 30.
161. Larroque, C.; Pelegrin, A.; Van Lier, J. Serum albumin as a vehicle for zinc phthalocyanine: photodynamic activities in solid tumour models. *Br. J. Cancer* **1996**, *74*, 1886.
162. Reddi, E.; Zhou, C.; Biolo, R.; Menegaldo, E.; Jori, G. Liposome-or LDL-administered Zn (II)-phthalocyanine as a photodynamic agent for tumours. I. Pharmacokinetic properties and phototherapeutic efficiency. *Br. J. Cancer* **1990**, *61*, 407.
163. Krieger, M.; Acton, S.; Ashkenas, J.; Pearson, A.; Penman, M.; Resnick, D. Molecular flypaper, host defense, and atherosclerosis. Structure, binding properties, and functions of macrophage scavenger receptors. *J. Biol. Chem.* **1993**, *268*, 4569 - 4569.
164. Allen, C. M.; Sharman, W. M.; van Lier, J. E. Photodynamic therapy: targeting cancer cells with photosensitizer-bioconjugates; In *Tumor Targeting in Cancer Therapy*; Springer: 2002; pp 329 - 361.
165. Hamblin, M. R.; Newman, E. L. Photosensitizer targeting in photodynamic therapy I. Conjugates of haematoporphyrin with albumin and transferrin. *Journal of Photochemistry and Photobiology B: Biology* **1994**, *26*, 45 - 56.
166. Brasseur, N.; Langlois, R.; Madeleine, C. L.; Ouellet, R.; Lier, J. E. Receptor-Mediated Targeting of Phthalocyanines to Macrophages Via Covalent Coupling to Native or Maleylated Bovine Serum Albumin. *Photochem. Photobiol.* **1999**, *69*, 345 - 352.
167. Hamblin, M. R.; Miller, J. L.; Ortel, B. Scavenger-receptor targeted photodynamic therapy. *Photochem. Photobiol.* **2000**, *72*, 533 - 540.
168. Hamblin, M. R.; Huzaira, M.; O'Donnell, D. A. Scavenger receptor-targeted photodynamic therapy of murine tumors in vivo; In *13th International Congress on Photobiology*; 2000.



169. Stryer, L. *Biochemistry*; W. H. Freeman and Company: New York, 1988.
170. Gueddari, N.; Favre, G.; Hachem, H.; Marek, E.; Le Gaillard, F.; Soula, G. Evidence for up-regulated low density lipoprotein receptor in human lung adenocarcinoma cell line A549. *Biochimie* **1993**, *75*, 811 - 819.
171. Maziere, J.; Morliere, P.; Santus, R. New trends in photobiology: The role of the low density lipoprotein receptor pathway in the delivery of lipophilic photosensitizers in the photodynamic therapy of tumours. *Journal of Photochemistry and Photobiology B: Biology* **1991**, *8*, 351 - 360.
172. Polo, L.; Valduga, G.; Jori, G.; Reddi, E. Low-density lipoprotein receptors in the uptake of tumour photosensitizers by human and rat transformed fibroblasts. *Int. J. Biochem. Cell Biol.* **2002**, *34*, 10 - 23.
173. De Smidt, P. C.; Versluis, A. J.; Van Berkel, T. J. Properties of incorporation, redistribution, and integrity of porphyrin-low-density lipoprotein complexes. *Biochemistry (N. Y.)* **1993**, *32*, 2916 - 2922.
174. Zhou, C.; Milanese, C.; Jori, G. An ultrastructural comparative evaluation of tumors photosensitized by porphyrins administered in aqueous solution, bound to liposomes or to lipoproteins. *Photochem. Photobiol.* **1988**, *48*, 487 - 492.
175. Hamblin, M. R.; Newman, E. L. Photosensitizer targeting in photodynamic therapy II. Conjugates of haematoporphyrin with serum lipoproteins. *Journal of Photochemistry and Photobiology B: Biology* **1994**, *26*, 147 - 157.
176. Schmidt-Erfurth, U.; Diddens, H.; Birngruber, R.; Hasan, T. Photodynamic targeting of human retinoblastoma cells using covalent low-density lipoprotein conjugates. *Br. J. Cancer* **1997**, *75*, 54.
177. Conrad, M. E.; Umbreit, J. N. Iron absorption and transport—an update. *Am. J. Hematol.* **2000**, *64*, 287 - 298.
178. Ponka, P.; Beaumont, C.; Richardson, D. R. Function and regulation of transferrin and ferritin. In *Seminars in hematology*; 1998; Vol. 35, pp 35.
179. Testa, U.; Pelosi, E.; Peschle, C. The transferrin receptor. *Crit. Rev. Oncog.* **1993**, *4*, 241.

180. Singh, M. Targeting with transferrin; Page, M., Ed.; In *Tumor Targeting in Cancer Therapy*; Humana Press: New Jersey, 2002; pp 151 - 164.
181. Cavanaugh, P. G. Synthesis, and photodynamic therapy-mediated anti-cancer, and other uses of chlorin e6-transferrin; US Patent application Publication Number US 2002 / 0137901 A1; Sept. 26, 2002.
182. Cavanaugh, P. G. Synthesis of chlorin e6-transferrin and demonstration of its light-dependent in vitro breast cancer cell killing ability. *Breast Cancer Res. Treat.* **2002**, 72, 117 - 130.
183. Whitfield, J. F.; Morley, P.; Willick, G. E. *The Parathyroid Hormone: An Unexpected Bone Builder for Treating Osteoporosis*; R. G. Landes Company: Georgetown, TX, 1998.
184. Ducy, P.; Schinke, T.; Karsenty, G. The osteoblast: a sophisticated fibroblast under central surveillance. *Science* **2000**, 289, 1501 - 1504.
185. Teitelbaum, S. L. Bone resorption by osteoclasts. *Science* **2000**, 289, 1504 - 1508.
186. Rodan, G. A.; Martin, T. J. Therapeutic approaches to bone diseases. *Science* **2000**, 289, 1508 - 1514.
187. Chen, J. Compositions and methods for the treatment of metabolic bone disorders and bone metastases; WO Patent application Publication Number WO 00 / 41725; July 20, 2000.
188. Fleisch, H. Bisphosphonates: mechanism of action and clinical use; Bilezikian, J. P., Raisz, L. G. and Rodan, G. A., Eds.; In *Principles of Bone Biology*; Academic Press: San Diego, 1996; pp 1037 - 1052.
189. Ali, H.; van Lier, J. E. Metal complexes as photo- and radiosensitizers. *Chem. Rev.* **1999**, 99, 2379 - 2450.
190. Decréau, R.; Chanon, M.; Julliard, M. Synthesis of silicon phthalocyanines bearing two cholesterol moieties. *Synlett* **1998**, 375 - 376.
191. Ğb, J. G.; Nowis, D.; Skrzycki, M.; Czczot, H.; Barańczyk-Kuźma, A.; Wilczyński, G. M.; Makowski, M.; Mróz, P.; Kozar, K.; Kamiński, R. Antitumor effects of photodynamic therapy are potentiated by 2-methoxyestradiol. *J. Biol. Chem.* **2003**, 278, 407 - 414.

192. Cowled, P.; Mackenzie, L.; Forbes, I. Potentiation of photodynamic therapy with haematoporphyrin derivatives by glucocorticoids. *Cancer Lett.* **1985**, *29*, 107 - 114.
193. Aranda, A.; Pascual, A. Nuclear hormone receptors and gene expression. *Physiol. Rev.* **2001**, *81*, 1269 - 1304.
194. Kumar, R.; Thompson, E. B. The structure of the nuclear hormone receptors. *Steroids* **1999**, *64*, 310 - 319.
195. Whitfield, G. K.; Jurutka, P. W.; Haussler, C. A.; Haussler, M. R. Steroid hormone receptors, evolution, ligands and molecular basis of biological function. *J. Cell. Biochem.* **1999**, *S32 - 33*, 110 - 122.
196. Hager, G. L.; Lim, C. S.; Elbi, C.; Baumann, C. T. Trafficking of nuclear receptors in living cells. *J. Steroid Biochem. Mol. Biol.* **2000**, *74*, 249 - 254.
197. Ferguson, A. T.; Lapidus, R. G.; Davidson, N. E. The regulation of estrogen receptor expression and function in human breast cancer. *Cancer Treat. Res.* **1998**, *94*, 255 - 278.
198. Murphy, L.; Hilsenbeck, S.; Dotzlaw, H.; Fuqua, S. Relationship of clone 4 estrogen receptor variant messenger RNA expression to some known prognostic variables in human breast cancer. *Clinical cancer research* **1995**, *1*, 155 - 159.
199. Gotteland, M.; May, E.; May-Levin, F.; Contesso, G.; Delarue, J. C.; Mouriessse, H. Estrogen receptors (ER) in human breast cancer. The significance of a new prognostic factor based on both ER protein and ER mRNA contents. *Cancer* **1994**, *74*, 864 - 871.
200. Boyle, R. W.; Dolphin, D.; Johnson, C. K. US Patent 5,703,230.
201. Khan, E. H.; Ali, H.; Shafiullah; van Lier, J. E. Unpublished results.
202. Katzenellenbogen, J. A.; O'Malley, B. W.; Katzenellenbogen, B. S. Tripartite steroid hormone receptor pharmacology: interaction with multiple effector sites as a basis for the cell-and promoter-specific action of these hormones. *Molecular Endocrinology* **1996**, *10*, 119 - 131.

203. Anstead, G. M.; Carlson, K. E.; Katzenellenbogen, J. A. The estradiol pharmacophore: ligand structure-estrogen receptor binding affinity relationships and a model for the receptor binding site. *Steroids* **1997**, *62*, 268 - 303.
204. Brzozowski, A. M.; Pike, A. C.; Dauter, Z.; Hubbard, R. E.; Bonn, T.; Engstrom, O.; Ohman, L.; Greene, G. L.; Gustafsson, J.; Carlquist, M. Molecular basis of agonism and antagonism in the oestrogen receptor. *Nature* **1997**, *389*, 753 - 758.
205. Tanenbaum, D. M.; Wang, Y.; Williams, S. P.; Sigler, P. B. Crystallographic comparison of the estrogen and progesterone receptor's ligand binding domains. *Proceedings of the National Academy of Sciences* **1998**, *95*, 5998 - 6003.
206. Ray, R.; Mohr, S. C.; Swamy, N. Selective nuclear receptor-targeted systems for delivery of cytotoxins to cancer cells for targeted photodynamic therapy; WO Patent application Publication Number WO 01 / 78606; Oct. 25, 2001.
207. Mohr, S. C.; Ray, R. Photodynamic therapy using nuclear hormone receptors to target photosensitizers; WO Patent application Publication Number WO97 / 34637; Sept. 25, 1997.
208. Xia, W.; Low, P. S. Folate-targeted therapies for cancer. *J. Med. Chem.* **2010**, *53*, 6811.
209. Low, P. S.; Kularatne, S. A. Folate-targeted therapeutic and imaging agents for cancer. *Curr. Opin. Chem. Biol.* **2009**, *13*, 256 - 262.
210. Leamon, C. P.; Parker, M. A.; Vlahov, I. R.; Xu, L.; Reddy, J. A.; Vetzal, M.; Douglas, N. Synthesis and biological evaluation of EC20: a new folate-derived, <sup>99m</sup>Tc-based radiopharmaceutical. *Bioconjug. Chem.* **2002**, *13*, 1200 - 1210.
211. Thomas, M.; Kularatne, S. A.; Qi, L.; Kleindl, P.; Leamon, C. P.; Hansen, M. J.; Low, P. S. Ligand-Targeted Delivery of Small Interfering RNAs to Malignant Cells and Tissues. *Ann. N. Y. Acad. Sci.* **2009**, *1175*, 32 - 39.
212. Low, P. S.; Henne, W. A.; Doorneweerd, D. D. Discovery and development of folic-acid-based receptor targeting for imaging and therapy of cancer and inflammatory diseases. *Acc. Chem. Res.* **2008**, *41*, 120 - 129.

213. Tranoy-Opalinski, I.; Fernandes, A.; Thomas, M.; Gesson, J.; Papot, S. Design of self-immolative linkers for tumour-activated prodrug therapy. *Anti-Cancer Agents in Medicinal Chemistry* **2008**, *8*, 618 - 637.
214. Ojima, I. Guided molecular missiles for tumor-targeting chemotherapy—case studies using the second-generation taxoids as warheads. *Acc. Chem. Res.* **2007**, *41*, 108 - 119.
215. Matherly, L. H.; Hou, Z.; Deng, Y. Human reduced folate carrier: translation of basic biology to cancer etiology and therapy. *Cancer Metastasis Rev.* **2007**, *26*, 111 - 128.
216. Zhao, R.; Min, S. H.; Wang, Y.; Campanella, E.; Low, P. S.; Goldman, I. D. A role for the proton-coupled folate transporter (PCFT-SLC46A1) in folate receptor-mediated endocytosis. *J. Biol. Chem.* **2009**, *284*, 4267 - 4274.
217. Parker, N.; Turk, M. J.; Westrick, E.; Lewis, J. D.; Low, P. S.; Leamon, C. P. Folate receptor expression in carcinomas and normal tissues determined by a quantitative radioligand binding assay. *Anal. Biochem.* **2005**, *338*, 284 - 293.
218. Ross, J. F.; Chaudhuri, P. K.; Ratnam, M. Differential regulation of folate receptor isoforms in normal and malignant tissues in vivo and in established cell lines. Physiologic and clinical implications. *Cancer* **1994**, *73*, 2432 - 2443.
219. Kalli, K. R.; Oberg, A. L.; Keeney, G. L.; Christianson, T. J.; Low, P. S.; Knutson, K. L.; Hartmann, L. C. Folate receptor alpha as a tumor target in epithelial ovarian cancer. *Gynecol. Oncol.* **2008**, *108*, 619 - 626.
220. Nakashima-Matsushita, N.; Homma, T.; Yu, S.; Matsuda, T.; Sunahara, N.; Nakamura, T.; Tsukano, M.; Ratnam, M.; Matsuyama, T. Selective expression of folate receptor  $\beta$  and its possible role in methotrexate transport in synovial macrophages from patients with rheumatoid arthritis. *Arthritis & Rheumatism* **1999**, *42*, 1609 - 1616.
221. Van Der Heijden, Joost W; Oerlemans, R.; Dijkmans, B. A.; Qi, H.; Vander Laken, C. J.; Lems, W. F.; Jackman, A. L.; Kraan, M. C.; Tak, P. P.; Ratnam, M. Folate receptor  $\beta$  as a potential delivery route for novel folate antagonists to macrophages in the synovial tissue of rheumatoid arthritis patients. *Arthritis & Rheumatism* **2008**, *60*, 12 - 21.

222. Xia, W.; Hilgenbrink, A. R.; Matteson, E. L.; Lockwood, M. B.; Cheng, J.; Low, P. S. A functional folate receptor is induced during macrophage activation and can be used to target drugs to activated macrophages. *Blood* **2009**, *113*, 438 - 446.
223. Turk, M. J.; Breur, G. J.; Widmer, W. R.; Paulos, C. M.; Xu, L.; Grote, L. A.; Low, P. S. Folate-targeted imaging of activated macrophages in rats with adjuvant-induced arthritis. *Arthritis & Rheumatism* **2002**, *46*, 1947 - 1955.
224. Elnakat, H.; Ratnam, M. Distribution, functionality and gene regulation of folate receptor isoforms: implications in targeted therapy. *Adv. Drug Deliv. Rev.* **2004**, *56*, 1067 - 1084.
225. Kamen, B. A.; Smith, A. K. A review of folate receptor alpha cycling and 5-methyltetrahydrofolate accumulation with an emphasis on cell models in vitro. *Adv. Drug Deliv. Rev.* **2004**, *56*, 1085 - 1097.
226. Yang, J.; Chen, H.; Vlahov, I. R.; Cheng, J.; Low, P. S. Evaluation of disulfide reduction during receptor-mediated endocytosis by using FRET imaging. *Proceedings of the National Academy of Sciences* **2006**, *103*, 13872 - 13877.
227. Cookson, B. D. The emergence of mupirocin resistance: a challenge to infection control and antibiotic prescribing practice. *J. Antimicrob. Chemother.* **1998**, *41*, 11 - 18.
228. Pfeltz, R. F.; Singh, V. K.; Schmidt, J. L.; Batten, M. A.; Baranyk, C. S.; Nadakavukaren, M. J.; Jayaswal, R. K.; Wilkinson, B. J. Characterization of passage-selected vancomycin-resistant *Staphylococcus aureus* strains of diverse parental backgrounds. *Antimicrob. Agents Chemother.* **2000**, *44*, 294 - 303.
229. Kömerik, N.; Wilson, M.; Poole, S. The Effect of Photodynamic Action on Two Virulence Factors of Gram-negative Bacteria. *Photochem. Photobiol.* **2000**, *72*, 676 - 680.
230. Brown, S. B. Clinical studies using antimicrobial PDT; In *Proceedings of the 11th Congress of the International Photodynamic Association*; Shanghai, China; Mar. 28-31, 2007; p 51.

231. Akilov, O. E.; Kosaka, S.; O'Riordan, K.; Hasan, T. Photodynamic therapy for cutaneous leishmaniasis: the effectiveness of topical phenothiaziniums in parasite eradication and Th1 immune response stimulation. *Photochem.Photobiol.Sci.* **2007**, *6*, 1067 - 1075.
232. Demidova, T.; Hamblin, M. Macrophage-targeted photodynamic therapy. *Int. J. Immunopathol. Pharmacol.* **2004**, *17*, 117.
233. van Berkel, T. J.; Out, R.; Hoekstra, M.; Kuiper, J.; Biessen, E.; van Eck, M. Scavenger receptors: friend or foe in atherosclerosis? *Curr. Opin. Lipidol.* **2005**, *16*, 525 - 535.
234. Jenkins, M.; Buonaccorsi, G.; Raphael, M.; Nyamekye, I.; McEwan, J.; Bown, S.; Bishop, C. Clinical study of adjuvant photodynamic therapy to reduce restenosis following femoral angioplasty. *Br. J. Surg.* **1999**, *86*, 1258 - 1263.
235. Rockson, S. G.; Kramer, P.; Razavi, M.; Szuba, A.; Filardo, S.; Fitzgerald, P.; Cooke, J. P.; Yousuf, S.; DeVault, A. R.; Renschler, M. F. Photoangioplasty for human peripheral atherosclerosis: results of a phase I trial of photodynamic therapy with motexafin lutetium (Antrin). *Circulation* **2000**, *102*, 2322 - 2324.
236. Kereiakes, D. J.; Szyniszewski, A. M.; Wahr, D.; Herrmann, H. C.; Simon, D. I.; Rogers, C.; Kramer, P.; Shear, W.; Yeung, A. C.; Shunk, K. A. Phase I Drug and Light Dose-Escalation Trial of Motexafin Lutetium and Far Red Light Activation (Phototherapy) in Subjects With Coronary Artery Disease Undergoing Percutaneous Coronary Intervention and Stent Deployment. *Circulation* **2003**, *108*, 1310 - 1315.
237. Saia, F.; Marzocchi, A.; Serruys, P. W. Drug-eluting stents. The third revolution in percutaneous coronary intervention. *Ital. Heart J.* **2005**, *6*, 289 - 303.
238. Kivelä, A.; Hartikainen, J. Restenosis related to percutaneous coronary intervention has been solved? *Ann. Med.* **2006**, *38*, 173 - 187.
239. Stone, G. W.; Moses, J. W.; Ellis, S. G.; Schofer, J.; Dawkins, K. D.; Morice, M.; Colombo, A.; Schampaert, E.; Grube, E.; Kirtane, A. J. Safety and efficacy of sirolimus-and paclitaxel-eluting coronary stents. *N. Engl. J. Med.* **2007**, *356*, 998 - 1008.

240. Bressler, N. M.; Bressler, S. B.; Fine, S. L. Age-related macular degeneration. *Surv. Ophthalmol.* **1988**, *32*, 375 - 413.
241. Friedman, D. S.; O'colmain, B.; Munoz, B.; Tomany, S.; McCarty, C.; De Jong, P.; Nemesure, B.; Mitchell, P.; Kempen, J. Prevalence of age-related macular degeneration in the United States. *Arch. Ophthalmol.* **2004**, *122*, 564 - 572.
242. Mitchell, P.; Smith, W.; Attebo, K.; Wang, J. J. Prevalence of age-related maculopathy in Australia. The Blue Mountains Eye Study. *Ophthalmology* **1995**, *102*, 1450 - 1460.
243. Vingerling, J. R.; Dielemans, I.; Hofman, A.; Grobbee, D. E.; Hijmering, M.; Kramer, C. F.; Jong, P. T. d. The prevalence of age-related maculopathy in the Rotterdam Study. *Ophthalmology* **1995**, *102*, 205 - 210.
244. Bressler, S.; Bressler, N.; Fine, S.; Hillis, A.; Murphy, R.; Olk, R.; Patz, A. Natural course of choroidal neovascular membranes within the foveal avascular zone in senile macular degeneration. *Am. J. Ophthalmol.* **1982**, *93*, 157 - 163.
245. Ferris III, F. L.; Fine, S. L.; Hyman, L. Age-related macular degeneration and blindness due to neovascular maculopathy. *Arch. Ophthalmol.* **1984**, *102*, 1640 - 1642.
246. Sarks, S. Ageing and degeneration in the macular region: a clinico-pathological study. *Br. J. Ophthalmol.* **1976**, *60*, 324 - 341.
247. Sarks, J.; Sarks, S.; Killingsworth, M. Evolution of geographic atrophy of the retinal pigment epithelium. *Eye* **1988**, *2*, 552 - 577.
248. Renno, R. Z.; Terada, Y.; Haddadin, M. J.; Michaud, N. A.; Gragoudas, E. S.; Miller, J. W. Selective photodynamic therapy by targeted verteporfin delivery to experimental choroidal neovascularization mediated by a homing peptide to vascular endothelial growth factor receptor-2. *Arch. Ophthalmol.* **2004**, *122*, 1002.
249. Schmidt-Erfurth, U.; Hasan, T.; Gragoudas, E.; Michaud, N.; Flotte, T. J.; Birngruber, R. Vascular targeting in photodynamic occlusion of subretinal vessels. *Ophthalmology* **1994**, *101*, 1953.
250. Pournaras, C. J. Retinal oxygen distribution. Its role in the physiopathology of vasoproliferative microangiopathies. *Retina* **1995**, *15*, 332.



251. Fingar, V. H. Vascular effects of photodynamic therapy. *J. Clin. Laser Med. Surg.* **1996**, *14*, 323 - 328.
252. Henderson, B. W.; Dougherty, T. J. How does photodynamic therapy work? *Photochem. Photobiol.* **1992**, *55*, 145 - 157.
253. Sporn, L. A.; Foster, T. H. Photofrin and light induces microtubule depolymerization in cultured human endothelial cells. *Cancer Res.* **1992**, *52*, 3443 - 3448.
254. Kalka, K.; Merk, H.; Mukhtar, H. Photodynamic therapy in dermatology. *J. Am. Acad. Dermatol.* **2000**, *42*, 389 - 413.
255. Mukhtar, H.; Agarwal, R.; Athar, M.; Lewen, R. L.; Elmets, C. A.; Bickers, D. R. Photodynamic therapy of murine skin tumors using Photofrin-II. *Photodermatol. Photoimmunol. Photomed.* **1991**, *8*, 169 - 175.
256. Kennedy, J.; Pottier, R.; Pross, D. Photodynamic therapy with endogenous protoporphyrin: IX: basic principles and present clinical experience. *Journal of Photochemistry and Photobiology B: Biology* **1990**, *6*, 143 - 148.
257. Schwartz, R. A. et al. The actinic keratosis. A perspective and update. *Dermatologic surgery: official publication for American Society for Dermatologic Surgery* **1997**, *23*, 1009.
258. Salasche, S. J. Epidemiology of actinic keratoses and squamous cell carcinoma. *J. Am. Acad. Dermatol.* **2000**, *42*, 4.
259. Chamberlain, A. J.; Kurwa, H. A. Photodynamic Therapy: Is it a Valuable Treatment Option for Actinic Keratoses? *American journal of clinical dermatology* **2003**, *4*, 149 - 155.
260. Dinehart, S. M. The treatment of actinic keratoses. *J. Am. Acad. Dermatol.* **2000**, *42*, S25 - S28.
261. Fowler Jr, J.; Zax, R. Aminolevulinic acid hydrochloride with photodynamic therapy: efficacy outcomes and recurrence 4 years after treatment. *Cutis* **2002**, *69*, 2 - 7.
262. Marcus, L. Photodynamic Therapy for Actinic Keratosis Followed by 5-Fluorouracil Reaction. *Dermatologic surgery* **2003**, *29*, 1061 - 1065.

263. Szeimies, R.; Karrer, S.; Sauerwald, A.; Landthaler, M. Photodynamic therapy with topical application of 5-aminolevulinic acid in the treatment of actinic keratoses: an initial clinical study. *Dermatology* **1996**, *192*, 246 - 251.
264. Tschen, E.; Wong, D.; Pariser, D.; Dunlap, F.; Houlihan, A.; Ferdon, M. Photodynamic therapy using aminolaevulinic acid for patients with nonhyperkeratotic actinic keratoses of the face and scalp: phase IV multicentre clinical trial with 12-month follow up. *Br. J. Dermatol.* **2006**, *155*, 1262 - 1269.
265. Hongcharu, W.; Taylor, C. R.; Chang, Y.; Aghassi, D.; Suthamjariya, K.; Anderson, R. R. Topical ALA-photodynamic therapy for the treatment of acne vulgaris. *J. Invest. Dermatol.* **2000**, *115*, 183 - 192.
266. Kennedy, J. C.; Pottier, R. H. New trends in photobiology: endogenous protoporphyrin IX, a clinically useful photosensitizer for photodynamic therapy. *Journal of Photochemistry and Photobiology B: Biology* **1992**, *14*, 275 - 292.
267. Divaris, D.; Kennedy, J.; Pottier, R. Phototoxic damage to sebaceous glands and hair follicles of mice after systemic administration of 5-aminolevulinic acid correlates with localized protoporphyrin IX fluorescence. *The American journal of pathology* **1990**, *136*, 891.
268. Goldman, M.; Boyce, S. A single-center study of aminolevulinic acid and 417 NM photodynamic therapy in the treatment of moderate to severe acne vulgaris. *Journal of drugs in dermatology: JDD* **2003**, *2*, 393.
269. Gold, M.; Bridges, T. M.; Bradshaw, V. L.; Boring, M. ALA-PDT and blue light therapy for hidradenitis suppurativa. *J. Drugs Dermatol.* **2004**, *3*, S32 - S35.
270. DeVita, E.; Taub, A. F. Photodynamic therapy for the treatment of hidradenitis suppurativa; In *Annual Meeting of the American Society of Laser Medicine and Surgery*; Grapevine, TX; April, 2007.
271. Siemann, D. W.; Chaplin, D. J.; Horsman, M. R. Vascular-targeting therapies for treatment of malignant disease. *Cancer* **2004**, *100*, 2491 - 2499.

272. Fukumura, D.; Jain, R. K. Tumor microenvironment abnormalities: causes, consequences, and strategies to normalize. *J. Cell. Biochem.* **2006**, *101*, 937 - 949.
273. Siemann, D. W.; Bibby, M. C.; Dark, G. G.; Dicker, A. P.; Eskens, F. A.; Horsman, M. R.; Marmé, D.; LoRusso, P. M. Differentiation and definition of vascular-targeted therapies. *Clinical Cancer Research* **2005**, *11*, 416 - 420.
274. Thorpe, P. E. Vascular targeting agents as cancer therapeutics. *Clinical Cancer Research* **2004**, *10*, 415 - 427.
275. Gross, S.; Gilead, A.; Scherz, A.; Neeman, M.; Salomon, Y. Monitoring photodynamic therapy of solid tumors online by BOLD-contrast MRI. *Nat. Med.* **2003**, *9*, 1327 - 1331.
276. Fingar, V. H.; Wieman, T. J.; Haydon, P. S. The effects of thrombocytopenia on vessel stasis and macromolecular leakage after photodynamic therapy using photofrin. *Photochem. Photobiol.* **1997**, *66*, 513 - 517.
277. Ben-Hur, E.; Barshtein, G.; Chen, S.; Yedgar, S. Photodynamic treatment of red blood cell concentrates for virus inactivation enhances red blood cell aggregation: protection with antioxidants. *Photochem. Photobiol.* **1997**, *66*, 509 - 512.
278. Fingar, V. H.; Wieman, T. J.; Doak, K. W. Role of thromboxane and prostacyclin release on photodynamic therapy-induced tumor destruction. *Cancer Res.* **1990**, *50*, 2599 - 2603.
279. Foster, T. H.; Primavera, M. C.; Marder, V. J.; Hilf, R.; Sporn, L. A. Photosensitized release of von Willebrand factor from cultured human endothelial cells. *Cancer Res.* **1991**, *51*, 3261 - 3266.
280. Henderson, B.; Owczarczak, B.; Sweeney, J.; Gessner, T. Effects of photodynamic treatment of platelets or endothelial cells in vitro on platelet aggregation. *Photochem. Photobiol.* **1992**, *56*, 513 - 521.
281. Dolmans, D. E.; Kadambi, A.; Hill, J. S.; Waters, C. A.; Robinson, B. C.; Walker, J. P.; Fukumura, D.; Jain, R. K. Vascular accumulation of a novel photosensitizer, MV6401, causes selective thrombosis in tumor vessels after photodynamic therapy. *Cancer Res.* **2002**, *62*, 2151 - 2156.

282. Vaupel, P.; Mayer, A. Hypoxia in cancer: significance and impact on clinical outcome. *Cancer Metastasis Rev.* **2007**, *26*, 225 - 239.
283. Fingar, V.; Wieman, T.; Doak, K. Changes in tumor interstitial pressure induced by photodynamic therapy. *Photochem. Photobiol.* **1991**, *53*, 763.
284. Leunig, M.; Goetz, A.; Gamarra, F.; Zetterer, G.; Messmer, K.; Jain, R. Photodynamic therapy-induced alterations in interstitial fluid pressure, volume and water content of an amelanotic melanoma in the hamster. *Br. J. Cancer* **1994**, *69*, 101.
285. Chen, B.; Pogue, B. W.; Hoopes, P. J.; Hasan, T. Combining vascular and cellular targeting regimens enhances the efficacy of photodynamic therapy. *Int. J. Radiat. Oncol. Biol. Phys.* **2005**, *61*, 1216.
286. Chen, B.; Roskams, T.; Witte, P. A. Antivascular Tumor Eradication by Hypericin-mediated Photodynamic Therapy. *Photochem. Photobiol.* **2002**, *76*, 509 - 513.
287. Boucher, Y.; Jain, R. K. Microvascular pressure is the principal driving force for interstitial hypertension in solid tumors: implications for vascular collapse. *Cancer Res.* **1992**, *52*, 5110 - 5114.
288. Rofstad, E. K.; Tunheim, S. H.; Mathiesen, B.; Graff, B. A.; Halsør, E. F.; Nilsen, K.; Galappathi, K. Pulmonary and lymph node metastasis is associated with primary tumor interstitial fluid pressure in human melanoma xenografts. *Cancer Res.* **2002**, *62*, 661 - 664.
289. Pinthus, J. H.; Bogaards, A.; Weersink, R.; Wilson, B. C.; Trachtenberg, J. Photodynamic therapy for urological malignancies: past to current approaches. *J. Urol.* **2006**, *175*, 1201 - 1207.
290. Birchler, M.; Viti, F.; Zardi, L.; Spiess, B.; Neri, D. Selective targeting and photocoagulation of ocular angiogenesis mediated by a phage-derived human antibody fragment. *Nat. Biotechnol.* **1999**, *17*, 984 - 988.
291. Tirand, L.; Frochot, C.; Vanderesse, R.; Thomas, N.; Trinquet, E.; Pinel, S.; Viriot, M.; Guillemin, F.; Barberi-Heyob, M. A peptide competing with VEGF165 binding on neuropilin-1 mediates targeting of a chlorin-type photosensitizer and potentiates its photodynamic activity in human endothelial cells. *Journal of controlled release: official journal of the Controlled Release Society* **2006**, *111*, 153 - 164.

292. Ichikawa, K.; Hikita, T.; Maeda, N.; Yonezawa, S.; Takeuchi, Y.; Asai, T.; Namba, Y.; Oku, N. Antiangiogenic photodynamic therapy (PDT) by using long-circulating liposomes modified with peptide specific to angiogenic vessels. *Biochimica et Biophysica Acta (BBA)-Biomembranes* **2005**, 1669, 69 - 74.
293. Reddy, G. R.; Bhojani, M. S.; McConville, P.; Moody, J.; Moffat, B. A.; Hall, D. E.; Kim, G.; Koo, Y. L.; Woolliscroft, M. J.; Sugai, J. V. Vascular targeted nanoparticles for imaging and treatment of brain tumors. *Clinical Cancer Research* **2006**, 12, 6677 - 6686.
294. Frochot, C.; Stasio, B. D.; Vanderesse, R.; Belgy, M.; Dodeller, M.; Guillemin, F.; Viriot, M.; Barberi-Heyob, M. Interest of RGD-containing linear or cyclic peptide targeted tetraphenylchlorin as novel photosensitizers for selective photodynamic activity. *Bioorg. Chem.* **2007**, 35, 205 - 220.
295. Korbelik, M.; Cecic, I. Mechanism of tumor destruction by photodynamic therapy. *Handbook of photochemistry and photobiology* **2003**, 4, 39 - 77.
296. Korbelik, M. PDT-associated host response and its role in the therapy outcome. *Lasers Surg. Med.* **2006**, 38, 500 - 508.
297. Galin, J. I.; Snyderman, R. *Inflammation: Basic Principles and Clinical Correlations*; Lippincott Williams and Wilkins: Philadelphia, PA, 1999.
298. Korbelik, M.; Merchant, S.; Stott, B.; Cecic, I.; Payne, P.; Sun, J. Acute phase response induced following tumor treatment by photodynamic therapy: relevance for the therapy outcome. *Proc. SPIE* **2006**, 6087, 0C1 - 0C7.
299. Cecic, I.; Scott, B.; Jinghai, S.; Korbelik, M. Relevance of innate immunity recognition of altered self in the induction of host response associated with photodynamic therapy. *Recent research developments in cancer* **2004**, 153 - 161.
300. Matzinger, P. The danger model: a renewed sense of self. *Science Signalling* **2002**, 296, 301.
301. Seong, S.; Matzinger, P. Hydrophobicity: an ancient damage-associated molecular pattern that initiates innate immune responses. *Nature Reviews Immunology* **2004**, 4, 469 - 478.

302. Korbelik, M. Role of Toll-like receptors in photodynamic-therapy-elicited host response. *Proc. SPIE* **2004**, 5319, 87 - 95.
303. Andrews, N. W. Membrane repair and immunological danger. *EMBO Rep.* **2005**, 6, 826 - 830.
304. Agarwal, M. L.; Larkin, H. E.; Zaidi, S.; Mukhtar, H.; Oleinick, N. L. Phospholipase activation triggers apoptosis in photosensitized mouse lymphoma cells. *Cancer Res.* **1993**, 53, 5897 - 5902.
305. Musser, D. A.; Wagner, J.; Weber, F.; Datta-Gupta, N. The binding of tumor localizing porphyrins to a fibrin matrix and their effects following photoirradiation. *Res. Commun. Chem. Pathol. Pharmacol.* **1980**, 28, 505.
306. Beg, A. A. Endogenous ligands of Toll-like receptors: implications for regulating inflammatory and immune responses. *Trends Immunol.* **2002**, 23, 509 - 512.
307. Termeer, C.; Benedix, F.; Sleeman, J.; Fieber, C.; Voith, U.; Ahrens, T.; Miyake, K.; Freudenberg, M.; Galanos, C.; Simon, J. C. Oligosaccharides of Hyaluronan activate dendritic cells via toll-like receptor 4. *J. Exp. Med.* **2002**, 195, 99 - 111.
308. Okamura, Y.; Watari, M.; Jerud, E. S.; Young, D. W.; Ishizaka, S. T.; Rose, J.; Chow, J. C.; Strauss III, J. F. The extra domain A of fibronectin activates Toll-like receptor 4. *J. Biol. Chem.* **2001**, 276, 10229 - 10233.
309. Smiley, S. T.; King, J. A.; Hancock, W. W. Fibrinogen stimulates macrophage chemokine secretion through toll-like receptor 4. *The Journal of Immunology* **2001**, 167, 2887 - 2894.
310. Medzhitov, R.; Janeway, C. A. Innate immunity. *New England Journal of Medicine* **2000**, 343, 338 - 344.
311. Lee, M. S.; Kim, Y. Pattern-recognition receptor signaling initiated from extracellular, membrane, and cytoplasmic space. *Mol. Cells* **2007**, 23, 1.
312. Lentsch, A. B.; Ward, P. A. Regulation of inflammatory vascular damage. *J. Pathol.* **2000**, 190, 343 - 348.
313. Pober, J. S.; Sessa, W. C. Evolving functions of endothelial cells in inflammation. *Nature Reviews Immunology* **2007**, 7, 803 - 815.

314. Henderson, B. W.; Donovan, J. M. Release of prostaglandin E2 from cells by photodynamic treatment *in vitro*. *Cancer Res.* **1989**, *49*, 6896 - 6900.
315. Krosi, G.; Korbelik, M.; Dougherty, G. Induction of immune cell infiltration into murine SCCVII tumour by photofrin-based photodynamic therapy. *Br. J. Cancer* **1995**, *71*, 549 - 555.
316. Gollnick, S. O.; Liu, X.; Owczarczak, B.; Musser, D. A.; Henderson, B. W. Altered expression of interleukin 6 and interleukin 10 as a result of photodynamic therapy *in vivo*. *Cancer Res.* **1997**, *57*, 3904 - 3909.
317. Sun, J.; Cecic, I.; Parkins, C. S.; Korbelik, M. Neutrophils as inflammatory and immune effectors in photodynamic therapy-treated mouse SCCVII tumours. *Photochem.Photobiol.Sci.* **2002**, *1*, 690 - 695.
318. Korbelik, M. Induction of tumor immunity by photodynamic therapy. *J. Clin. Laser Med. Surg.* **1996**, *14*, 329 - 334.
319. van Duijnhoven, F. H.; Aalbers, R. I.; Rovers, J. P.; Terpstra, O. T.; Kuppen, P. J. The immunological consequences of photodynamic treatment of cancer, a literature review. *Immunobiology* **2003**, *207*, 105 - 113.
320. Canti, G.; De Simone, A.; Korbelik, M. Photodynamic therapy and the immune system in experimental oncology. *Photochemical & Photobiological Sciences* **2002**, *1*, 79 - 80.
321. Scheffer, S. R.; Nave, H.; Korangy, F.; Schlote, K.; Pabst, R.; Jaffee, E. M.; Manns, M. P.; Greten, T. F. Apoptotic, but not necrotic, tumor cell vaccines induce a potent immune response *in vivo*. *International journal of cancer* **2003**, *103*, 205 - 211.
322. Shaif-Muthana, M.; McIntyre, C.; Sisley, K.; Rennie, I.; Murray, A. Dead or alive: immunogenicity of human melanoma cells when presented by dendritic cells. *Cancer Res.* **2000**, *60*, 6441 - 6447.
323. Zitvogel, L.; Casares, N.; Péquignot, M. O.; Chaput, N.; Albert, M. L.; Kroemer, G. Immune response against dying tumor cells. *Adv. Immunol.* **2004**, *84*, 131 - 179.
324. Melcher, A.; Gough, M.; Todryk, S.; Vile, R. Apoptosis or necrosis for tumor immunotherapy: what's in a name? *Journal of molecular medicine* **1999**, *77*, 824 - 833.

325. Yenari, M. A.; Liu, J.; Zheng, Z.; Vexler, Z. S.; Lee, J. E.; Giffard, R. G. Antiapoptotic and Anti-inflammatory Mechanisms of Heat-Shock Protein Protection. *Ann. N. Y. Acad. Sci.* **2005**, *1053*, 74 - 83.
326. Korbelik, M.; Sun, J.; Cecic, I. Photodynamic therapy-induced cell surface expression and release of heat shock proteins: relevance for tumor response. *Cancer Res.* **2005**, *65*, 1018 - 1026.
327. Todryk, S.; Melcher, A. A.; Hardwick, N.; Linardakis, E.; Bateman, A.; Colombo, M. P.; Stoppacciaro, A.; Vile, R. G. Heat shock protein 70 induced during tumor cell killing induces Th1 cytokines and targets immature dendritic cell precursors to enhance antigen uptake. *The Journal of Immunology* **1999**, *163*, 1398 - 1408.
328. Gomer, C. J.; Ryter, S. W.; Ferrario, A.; Rucker, N.; Wong, S.; Fisher, A. M. Photodynamic therapy-mediated oxidative stress can induce expression of heat shock proteins. *Cancer Res.* **1996**, *56*, 2355 - 2360.
329. Takeda, K.; Kaisho, T.; Akira, S. Toll-Like Receptors. *Annu. Rev. Immunol.* **2003**, *21*, 335 - 376.
330. Steubing, R. W.; Yeturu, S.; Tuccillo, A.; Sun, C.; Berns, M. Activation of macrophages by Photofrin II during photodynamic therapy. *Journal of Photochemistry and Photobiology B: Biology* **1991**, *10*, 133 - 145.
331. Evans, S.; Matthews, W.; Perry, R.; Fraker, D.; Norton, J.; Pass, H. I. Effect of photodynamic therapy on tumor necrosis factor production by murine macrophages. *J. Natl. Cancer Inst.* **1990**, *82*, 34 - 39.
332. Korbelik, M.; Krosi, G. Enhanced macrophage cytotoxicity against tumor cells treated with photodynamic therapy. *Photochem. Photobiol.* **1994**, *60*, 497 - 502.
333. Canti, G.; Lattuada, D.; Nicolin, A.; Taroni, P.; Valentini, G.; Cubeddu, R. Antitumor immunity induced by photodynamic therapy with aluminum disulfonated phthalocyanines and laser light. *Anticancer Drugs* **1994**, *5*, 443.
334. Rawls, H. R.; Van Santen, P. A possible role for singlet oxygen in the initiation of fatty acid autoxidation. *J. Am. Oil Chem. Soc.* **1970**, *47*, 121 - 125.



335. Adams, G.; Willson, R. Pulse radiolysis studies on the oxidation of organic radicals in aqueous solution. *Trans.Faraday Soc.* **1969**, 65, 2981 - 2987.
336. Hastings, J. W.; Wilson, T. Bioluminescence and chemiluminescence. *Photochem. Photobiol.* **1976**, 23, 461 - 473.
337. Mazur, S.; Foote, C. S. Chemistry of singlet oxygen. IX. Stable dioxetane from photooxygenation of tetramethoxyethylene. *J. Am. Chem. Soc.* **1970**, 92, 3225 - 3226.
338. King, A. O.; Yasuda, N. Palladium-catalyzed cross-coupling reactions in the synthesis of pharmaceuticals. *Organometallics in Process Chemistry* **2004**, 205 - 245.
339. Torborg, C.; Beller, M. Recent Applications of Palladium-Catalyzed Coupling Reactions in the Pharmaceutical, Agrochemical, and Fine Chemical Industries. *Advanced Synthesis & Catalysis* **2009**, 351, 3027 - 3043.
340. Carey, J. S.; Laffan, D.; Thomson, C.; Williams, M. T. Analysis of the reactions used for the preparation of drug candidate molecules. *Organic & biomolecular chemistry* **2006**, 4, 2337 - 2347.
341. Surry, D. S.; Buchwald, S. L. Biaryl Phosphane Ligands in Palladium-Catalyzed Amination. *Angewandte Chemie International Edition* **2008**, 47, 6338 - 6361.
342. Horton, D. A.; Bourne, G. T.; Smythe, M. L. The combinatorial synthesis of bicyclic privileged structures or privileged substructures. *Chem. Rev.* **2003**, 103, 893 - 930.
343. Bikker, J.; Brooijmans, N.; Wissner, A.; Mansour, T. Kinase domain mutations in cancer: implications for small molecule drug design strategies. *J. Med. Chem.* **2009**, 52, 1493.
344. Quintás-Cardama, A.; Kantarjian, H.; Cortes, J. Flying under the radar: the new wave of BCR–ABL inhibitors. *Nature Reviews Drug Discovery* **2007**, 6, 834 - 848.

345. Brickner, S. J.; Hutchinson, D. K.; Barbachyn, M. R.; Manninen, P. R.; Ulanowicz, D. A.; Garmon, S. A.; Grega, K. C.; Hendges, S. K.; Toops, D. S.; Ford, C. W. Synthesis and antibacterial activity of U-100592 and U-100766, two oxazolidinone antibacterial agents for the potential treatment of multidrug-resistant gram-positive bacterial infections. *J. Med. Chem.* **1996**, *39*, 673 - 679.
346. Ronald, A. R.; Low, D. E. *Fluoroquinolone antibiotics*; Birkhäuser: Basel, Boston, 2003.
347. Nilsson, J. W.; Thorstensson, F.; Kvarnström, I.; Oprea, T.; Samuelsson, B.; Nilsson, I. Solid-phase synthesis of libraries generated from a 4-phenyl-2-carboxy-piperazine scaffold. *J. Comb. Chem.* **2001**, *3*, 546 - 553.
348. Wolfe, J.; Wagaw, S.; Buchwald, S. An Improved Catalyst System for Aromatic Carbon-Nitrogen Bond Formation-The Possible Involvement of bis (Phosphine) Palladium Complexes as Key Intermediates. *J. Am. Chem. Soc.* **1996**, *118*, 7215 - 7216.
349. Wolfe, J. P.; Buchwald, S. L. Scope and limitations of the Pd/BINAP-catalyzed amination of aryl bromides. *J. Org. Chem.* **2000**, *65*, 1144 - 1157.
350. Driver, M.; Hartwig, J. A 2nd-Generation Catalyst for Aryl Halide Amination-Mixed Secondary-Amines from Aryl Halides and Primary Amines Catalyzed by (Dppf) PdCl<sub>2</sub>. *J. Am. Chem. Soc.* **1996**, *118*, 7217 - 7218.
351. Guari, Y.; van Es, D. S.; Reek, J. N.; Kamer, P. C.; van Leeuwen, P. W. An efficient, palladium-catalysed, amination of aryl bromides. *Tetrahedron Lett.* **1999**, *40*, 3789 - 3790.
352. Shen, Q.; Ogata, T.; Hartwig, J. F. Highly Reactive, General and Long-Lived Catalysts for Palladium-Catalyzed Amination of Heteroaryl and Aryl Chlorides, Bromides, and Iodides: Scope and Structure-Activity Relationships. *J. Am. Chem. Soc.* **2008**, *130*, 6586 - 6596.
353. Marion, N.; Navarro, O.; Mei, J.; Stevens, E. D.; Scott, N. M.; Nolan, S. P. Modified (NHC) Pd (allyl) Cl (NHC= N-heterocyclic carbene) complexes for room-temperature Suzuki-Miyaura and Buchwald-Hartwig reactions. *J. Am. Chem. Soc.* **2006**, *128*, 4101 - 4111.

354. Nishiyama, M.; Yamamoto, T.; Koie, Y. Synthesis of N-arylpiperazines from aryl halides and piperazine under a palladium tri-tert-butylphosphine catalyst. *Tetrahedron Lett.* **1998**, *39*, 617 - 620.
355. Fleckenstein, C. A.; Plenio, H. Sterically demanding trialkylphosphines for palladium-catalyzed cross coupling reactions—alternatives to PtBu<sub>3</sub>. *Chem. Soc. Rev.* **2010**, *39*, 694 - 711.
356. Hartwig, J. F. Evolution of a fourth generation catalyst for the amination and thioetherification of aryl halides. *Acc. Chem. Res.* **2008**, *41*, 1534 - 1544.
357. Marion, N.; Nolan, S. P. Well-Defined N-Heterocyclic Carbenes– Palladium (II) Precatalysts for Cross-Coupling Reactions. *Acc. Chem. Res.* **2008**, *41*, 1440 - 1449.
358. Old, D.; Wolfe, J.; Buchwald, S. A highly active catalyst for palladium-catalyzed cross-coupling reactions: Room-temperature Suzuki couplings and amination of unactivated aryl chlorides. *J. Am. Chem. Soc.* **1998**, *120*, 9722 - 9723.
359. Singer, R. A.; Caron, S.; McDermott, R. E.; Arpin, P.; Do, N. M. *Synlett* **2003**, 1727 - 1731.
360. Rataboul, F.; Zapf, A.; Jackstell, R.; Harkal, S.; Riermeier, T.; Monsees, A.; Dingerdissen, U.; Beller, M. New Ligands for a General Palladium-Catalyzed Amination of Aryl and Heteroaryl Chlorides. *Chemistry-A European Journal* **2004**, *10*, 2983 - 2990.
361. Dai, Q.; Gao, W.; Liu, D.; Kapes, L. M.; Zhang, X. Triazole-based monophosphine ligands for palladium-catalyzed cross-coupling reactions of aryl chlorides. *J. Org. Chem.* **2006**, *71*, 3928 - 3934.
362. Singer, R. A.; Doré, M.; Sieser, J. E.; Berliner, M. A. Development of nonproprietary phosphine ligands for the Pd-catalyzed amination reaction. *Tetrahedron Lett.* **2006**, *47*, 3727 - 3731.
363. Fleckenstein, C. A.; Plenio, H. 9-Fluorenylphosphines for the Pd-Catalyzed Sonogashira, Suzuki, and Buchwald–Hartwig Coupling Reactions in Organic Solvents and Water. *Chemistry-A European Journal* **2007**, *13*, 2701 - 2716.

364. Schwarz, N.; Tillack, A.; Alex, K.; Sayyed, I. A.; Jackstell, R.; Beller, M. A novel palladium catalyst for the amination of electron-rich indole derivatives. *Tetrahedron Lett.* **2007**, *48*, 2897 - 2900.
365. Doherty, S.; Knight, J. G.; Smyth, C. H.; Jorgenson, G. A. Electron-Rich, Bicyclic Biaryl-Like KITPHOS Monophosphines via [4 2] Cycloaddition between 1-Alkynylphosphine Oxides and Anthracene: Highly Efficient Ligands for Palladium-Catalysed C-N and C-C Bond Formation. *Advanced Synthesis & Catalysis* **2008**, *350*, 1801 - 1806.
366. So, C. M.; Zhou, Z.; Lau, C. P.; Kwong, F. Y. Palladium-Catalyzed Amination of Aryl Mesylates. *Angewandte Chemie International Edition* **2008**, *47*, 6402-6406.
367. Suzuki, K.; Hori, Y.; Kobayashi, T. A New Hybrid Phosphine Ligand for Palladium-Catalyzed Amination of Aryl Halides. *Advanced Synthesis & Catalysis* **2008**, *350*, 652 - 656.
368. Withbroe, G. J.; Singer, R. A.; Sieser, J. E. Streamlined Synthesis of the Bippyphos Family of Ligands and Cross-Coupling Applications. *Organic Process Research & Development* **2008**, *12*, 480 - 489.
369. Pratap, R.; Parrish, D.; Gunda, P.; Venkataraman, D.; Lakshman, M. K. Influence of Biaryl Phosphine Structure on C-N and C-C Bond Formation. *J. Am. Chem. Soc.* **2009**, *131*, 12240 - 12249.
370. Ruan, J.; Shearer, L.; Mo, J.; Bacsa, J.; Zanotti-Gerosa, A.; Hancock, F.; Wu, X.; Xiao, J. [2.2] Paracyclophane-based monophosphine ligand for palladium-catalyzed cross-coupling reactions of aryl chlorides. *Organic & biomolecular chemistry* **2009**, *7*, 3236 - 3242.
371. Suzuki, K.; Hori, Y.; Nishikawa, T.; Kobayashi, T. A Novel (2, 2-Diarylvinyl) phosphine/Palladium Catalyst for Effective Aromatic Amination. *Advanced Synthesis & Catalysis* **2007**, *349*, 2089 - 2091.
372. Burgos, C. H.; Barder, T. E.; Huang, X.; Buchwald, S. L. Significantly Improved Method for the Pd-Catalyzed Coupling of Phenols with Aryl Halides: Understanding Ligand Effects. *Angewandte Chemie International Edition* **2006**, *45*, 4321 - 4326.
373. Vorogushin, A. V.; Huang, X.; Buchwald, S. L. Use of tunable ligands allows for intermolecular Pd-catalyzed CO bond formation. *J. Am. Chem. Soc.* **2005**, *127*, 8146 - 8149.

374. Moradi, W. A.; Buchwald, S. L. Palladium-Catalyzed  $\alpha$ -Arylation of Esters. *J. Am. Chem. Soc.* **2001**, *123*, 7996 - 8002.
375. Martin, R.; Buchwald, S. L. Palladium-Catalyzed Suzuki–Miyaura Cross-Coupling Reactions Employing Dialkylbiaryl Phosphine Ligands. *Acc. Chem. Res.* **2008**, *41*, 1461 - 1473.
376. Molander, G. A.; Canturk, B. Organotrifluoroborates and monocoordinated palladium complexes as catalysts—a perfect combination for Suzuki–Miyaura coupling. *Angewandte Chemie International Edition* **2009**, *48*, 9240 - 9261.
377. Surry, D. S.; Buchwald, S. L. Dialkylbiaryl phosphines in Pd-catalyzed amination: a user's guide. *Chemical Science* **2011**, *2*, 27 - 50.
378. Biscoe, M. R.; Barder, T. E.; Buchwald, S. L. Electronic Effects on the Selectivity of Pd-Catalyzed C–N Bond-Forming Reactions Using Biarylphosphine Ligands: The Competitive Roles of Amine Binding and Acidity. *Angewandte Chemie International Edition* **2007**, *46*, 7232 - 7235.
379. Barder, T. E.; Buchwald, S. L. Rationale behind the resistance of dialkylbiaryl phosphines toward oxidation by molecular oxygen. *J. Am. Chem. Soc.* **2007**, *129*, 5096 - 5101.
380. Huang, X.; Anderson, K. W.; Zim, D.; Jiang, L.; Klapars, A.; Buchwald, S. L. Expanding Pd-catalyzed CN bond-forming processes: The first amidation of aryl sulfonates, aqueous amination, and complementarity with Cu-catalyzed reactions. *J. Am. Chem. Soc.* **2003**, *125*, 6653 - 6655.
381. Charles, M. D.; Schultz, P.; Buchwald, S. L. Efficient Pd-catalyzed amination of heteroaryl halides. *Org. Lett.* **2005**, *7*, 3965 - 3968.
382. Fors, B. P.; Buchwald, S. L. Pd-Catalyzed Conversion of Aryl Chlorides, Triflates, and Nonafates to Nitroaromatics. *J. Am. Chem. Soc.* **2009**, *131*, 12898 - 12899.
383. Biscoe, M. R.; Fors, B. P.; Buchwald, S. L. A New Class of Easily Activated Palladium Precatalysts for Facile C–N Cross-Coupling Reactions and the Low Temperature Oxidative Addition of Aryl Chlorides. *J. Am. Chem. Soc.* **2008**, *130*, 6686 - 6687.

384. Barder, T. E.; Buchwald, S. L. Insights into amine binding to biaryl phosphine palladium oxidative addition complexes and reductive elimination from biaryl phosphine arylpalladium amido complexes via density functional theory. *J. Am. Chem. Soc.* **2007**, *129*, 12003 - 12010.
385. Wolfe, J. P.; Tomori, H.; Sadighi, J. P.; Yin, J.; Buchwald, S. L. Simple, efficient catalyst system for the palladium-catalyzed amination of aryl chlorides, bromides, and triflates. *J. Org. Chem.* **2000**, *65*, 1158 - 1174.
386. Ikawa, T.; Barder, T. E.; Biscoe, M. R.; Buchwald, S. L. Pd-catalyzed amidations of aryl chlorides using monodentate biaryl phosphine ligands: A kinetic, computational, and synthetic investigation. *J. Am. Chem. Soc.* **2007**, *129*, 13001 - 13007.
387. Old, D. W.; Harris, M. C.; Buchwald, S. L. Efficient palladium-catalyzed N-arylation of indoles. *Org. Lett.* **2000**, *2*, 1403 - 1406.
388. Harris, M. C.; Huang, X.; Buchwald, S. L. Improved functional group compatibility in the palladium-catalyzed synthesis of aryl amines. *Org. Lett.* **2002**, *4*, 2885 - 2888.
389. Anderson, K. W.; Mendez-Perez, M.; Priego, J.; Buchwald, S. L. Palladium-catalyzed amination of aryl nonaflates. *J. Org. Chem.* **2003**, *68*, 9563 - 9573.
390. Surry, D. S.; Buchwald, S. L. Selective palladium-catalyzed arylation of ammonia: Synthesis of anilines as well as symmetrical and unsymmetrical Di- and triarylamines. *J. Am. Chem. Soc.* **2007**, *129*, 10354 - 10355.
391. Fors, B. P.; Davis, N. R.; Buchwald, S. L. An Efficient Process for Pd-Catalyzed C-N Cross-Coupling Reactions of Aryl Iodides: Insight Into Controlling Factors. *J. Am. Chem. Soc.* **2009**, *131*, 5766 - 5768.
392. Amatore, C.; Jutand, A. Role of dba in the reactivity of palladium (0) complexes generated in situ from mixtures of Pd(dba)<sub>2</sub> and phosphines. *Coord. Chem. Rev.* **1998**, *178*, 511 - 528.
393. Macé, Y.; Kapdi, A. R.; Fairlamb, I. J.; Jutand, A. Influence of the dba Substitution on the Reactivity of Palladium (0) Complexes Generated from Pd<sub>2</sub>(dba)<sub>3</sub> or Pd(dba)<sub>2</sub> and PPh<sub>3</sub> in Oxidative Addition with Iodobenzene. *Organometallics* **2006**, *25*, 1795 - 1800.

394. Shekhar, S.; Hartwig, J. F. Effects of Bases and Halides on the Amination of Chloroarenes Catalyzed by Pd(Pt Bu<sub>3</sub>)<sub>2</sub>. *Organometallics* **2007**, *26*, 340 - 351.
395. Guram, A. S.; Rennels, R. A.; Buchwald, S. L. A simple catalytic method for the conversion of aryl bromides to arylamines. *Angewandte Chemie International Edition* **1995**, *34*, 1348 - 1350.
396. Amatore, C.; Jutand, A. Anionic Pd (0) and Pd (II) intermediates in palladium-catalyzed Heck and cross-coupling reactions. *Acc. Chem. Res.* **2000**, *33*, 314 - 321.
397. Amatore, C.; Jutand, A. Mechanistic and kinetic studies of palladium catalytic systems. *Journal of organometallic chemistry* **1999**, *576*, 254 - 278.
398. Roy, A. H.; Hartwig, J. F. Oxidative addition of aryl sulfonates to Palladium (0) complexes of mono- and bidentate phosphines. Mild addition of aryl tosylates and the effects of anions on rate and mechanism. *Organometallics* **2004**, *23*, 194 - 202.
399. Grushin, V. V.; Alper, H. Transformations of chloroarenes, catalyzed by transition-metal complexes. *Chem. Rev.* **1994**, *94*, 1047 - 1062.
400. Littke, A. F.; Fu, G. C. Palladium-catalyzed coupling reactions of aryl chlorides. *Angewandte Chemie International Edition* **2002**, *41*, 4176 - 4211.
401. Colacot, T. J. The 2010 Nobel Prize in Chemistry: Palladium-Catalyzed Cross-Coupling. *Platinum Metals Review* **2011**, *55*, 84 - 90.
402. Colacot, T. CRC International Symposium: Cross Coupling and Organometallics. *Platinum Metals Review* **2008**, *52*, 172.
403. Mizoroki, T.; Mori, K.; Ozaki, A. Arylation of olefin with aryl iodide catalyzed by palladium. *Bull. Chem. Soc. Jpn.* **1971**, *44*, 581.
404. Mori, K.; Mizoroki, T.; Ozaki, A. Arylation of olefin with iodobenzene catalyzed by Palladium. *Bull. Chem. Soc. Jpn.* **1973**, *46*, 1505 - 1508.
405. Heck, R. F. Acylation, methylation, and carboxyalkylation of olefins by Group VIII metal derivatives. *J. Am. Chem. Soc.* **1968**, *90*, 5518 - 5526.

406. Heck, R. F.; Nolley Jr, J. Palladium-catalyzed vinylic hydrogen substitution reactions with aryl, benzyl, and styryl halides. *J. Org. Chem.* **1972**, *37*, 2320 - 2322.
407. Dieck, H.; Heck, R. Organophosphinepalladium complexes as catalysts for vinylic hydrogen substitution reactions. *J. Am. Chem. Soc.* **1974**, *96*, 1133 - 1136.
408. Negishi, E.; Baba, S. Novel stereoselective alkenyl-aryl coupling via nickel-catalysed reaction of alkenylzinc reagents with aryl halides. *J. Chem. Soc., Chem. Commun.* **1976**, 596b - 597b.
409. Negishi, E.; King, A. O.; Okukado, N. Selective carbon-carbon bond formation via transition metal catalysis. 3. A highly selective synthesis of unsymmetrical biaryls and diarylmethanes by the nickel-or palladium-catalyzed reaction of aryl- and benzylzinc derivatives with aryl halides. *J. Org. Chem.* **1977**, *42*, 1821 - 1823.
410. King, A. O.; Okukado, N.; Negishi, E. Highly general stereo-, regio-, and chemo-selective synthesis of terminal and internal conjugated enynes by the Pd-catalysed reaction of alkynylzinc reagents with alkenyl halides. *J. Chem. Soc., Chem. Commun.* **1977**, 683 - 684.
411. Hirashima, S.; Aoyagi, S.; Kibayashi, C. Total synthesis of pumiliotoxins A and 225F. *J. Am. Chem. Soc.* **1999**, *121*, 9873 - 9874.
412. Wipf, P.; Lim, S. Total synthesis of the enantiomer of the antiviral marine natural product hennoxazole A. *J. Am. Chem. Soc.* **1995**, *117*, 558 - 559.
413. Anderson, B. A.; Becke, L. M.; Booher, R. N.; Flaugh, M. E.; Harn, N. K.; Kress, T. J.; David, L.; Wepsiec, J. P. Application of palladium (0)-catalyzed processes to the synthesis of oxazole-containing partial ergot alkaloids. *J. Org. Chem.* **1997**, *62*, 8634 - 8639.
414. Miyaura, N.; Suzuki, A. Stereoselective synthesis of arylated (E)-alkenes by the reaction of alk-1-enylboranes with aryl halides in the presence of palladium catalyst. *J. Chem. Soc., Chem. Commun.* **1979**, 866 - 867.
415. Dieck, H. A.; Heck, R. F. Palladium-catalyzed conjugated diene synthesis from vinylic halides and olefinic compounds. *J. Org. Chem.* **1975**, *40*, 1083 - 1090.



416. Evano, G.; Blanchard, N.; Toumi, M. Copper-Mediated Coupling Reactions and Their Applications in Natural Products and Designed Biomolecules Synthesis. *Chem. Rev.* **2008**, *108*, 3054 - 3131.
417. Chan, D. M.; Monaco, K. L.; Wang, R.; Winters, M. P. New N-and O-arylations with phenylboronic acids and cupric acetate. *Tetrahedron Lett.* **1998**, *39*, 2933 - 2936.
418. Lam, P.; Clark, C. G.; Saubern, S.; Adams, J.; Winters, M. P.; Chan, D. M.; Combs, A. New aryl/heteroaryl C-N bond cross-coupling reactions via arylboronic acid/cupric acetate arylation. *Tetrahedron Lett.* **1998**, *39*, 2941 - 2944.
419. Ley, S. V.; Thomas, A. W. Modern Synthetic Methods for Copper-Mediated C (aryl)-O, C (aryl)-N, and C (aryl)-S Bond Formation. *Angewandte Chemie International Edition* **2003**, *42*, 5400 - 5449.
420. Jones, H. W., Jr; McKusick, V. A.; Harper, P. S.; Wu, K. D. George Otto Gey. (1899-1970). The HeLa cell and a reappraisal of its origin. *Obstet. Gynecol.* **1971**, *38*, 945 - 949.
421. Masters, J. R. HeLa cells 50 years on: the good, the bad and the ugly. *Nature Reviews Cancer* **2002**, *2*, 315 - 319.
422. Skloot, R. *The immortal life of Henrietta Lacks*; Crown, 2010.
423. Boateng, G. Design, Synthesis, and Biological Evaluation of Folate-Targeted Photodynamic Therapy Agents, Loyola University Chicago, 2009.
424. <http://academic.brooklyn.cuny.edu/biology/bio4fv/page/endocyta.htm>. [accessed May 5, 2011].
425. Chatterjee, R.; Iwai, Y.; Walder, R. Y.; Walder, J. A. Structural features required for the reactivity and intracellular transport of bis(3,5-dibromosalicyl)fumarate and related anti-sickling compounds that modify hemoglobin S at the 2,3-diphosphoglycerate binding site. *J. Biol. Chem.* **1984**, *259*, 14863 - 14873.
426. Patrick, G. L. *An Introduction to Medicinal Chemistry, 4th Ed.* Oxford University Press: Oxford, 2009.
427. <http://www.statemaster.com/encyclopedia/Photodynamic-therapy>. [accessed April 16, 2010].

428. Sanjeevaiah, P. B. Synthesis and Characterization of Phenothiazine Based Photosensitizers for Photodynamic Therapy, Loyola University Chicago, 2008.
429. Sang, G.; Zou, Y.; Li, Y. Two Polythiophene Derivatives Containing Phenothiazine Units: Synthesis and Photovoltaic Properties. *The Journal of Physical Chemistry C* **2008**, *112*, 12058 - 12064.
430. Zhang, Z.; Chen, Z.; Du, Q.; Feng, Y.; Xia, C. Synthesis of N-Aryl substituted heterocyclic compounds by copper (0) catalyst. *Youji Huaxue* **1989**, *9*, 555 - 557.
431. Okamoto, T.; Kuratsu, M.; Kozaki, M.; Hirotsu, K.; Ichimura, A.; Matsushita, T.; Okada, K. Remarkable Structure Deformation in Phenothiazine Trimer Radical Cation. *Org. Lett.* **2004**, *6*, 3493 - 3496.
432. Wang, Z.; Fu, H.; Jiang, Y.; Zhao, Y. Iron/Copper-Cocatalyzed Ullmann N, O-Arylation Using FeCl<sub>3</sub>, CuO, and rac-1, 1'-Binaphthyl-2, 2'-diol. *Synlett* **2008**, *2008*, 2540 - 2546.
433. Lulinski, P.; Skulski, L. Oxidative Iodination of Arenes with Manganese (IV) Oxide or Potassium Permanganate as the Oxidants. *Bull. Chem. Soc. Jpn.* **1999**, *72*, 115 - 120.
434. Zhu, R.; Xing, L.; Wang, X.; Cheng, C.; Su, D.; Hu, Y. Highly Practical "Ligand-Free-Like" Copper-Catalyzed N-Arylation of Azoles in Lower Nitrile Solvents. *Advanced Synthesis & Catalysis* **2008**, *350*, 1253 - 1257.
435. Maiti, D.; Fors, B. P.; Henderson, J. L.; Nakamura, Y.; Buchwald, S. L. Palladium-catalyzed coupling of functionalized primary and secondary amines with aryl and heteroaryl halides: two ligands suffice in most cases. *Chemical Science* **2011**, *2*, 57 - 68.
436. Ram, S.; Spicer, L. D. Debenzylation of N-benzylamino derivatives by catalytic transfer hydrogenation with ammonium formate. *Synthetic Communications* **1987**, *17*, 415 - 418.
437. Johnstone, R. A.; Wilby, A. H.; Entwistle, I. D. Heterogeneous catalytic transfer hydrogenation and its relation to other methods for reduction of organic compounds. *Chem. Rev.* **1985**, *85*, 129 - 170.

438. Bajwa, J. S.; Slade, J.; Repič, O. Chemoselective deprotection of tertiary benzylamines and reduction of carbon–carbon double bonds in the presence of benzyl and benzyloxymethyl ethers. *Tetrahedron Lett.* **2000**, *41*, 6025 - 6028.
439. Elamin, B.; Anantharamaiah, G. M.; Royer, G. P.; Means, G. E. Removal of benzyl-type protecting groups from peptides by catalytic transfer hydrogenation with formic acid. *J. Org. Chem.* **1979**, *44*, 3442 - 3444.
440. Gilman, H.; Nelson, R. D. Oxidation of 10-Acyl-and 10-Alkylphenothiazines. *J. Am. Chem. Soc.* **1953**, *75*, 5422 - 5425.
441. Sabot, C.; Kumar, K. A.; Meunier, S.; Mioskowski, C. A convenient aminolysis of esters catalyzed by 1, 5, 7-triazabicyclo [4.4. 0] dec-5-ene (TBD) under solvent-free conditions. *Tetrahedron Lett.* **2007**, *48*, 3863 - 3866.
442. Kawauchi, H.; Suzuki, S.; Kozaki, M.; Okada, K.; Islam, D. M. S.; Araki, Y.; Ito, O.; Yamanaka, K. Photoinduced charge-separation and charge-recombination processes of fullerene [60] dyads covalently connected with phenothiazine and its trimer. *J. Phys. Chem. A.* **2008**, *112*, 5878 – 5884.
443. Hrdina, R.; Muller, C. E.; Wende, R. C.; Wanka, L.; Schreiner, P. R. Enantiomerically enriched *trans*-diols from alkenes in one pot: a multicatalyst approach. *Chem. Commun.* **2012**, *48*, 2498 - 2500.
444. CellTiter-Blue Cell Viability Assay - Instructions for Use of Products G8080, G8081, and G8082. <http://www.promega.com/~media/files/resources/protocols/technical%20bulletins/101/celltiter-blue%20cell%20viability%20assay%20protocol.pdf> [accessed August 19, 2014].
445. Chen, C.; Ke, J.; Zhou, X.E.; Yi, W.; Brunzelle, J.S.; Li, J.; Yong, E.; Xu, H.E.; Melcher, K. Structural basis for molecular recognition of folic acid by folate receptors. *Nature* **2013**, *500*, 486 – 490.
446. Li, Donghong; Li, Pengxi; Lin, Huiyun; Jiang, Zonglin; Guo, Linfeng; Li, Buhong. A novel chorin-PEG-folate conjugate with higher water solubility, lower cytotoxicity, better tumor targeting, and photodynamic activity. *J. Photochem. Photobiol. B Biol.* **2013**, *127*, 28 – 37.

## VITA

Laura Donahue was born on August 26, 1959 in Freeport, IL. She graduated from St. Xavier University, Chicago, in 1981 with a Bachelor of Science degree in Biology. She then completed an internship in Medical Technology at St. Francis Hospital, Blue Island, IL and became a certified Medical Technologist in 1983. After working in this field for a while, Laura continued her education at Governors State University, University Park, IL, and received a 6 – 12 science education teaching certificate in 1987. She later received a Master of Science degree in Analytical Chemistry from Governors State University in 1992. Since that time, she has been an adjunct professor of chemistry at Moraine Valley Community College, Triton Community College, Governors State University, and Lewis University. She began her doctoral studies at Loyola University Chicago in 2008 working on Photodynamic Therapy research with Dr. David Crumrine. She was awarded a Teaching Scholars Fellowship for the academic year 2010 - 2011. Laura has two sons, Michael (24), and Matthew (21). Her son Matt is pursuing a Biochemistry degree at Loyola University Chicago, and Mike is a graduate of DePaul University with a degree in Political Science.